

**Tumor-intrinsic signaling pathways that coordinate breast cancer  
immunosuppression.**

Ryuhjin Ahn  
Division of Experimental Medicine  
McGill University  
Montreal, Quebec, Canada  
2019

---

A Thesis submitted to McGill University in partial fulfillment of the requirements of the  
degree of Doctor of Philosophy.

©Ryuhjin Ahn, 2019

## Table of Contents

Abstract	7
Resume	8
Original Contributions to Knowledge	9
Acknowledgements	10
Preface	10
Contribution of Authors	10
Mouse strains and reagents	10
Experimental contributions	11
Technical services	11
List of Figures	13
List of Tables	16
List of Abbreviations	17
Chapter 1: Literature Review	21
1.1 Breast architecture	21
1.2 Breast cancer	21
1.2.1 Statistics	21
1.2.2 Development and progression	22
1.2.3 Staging and subtypes	23
1.2.4 Standard of treatment and the need for improvement	23
1.3 Cancer and immune response	24
1.3.1 Tumor elimination by adaptive and innate immune cells	26
1.3.2 Immune escape, suppression and resistance to therapy	27
1.3.3 Breast cancer and immune response	29
1.3.4 Oncogenic signaling pathways suppress immune response	30
1.3.5 Cancer immunotherapy	32
1.3.6 Breast cancer immunotherapy: where are we?	33
1.3.7 Combination of kinase inhibitors and immunotherapy	34
1.4 Receptor tyrosine kinases signaling	35
1.5 Shc1 adaptor protein	36
1.5.1 Shc1 phospho-tyrosine signaling	38

1.5.2	Shc1-p66 isoform	42
1.5.3	Shc1 in cancer	43
1.5.4	Shc1 in anti-tumor immunity	44
1.6	STAT1 and STAT3 transcription factors	45
1.6.1	STAT3	45
1.6.1.1	STAT3 in cancer	49
1.6.1.2	Tumor intrinsic STAT3-mediated immunosuppression	50
1.6.1.3	Unphosphorylated STAT3	51
1.6.2	STAT1	52
1.6.2.1	STAT1 signaling	52
1.6.2.2	STAT1 in anti-tumorigenic roles	53
1.6.2.3	STAT1 in pro-tumorigenic roles	54
1.6.3	Interaction between STAT1 and STAT3	55
1.7	Mouse models used in this thesis	57
1.7.1	Middle T antigen driven mouse model of breast cancer	57
1.7.2	HER2 driven mouse model of breast cancer	59
1.7.3	CD8 null mouse model	60
1.7.4	IFN $\gamma$ null mouse model	60
1.8	Experimental rationale	61
Chapter 2: Materials and Methods		63
2.1	Animal Work	63
2.1.1	General mouse husbandry	63
2.1.2	Generation of mouse strains	63
2.1.3	Tail DNA Extraction and genotyping	63
2.1.4	Mammary fat pad (MFP) injections	65
2.1.5	Tumor monitoring	65
2.1.6	Tumor vaccination	65
2.1.7	Immune checkpoint inhibitor treatment	65
2.1.8	Necropsies and tissue collections	66
2.2	Plasmid constructs and cloning	66
2.2.1	CRISPR/Cas9 against STAT1 and STAT3	66

2.2.2	BiID and affinity purification constructs	66
2.2.3	STAT3 wild-type and STAT3 mutants	67
2.2.4	Knock-down using shRNA	67
2.3	Cell culture	68
2.3.1	General cell culture	68
2.4	Flow cytometry	68
2.4.1	Cell lines	68
2.4.2	Breast tumor	69
2.5	Mass spectrometry	70
2.5.1	Coomassie blue staining	70
2.5.2	BiID-MS	70
2.5.3	AP-MS	72
2.5.4	ProHits-vis analysis	72
2.6	Protein analyses	73
2.6.1	Protein lysis and immunoblot	73
2.6.2	ELISA	74
2.6.3	Immunohistochemistry (IHC)	74
2.7	RNA analyses	75
2.7.1	RNA extraction for in vitro and in vivo studies	75
2.7.2	RNA sequencing and analysis	76
2.7.3	Real time quantitative reverse transcription PCR (RT-qPCR)	78
2.8	Data availability	79
2.9	Statistics	79
Chapter 3:	Shc1 phospho-tyrosine signaling promotes immunosuppression	80
3.1	Experimental rationale	80
3.2	Phospho-Y239/240-Shc1 signaling suppresses anti-tumor immune response	81
3.3	Phospho-Y313-Shc1 signaling suppresses the antigen presentation machinery	83
3.4	Shc1 signaling promotes STAT3 signaling and suppresses STAT1 signaling	85

3.5	STAT1 and STAT3 activation are concomitantly increased and sustained specifically with phospho-Y313-Shc1 signaling loss	87
3.6	Y313-Shc1 signaling suppresses STAT1 to decrease expression of APP machinery and surface MHC class I	87
3.7	STAT3 is critical for promoting tumor onset and growth in the presence of CTL immune response	88
3.8	Phosphorylation status of Shc1 impacts breast tumor sensitivity to immunotherapy	90
3.9	Shc1 phospho-signaling and immune evasion in human breast cancer	92
Chapter 4: Shc1 phospho-tyrosine dependent interactors that mediate immunosuppression		
		153
4.1	Experimental rationale	153
4.2	Identification of Shc1 phospho-tyrosine dependent and independent interactome	153
4.3	Map4k5 and Grb2 as Shc1 interactor that mediates immunosuppression	156
4.4	Loss of Grb2 leads to STAT3 activation	158
4.5	Map4k5 is a novel Shc1 interactor	158
4.6	MEK pathway and JAK2/3 phosphorylates S727- and Y705-STAT3	159
Chapter 5: Mechanism of STAT3 driven immunosuppression		
		173
5.1	Experimental rationale	173
5.2	Phospho-Y705 and phospho-S727 STAT3 signaling suppresses IFN $\gamma$ driven anti-tumor immunity	173
5.3	STAT3 localization and phosphorylation status	175
5.4	Summary	176
Chapter 6: Discussion and future directions		
		181
6.1	Mechanism of STAT3 activation by phospho-Y239/240-Shc1 signaling to promote immunosuppression	181
6.2	Mechanism of phospho-Y313-Shc1 signaling driven suppression of STAT1 signaling	183
6.3	Shc1 Interactome	184
6.4	Shc1 and immunotherapy	188

6.5 STAT3 and immunosuppression.....	191
Chapter 7: References.....	194

## Abstract

Dysregulated receptor and non-receptor tyrosine kinase signalling within malignant cells are central to cancer progression. Previously, the Shc1 scaffold, a critical downstream effector of numerous oncogenic tyrosine kinases, was shown to be essential for promoting breast cancer immunosuppression. To define the molecular mechanism(s), we employed the Polyoma virus middle T (MT) transgenic breast cancer mouse model (MMTV/MT) harbouring two wild-type Shc1 alleles or a homozygous knock-in of tyrosine-to-phenylalanine point mutations in key tyrosines (Y239/240 or Y313) that are critical for Shc1 signaling. Breast cancer cell lines generated from these mice were studied in the context of cytotoxic T cell or IFN $\gamma$  wild-type or deficient mice to address the tumor intrinsic function of Shc1 phospho-tyrosine signaling in suppressing anti-tumor responses during breast cancer progression. We show that Y239/240-Shc1 signaling node activates STAT3 (Y705 and S727) immunosuppressive signals, while Y313-Shc1 impairs the STAT1-driven anti-tumor immunity in breast cancer. Therapeutically, impaired Y239/240-Shc1 signaling sensitized tumors to immune checkpoint inhibitors and tumor vaccines while impaired Y313-Shc1 signaling only sensitized tumors to tumor vaccines. Transcriptomic signatures unique to each Shc1 phospho-tyrosine signaling pathway were used to stratify TCGA breast cancer patient samples. Proteomic analysis on breast tumors harbouring wild-type or the phospho-tyrosine deficient Shc1 mutants were done using mass spectrometry to define the interactome unique to each phospho-tyrosine signaling node. In particular, we provide evidence that Map4k5 is a novel Shc1 interactor. Finally, given the importance of STAT3 activation downstream of Shc1 for breast tumor immunity, we focused our efforts on understanding the mechanistic basis by which both Y705 and S727-STAT3 contribute to immune evasion. We show that these STAT3 phosphorylation sites confer important and non-overlapping roles to induce breast cancer immune suppression. Combined, these data suggest that inhibition of phospho-Y239/240-Shc1 dependent STAT3 signalling may represent a therapeutic strategy to sensitize breast tumors to multiple immunotherapies. Together, we provide the first experimental evidence that post-translational modification of an adaptor protein downstream of tyrosine kinases attenuates anti-tumor immune responses and impairs sensitivity of tumors to various immunotherapies in a preclinical model of breast cancer.

## Resume

Les signalisations par tyrosine kinases dans les cellules malignes sont essentielles pour la progression du cancer. Shc1, un régulateur critique et un point de convergence de la signalisation de la tyrosine kinase, a été ultérieurement montré comme favorisant la suppression immunitaire du cancer du sein. Cependant, le mécanisme moléculaire était inconnu. En combinant des modèles *in vivo*, des techniques de biologie cellulaire et de la bioinformatique, nous avons identifié des noyaux de signalisation de phospho-tyrosine spécifiques (Y239/240 ou Y313) de protéines adaptatrices Shc1 qui régulent des voies inflammatoires importantes, permettant finalement aux tumeurs d'échapper à la réponse immunitaire anti-tumorale. Nous montrons que la modulation des noyaux spécifiques de signalisation de l'adaptateur Shc1 pourrait sensibiliser de manière différentielle le cancer du sein à l'inhibiteur du point de contrôle immunitaire ou à la vaccination tumorale. Les biomarqueurs pour les patients qui bénéficieraient de l'immunothérapie ont été identifiés. Des analyses protéomiques sur des tumeurs du sein hébergeant Shc1 de type sauvage ou Shc1 déficients en phospho-tyrosine ont été effectuées en utilisant la spectrométrie de masse pour définir l'interactome unique de chaque noeud de signalisation de phospho-tyrosine. En particulier, nous apportons la preuve que Map4k5 est un nouvel interacteur pour Shc1. Additionnellement, nous montrons que les deux phosphorylations Y705 et S727 de STAT3 confèrent des rôles importants pour induire une suppression immunitaire du cancer du sein. Cette étude met en évidence Shc1 comme une cible idéale pour surmonter deux obstacles majeurs dans la thérapie du cancer aujourd'hui: la résistance à une thérapie ciblée, comme les inhibiteurs de la kinase, et l'immunodétection tumorale qui entrave l'immunothérapie réussie. À notre connaissance, ce travail fournit la première preuve que la modification post-traductionnelle d'une protéine adaptateur pourrait réguler différemment la sensibilité à l'immunothérapie dans un modèle préclinique et soutient le développement de méthodes visant à cibler les protéines adaptatrices dans le traitement du cancer.

## **Original Contributions to Knowledge**

1. Posttranslational modification of an adaptor protein regulates an anti-tumor immune response and sensitivity to immunotherapies in preclinical model of breast cancer.
2. Y239/240-Shc1 signaling node activates STAT3 (Y705 and S727) immunosuppressive signals, while Y313-Shc1 impairs STAT1-driven anti-tumor immune response in breast cancer.
3. Impaired Y239/240-Shc1 sensitizes tumors to immune checkpoint inhibitors and tumor vaccines while impaired Y313-Shc1 sensitizes tumors to tumor vaccines.
4. Map4k5 is a novel Shc1 interactor
5. Both phospho-Y705 and S727-STAT3 signaling are important to suppress IFN $\gamma$  anti-tumor immune during breast cancer progression

## **Acknowledgements**

I want to express my deepest gratitude to Dr. Josie Ursini-Siegel for giving me the opportunity to pursue this degree, for her unwavering mentorship and supervision over the years, and for inspiring me to always strive for excellence. I am immensely grateful to Dr. Stephane Richard, Dr. Peter Siegel, Dr. Koren Mann, Dr. David Dankort, Dr. Connie Krawczyk, Dr. Stephanie Lehoux, Dr. Morag Park, and Dr. William Muller for their crucial guidance on my thesis project and support with professional development throughout my degree. I am greatly indebted to past and present lab members for their monumental support and experimental contribution to this thesis and the publications associated. I would like to thank Rhona Rosenzweig and Talia Rosberger for their kind assistance with ordering. My sincerest thanks go to Mona Wu, Mike Dahabieh, Ronan Hanley, and Kévin Jacquet for their incredible help and advice. I owe everything to Kenny Ah-Lan, my parents, and my brother for their unconditional love and support through thick and thin. Lastly, I dedicate this thesis to my late grandfather Myung-Choo Ahn who inspired me throughout my life to persistently follow my passion, to pursue a career in scientific research, and to never give up.

## **Preface**

This thesis is presented in the traditional thesis format.

Peer-reviewed publication arising from this thesis is “The Shc1 adaptor simultaneously balances STAT1 and STAT3 activity to promote breast cancer immune suppression” published in Nature Communications (Ahn et al., 2017). Parts of the data presented in Chapter 3 were published in a book chapter titled “Analyzing the Tumor Microenvironment by Flow Cytometry” (Young et al., 2016). Parts of the data presented in Chapter 4 have been included in a manuscript (Kiepas *et al.*) recently submitted.

## **Contribution of Authors**

### **Mouse strains and reagents**

Shc1<sup>flx/flx</sup> mice and Shc<sup>2F/2F</sup> and Shc<sup>313F/313F</sup> mice were provided by Dr. Tony Pawson. MMTV/MT mice, MMTV/NIC mice, and two MT cell lines (864, 4788) were provided by Dr. William Muller of McGill University. Grb2 shRNA constructs were provided by Dr.

Sidong Huang of McGill University. IFN $\gamma$ <sup>-/-</sup> and CD8<sup>-/-</sup> mice were purchased from JAX Laboratory and were backcrossed in-house onto FVB background (F8). FVB mice were purchased from Charles River Laboratories. FVB, IFN $\gamma$ <sup>-/-</sup> and CD8<sup>-/-</sup> mice were in part maintained by Valerie Sabourin, Stephanie Totten, and Julie Lamarche. BioID constructs were made by Young Kyuen Im and Jacqueline Ha. Protocol for fractionation was optimized and shared by Dr. Shuo Wang of Dr. Antonis Koromilas lab at the Lady Davis Institute.

### **Experimental contributions**

RNA-seq bioinformatics analysis was done by Nicolas De Jay, Steven Hébert, and Dr. Claudia Kleinman of the Lady Davis Institute. Flow cytometry experiment for animal tissue was done and analyzed with Dr. Alicia Bolt, Yoon Kow (Christian) Young and Dr. Koren Mann of the Lady Davis Institute. MHC class I flow cytometric analysis for CRISPR/cas9-edited cell lines were done by Stephanie Totten. Part of MT/Shc1<sup>fl/fl</sup>, MT/Shc<sup>2F/2F</sup> and MT/Shc<sup>313F/313F</sup> transgenic mice cohorts were generated, palpated and necropsied by Valerie Sabourin and Young Kyuen Im. Valerie Sabourin contributed to immunohistochemical staining of breast tumor tissues and mammary fat pad injections. Rachel La Selva contributed to mammary fat pad injection, palpation and necropsy of STAT3 wild-type and mutant tumors. Affinity purified and BioID samples were trypsinized and subjected to mass spectrometry analysis by Dr. Nicolas Bisson and Kévin Jacquet of University of Laval. NIC/Shc1<sup>+/+</sup> and NIC/Shc1<sup>fl/fl</sup> RT-qPCR experiment was performed by Dr. Josie Ursini-Siegel. Summer student Maria Carolina Festa assisted with some of the experiments associated with Chapter 2. Undergraduate students Matthew Siegel and Beatrice Collibee assisted with some of the experiments associated with Chapter 3 and 4.

### **Technical services**

Services from pathology cores at the Jewish General Hospital and McGill University were purchased for paraffin embedding of tissues and scanning of immunohistochemically stained tissues. Genome Quebec service was purchased for RNA-sequencing. The

Animal quarter facility of the Lady Davis Institute was used for animal husbandry and training for animal surgery. Mutagenesis service was purchased from GenScript.

## List of Figures

- Figure 1. Schematic of normal breast architecture in adult human and adult mouse.
- Figure 2. Immune infiltrate and their immune modulatory effect in breast cancer.
- Figure 3. Antigen processing and presentation by tumor
- Figure 4. Tumors express checkpoint ligands to suppress effector T cell function
- Figure 5. Receptor tyrosine kinases (RTKs) involved in breast tumorigenesis.
- Figure 6. Schematic of Shc1 adaptor protein.
- Figure 7. STAT3 signaling
- Figure 8. Interferon induced STAT1 activation
- Figure 9. Tumor intrinsic STAT1 and STAT3 signaling pathways in tumorigenesis.
- Figure 10. Impaired phospho-Y239/240-Shc1 signaling delays breast tumor onset in a CD8+ T cell-dependent manner.
- Figure 11. *Morphology of cell lines in vitro and histology of mammary tumors in vivo.*
- Figure 12. Tumour onset of Shc1 wild-type and phospho-tyrosine *mutant expressing cell lines in vivo.*
- Figure 13. Phospho-Y239/240-Shc1 signaling suppresses CTL and IFN $\gamma$  driven anti-tumor immunity.
- Figure 14. Phospho-Y239/240-Shc1 signaling suppresses Granzyme B+ and CD3+ T cell infiltration.
- Figure 15. Phospho-Y239/240-Shc1 signaling suppresses CTL infiltration.
- Figure 16. Shc1 phospho-tyrosine signaling do not alter global transcriptome.
- Figure 17. Antigen processing and presentation machinery (APP) and MHC class I surface expression are increased with impaired phospho-Y313-Shc1 signaling.
- Figure 18. Surface MHC class I is increased with loss of phospho-Y313-Shc1 signaling.
- Figure 19. Impaired phospho-Y239/240-Shc1 *signaling* leads to increased IFN $\gamma$  and CXCL9 expression in mammary tumors.
- Figure 20. STAT1 and STAT3 pathways
- Figure 21. Phospho-Y239/240-Shc1 signaling promotes STAT3 activation while phospho-Y313-Shc1 signaling suppresses STAT1 expression.
- Figure 22. STAT3 activation at baseline and with IFN $\gamma$  treatment.

Figure 23. Impaired phospho-Y239/240-Shc1 *induces increased* STAT1 signaling *in vivo* in an IFN $\gamma$  dependent manner.

Figure 24. Two groups of tumors arise with loss of phospho-Y239/240-Shc1 signaling.

Figure 25. Phospho-Y239/240-Shc1 promotes STAT3 signaling.

Figure 26. STAT1 CRISPR/cas9 deletion and its impact on STAT3 activation.

Figure 27. STAT3 CRISPR/cas9 deletion and its impact on STAT1 activation.

Figure 28. Enhanced MHC class I expression due to impaired phospho-Y313-Shc1 signaling is STAT1 dependent.

Figure 29. IFN inducible genes upregulated upon loss of phospho-Y313-Shc1 signaling is STAT1 dependent.

Figure 30. Confirmation of mammary epithelial STAT1 *loss in breast tumors in vivo*.

Figure 31. Confirmation of mammary epithelial STAT3 *loss in breast tumors in vivo*.

Figure 32. STAT3 promotes suppression of CTL tumor killing and STAT1 is important for CTL anti-tumor immune response upon loss of phospho-Y239/240-Shc1 signaling.

Figure 33. STAT1 and STAT3 are both positive regulators of tumor progression in Shc1-proficient breast cancer cells in a CTL dependent manner.

Figure 34. STAT3 activation status may dictate whether STAT1 plays pro- or anti-tumorigenic role, and Shc1 may modulates this process.

Figure 35. CD3+ T cell infiltration is dependent on tumor intrinsic STAT1 activation.

Figure 36. Increased Granzyme B+ cell infiltration in phospho-Y239/240-Shc1 deficient tumors is STAT1 independent.

Figure 37. Loss of phospho-tyrosine Shc1 *signaling leads to* increased *PD-L1* expression.

Figure 38. Loss of phospho-Y239/240-Shc1 signaling sensitizes tumors to immune checkpoint inhibition and tumor vaccination, while loss of phospho-Y313-Shc1 signaling sensitizes tumors to tumor vaccination.

Figure 39. Shortened DM, 2F and 313F gene signatures used for breast cancer patient TCGA analysis accurately predict their respective Shc1 genotypes in cell lines.

Figure 40. Relevance of Shc1 gene signature in human breast cancer patients.

Figure 41. Positive correlation between STAT1, STAT3, phospho-Y705-STAT3 expression and their target gene transcription.

Figure 42. STAT1 and STAT3 activation status in mouse breast cancer cell lines correlate with the level of respective transcriptional target genes.

Figure 43. Schematic diagram of Shc1 driven immunosuppression and impact on immunotherapy.

Figure 44. Schematic of Myc-BirA-Shc1-3xFLAG constructs used in the study.

Figure 45. Validation of BioID constructs.

Figure 46. BioID/MS interactome of Shc1.

Figure 47. AP/MS interactome of Shc1.

Figure 48. AKT activation is impaired with loss of phospho-Y239/240-Shc1 signaling.

Figure 49. EGF induced AKT activation is debilitated in phospho-Y239/240-Shc1 impaired cells.

Figure 50. Grb2 and Map4k5 interaction with Shc1 affinity purification.

Figure 51. Predicted model of how Map4k5 promotes immunosuppression in cancer.

Figure 52. ShRNA induced knock-down of Grb2.

Figure 53. Map4k5 engages Shc1 independently of phospho-tyrosine in BioID assay.

Figure 54. ERK and JAK2/3 phosphorylate STAT3.

Figure 55. STAT3 wild-type and mutant models successfully generated.

Figure 56. Phospho-Y705-STAT3 and phospho-S727-STAT3 signaling suppresses IFN $\gamma$  driven anti-tumor immune response.

Figure 57. Level of SOCS3 expression *in vivo*.

Figure 58. STAT3 localizes to nucleus regardless of its phosphorylation status.

## List of Tables

- Table 1. Subtypes, frequency, molecular phenotype, staging and overall survival (OS) of breast cancer patients.
- Table 2. Pathways and/or molecular interactors of Shc1 (p52/p46 isoforms) and their known roles in tyrosine phosphorylation.
- Table 3. List of phospho-Y705 or phospho-S727 regulators.
- Table 4. Composition of PCR reaction for each genotype
- Table 5. List of primers used for PCR genotyping.
- Table 6. List of antibodies and reagents used for immune panel flow cytometry
- Table 7. List of reagents used for immune panel flow cytometry
- Table 8. List of antibodies used for immunoblotting
- Table 9. List of antibodies used for immunohistochemistry
- Table 10. List of mouse primers used for RT-qPCR
- Table 11. Differentially regulated genes in Shc2F (n=4 cell lines) by RNA-seq.
- Table 12. Differentially regulated genes in Shc313F (n=4 cell lines) by RNA-seq.
- Table 13. Differentially regulated genes in both Shc2F and Shc313F by RNA-seq.
- Table 14. IFN $\alpha$ , IFN $\beta$ , and IFN $\gamma$  protein levels detected by ELISA in the supernatants of ShcWT, Shc2F and Shc313F cells in culture (n=3-4 wells per cell line).
- Table 15. Number of reads of IFN genes in ShcWT, Shc2F and Shc313F cells based on RNA-seq analysis.
- Table 16. List of STAT1 target genes that define the STAT1 ssGSEA signature.
- Table 17. List of STAT3 target genes that define the STAT3 ssGSEA signature.
- Table 18. STRING analysis results for each condition (top two GO terms are shown)
- Table 19. List of 16 proteins discovered in both BioID-MS and AP-MS. Indicated are the tyrosines requirements for interaction.

## **List of Abbreviations**

AKT	v-akt Thymoma Viral Oncogene Homolog
AP-MS	Affinity purification mass spectrometry
APP	Antigen processing and presentation
B2M	$\beta$ -2-microglobulin
BFDR	Bayesian false discovery rate
BioID-MS	Proximity-dependent Biotin Identification mass spectrometry
BirA	Bifunctional ligase/repressor
BT	Breast tumor
Cas9	CRISPR associated protein 9
CD274	Cluster of differentiation 274
CD3	Cluster of differentiation 3
CD8	Cluster of differentiation 8
Cre	Cre recombinase
CRISPR	Clustered regularly interspaced short palindromic repeats
CTL	cytotoxic T lymphocyte
Ctrl	Control
CXCL9	Chemokine (C-X-C motif) ligand 9
DC	Dendritic cells
DCIS	Ductal Carcinoma In Situ
DDX60	DEAD/H-Box Helicase 60
EGF	Epidermal Growth Factor
EGFR	Epidermal Growth Factor Receptor
ELISA	Enzyme-linked immunosorbent assay
ER	Estrogen Receptor
ERAP1	Endoplasmic reticulum aminopeptidase 1
ErB2	epidermal growth factor 2
ErbB2	Epidermal Growth Factor 2
ERK	Extracellular signal-regulated kinase
Fas	Apoptosis antigen 1
FGFR	Fibroblast growth factor receptor

FLAG	peptide sequence DYKDDDDK
Flx	Floxed allele
FoxP3	Forkhead Box P3
FVB	friend virus B-type; strain of mouse
GAPDH	Glyceraldehyde 3-phosphate dehydrogenase
Grb2	Growth Factor Receptor-bound Protein 2
GZMB	Granzyme B
H&E	Hematoxylin and Eosin
IB	immunoblot
IFN $\gamma$	interferon gamma
IGF1R	Insulin-like growth factor 1 receptor
IHC	Immunohistochemistry
IL	Interleukin
IRES	Internal Ribosome Entry Site
JAK	Janus Kinase
LCIS	Lobular carcinoma in situ
LTR	Long Terminal Region
MAPK	Mitogen-activated Protein Kinase
MDSC	Myeloid Derived Suppressor Cell
MEF	Mouse embryonic fibroblast
MFP	mammary fat pad
MHC	Major Histocompatibility
ML	microscopic lesions
MMTV	Mouse Mammary Tumour Virus
mRNA	messenger RNA
MT	polymavirus middle T oncoprotein
MUC1	Mucin 1, Cell Surface Associated
Neu	Neuro/glioblastoma Derived Oncogene Homologue, ErbB2
NIC	NDL2-5-IRES-Cre recombinase; MMTV-NIC
NK	Natural killer cells
OCT	Optimal Cutting Temperature compound

OS	Overall survival
PBS	Phosphate-buffered saline
PCA	Principal component
PCR	Polymerase Chain Reaction
PD	Progressive disease
PD-1	Programmed Cell Death Protein 1
PD-L1	Programmed Death-Ligand 1
PI3K	Phosphatidylinositol-3-Kinase
PPC	Positive pixel count
PR	Progesterone receptor
PSMB8	Proteasome subunit beta type-8
PTB	Phosphotyrosine-Binding domain
qRT-PCR	Quantitative Real-Time PCR
RAG2	Recombination Activating 2
Ras	Rat Sarcoma Viral oncogene
RNA-seq	RNA sequencing
RTK	Receptor Tyrosine Kinases
S.D.	Standard deviation
S.E.M.	Standard error of the mean
SAINT	Significance Analysis of INTeractome
SD	Stable disease
SH2	Src Homology 2
Shc1	Src Homology 2 Domain-Containing Transforming Protein 1
shRNA	Short hairpin RNA
SOCS	Suppressors of Cytokine Signaling
SOS	Son of Sevenless
Src	v-Src Sarcoma Viral Oncogene Homolog
ssGSEA	Single-sample Gene Set Enrichment Analysis
STAT3	Signal Transducer and Activator of Transcription 3
TAP	Transporter associated with Antigen Processing 1
TBP	TATA-binding protein

TCR	T cell receptor
TLS	Tertiary lymphoid structures
TNBC	Triple negative breast cancer
TNF $\alpha$	Tumor necrosis factor alpha
Treg	T regulatory cells
VEGF	Vascular Endothelial Growth Factor
WT	Wild-type

## Chapter 1: Literature Review

### 1.1 Breast architecture

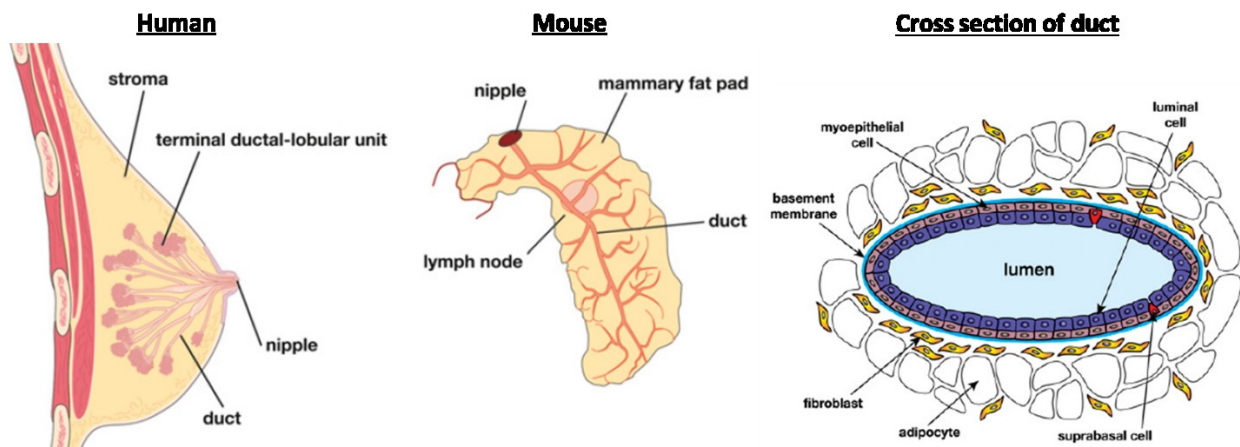


**Figure 1. Schematic of normal breast architecture in adult human and adult mouse.** Figures extracted from (Polyak and Hu, 2005; Visvader, 2009).

In the normal ducts of human and mouse mammary glands, a continuous layer of myoepithelial cells surrounds and separates the luminal epithelial cells from the basement membrane and stroma (**Fig. 1**) (Gudjonsson et al., 2005; Polyak and Hu, 2005). Stromal cells in the mammary gland include endothelial cells, macrophages, adipocytes, and fibroblasts (Neville et al., 1998). In humans, this network of ducts ends in clusters of terminal ductal lobular units (TDLUs), the milk producing glandular unit of the breast (Gudjonsson et al., 2005). Mice, instead of having TDLUs, have alveolar bud formation during each estrous cycle and pregnancy that give rise to milk producing cells (Paine and Lewis, 2017). While the architecture, adipocyte content, connective tissue amount and some cell lineage markers differ between mouse and human mammary glands, epithelial hierarchies of breast development and the expression pattern of key proteins (e.g. estrogen receptor alpha, progesterone receptor, ErbB2/HER2 receptor) show significant parallels (Fu et al., 2014; Visvader, 2009).

## 1.2 Breast cancer

### 1.2.1 Statistics

One in eight women are expected to develop breast cancer during their lifetime and 1 in 31 will die from it in the United States (Waks and Winer, 2019). According to the Government of Canada online database, breast cancer accounts for approximately 26% of new cases of cancer and 13% of all cancer deaths in Canadian women, making breast cancer the most common cancer in women with the exception of non-melanoma skin cancer.

### 1.2.2 Development and progression

It is postulated that most human breast cancer and benign lesions arise from inside or proximal to the terminal ductal lobular units (TDLUs) (Bodelon et al., 2017; Figueroa et al., 2014; Wellings, 1980; Yang et al., 2012). Breast cancer is classified into carcinomas (arising from ductal or lobular epithelium) and sarcomas (stromal component of breast; <1% of primary breast cancer) (Feng et al., 2018). Epidemiological and morphological observations have established a linear model of breast cancer progression where atypical ductal (or lobular) hyperplasia and ductal (or lobular) carcinoma in situ (DCIS) are suggested as non-obligate precursors of invasive and metastatic ductal (or lobular) carcinoma (Bombonati and Sgroi, 2011).

The pathogenesis of breast cancer involves both environmental (e.g. ionizing radiation, carcinogens, oral contraceptives, hormone replacement therapy, parity and menstrual history) and genetic risk factors (e.g. mutations, being a female) (Lippi et al., 2017). Genetic alterations contributing to breast cancer include whole or partial chromosome copy gain or loss, amplification, deletions, insertions, translocations, and mutations of single genes (Neve et al., 2006). Ultimately, dysregulation of various signaling pathways in the mammary epithelium leads to breast cancer. Systemic whole exome or genome sequencing studies of 103 breast cancer patients have identified the top 21 most commonly mutated genes in all of breast cancer: *TP53* (35%), *PIK3CA* (34%), *GATA3* (9%), *MAP3K1* (8%), *MLL3* (6%), *CDH1* (6%), *USH2A* (5%), *PTEN* (3%), *RUNX1* (3%), *MAP2K4* (3%), *NCOR1* (3%), *RB1* (3%), *TBX3* (2%), *PIK3R1* (2%), *CTCF* (2%), *NF1* (2%), *SF3B1* (2%), *AKT1* (2%), *CBFB* (1%), *FOXA1* (1%), and *CDKN1B* (1%) (Banerji et al., 2012). Proteins transcribed by *PIK3CA*, *MAP3K1*, *PTEN*, *MAP2K4*, *PIK3R1*, *NF1*, and *AKT1* are important signaling mediators of oncogenic receptor tyrosine

kinases (e.g. EGFR, HER2, FGFR, IGF1R) and non-receptor tyrosine kinase (e.g. SRC) (Polyak and Metzger Filho, 2012). Additionally, BRCA1 and BRCA2 mutations are well established risk factors of breast cancer development (present in approximately 3% of all breast cancer patients) (Lippi et al., 2017; Whittemore et al., 1997).

### 1.2.3 Staging and subtypes

Breast cancer is staged based on the size of tumor, armpit lymph node positive status, and metastasis status. Stage 0 indicates pre-cancerous DCIS or LCIS, stage 1 to 3 is assigned when malignant cells are within the breast or regional lymph node, and stage 4 is assigned when metastasis has occurred.

Molecularly, breast cancer is categorized into subtypes based on the status of estrogen receptor (ER+), progesterone receptor (PR+), and epidermal growth factor 2 (HER2/ErbB2) and Ki67 expression. Luminal A (ER+PR+HER2-Ki67<sup>low</sup>) or luminal B subtypes (ER+/PR+/HER2-/Ki67<sup>high</sup>) make up 70% of patients. The HER2 subtype (ER-/PR-/HER2+) makes up 15-20% of patients and triple negative (ER-/PR-/HER2-; TNBC) makes up 10-15% of patients. While breast cancer is heterogenous, subsets display recurrent patterns of transcriptional, genomic, and biological abnormalities (Neve et al., 2006). The HER2 subtype can be further subdivided into three molecularly and prognostically distinct groups (Staaf et al., 2010). Similarly, the TNBC subtype can be further subdivided into six (Lehmann et al., 2011) or four subtypes (Burstein et al., 2015). Depending on the stage and subtype, patients have varying overall survival (OS) rate (**Table 1**) (Polyak and Metzger Filho, 2012; Waks and Winer, 2019).

**Table 1. Subtypes, frequency, molecular phenotype, staging and overall survival (OS) of breast cancer patients.**

Adapted from (Polyak and Metzger Filho, 2012)

Subtype	Frequency	Phenotype	stage	5 year OS (%)	10 year OS (%)
DCIS	N/A	pre-invasive	0	99	98
luminal	70%	ER+, PR+	I	98	95

<b>(non HER2+)</b>			II	91	81
			III	72	54
			IV	33	17
<b>HER2+ (estimated using HER2 targeted therapies)</b>	20%	ERBB2 gene amplification and overexpression	I	98	95
			II	92	86
			III	85	75
			IV	40	15
<b>TNBC</b>	10%	ER-PR-HER2-, overlaps with basal subtype (defined by differentiation state and gene expression profile)	I	93	90
			II	76	70
			III	45	37
			IV	15	11

#### 1.2.4 Standard of treatment and the need for improvements

Treatment for breast cancer is determined by subtype, stage, and patient preference (Waks and Winer, 2019). ER+ and PR+ tumors (hormone receptor positive; HR+) are treated with endocrine therapy with or without chemotherapy, as these cells rely on ER and PR to proliferate (Polyak and Metzger Filho, 2012). This involves aromatase inhibitors (deprives estrogen) and blocking the binding of estrogen to ER using selective ER modulators (e.g. Tamoxifen in pre- and postmenopausal patients) or ER down-regulators (e.g. Fulvestrant; binds ER, leads to ER degradation) (Johnston and Cheung, 2018). HER2+ tumors are targeted with a HER2 monoclonal antibody (e.g. Trastuzumab) or small molecular inhibitor therapy combined with chemotherapy (Waks and Winer, 2019). TNBC patients are treated with chemotherapy (e.g. taxanes, anthracyclines) as first-line therapy (Schmid et al., 2018). As evident from **Table 1**, therapeutic challenges remain in advanced and/or metastatic HR+, HER2+ and TNBC subtypes, and especially where the disease is refractory to therapy or has relapsed after therapy. Multiple therapeutic options are being tested in clinical trials as discussed below.

### 1.3 Cancer and immune response

The true appreciation of the immune response in suppressing tumor formation came when mice lacking adaptive immunity (RAG2 knock-out) showed an increased tumor incidence upon carcinogen exposure (Shankaran et al., 2001). Since then, the ability of malignant cells to escape from anti-tumor immune responses through promoting immunosuppression has been established as a key hallmark of cancer (Hanahan and Weinberg, 2011). To achieve this, malignant cells organize into a complex structure composed of diverse cell types including stromal cells, immune cells, and endothelial cells, all of which are in constant communication (Ott and Adams, 2011) (**Fig. 2**).

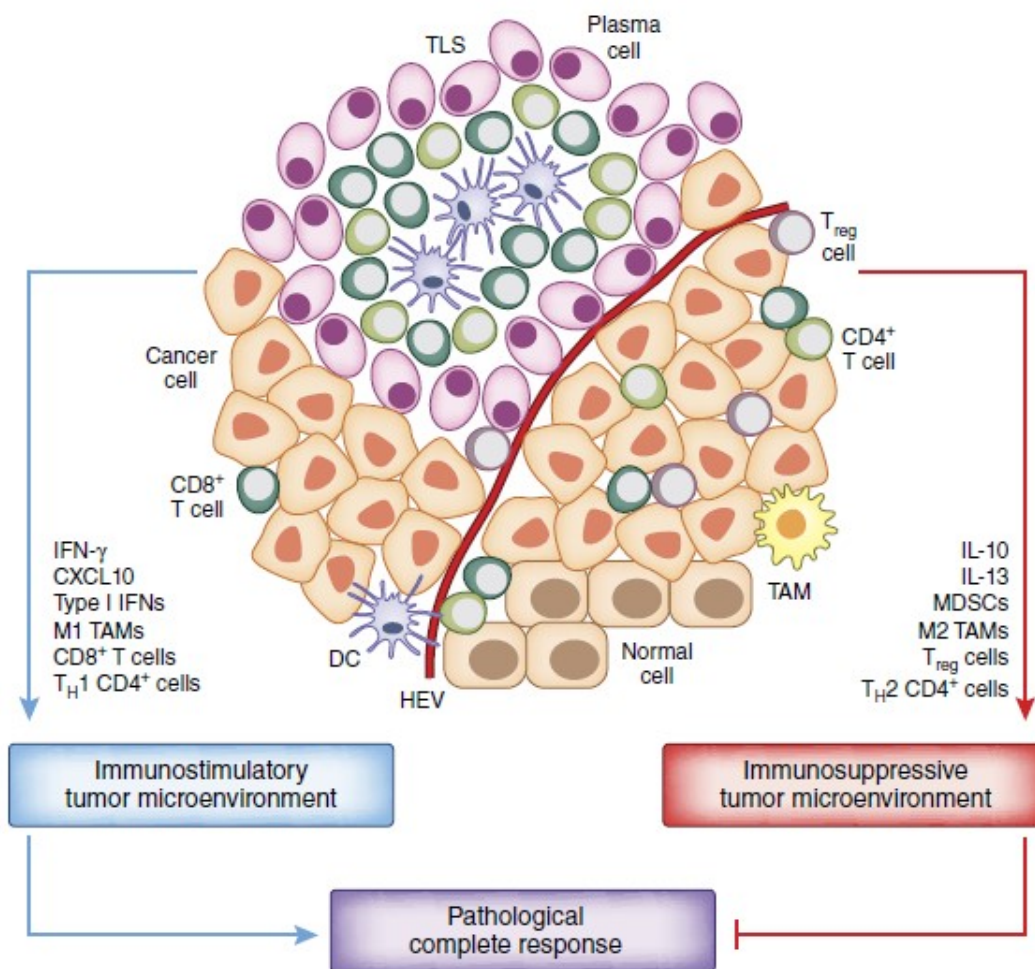


**Figure 2. Immune infiltrate and their immune modulatory effect in breast cancer.** Figure extracted from (Kroemer et al., 2015). Breast tumor microenvironment includes cancer cells, CD8<sup>+</sup> T effector cells, dendritic cells (DC), normal breast epithelium, tumor associated macrophages (TAM), plasma cells, tertiary lymphoid structures (TLS), CD4<sup>+</sup>

T helper cells, and myeloid derived suppressor cells (MDSC), and T regulatory cells ( $T_{reg}$ ). Immunostimulatory cytokines and immune effectors are listed on the left while those promoting immunosuppressive tumor microenvironment are listed on the right. The balance of the two forces influence eradication of tumors. HEV, high endothelial venules.

### 1.3.1 Tumor elimination by adaptive and innate immune cells

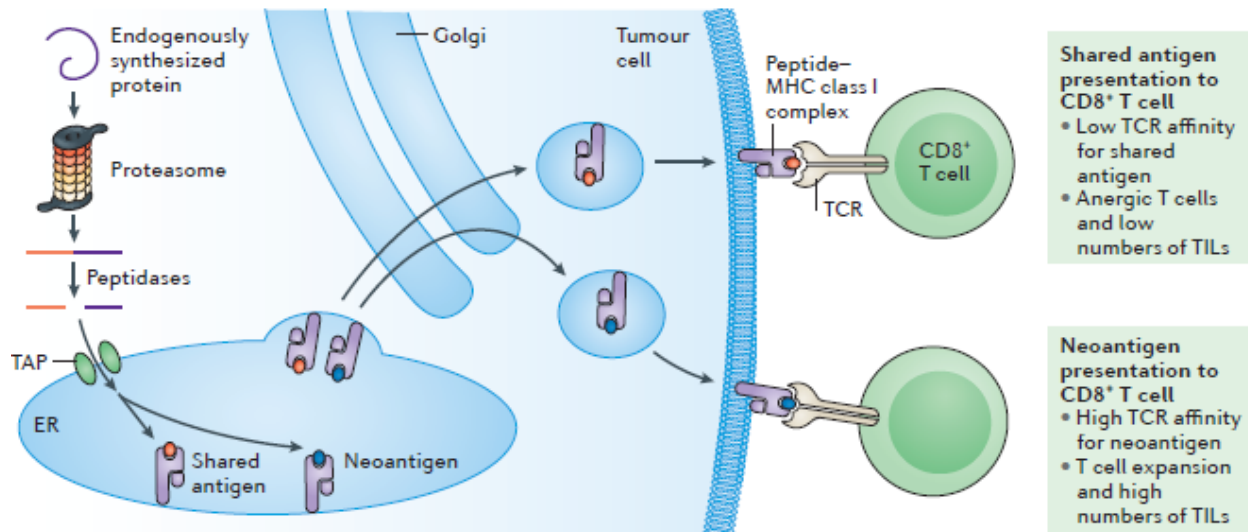


**Figure 3. Antigen processing and presentation by tumor**

Figure extracted from (Yarchoan et al., 2017). In order for CD8+ cytotoxic T cells to recognize tumors, antigens are processed by the immunoproteasome, peptides of size 8-11 amino acid lengths are generated through processing by peptidases such as ERAP1, transported into the endoplasmic reticulum (ER) by TAP1/2 proteins, and the antigens are loaded onto MHC class I complex along with  $\beta$ -2-microglobulin (B2M). Shared antigens such as tumor associated antigens (TAA) are overexpressed by both host and tumor cells while neoantigens (tumor specific antigens; TSA) arise by mutation specifically in tumor. TCR, T cell receptor. (Yarchoan et al., 2017).

Mechanisms of immune mediated tumor killing include (1) recognition of tumor associated antigen or tumor specific antigens by the adaptive immune system, and (2) non-antigen dependent killing by the innate immune system. Cytotoxic T cells (CD8+CD3+; CTL) are part of the adaptive immune system that eliminates tumors by (1) recognition of antigens presented in the context of MHC class I expressed on all nucleated

cells (**Fig. 3**) and (2) recognition of Fas on tumors via FasL to initiate apoptosis. Upon being activated by antigen recognition, CTLs form pores on target cells, through secretion of perforin, permitting the serine protease Granzyme B (GZMB) to be released in the target cells. Granzyme B mediated proteolysis of intracellular largest leads to apoptosis of the target cells. CTLs also release cytokines such as TNF $\alpha$  and IFN $\gamma$  to promote cell cycle arrest in tumors (DeNardo et al., 2010; Dunn et al., 2002; Dunn et al., 2004; Kim and Cantor, 2014; Zitvogel et al., 2006). While CTLs mount their attacks via T cell receptor (TCR) mediated recognition of antigen-MHC complexes, natural killer (NK) cells engage based on the balance of stimulatory versus inhibitory signals expressed by target cells (Voskoboinik et al., 2015; Wang et al., 2015b). Nonmicrobial cell death (necrosis or apoptosis) occurring in the context of an unfolded protein response (UPR) and autophagy can lead to the release of damage associated molecular patterns (DAMPs) which can elicit immunogenic cell death (ICD), inducing anti-tumor immune response by the innate immune system. B cells of the adaptive immune system have also emerged as potentially playing anti-tumorigenic roles through (1) release of tumor antigen specific antibodies (once B cell differentiates into plasma cells) that trigger antibody dependent cellular cytotoxicity (ADCC) by NK cells or complement-dependent cytotoxicity (CDC), and (2) B cell receptor mediated antigen presentation to CD8 $^+$  or naïve CD4 $^+$  cells for tumor killing (Mahmoud et al., 2012; Tsou et al., 2016; Wouters and Nelson, 2018). ADCC involves recognition of antibody to its corresponding epitope and recognition of the Fc region of the antibody by Fc receptors on immune effector cells such as NK cells. Coating of the tumors with antibodies thus triggers immune cell activation, leading to lysis of tumors (Boero et al., 2015).

### **1.3.2 Immune escape, suppression and resistance to therapy**

Tumors develop multiple tiers of immunosuppressive mechanisms to escape the host immune response (Gabrilovich et al., 2012; Kroemer et al., 2015). This involves (1) secretion of immunosuppressive cytokines that inhibit anti-tumor adaptive (e.g. CTLs) and innate immune cells (e.g. NK cells) and polarize immune cells to pro-tumorigenic subtypes (e.g. T regulatory cells; T<sub>reg</sub>), (2) secretion of chemokines that recruit immunosuppressive stromal and immune cells (e.g. myeloid derived suppressor cells,

tumor associated fibroblasts and macrophages) that in turn secrete immunosuppressive cytokines (e.g. IL-10, TGF $\beta$ ), (3) promotion of anergy and tolerance in anti-tumor immune cells through expression of surface inhibitory ligands (e.g. PD-L1) and persistent self-antigen presentation, (4) suppression of antigen presentation through e.g. epigenetic mechanisms (Heninger et al., 2015), to avoid detection by adaptive immunity through, and (5) upregulation of signaling pathways that reduce necessary metabolites (e.g. ATP) for immune cell (e.g. immature DC) activation in the tumor microenvironment (Kroemer et al., 2015).

Immunosuppressive pathways being successfully targeted in subgroups of patients include the PD-1/PD-L1 and CTLA4 immune checkpoint pathways (Topalian et al., 2015; Xia et al., 2015). They are necessary to maintain self-tolerance by limiting effector T cell function during an immune response (Xia et al., 2015). Normally, PD-1 expressed on T cells restricts peripheral tissue damage and inflammation during infection (**Fig. 4**). Once PD-1 binds PD-L1, TCR mediated effector functions of T cells are inhibited and T cell migration is reduced, leading to suppression of T cell activity (**Fig. 4**). Tumors can co-opt this and promote immunosuppression by expressing PD-L1 downstream of oncogenic signaling pathways (e.g. STAT3, STAT1, Myc, 9p24.1 amplification) or upon being exposed to IFN $\gamma$  secreted by T cells (Xia et al., 2015) (**Fig. 4**).

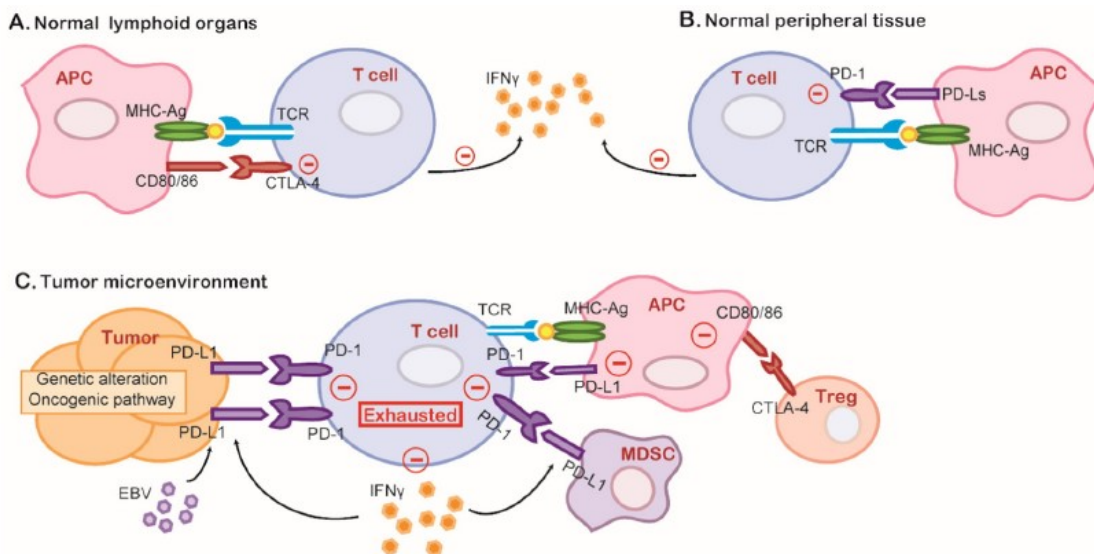


**Figure 4. Tumors express checkpoint ligands to suppress effector T cell function**

Figure extracted from (Xia et al., 2015). IFN $\gamma$  secreted by activated T cells induces STAT1 transcription factor signaling pathway, which lead to expression of PD-L1 on tumors and tumor associated myeloid cells (e.g. MDSC), leading to effector T cell exhaustion (Topalian et al., 2015).

### 1.3.3 Breast cancer and immune response

Stanton *et al.* in 2016 examined 13,914 patient samples and determined that 5%-26% of breast cancers have high infiltration of lymphocytes while 16% of cancers showed no infiltration. Median of 20% triple negative (TN), 16% HER2+, and 6% ER+/PR+/HER2- (HR+) breast cancers show predominant lymphocyte infiltration (defined as >50% lymphocytic infiltrate) (Stanton et al., 2016). CD8+ CTLs which are indicative of an anti-tumor immune response, as well as FOXP3+ T<sub>reg</sub> cells indicative of a pro-tumorigenic immune response, were most prominent in TNBC (60% infiltrated with CTLs and 70% infiltrated with T<sub>reg</sub>) and HER2+ (61% and 67%) tumors compared to HR+ breast cancers (43% and 38%) (Stanton et al., 2016). This observation is supported by other studies establishing that subsets of breast cancers are immunogenic and contain high TILs (Cimino-Mathews et al., 2016; Loi et al., 2013). Based on this concept of tumors being immune cold (lack of immune infiltration in part due to lack of tumor antigens, antigen presenting cell deficiency, absence of T cell priming, and impaired T cell trafficking) and immune hot (high immune infiltration) have emerged (Bonaventura et al., 2019). Importantly, high TILs are associated with improved prognosis in early stage TNBCs and HER2+ breast cancers (Ali et al., 2014; Burstein et al., 2015; Li et al., 2019; Savas et al., 2016), while the opposite is true in luminal breast cancer (Denkert et al., 2018). Given that TNBCs and HER2+ subtypes have worse prognosis, it has brought optimism for immunomodulation benefiting these subgroups of patients. Thus, immunotherapy approaches have been recently explored in these subtypes and are discussed below.

Not only the quantity of TILs (especially CD8+ T cells) but their spatial organization contribute to prognostic and predictive stratification in breast cancer (Heindl et al., 2018; König et al., 2019; Li et al., 2019; Nawaz et al., 2015; Saltz et al., 2018). This was also observed in ovarian cancer (Zhang et al., 2018) and early-stage non-small cell lung cancer (Corredor et al., 2019). Thus, a distinct immune response to tumors exists

between breast cancer subtypes, and spatial, quantitative and qualitative differences in type of immune infiltrates in the tumor microenvironment are prognostic of disease outcome.

#### **1.3.4 Oncogenic signaling pathways suppress immune response.**

Over the past decades, evidence that malignant progression of neoplastic cells not only relies on intrinsic signaling (loss of tumor suppressors and gain of oncogenes due to genetic aberrations) but also on extrinsic cellular players from the local microenvironment have extensively accumulated (Spranger and Gajewski, 2018). With the emergence of the concept that cancer is a wound that never heals (Dvorak, 1986), studies emerged in the 1990s demonstrating that tumors co-opt inflammation for survival (Cordon-Cardo and Prives, 1999; Coussens et al., 1999; Coussens et al., 2000; Hudson et al., 1999). Today, it is fully established that the tumor cell intrinsic mechanisms continuously shape the tumor immune landscape to favor cancer progression and therapeutic resistance (Wellenstein and de Visser, 2018). One of the first demonstrations of an oncogene directly impacting the immune landscape came in 2004 whereby the H-RasG12V oncogene was shown to induce *CXCL8* transcription in various cancer cell lines to promote macrophage infiltration and vascularization *in vivo* to favor tumor growth (Sparmann and Bar-Sagi, 2004). In 2006, BRAF<sup>V600E</sup>, a constitutively active form of the BRAF serine/threonine kinase that drives melanoma, was shown to promote IL-6, IL-10, and VEGF secretion in a STAT3 dependent manner (Sumimoto et al., 2006). This in turn could suppress LPS induced inflammation by dendritic cells. Numerous other studies directly linking (proto)oncogene signaling to inflammation have emerged afterward. Loss of Shc1 adaptor protein signaling downstream of ErbB2 and polyomavirus middle T antigen (MT) led to increased CTL infiltration and IFN $\gamma$  driven immune response during early stages of mammary tumorigenesis in mice (Ursini-Siegel et al., 2010). In human leukemia and lymphomas, Myc oncogene has been shown to bind the promoters and regulate transcription of CD47 and PD-L1, two proteins that suppress anti-tumor immunity (Casey et al., 2016). Crk, an adaptor protein largely known for being involved in cell adhesion and growth factor signaling, was demonstrated to promote immunosuppression in 4T1 murine model of breast cancer (Kumar et al., 2017). Deletion of Crk enhances anti-tumor

immune responses and secretion of cytokines favouring immune surveillance, leading to reduced tumor growth and metastasis. Loss of Crk also enhanced tumor clearance upon PD-1 checkpoint inhibition (Kumar et al., 2017). In melanoma, loss of PTEN (tumor suppressor that negatively regulates AKT/PI3K activity) leads to decreased TIL and reduced responsiveness to PD-1 checkpoint inhibition and increased immunosuppressive cytokines secretion (Peng et al., 2016).

In line with studies demonstrating how oncogenic signaling pathways potentiate immunosuppression, therapies targeting these pathways can elicit and/or depend on immune responses for their efficacy. In breast cancer patients, inhibition of cyclin-dependent kinases 4 and 6 (CDK4/6), which are fundamental drivers of cell cycle progression downstream of oncogenic signaling pathways, induces significant anti-tumor immune responses (Goel et al., 2017). This is in part due to increased expression of endogenous retroviral elements and intracellular levels of double stranded RNA (Goel et al., 2017). In squamous cell carcinoma, nuclear focal adhesion kinase (FAK) regulates transcription of CCL5 to promote T<sub>reg</sub> recruitment and exhaustion of CD8<sup>+</sup> T cells to promote tumor growth, and treatment with FAK inhibitors reactivates anti-tumor immune responses (Serrels et al., 2015). Taken together, these studies demonstrate the immunosuppressive role of oncogenic signaling pathways and how they can be effectively targeted.

Multiple RTK inhibitors have been shown to elicit anti-tumor immune responses in cancer. Sunitinib (targets VEGFR, PDGFR $\alpha$ , Ret and Kit; all recruit Shc1) has been shown to elicit CTL driven anti-tumor immune responses partially through suppression of the STAT3 signaling pathway in renal cell carcinoma (Xin et al., 2009). Lapatinib (dual ErbB1/2 inhibitor) treatment of an ErbB2 driven breast cancer mouse model (MMTV/Neu) increases IFN $\gamma$  driven anti-tumor adaptive immune responses in a STAT1 dependent manner (Hannesdottir et al., 2013). Ron-selective kinase inhibitor reduces lung metastases in a breast cancer in mouse model through promoting anti-tumor immune responses (Eyob et al., 2013). Epidermal growth factor receptor (EGFR) signalling in lung cancer activates the PD-1 immune checkpoint to promote immune evasion (Akabay et al., 2013). Inhibition of TAM tyrosine kinase receptors (Tyro3, Axl, Mer) expressed on NK cells leads to rejection of breast cancer metastasis in mouse models (Paolino et al., 2014).

Cabozantinib (targets RET and MET) has been shown to increase MHC class I (H-2Db) and Fas expression in colon cancer cell lines (Kwilas et al., 2014). Mutation or overexpression of EGFR, in NSCLC have been shown to promote immunosuppression, and its inhibition (e.g. gefitinib, erlotinib) restores MHC class I expression, reduces PD-L1 expression or upregulates expression of NKG2D ligands for NK cell tumor killing (Liang et al., 2018). One high-throughput immune oncology screen identified the EGFR inhibitor Erlotinib as a potent enhancer of antigen specific CTL tumor cell killing (Lizotte et al., 2018). They further showed that Erlotinib treatment synergizes with anti-PD-1 checkpoint inhibition to suppress colon cancer growth (Lizotte et al., 2018). Thus, these studies have provided bases for combining TK inhibitors with immune-based therapy for the treatment of cancer.

Effective monoclonal antibody based targeted therapies rely on an intact innate immune system. EGFR-neutralizing antibody combined with chemotherapy depends on immunogenic cell death (ICD) for clearance of colorectal cancers (Pozzi et al., 2016). Trastuzumab, a recombinant humanized monoclonal antibody directed against the human HER2 receptor tyrosine kinase, mediates tumor killing partially through inducing antibody-dependent cell-mediated cytotoxicity (ADCC) against HER2 overexpressing tumor cells. Accordingly, the therapeutic effect of trastuzumab is diminished in mice that lack NK cells or those that have macrophages disabled to bind the Fc region of trastuzumab (Muntasell et al., 2017). Similarly, NK cell-derived IFN $\gamma$  induced PD-L1 expression in tumors and enhanced cetuximab (EGFR inhibitor)-mediated ADCC (Concha-Benavente and Ferris, 2015).

### **1.3.5 Cancer immunotherapy**

Cancer immunotherapy aims to reactivate anti-tumor immune responses, turning cold tumors into hot tumors in order to eradicate cancer (Bonaventura et al., 2019). Important cancer immunotherapy modalities include: (1) checkpoint inhibitors, (2) engineered T cells, (3) cancer vaccines, among others (Riley et al., 2019). Checkpoint inhibitors such as Nivolumab (anti-PD-1 monoclonal antibody) prevent binding of PD-L1 on tumors to PD-1 on immune cells, which normally would lead to inactivation of the immune cells (Riley et al., 2019). Engineered T cells such as chimeric antigen receptor T

cells (CAR T cell) are generated by isolating and engineering the T cell collected from patients to express T cell receptors specific to tumor associated or specific antigens. Therapeutic cancer vaccines include: (1) dendritic cell (DC) vaccine where DC from patients are engineered to express tumor associated antigens to directly activate T cells, (2) nucleic acid based vaccines where DNA or mRNA are delivered to antigen presenting cells which can then induce antigen expression and presentation to T cells, (3) neoantigen vaccines where tumor specific antigens from somatic DNA mutations in cancer are identified and used to boost patients immune system, and (4) whole tumor lysate vaccines where tumor derived proteins are used to pulse and prime DC (Chiang et al., 2015; Riley et al., 2019).

### **1.3.6 Breast cancer immunotherapy: where are we?**

Recently, chemotherapies combined with antibody-drug conjugates (ADC) or immune checkpoint inhibitors aimed to reinstate immunosurveillance have been explored in advanced or poorly prognostic breast cancer (Makhoul et al., 2018). As of 2019 May, only one immunotherapy has been approved by the FDA for breast cancer using immunotherapy: atezolizumab (anti-PD-L1 monoclonal antibody) with protein-bound paclitaxel for locally advanced, non-removable TNBC or metastatic TNBC that are PD-L1 positive (IMpassion130 trial) (Schmid et al., 2018). Lessons learned from breast cancer clinical trials using various treatment modalities in combination with immunotherapy are (1) tumor mutational burden predicts prolonged survival associated with high (and not low) immune infiltration in breast cancer (Thomas et al., 2018), especially in TNBC and HER2+ subtypes (Makhoul et al., 2018), which is consistent with observations made in lung cancer and melanoma (Goodman et al., 2017), and (2) only a subset of patients, especially those expressing high tumor PD-L1, show benefit from immune checkpoint blockade therapy. Thus, clinical trials using checkpoint inhibitors in combination with chemotherapy or other agents are mostly being explored in TNBC tumors as this subtype displays the highest immunogenicity (PD-L1+ TIL, PD-L1+ tumor, mutation, neoantigen load, and MHC expression) (Makhoul et al., 2018). Efforts to take advantage of immunotherapy are ongoing in advanced HR+ cancers resistant to tamoxifen (NCT02779751). Recently, combining cell cycle inhibitors (CDK4/6) with endocrine

therapy (MONALEESA-7 trial) has shown great promise in this group of patients in need of options. It will be important to assess how the immune response impacts this treatment regiment given that CDK4/6 inhibitors have been shown to elicit anti-tumor immune responses (Goel et al., 2017).

However, key questions remain in the field of immunotherapy. First, what dictates immunotherapeutic responsiveness (e.g. composition and the landscape of immune cells in the tumor microenvironment, unique tumor specific signaling mechanisms) or lack thereof? Second, biomarkers to predict or to readout responsiveness are lacking. Third, resistance mechanisms conferred by tumor and surrounding stroma and host immune cells are less understood. Based on the molecular understanding of how tumor intrinsic signaling alters the immune response, rational combination of chemotherapy, targeted therapy, and cancer immunotherapy methods need to be explored.

### **1.3.7 Combination of kinase inhibitors and immunotherapy**

Kinase inhibitors inevitably lead to acquired resistance after long-term exposure due to functional redundancy of the tyrosine kinome (Ha et al., 2016). For example, while trastuzumab has become a standard treatment option for early and late stage HER2+ breast cancer, intrinsic and acquired trastuzumab resistance remains a challenge. Armed with the knowledge that oncogenic kinase signaling contribute to immunosuppression and its blockade induces anti-tumor immune responses, clinical trials that combine kinase inhibitors with immunotherapy to further boost the anti-tumor immune response are currently ongoing for various types of cancers including breast cancer (Makhoul et al., 2018), non-small cell lung cancer (Yang and Tam, 2018), and advanced renal cell carcinoma (Atkins and Tannir, 2018). Current clinical trials combining kinase inhibitors with checkpoint inhibitors in breast cancer include: (1) Pembrolizumab with trastuzumab emtansine (an ADC composed of HER2 targeting trastuzumab covalently linked to the cytotoxic agent DM1) in HER2+ metastatic breast cancer (NCT03032107). (2) pembrolizumab with BGB324 (Axl kinase inhibitor) in metastatic TNBC (NCT03184558), (3) pembrolizumab with JAK2 inhibitor in HR negative or TNBC (NCT03012230), (4) Pembrolizumab with Binimetinib (MEK inhibitor) in various breast cancer subtypes (NCT03106415), (5) pembrolizumab with Abemaciclib (CDK4/6 inhibitor) in HR+

metastatic breast cancer (NCT02779751). The efficacy of these treatments remains to be assessed. Previously, a single-arm, non-randomized feasibility study in HER2+ metastatic breast cancer patients (n=20) was done using a HER2+ whole-cell breast cancer vaccine and weekly trastuzumab. This showed a 6 month clinical benefit of 55%, which was supported by mouse model studies with control groups (Chen et al., 2014). While the results were encouraging, further studies with bigger cohorts and control arms are necessary to determine the true benefit of this treatment. In May 2019, a breakthrough randomized clinical trial in renal cell carcinoma (JAVELIN Renal 101) showed Avelumab (PD-L1 checkpoint inhibitor) in combination with axitinib (VEGFR1-3, c-kit, PDGFR tyrosine kinase inhibitor) resulted in a significant survival benefit compared to standard of care sunitinib (inhibitor of multiple RTKs including PDGFR and VEGFR), leading to the FDA approval of this regimen (Motzer et al., 2019). Thus, combination of kinase inhibitors and immunotherapy hold promise in cancer treatment, and it remains to be seen whether kinase inhibitors combined with immunotherapy will be effective in different subtypes of breast cancer. Where efficacy is seen, we must understand if a combination approach - over single-agent approach - is always preferred, and whether sequential use of the drugs is as effective.

#### 1.4 Receptor tyrosine kinases signaling

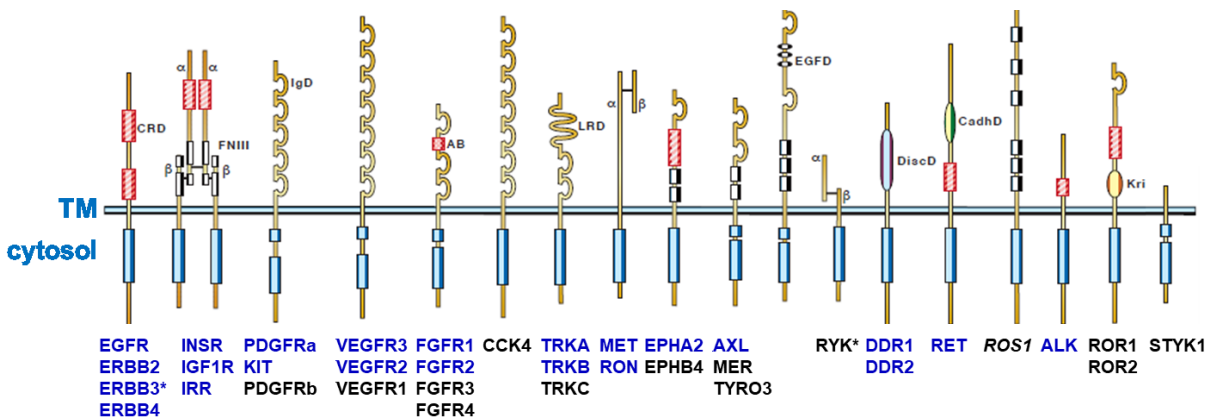


**Figure 5. Receptor tyrosine kinases (RTKs) involved in breast tumorigenesis.**

Some of the RTKs involved in breast tumorigenesis or listed and those that have been shown to directly engage Shc1 (PTB or SH2 domain) or indirectly in a signaling complex

(by affinity purification or immunoprecipitation) are highlighted in blue (further discussed in section 2.1.4)

Receptor tyrosine kinases (RTKs) are single-pass transmembrane proteins expressed on the surface of various cell types that regulate proliferation, differentiation, survival, metabolism, migration, and invasion (Lemmon and Schlessinger, 2010). There are 58 known RTKs that fall into 20 subfamilies (Lemmon and Schlessinger, 2010). In general, upon binding to their cognate ligands, RTKs undergo conformational changes, receptor dimerization and activation of their tyrosine kinase domains. These activated kinases then trans-phosphorylate key tyrosine residues in their cytoplasmic tails, leading to the recruitment of adaptor proteins (containing SH2 or PTB domains) that initiate downstream signaling pathways such as mitogen-activated protein kinase (MAPK) and phosphoinositide 3- kinase (PI3K)/AKT pathways (Butti et al., 2018). Overexpression or mutations in RTKs leading to their aberrant activation of such downstream pathways have been causally linked to cancers (Lemmon and Schlessinger, 2010). RTK families that are aberrantly activated in breast cancer include epidermal growth factor receptors (EGFR, ErbB2, ErbB3, ErbB4), vascular endothelial growth factor receptors (VEGFR1/2/3), platelet-derived growth factor receptors (PDGFR $\alpha/\beta$ ), insulin-like growth factor receptors (IGFRs), and fibroblast growth factor receptors (FGFRs), among others (Butti et al., 2018) (**Fig. 5**)

### **1.5 Shc1 adaptor protein**

Adaptor proteins serve as a critical integration point downstream of RTKs in the cytosol. While adaptor proteins lack enzymatic function, they contain two or more protein binding modules that link them with other protein binding partners to form signaling complexes in a spatially and temporally dynamic manner (Flynn, 2001). Their specificity in signaling is conferred by their domains containing motifs and their post-translational modifications (PTM). Most common types of PTM in mammalian cells are phosphorylation of serine (Ser/S), threonine (Thr/T) and tyrosine (Tyr/Y) residues (White and Wolf-Yadlin, 2016). While it is estimated that approximately 500 kinases and 180 phosphatases exist in the human genome to regulate phosphorylation (and similar number of orthologues in

mouse genome) (Milanesi et al., 2005), the number of adaptor proteins have not been estimated in the literature. Through phosphorylation, adaptor proteins can alter their conformation or have novel motifs that serve as binding sites for protein-protein interactions. The type of stimuli and concentration of the same stimuli can alter the duration (transient or prolonged) and the type of signaling complexes formed, leading to different biological responses (White and Wolf-Yadlin, 2016).

Shc1 (ShcA) is a ubiquitously expressed adaptor protein that serve as a downstream effector of numerous receptor and non-receptor tyrosine kinase signaling (Migliaccio et al., 1997). It is one of the first adaptor proteins identified (Pelicci et al., 1992) and has served as a prototypical model for studying adaptor protein signaling in biology (Wills and Jones, 2012). It is located on chromosome 1q21 in human and chromosome 3 in mouse. Other members of the *Shc* gene family are ShcB (Shc2/Sli), ShcC (Shc3/Rai) and ShcD (Shc4/RaLP) (Fagiani et al., 2007; Jones et al., 2007; Ravichandran, 2001; Wills and Jones, 2012). ShcB and ShcC are highly expressed in neuronal cells while ShcD is expressed in adult brain and skeletal muscles (Jones et al., 2007) (Liu et al., 2018).

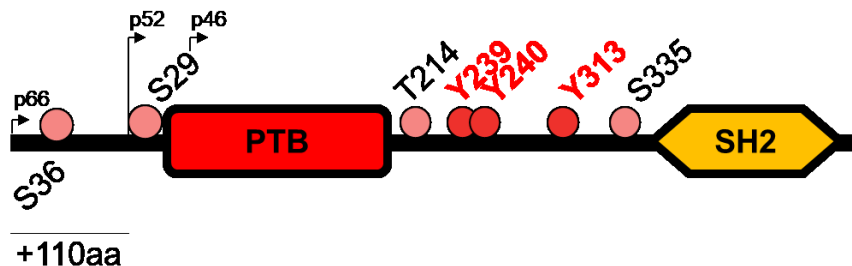


**Figure 6. Schematic of Shc1 adaptor protein.**

In mammals, the *Shc1* gene gives rise to three isoforms p46, p52 and p66, named based on their molecular weight in kDa (Wills and Jones, 2012) (**Fig. 6**). The isoforms p46 and p52 are encoded by the same transcript through an alternative use of two in-frame ATG sites (position 83 and 218) surrounded by consensus translation initiation sequences (Pelicci et al., 1992). Thus, isoform p52Shc1 is 45 amino acids longer than p46Shc1 in human. The two isoforms consist of a conserved PTB-CH1-SH2 domain structure, only distinguished by the length of their N-terminus. The p66 isoform is encoded

by a distinct promoter and an alternative spliced transcript resulting in an extra 110 amino acids at the N-terminus, giving p66 isoform a CH2-PTB-CH1-SH2 structure (Lotti et al., 1996; Pelicci et al., 1992). While selective deletion of the p66 isoform causes a 30% increased life-span in mice (Pelicci et al., 1992), concurrent deletion of the three isoforms cause embryonic lethality by day 11.5 (E11.5) due to cardiovascular defects, underscoring their importance in development (Lai and Pawson, 2000).

Shc1 engages numerous proteins in a temporally and spatially dynamic manner using its domains and motifs in various combinations. The PTB domain binds NPXY motifs while the SH2 domain binds YXXL/V/M motifs. This can occur through phosphotyrosine dependent and independent mechanisms (Pawson, 1997). Mouse Shc1 p52 can be phosphorylated at S29, T214, Y239, Y240, Y313 (Y317 in human) and S335 (S339 in human) (Zheng et al., 2013). Y239/240 were first identified by Gotoh *et al.* (Gotoh et al., 1997) after Y317 was identified (Salcini et al., 1994). In human, the p66 isoform is phosphorylated at S36, S139, Y340, Y350, Y427, S453. Upon ligand activation, receptor tyrosine kinases can be autophosphorylated at NXXY motifs to recruit Shc1 through its PTB2 domain. Shc1 also contains a lysine residue that has been shown to be N-acetylated. The structure of Shc1 has been studied in fragments by NMR.

### 1.5.1 Shc1 phospho-tyrosine signaling

Shc1 Y239/Y240 (pYYND) and Y313 (pYVNI) residues in the CH1 domain serve as substrates for many receptor tyrosine kinases and non-receptor tyrosine kinases (TKs). For instance, Src phosphorylates Y313 (Zheng et al., 2013). These motifs then serve as docking site for SH2 domain (Salcini et al., 1994) containing scaffold proteins such as Grb2 which, through its SH3 domain, can recruit SOS1 or GAB1 proteins (Nicholson et al., 2001) that initiate Ras-MAP kinase (MAPK) and phosphatidylinositol-3-OH kinase PI(3)K/AKT pathways (Liu et al., 2012a; Zheng et al., 2013). Upon EGF induction in Rat-2 cells, the p52 isoform is phosphorylated within 1-2 minute at all three tyrosines and dephosphorylated at baseline after 60 minutes while other phosphorylation sites at serine and threonine residues have various peaking time points, which coordinately reflect binding partners of Shc1 (Zheng et al., 2013). In this context, a significant portion of phospho-Y239/240/313 mediated signaling have been shown to be through Grb2, since

when Grb2 is conditionally knocked out, aside from upstream receptor tyrosine kinases, a majority of binders are lost from Shc1 (Zheng et al., 2013). It is unclear whether there are specific interactors lost or gained with debilitated phospho-Y239/240 or debilitated phospho-Y313 in this context, as all three tyrosines were mutated to phenylalanine.

In transgenic mice, homozygous expression of knock-in Shc1 alleles harbouring tyrosine to phenylalanine mutation at residues Y239/Y240 (Shc1<sup>2F/2F</sup>) or Y313 (Shc1<sup>313F/313F</sup>) appear normal postnatally, while mice harbouring homozygous tyrosine to phenylalanine mutation at all three residues (Shc1<sup>3F/3F</sup>) exhibit severely defective postnatal limb coordination (Hardy et al., 2007), possibly suggesting a level of functional redundancy or complementation between the Y239/Y240 and Y313 residues in motor function development. Interestingly Shc1<sup>313F/313F</sup> and Shc1<sup>3F/3F</sup> mice are born at a reduced Mendelian frequency while Shc1<sup>2F/2F</sup> mice do not, suggesting the existence of a distinct function of Y239/240 signaling from Y313 signaling (Hardy et al., 2007).

Numerous studies have further indicated that Y239/Y240 and Y313 play distinct roles, potentially depending on different downstream effectors recruited to phospho-Y239/240-Shc1 and phospho-Y313-Shc1 (**Table 2**). In Middle T oncoprotein (MT) expressing NIH3T3 fibroblasts, while both Y313 and Y239/240-Shc1 can engage Grb2-SH2, the latter is the predominant interactor linked to its transformation and colony forming ability (Blaikie et al., 1997). EGF induced c-Myc activation was significantly reduced in NIH3T3 cells expressing Y239/240F mutants, but not in those expressing Y317F mutants (Gotoh et al., 1997). This was also accompanied by a differential MAPK activating capacity between the two mutants (Gotoh et al., 1997). Induction of EGFR with EGF in Rat2 fibroblasts in the absence of Grb2 leads to a significantly elevated phosphorylation of Y239/240 over Y313, suggesting compensation or feedback mechanisms for the loss of Grb2 exists through Y239/240 (Zheng et al., 2013). In murine T-cell hybridomas, phospho-Y239/240-Shc1 signaling, and not phospho-Y313-Shc1 signaling is important for ERK activation. Phosphorylation of Y317 (Y313 in mouse) has been shown to cause structural rigidity in Shc1, suggesting that modulation of this site can cause changes in potential interactors (Suenaga et al., 2004). Adding to this complexity, studies have shown differential binding of downstream interactors to Y239F/Y240 and Y239/Y240F, suggesting singly phosphorylated Y239/240 motif may be

biologically relevant. The presence of an intact Y239 phosphorylation site lead to increased Gad adaptor Shc1 binding in 293T cells and this effect is Y240 independent (Liu and McGlade, 1998).

**Table 2. Pathways and/or molecular interactors of Shc1 (p52/p46 isoforms) and their known roles in tyrosine phosphorylation.**

<b>Context</b>	<b>Y239 /240</b>	<b>Y313</b>	<b>Details</b>
<b>Insulin receptor</b>	+	+++	Mitogenesis in Rat1 fibroblasts expressing insulin receptors. Associated with preferential Grb2 binding (Ishihara et al., 1998)
<b>Cell cycle progression</b>	?	+++	Ras-dependent cell cycle progression in ErbB2 overexpressing human breast cancer cell lines (e.g. SKBR3), but not in non-transformed mammary epithelial cells (Stevenson, 1999 #253). Arrests in G2-M checkpoint.
<b>Androgen induced ErbB2 signaling</b>	-	+++	Prostate cancer cells. Androgen stimulated ErbB2 driven proliferation, but not EGF induced proliferation. (Lee et al., 2004).
<b>IL3Rb</b>	+	+++	Ras pathway activation in mast cells (Velazquez et al., 2000) PTB, not SH2, domain dependent.
<b>IL3</b>	+	+++	c-Myc transcription for survival in Ba/F3 cells (Gotoh et al., 1996)
<b>Socs5</b>	-	+++	Interacts with Shc1 when overexpressed and pulled down. (Linossi et al., 2013)
<b><math>\beta</math>1/<math>\alpha</math>v integrins</b>	-	+++	Fibronectin induced Grb2 recruitment and ERK activation (Wary et al., 1998)
<b>Survival signaling</b>	-	+++	Breast tumor growth <i>in vivo</i> . Partially due to stroma phospho-Y313 missing (Ursini-Siegel et al., 2008)

<b>v-Src</b>	+++	+++	Phosphorylates p46-Shc1 (Sato et al., 1997a)
	+++	+	Phosphorylates Shc1 in COS cells. (van der Geer et al., 1996)
<b>c-Src</b>	+++	-	Phosphorylates p46-Shc1 (Sato et al., 1997a; Sato et al., 1998)
<b>CNTF</b>	?	?	Phosphorylates p52/46-Shc1 in EW-1 ewing sarcoma cells (Boulton et al., 1994)
<b>JAK3</b>	?	?	Shc1 directly phosphorylated on one tyrosine residue each in CH1 domain (Mishra and Kumar, 2014)
<b>EGFR</b>	+++	-	TC45 inhibited the EGF-induced association of p52Shc with Grb2, which was attributed to the ability of the TC45 to recognize specifically p52Shc phospho-Y239, but not phospho-Y317 (Tiganis et al., 1998)
	?	+++	Y317 and p705-STAT3 are constitutively phosphorylated in L858R-EGFR overexpressing NIH-3T3 fibroblasts (Greulich et al., 2005)
	?	+++	Blocking internal domain of EGFR during EGF-induced activation leads to reduced phosphorylation of Y317-p46 and STAT3 (Buerger et al., 2003)
	+++	+	Used for Grb2 interaction in COS1 cells. (van der Geer et al., 1996)
	+++	+	Grb2 knocked-out MEFs induced with EGF show enhanced feedback phosphorylation of Y239/240 than of Y313 (Zheng et al., 2013)
<b>ERK</b>	+++	-	Murine T-cell hybridoma (Pratt et al., 1999) Y239/240 is more critical for MAPK activation than Y317

<b>TGFβ/Crk</b>	+++	-	Endothelial cell recruitment in ErbB2 expressing breast cancer (Northey et al., 2012)
<b>TGFβ/Grb2</b>	-	+++	Promotes survival in ErbB2 expressing breast cancer cells (Northey et al., 2012)
<b>Angiogenesis</b>	+++	-	In breast cancer. (Ursini-Siegel et al., 2008)
<b>Lower organism</b>	+++	x	Nematodes e.g. <i>c. elegans</i>
<b>Higher organism</b>	+++	+++	Mammals
<b>TCR/CD3 cross-linking</b>	+++	+	P38MAPK and JNK. Myc transcription. Activation-induced cell death of Jurkat T cells (Patrussi et al., 2005)
<b>Metastasis</b>	+++	+++	Breast cancer lung metastasis. All three tyrosines necessary (Northey et al., 2012)
<b>Thrombin</b>	+++	+++	Src dependent phosphorylation. All three isoforms. Induce NFκB activation and IL8 release in human lung EC (A549 cells) (Lin et al., 2013)

? = not tested or shown; x = proven to not exist; +++ strongly phosphorylated/required. + weakly phosphorylated/less or independent

### 1.5.2 Shc1-p66 isoform

The p66-Shc1 (p66) isoform has been generally accepted to negatively regulate p52/p46 Shc1 function. Multiple studies have suggested this. In lymphocytes, EGFR activation lead to recruitment of p66/Grb2 complex but unlike p52/p46-Shc1, it does not lead to activation of the MAPK pathway; instead, it inhibits *Fos* promoter activation via its CH2 domain (Migliaccio et al., 1997). Other receptor tyrosine kinases such as INSR and PDGFR also recruit p66-Shc1/Grb2/SOS complex, leading to downregulation of Ras/MAPK/Fos pathway (Migliaccio et al., 2006). While high levels of ErbB2 and phospho-ErbB2 positively correlate with phospho-Y313-p52/46 isoforms, it negatively correlates with the level of p66 isoform expression (Stevenson and Frackelton, 1998). Consistently, high levels of phospho-Y313-p52/46 phosphorylation and low expression of p66 have been shown to correlate with increased risk of relapse in ER+ breast cancer (Frackelton et al., 2006). Under severe oxidative stress, p66 isoform can bind EGFR

through Grb2 and suppress p52/p46-Shc1/EGFR driven activation of the Ras/SOS/MAPK pathway (Arany et al., 2008). This suggests that p66 can act as a negative regulator of growth promoting pathways of the other two isoforms under stress. Furthermore, p66 can also be recruited to EGFR through Grb2 to either hinder Grb2/ARF1 GTPase activation or promote Grb2/ARF6 GTPase activation, ultimately regulating migration and invasion in breast cancer models (Haines et al., 2014). IL-6 stimulation and phosphorylation of gp130 causes p66 and Grb2 to directly interact, linking IL-6 signaling with Ras pathway (Giordano et al., 1997). Using HEK293T cells with exogenous expression of the p66 isoform and MET receptor, a p66/Grb2/Gab1 complex has been shown to interact with MET receptor constitutively, independently of MET kinase activity (Landry et al., 2016). Activation of MET receptor in this context leads to phosphorylation (unidentified whether Y239/240 or Y313) of p66 leading to reduced binding of Grb2/Gab1 to MET receptor itself. This demonstrates another negative regulatory role of p66 in RTK signaling.

### 1.5.3 Shc1 in cancer

Since Shc1 was first demonstrated to be able to transform NIH fibroblasts that formed tumors in nude mice (Pelicci et al., 1992), Shc1 has been demonstrated to play critical roles during breast tumorigenesis (Ursini-Siegel and Muller, 2008). This is through its ability to directly or indirectly engage numerous pro-tumorigenic tyrosine kinases (TKs) in a signaling complex (**Fig. 4**). The Shc1-PTB domain engages EGFR, ERBB2, ERBB3, ERBB4, INSR, IGF1R, VEGFR3, TrkA, and RET (Galvagni et al., 2010; Ishihara et al., 1997; Sasaoka and Kobayashi, 2000; Smith et al., 2006). The Shc1-SH2 domain engages MET, VEGFR2, c-kit (Foster et al., 2018) and Src (Ha et al., 2016). Shc1 requires an intact PTB domain to form a signaling complex with FGFR2, but this is indirectly mediated through Src binding to the SH2 of Shc1 (Schuller et al., 2008). Some TKs have been found in complex with Shc1: JAK3, EphA2, Alk, PDGFRa, Ron, TrkB, Axl, FGFR1 (Foster et al., 2018; Klint et al., 1995; Mishra and Kumar, 2014; Smith et al., 2006). Of the 22 TKs engaged by Shc1, small molecule inhibitors or monoclonal antibody based drugs approved by the FDA exist against 10 of them (ALK, MET, EGFR, ERBB2, JAK3, PDGFRa, RET, Src, VEGFR) as of 2018 (total of 39 tyrosine kinase inhibitors have been approved thus far, being the second most targeted group of proteins after G-protein

coupled receptors) (Bhullar et al., 2018). Furthermore, Raf and Mek1/2 which are kinases activated downstream of Shc1 are also targeted by various FDA approved drugs (Bhullar et al., 2018). Thus, as an integrator of various oncogenic signaling, breast tumor intrinsic Shc1 signaling has been shown to regulate tumor angiogenesis (Im et al., 2014; Ursini-Siegel et al., 2008), survival (Ursini-Siegel et al., 2012; Ursini-Siegel et al., 2008), metabolism (Im et al., 2018), tyrosine kinase inhibitor resistance (Ha et al., 2018a), initiation (Wright et al., 2019), Neu (ErbB2) driven epithelium transformation (Dankort et al., 2001; Ursini-Siegel et al., 2008), proliferation (Ahn et al., 2013), invasion and metastasis (Hudson et al., 2014; Northey et al., 2012), and motility (Northey et al., 2008).

In various cancer cell lines derived from stomach carcinoma, lung carcinoma, leukemia, thyroid carcinoma, melanoma, glioblastoma, pancreatic carcinoma, bladder carcinoma, hepatocellular carcinoma, as well as in small cohort of human breast tumor tissues compared to normal tissues, high levels of Shc1 phosphorylation are seen (Finlayson et al., 2003; Pelicci et al., 1995). In addition, ErbB2 activation in breast cancer positively correlates with Shc1 tyrosine phosphorylation (Stevenson and Frackelton, 1998). Further studies of breast tumor tissues revealed that high phospho-Y317-Shc1 status in primary breast tumors alone is associated with a higher incidence of relapse in breast cancer (Davol et al., 2003). Moreover, an increased ratio of phospho-Y317-Shc1 to p66-Shc1 expression levels positively correlates with nodal status, tumor stage, disease stage, and is two fold higher in breast cancer patients who relapse (Davol et al., 2003). Together, these data highlight the importance of Shc1 phosphotyrosine signaling in the context of breast cancer and possibly other types of cancers.

#### **1.5.3.1 Shc1 in anti-tumor immunity**

While Shc1 has become well-established to facilitate cancer progression through promoting the aforementioned pro-tumourigenic pathways (**Section 1.5.3**), its ability to also suppress anti-tumor immunity was only recently demonstrated. It was shown that the loss of Shc1 signaling downstream of the polyoma virus middle T (MT) oncogene in breast cancer mouse model leads to significant delays in tumor onset, which is accompanied by increased CD8<sup>+</sup> T cell infiltration, increased granzyme B positive cell presence, and

increased IFN $\gamma$  levels during the early stages of tumorigenesis (Ursini-Siegel et al., 2010). Importantly, mammary tumor progression of Shc1 deficient hyperplasias is significantly accelerated in athymic mice compared to that in immunocompetent mice, suggesting that Shc1 signaling suppresses T cell immune response to facilitate tumor progression (Ursini-Siegel et al., 2010). Additionally, in an ErbB2 driven breast cancer mouse model, loss of Shc1 in the mammary epithelium results in significantly reduced tumor incidence, accompanied by increased presence of proliferating CD4 $^{+}$  T cells, increased level of CXCL9 (chemoattractant for memory T cells and NK cells), and increased expression of inflammatory pathway genes *in vivo* (Ursini-Siegel et al., 2010). Thus, two transgenic mouse models of breast cancer have highlighted the role of Shc1 in regulating the tumor immunity. Supporting the clinical relevance of investigating how Shc1 regulates tumor immune responses, tissue microarray analysis (TMA) of 144 human breast tumor tissues revealed that high Shc1 expression is associated with decreased CD8 $^{+}$  T cell infiltration, (Ursini-Siegel et al., 2010). Furthermore, as highlighted in **Section 1.3.4**, targeting pathways closely upstream or downstream of Shc1 (e.g. ErbB2, EGFR, MEK, ERK, PTEN, PI3K, Crk) by drugs or molecular manipulation have been shown to enhance anti-tumor immune responses in various studies. Taken together, these data suggest Shc1 suppresses anti-tumor immunity to promote tumor progression through yet to be defined molecular mechanisms.

## **1.6 STAT1 and STAT3 transcription factors**

### **1.6.1 STAT3**

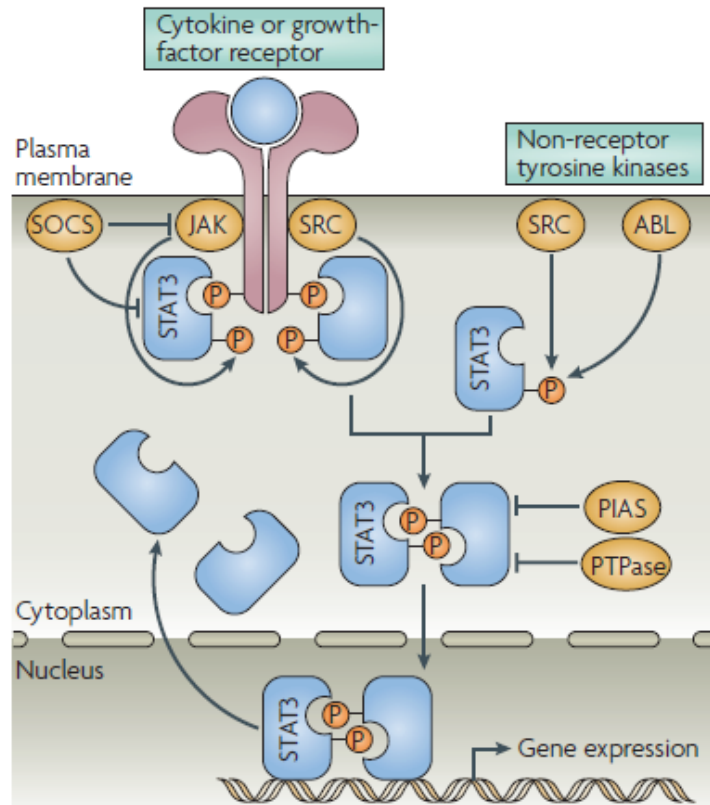


**Figure 7. STAT3 signaling.**

STAT3 signaling downstream of cytokine receptors, receptor tyrosine kinases and non-receptor tyrosine kinases. Figure extracted from (Yu et al., 2007).

STAT3 was first identified as an IL-6 family cytokine responsive member of the STAT transcription factor family (Akira et al., 1994). Germline STAT3 deletion leads to embryonic lethality and conditional deletion of various cell types has demonstrated extremely diverse functions for STAT3 (Maritano et al., 2004). STAT3 is activated downstream of cytokine receptors and RTKs, toll-like receptors (TLRs), microRNAs (miRNAs), and G-protein-coupled receptors (GPCR) (Yu et al., 2014). Various ligands (e.g. IL-6 family cytokines, IL-10 family cytokines, PDGF, EGF, IFNs) trigger STAT3 activation by phosphorylation (Schindler et al., 2007) (**Fig. 7, Table 3**). For example, IL-6 binding to IL6Ra forms a gp130/IL-6/IL6Ra complex, which activates JAK to phosphorylate gp130, recruiting cytoplasmic STAT3 to the complex (Yu et al., 2014). Once recruited, STAT3 is phosphorylated at tyrosine 705 (phospho-Y705) by JAK. This allows a STAT3 monomer to bind R603 residue within the SH2 domain of another STAT3

monomer, resulting in STAT3 dimerization (Bromberg et al.). This dimer can enter the nucleus to bind DNA and activate transcription of STAT3 targets (Domoszlai et al., 2014). Two isoforms STAT3 $\alpha$  and STAT3 $\beta$  are generated by alternative splicing of exon 23. STAT3 $\beta$  is truncated its c-terminus and lacks the S727 phosphorylation site.

**Table 3. List of phospho-Y705 or phospho-S727 regulators.**

Site	PO <sub>3</sub> <sup>-</sup>	Stimuli	Regulating kinase
<b>Y705</b>	+	IL-6	JAK (Yang et al., 2005; Yu et al., 2014)
	+	Growth factors	Src family kinases (Buchert et al., 2016; Laird et al., 2003), Abl (Buchert et al., 2016)
	+	IFN $\alpha$	(Huynh et al., 2016; Wen et al., 1995)
	+	IFN $\gamma$	(Beurel and Jope, 2008), Src (Qing and Stark, 2004)
	+	LIF	(Song et al., 2009)
	+	IL-10	(Cheng et al., 2014)
	-	UVB	SHP1, SHP2 (Kim et al., 2010)
	-	IL-6	PTPRT(Zhang et al., 2007)
	-		PTPRD (Peyser et al., 2015)
	-	GCSF, IL-6	TC45 (ten Hoeve et al., 2002; Yamamoto et al., 2002)
	-		DUSP2(Lu et al., 2015).
	-	IL-6, OM, CNTF	PIAS3 (Chung et al., 1997a)
	<b>S727</b>	+	Growth factors; PDGF, FGF, EGF
+		IFN $\gamma$	(Wen et al., 1995), PI3K (Ma et al., 2017; Nguyen et al., 2001)
+		DNA damage	CDK5 (Courapied et al., 2010)
+		UV	MSK1 (Roux and Blenis, 2004; Zhang et al., 2001), RSK2 (Zhang et al., 2003b),

		JNK1* (Lim and Cao, 1999b; Zhang et al., 2001)
+	Arsenic	*JNK (Liu et al., 2012b)
+	anisomycin	*JNK (Lim and Cao, 1999a)
	TNF $\alpha$	*(Lim and Cao, 1999a)
+	TGF $\beta$	TAK1 (Doerks et al., 2002), JAK1 (Tang et al., 2017)
+	IL-6	TAK1 (Kojima et al., 2005)
+	LPS	IRAK1(Huang et al., 2004), ERK, p70S6k (Park et al., 2008)
+	insulin	(Ceresa and Pessin, 1996) PKC $\delta$ (Dhar et al., 2013; Gartsbein et al., 2006)
+	IL32	PKC $\epsilon$ (Kang et al., 2012)
+	hypoxia	mTORC1(Dodd et al., 2015)
-	EGFR	Socs5(Kario et al., 2005)
-	others	PP2A(Liu et al., 2016; Togi et al., 2009; Woetmann et al., 1999), PP1(Zgheib et al., 2012), DUSP2(Lu et al., 2015).

PO<sub>3</sub><sup>-</sup> = phosphoryl group added (+) or removed (-). \* = independently of phospho-Y705

Numerous positive and negative regulators of STAT3 phosphorylation have been reported in various cell types in response to diverse stimuli (**Table 3**). S727 is located within a PMSF motif, which resembles the PXS/TP motif, a MAPK target (Decker and Kovarik, 2000). Numerous studies have defined the molecular function of S727-STAT3. It has been reported that S727 phosphorylation enhances the efficiency but not the STAT3-DNA binding activity (O'Rourke and Shepherd, 2002; Wen and Darnell, 1997; Wen et al., 1995). S727 also regulates the duration of STAT3 driven transcription (Wagner et al., 1990; Wakahara et al., 2012), as S727 is necessary for K140 methylation of the DNA bound STAT3 that leads to downregulation of STAT3 driven transcription (Yang et al., 2010). Interestingly, phosphorylation of Y705 is negatively regulated by S727 (Wakahara et al., 2012; Yang et al., 2010). Recruitment of STAT3 and its transcription partners to promoters depend on the type of stimulus. For example, SOCS3, a well-

studied STAT3 target gene, has both STAT3 and AP1 responsive element at its promoter (Wiejak et al., 2012). Upon EGF treatment, STAT3 and AP1 are both needed for SOCS3 transcriptional activity whereas upon IFN $\gamma$  treatment, STAT3 is sufficient (Breit et al., 2015).

#### **1.6.1.1 STAT3 in cancer**

STAT3 is constitutively activated, as marked by phosphorylation of Y705, in various cancers including breast cancer (Yu et al., 2014; Yue and Turkson, 2009). STAT3 promotes tumor progression through transcription of genes involved in tumor survival (Bcl-xL, Bcl-2, Fas), proliferation (cyclin D1, c-Myc, SERPIN family proteins), invasion (SERPINE2), metabolism (HIF1a), angiogenesis (VEGF), and immunosuppression (PD-L1) (Beigel et al., 2014; Demaria et al., 2010; Niu et al., 2008; Real et al., 2002; Yu et al., 2014). All these processes implicated phosphorylation of Y705-STAT3.

Multiple studies have identified a pro-tumorigenic role of S727 independently of Y705 in various cancers. In melanocytes, STAT3 is phosphorylated on S727 in the absence of Y705 phosphorylation, and in primary lesions of acral lentiginous melanoma, phosphorylation of S727 precedes phosphorylation of Y705 in the early stages of melanoma progression (Sakaguchi et al., 2012). Selective upregulation of phospho-S727 was also seen in tumor initiating cells to enable their survival in suspension (Liu et al., 2016). In chronic lymphocytic leukemia, constitutively high phospho-S727 has been observed in the absence of phospho-Y705 (although inducible) and the latter does not impact the DNA binding and transcriptional activity of phospho-S727-STAT3 (Hazan-Halevy et al., 2010). In prostate cancer, constitutive activation of S727 in the absence of phospho-Y705 leads to increased invasiveness, growth advantage following starvation, and nuclear localization at steady state compared to unphosphorylated STAT3 (Qin et al., 2008). In colorectal cancer cells, topoisomerase I inhibition leads to phosphorylation of S727 in the absence of Y705, and phospho-S727-STAT3 selectively associates with the promoter of *Eme1* (endonuclease involved in DNA repair) to reduce DNA damage (Courapied et al., 2010). In glioblastoma, phospho-S727-STAT3 positivity is an independent unfavorable prognostic factor in patients (Lin et al., 2014) and phosphorylation of S727 was associated with radiosensitivity independently of phospho-

Y705-STAT3 (Ouedraogo et al., 2016). In human breast cancer, level of phospho-S727 positively correlates with tumor stage and size (Yeh et al., 2006), and its nuclear localization positively correlates with PR expression (n=39) (Tkach et al., 2013). Consistent with this, progestin has been shown to induce S727 phosphorylation through ERK to promote cyclin D1 gene transcription (Tkach et al., 2013). Taken together, phospho-S727-STAT3 signaling has been suggested to be a non-canonical STAT3 signal (i.e. independent of Y705) important in regulating various aspects of cancer, meriting better understanding (Dimri et al., 2017).

While most studies have shown STAT3 to exert its function in the nucleus or cytoplasm, some studies have shown that STAT3 functions in the mitochondria. In liver and heart, STAT3 functions as a transcription factor within the mitochondria to regulate the electron transport chain (Wegrzyn et al., 2009). In mouse embryonic stem cells, LIF-activated STAT3 localizes to the mitochondria, transcribes mitochondrial genes (Nd1, Nd4), and enhances oxidative metabolism (Carbognin et al., 2016). In cancer, STAT3 has been shown to facilitate Ras driven malignant transformation in part through regulating metabolic function in the mitochondria (Gough et al., 2009). Interestingly, this was independent of phospho-Y705 (Gough et al., 2009).

#### **1.6.1.2 Tumor intrinsic STAT3-mediated immunosuppression**

Tumor intrinsic STAT3 signaling have several ways of promoting tumor immunosuppression. First, STAT3 can increase transcription of immune checkpoint ligands, PD-L1 (Marzec et al., 2008; Song et al., 2018) and PD-L2 (Garcia-Diaz et al., 2017), in malignant cells to promote effector T cell exhaustion. Second, tumor intrinsic STAT3 can directly promote transcription of immunosuppressive cytokines such as VEGF (Loeffler et al., 2005; Niu et al., 2002), IL-6 (Chang et al., 2013; Yoon et al., 2010), TGF $\beta$  (Rojas et al., 2016) and IL-10 (Herbeuval et al., 2004) to impede effector functions of T cells (Kim et al., 1995) and maturation of DCs for proper antigen presentation (Cheng et al., 2003; Haura et al., 2005; Johnson et al., 2018; Lee et al., 2011). Third, tumor intrinsic STAT3 can suppress anti-tumourigenic inflammatory signaling pathways initiated by interferons (Ito et al., 2007; Lu et al., 2018). Consistent with these molecular mechanisms, inducible loss of STAT3 in a breast cancer mice model leads to increased anti-

tumorigenic inflammation during early stages of tumor progression (Jones et al., 2015). Thus, STAT3 serves as an important regulator of immunosuppression exerted by malignant cells.

### **1.6.1.3 Unphosphorylated STAT3**

Studies have established that canonical STAT3 signaling and transcription requires Y705 phosphorylation. However, numerous groups have also shown the role of unphosphorylated STAT3 (U-STAT3) in regulating transcription in the absence of phospho-Y705 (Braunstein et al., 2003; Meyer et al., 2002; Yang et al., 2005; Yang et al., 2010).

Unphosphorylated STAT3 can dimerize. Using BRET and FRET, unphosphorylated STAT3 has been shown to dimerize in an SH2 domain dependent manner in the absence of stimuli (Domoszlai et al., 2014; Kretzschmar et al., 2004; Schroder et al., 2004b). Other studies also showed STAT3 can form dimers without being phosphorylated (Mukhopadhyay et al., 2008; Schroder et al., 2004b; Vinkemeier, 2004).

Nuclear accumulation, DNA binding, and/or transcription by unphosphorylated STAT3 has also been observed. Angiotensin II/All Type 1 Receptor (AT1R) signaling stimulates nuclear accumulation of U-STAT3 in myocytes and fibroblasts, where Y705F-STAT3 binds the OSN promoter (Yue et al., 2010). Constitutive nuclear presence of STAT3 is seen in various human and monkey cell lines, independently of phospho-Y705-STAT3 (Liu et al., 2005). This was shown to depend only on amino acid residues 150-162 (coiled-coil region) of STAT3 and importin- $\alpha$ 3 to be imported to the nucleus (Liu et al., 2005). In prostate and breast cancer cells, U-STAT3 binds regulatory regions of pro-apoptotic genes and negatively regulates their expression (Timofeeva et al., 2013). In untransformed, unstimulated human mammary epithelial hTERT-HME1 cells, Y705F-STAT3 has been shown to form a complex with unphosphorylated NF $\kappa$ B, bind NF $\kappa$ B elements of gene promoters (e.g. CCL5) and induce their transcription (Yang et al., 2007). Understanding the role of unphosphorylated STAT3 has important implications as (1) cancers often overexpress STAT3 and presumably not all STAT3 may be phosphorylated and (2) therapeutic targeting of kinases that induce STAT3 phosphorylation would lead to increased expression of unphosphorylated STAT3.

## 1.6.2 STAT1

### 1.6.2.1 STAT1 signaling

STAT1 is a transcription factor belonging to the same STAT family of transcription factors as STAT3. It is activated downstream of cytokines (e.g. IFN $\alpha$ , IFN $\beta$ , IFN $\gamma$ ) (Dunn et al., 2006) and growth factors (e.g. EGF, PDGF, CSF1; not FGF) (Fu and Zhang, 1993; Koromilas and Sexl, 2013; Meraz et al., 1996; Schindler and Darnell, 1995; Silvennoinen et al., 1993) to act as a transcription factor during cell growth regulation, antiviral and immune defense (**Fig. 8**).

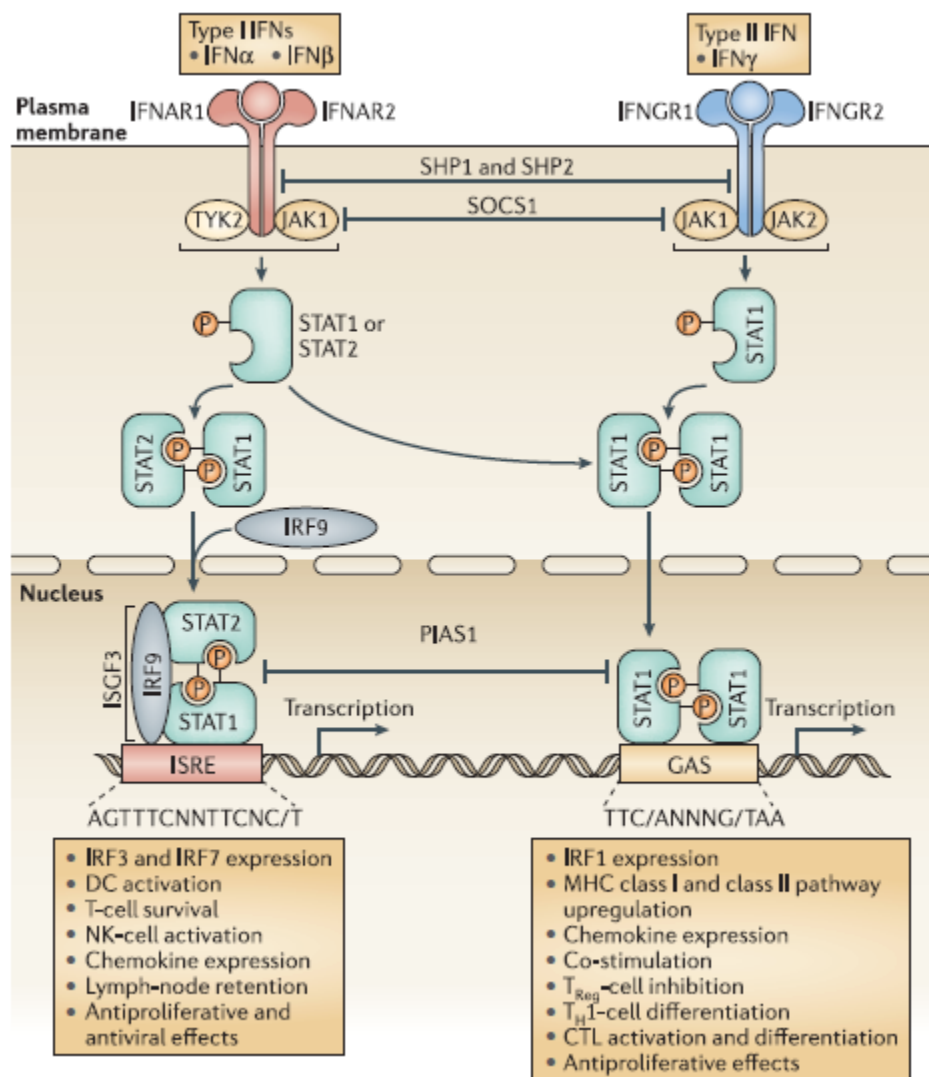


**Figure 8. Interferon induced STAT1 activation**

Interferon type I and type II activates STAT1 to regulate cell proliferation and immune response (Figure extracted from (Dunn et al., 2006)). STAT1 function depends on the type of cell (e.g. tumor or immune cell) being stimulated. GAS, gamma activated sequence; ISRE, Interferon-sensitive response element.

In resting cells, STAT1 largely remains in the cytoplasm as inactive homodimers (parallel form) (Braunstein et al., 2003; HAAN et al., 2000; Mertens et al., 2006; Schindler et al., 2007). Upon ligand binding to cytokine or certain growth factor receptors, receptor associated JAKs become activated, leading to phosphorylation of the receptor tyrosine residues. These residues serve as docking sites for SH2 domain of STAT1, which then becomes JAK substrates. Activated STAT1 is released from the receptor, reorients into the anti-parallel dimer where phospho-Y701-STAT1 binds SH2 domain of another phospho-Y701-STAT1, and translocate to the nucleus. STAT1 homodimers recognize GAS family of enhancers while type I interferon promote formation of STAT1/STAT2 (another STAT family member) heterodimers, which associates with IRF9, forming a ISGF3 complex that recognizes ISRE enhancers (Schindler et al., 2007) (**Fig. 8**).

Unphosphorylated STAT1 (U-STAT1) can migrate to the nucleus as shown by nuclear fractionation and immunofluorescence staining of cells (Shuai et al., 1992). Additionally, in normal human fibroblasts or mammary epithelial cells, U-STAT1 can localize to the nucleus under baseline conditions and induce various interferon responsive genes (IFI27, IFI44, OAS, BST2) long after IFN $\gamma$  stimulation is over (Cheon and Stark, 2009). In an adenovirus-infected fibrosarcoma cell setting, U-STAT1/IRF1 complex is required to activate the LMP2 promoter (Chatterjee-Kishore et al., 2000). This demonstrates the necessity to assess total as well as the phosphorylated level of STAT1.

In normal cells, the activation of STAT proteins is transient, ranging from between a few minutes to a few hours, due to negative feedback loops. However, numerous solid and non-solid tumors display constitutive activation of STAT1, STAT3 and STAT5 (Haura et al., 2005). Whether STAT1 plays a pro- or anti-tumorigenic role in cancer has been heavily studied over the years (Meissl et al., 2015).

### **1.6.2.2 STAT1 in anti-tumorigenic roles**

Multiple STAT1 target genes are anti-tumorigenic. First, STAT1 increases expression of antigen processing and presentation machinery (APP) genes (TAP1/2, B2M) and increases surface expression of MHC class I (Schroder et al., 2004a; Strehl et al., 2005; Zhou, 2009) on tumors for recognition by cytotoxic T cells. Second, it suppresses proliferation and promotes apoptosis through transcribing cell cycle inhibitors such as p27<sup>Kip1</sup> (Dimberg et al., 2003) and p21<sup>WAF1/CIP1</sup> (Burke et al., 1999). Third, it stabilizes the interaction of Rb with p16INK4a to promote senescence (Braumuller et al., 2013; Wang et al., 2014)). Fourth, it promotes apoptosis via regulating caspase 2, 3, and 7 (Sironi and Ouchi, 2004). In line with this, molecular players upstream of STAT1 such as interferon gamma receptor (IFN $\gamma$ R), JAK1 and JAK2 are mutated or lost in lung cancer cell lines (Haura et al., 2005).

Various studies established that STAT1 is a tumor suppressor. The MMTV/Neu/STAT1<sup>-/-</sup> model show slightly accelerated tumor onset (Hannedottir et al., 2013) and increased tumor burden (Klover et al., 2010). STAT1<sup>-/-</sup> mouse was used in a landmark paper to highlight a protective role for immune system during tumor formation (Shankaran et al., 2001). STAT1<sup>-/-</sup> mice display increased susceptibility to 3-methylcholanthrene induced tumor development, and RAG2<sup>-/-</sup>STAT1<sup>-/-</sup> mice show increased spontaneous neoplastic disease compared to RAG2<sup>-/-</sup> or wild-type mice (Haura et al., 2005; Shankaran et al., 2001). STAT1 deficient mice display defective NK cell activity and response to IFN $\gamma$  (Haura et al., 2005), and are more prone to tumor development than controls (Durbin et al., 1996; Yu and Jove, 2004). In ER $\alpha$  positive cancer, the absence of STAT1 (and therefore SOCS1 expression) allows for persistent JAK2/STAT3 and STAT5 pathway activation, leading to continued ER $\alpha$  disease progression (Chan et al., 2014).

### **1.6.2.3 STAT1 in pro-tumorigenic roles**

Due to the need to limit inflammation, IFN $\gamma$ /STAT1 pathway targets include immunosuppressive genes such as PD-L1 and IDO1, inadvertently contributing to cancer progression (Spranger et al., 2013). Constitutive upregulation of STAT1 in type II endometrial cancer promotes proliferation, survival and invasion through upregulation of ICAM1 and PD-L1 (Kharma et al., 2014). In breast cancer patients, tissue samples from

132 breast cancer patients showed that high *STAT1* mRNA level (but not phospho-Y701-STAT1) was associated with high enrichment of immunosuppressive T cells and tumor associated macrophages, and poor prognosis (Tymoszuk et al., 2014). Co-expression of *STAT1* and immunosuppressive *MUC1* was associated with decreased recurrence-free and overall survival (Khodarev et al., 2010).

Studies have linked tumor intrinsic *STAT1* to drug resistance in cancer. *STAT1* can mediate resistance to anti-tumor drugs via downregulating protein synthesis (through upregulation of 4EBP) and promoting cap-independent translation of Bcl-XL (anti-apoptotic) and *p27<sup>kip1</sup>* (suppressor of cell cycle) (Wang et al., 2015a). *STAT1* is also critical for docetaxel resistance in prostate cancer (independently of *STAT3* or phospho-*STAT3* expression) (Patterson et al., 2006). Resistance to Vorinostat (histone deacetylase inhibitor; HDACi) in cutaneous T-cell lymphoma is due to constant activation, accumulation of *STAT1* and high levels of phospho-*STAT3* in the nucleus (Fantin et al., 2008).

### 1.6.3 Interaction between *STAT1* and *STAT3*

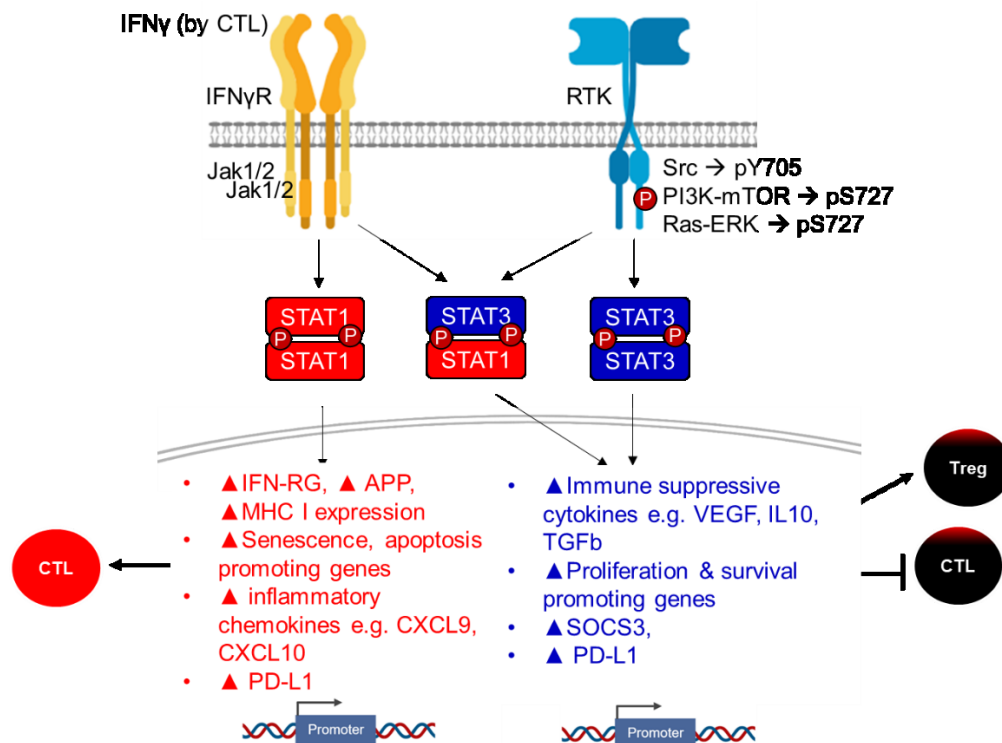


**Figure 9. Tumor intrinsic *STAT1* and *STAT3* signaling pathways in tumorigenesis.**

Under physiological conditions, STAT1 and STAT3 activation are tightly regulated to control proliferation, cell cycle, survival, angiogenesis, invasion and inflammation as discussed above, where they often play opposing functions, (Schindler et al., 2007; Yu et al., 2009) (**Fig. 9**). In numerous cancers including breast cancer, STAT1 and STAT3 are both persistently activated (Yu and Jove, 2004). Multiple ligands activate both STAT1 and STAT3: IFN $\alpha$ , IFN $\beta$ , IFN $\gamma$  (Ma et al., 2017; Plataniias, 2005; Sato et al., 1997b) and EGF, TGF $\beta$ , PDGF, CSF1, IL-6, IL-10, amphiregulin (Cao et al., 1996; Darnell et al., 1994; David et al., 1996; Grandis et al., 1998; Olayioye et al., 1999; Schindler and Darnell, 1995; Silvennoinen et al., 1993; Stark et al., 1998; Wen et al., 1995; Zhong et al., 1994). This may reflect their reciprocal modulatory roles (Schindler et al., 2007).

STAT1 and STAT3 have been shown to form heterodimers (how STAT3 was discovered) (Zhong et al., 1994) in a phospho-tyrosine dependent manner (Yang et al., 2010). The crystal structure of STAT1 and STAT3 are virtually superimposable (Bromberg et al.), and they share high sequence homology in their SH2 domains (Zhong et al., 1994).

Multiple studies have demonstrated that STAT3 and STAT1 negatively regulate each other. In MEFs, STAT3 deficiency leads to an enhanced STAT1, and ISG expression in response to IFN $\alpha/\beta$  (Wang et al., 2011), while STAT1 deficiency prolongs Y705-STAT3 phosphorylation (Qing and Stark, 2004). SOCS1, a STAT1 transcription target whose promoter is often methylated in gastric cancer, suppresses STAT3 activation (Souma et al., 2012). In multiple myeloma cells, IFN $\alpha$  induces STAT1/STAT3 dimer formation (Thyrell et al., 2007). Studies in immune cells have well established the reciprocal regulatory roles of STAT1 and STAT3. In myeloid cells, IFN $\alpha$ -activated STAT3 decreases STAT1 driven induction of inflammatory chemokines while promoting antiviral gene transcription, in part through sequestering STAT1 and preventing STAT1 homodimer formation and DNA binding (Ho and Ivashkiv, 2006). Macrophage specific deletion of STAT3 leads to significantly enhanced LPS induced inflammation leading to secretion of TNF $\alpha$ , IL-1, IFN $\gamma$  (Takeda et al., 1999). In CD4 $^+$  T cells, STAT1 suppresses IL-6/STAT3 pathway driven Th17 cell differentiation (Meyer Zu Horste et al., 2018).

Transcriptionally, STAT1 and STAT3 can compensate for each other under certain circumstances. The SOCS3 gene, which contains a GAS motif in its promoter, can be

transcribed by both STAT1 and STAT3 and STAT3 can compensate for the absence of STAT1 (Qing and Stark, 2004). Some negative regulators are shared. Nuclear tyrosine phosphatases, such as TC45 (a nuclear isoform of the T-cell PTP), dephosphorylate both STAT1 and STAT3 in the nucleus, but not STAT5 or STAT6, in HeLa cells (ten Hoeve et al., 2002). In tumors, both STAT1 (in response to IFN $\gamma$ ) and STAT3 (in response to growth factors) promote transcription of the PD-L1 checkpoint, ultimately promoting immunosuppression (Garcia-Diaz et al., 2017; Marzec et al., 2008; Song et al., 2018).

## **1.7 Mouse models used in this thesis**

Mice models provide critical insight into host-tumor interaction. Transcriptional profiles of human and mouse immune cell types demonstrated largely conserved global expression and underlying regulatory profiles of orthologous genes (Shay et al., 2013). Critically, mice models have been pivotal in furthering our understanding of immune and stromal compartment in cancer progression, as well as in metastasis, cancer initiation, invasion and angiogenesis (Walrath et al., 2010). Transcriptomic and signaling pathway analysis of oncogene driven breast cancer mouse models have shown significant molecular similarities with different subtypes of human breast cancers (Hollern and Andrechek, 2014). On the other hand, numerous differences in immune response mechanisms have also been well established (Mestas and Hughes, 2004). Altogether, combinatorial analysis of the observations made in mice models with that of human patient samples is necessary.

### **1.7.1 Middle T antigen driven mouse model of breast cancer**

Polyomavirus Middle T antigen (MT) is a protein normally encoded by murine polyomavirus that when expressed in fibroblasts (or in various tissues) can act as a potent oncogene through assembling and recruiting various host mitogenic signaling molecules, mimicking an activated form of receptor tyrosine kinases (Dilworth, 1995; Fluck and Schaffhausen, 2009). We employed the MMTV/MT mouse model of breast cancer where MT is expressed under mouse mammary tumor virus (MMTV) long terminal repeat (LTR) (Guy et al., 1992). MMTV LTR encodes transcriptional regulatory elements (termed

mammary gland enhancer region) that direct high and targeted expression of MT in both lactating and non-lactating mammary epithelial cells (Qin et al., 1999; Ross, 2008; Taneja et al., 2009) and at low levels in salivary gland and ovaries (Guy et al., 1992). MMTV, since it was discovered in the 1920's, has been extensively used as driver of transgene expression in the mammary epithelium (e.g. Neu/ERBB2, cyclin D1, Ras, Myc, c-Rel) for various mouse cancer models (Ross, 2008; Taneja et al., 2009). The hormone response element (located -202 and -59 upstream of LTR transcription start site) is regulated by glucocorticoids, progestins and androgens (Cato et al., 1987). The tumors significantly depend on c-Src for tumor formation, and on TGF $\beta$  for lung metastasis (Hollern and Andrechek, 2014). The molecular mechanism of MT-driven transformation is well characterized. Briefly, MT recruits A and C subunits of protein phosphatase 2A (PP2A) (Dilworth et al., 1994) as well as Src tyrosine kinase family (SFK) members such as c-Src, c-Fyn and c-Yes to residues 185 to 210 (Glover et al., 1999). MT does not have endogenous tyrosine kinase activity (Blaikie et al., 1997). SFKs in turn phosphorylates three tyrosine residues in the c-terminus of MT, Y315, Y322, and Y250. Phospho-Y315-MT binds the SH2 domain of PI3K, phospho-Y322 binds the SH2 domain of PLC $\gamma$ -1 and phospho-Y250 binds to the PTB domain of Shc1 (Campbell et al., 1994). These recruited proteins can in turn be phosphorylated by SFKs to initiate various signalling pathways that leads to persistent activation of Erk, AKT, AP1 and transcription of c-Myc, thus allowing MT to act analogous to a permanently activated growth factor receptor (Dilworth et al., 1994).

MMTV/MT is an ideal model for the current study. First, MMTV/MT driven breast cancer in mice recapitulates multiple stages of human breast cancer progression including metastasis (Lin et al., 2003). They first develop early proliferative lesions that harbour heterogenous malignant potential as seen in human patients (Maglione et al., 2001). Hyperplastic MT breast epithelium contains 30-40% ER $\alpha$  nuclear stain while normal mammary epithelium at this age does not (Lin et al., 2003). At the adenoma stage, 50-80% of cells are positive for ER $\alpha$ . As the cells become early stage carcinoma, a mosaic pattern of high ER $\alpha$  is seen, which disappears as the tumor progresses to late carcinoma (Lin et al., 2003). It was shown that adenoma contains 70-80% PR+ stain while normal ducts do not, and as tumors progress to late stage carcinoma, PR is undetectable (Lin et

al., 2003). At late stages, MT tumors are also marked by significantly increased ErbB2 levels compared to normal tissue. These trends are also seen in human breast tissues: around 30% of human breast cancer patients lose ER and PR signaling, accompanied by ErbB2 overexpression, all of which correlate with poor prognosis (Lapidus et al., 1998; Lin et al., 2003). Importantly, transcriptomic analysis of MMTV/MT tumors revealed they resemble luminal B subtype of human breast cancer (Guy et al., 1992; Herschkowitz et al., 2007), demonstrating the clinical relevance of using the MMTV/MT mouse model. Second, Shc1 engages MT through phosphorylated Y250 of MT (at NPTpY; member of general NPXpY motif) (Campbell et al., 1994), and this interaction and the subsequent phosphorylation of Y239/240 and Y313 on Shc1 are critical and sufficient for mammary gland transformation and progression in mice (Blaikie et al., 1997; Dilworth et al., 1994; Ursini-Siegel et al., 2008; Webster et al., 1998). This makes MMTV/MT ideal for studying Shc1 phosphotyrosine signaling in the context of mammary tumorigenesis. On the other hand, MMTV/MT mice model has important limitations. First, MT is a viral kinase that does not exist in human breast cancer patients. While it mimics RTK functions by initiating the PI3K/AKT and Ras/MAPK pathways, the complexity and the dynamics of signaling complexes formed by MT differ from that of RTKs commonly overexpressed in breast cancer patients. Second, MMTV/MT tumors carry characteristic chromosome 11 amplification (17q21-25 in human) and chromosome 4 deletions (1p35-36 in human), the significance of which in relation to human breast cancers are unclear (Hodgson et al., 2005). Thus, while the MMTV/MT mouse model can extensively contribute to our understanding of underlying molecular mechanisms and tumor-host interaction at play during breast cancer progression, it is necessary to validate the findings in various model systems prior to making therapeutic predictions.

### **1.7.2 HER2 driven mouse model of breast cancer**

HER2 (Neu in rat), a member of epidermal growth factor receptor tyrosine kinase family, is overexpressed in 20-30% of primary human breast cancer (Iqbal and Iqbal, 2014). Thus, we employed the MMTV/NIC mouse model of breast cancer (Ursini-Siegel et al., 2008). In this model, an oncogenic Neu (contains in-frame deletions in extracellular domain proximal to the transmembrane domain; results in formation of intermolecular

dimers stabilized by disulfide bonds and constitutive activation; ND2-5 (Siegel et al., 1999)) and Cre recombinase are expressed from the same bicistronic transcript where their cDNA sequences are joined by an internal ribosome entry site. These mice were then bred with *Shc1<sup>fl/fl</sup>* mice (MMTV/NIC/*Shc1<sup>fl/fl</sup>*) to delete *Shc1* from mammary epithelium. This eliminates the possibility that stochastic nature of Cre expression downstream of MMTV will not give rise to select population of cells expressing both oncogenic ErbB2 and *Shc1* (White et al., 2004). The average tumor onset of MMTV/NIC mice occurs at 146 days and tumors resemble solid or nodular adenocarcinomas (Ursini-Siegel et al., 2008).

### **1.7.3 CD8 null mouse model**

CD8, composed of CD8a and CD8b, is a co-receptor to T cell receptor complex on T cells that recognizes antigens presented in the context of MHC class I. CD8a in particular engages the  $\alpha 3$  chain of MHC class I. Mice homozygous for CD8a mutation lack functional cytotoxic T cells while having normal to comparable CD4<sup>+</sup> helper T cell thymic development and maturation (Fung-Leung et al., 1991). These mice have (1) significant debilitation in cytotoxic T cell responses to alloantigens and viral antigens, (2) normal CD4<sup>+</sup> helper cell recognition and response to alloantigens presented on MHC class II, and (3) normal IgM and IgG antibody production by B cells, (4) normal lymphoid organ anatomy and the ratio of T and B cells in lymph nodes (Fung-Leung et al., 1991). Loss of CD8a leads to as significant reduction in CD8b, suggesting the surface expression of CD8b is dependent on CD8a, and effectively CD8a mutant mice are null for surface expression of CD8 co-receptor.

### **1.7.4 IFN $\gamma$ null mouse model**

IFN $\gamma$  is involved in numerous signaling pathways of immune cell development and function in addition to exerting pleiotropic effects on various tissues expressing IFN $\gamma$ R (Cantin et al., 1999; Sercan et al., 2006). In cancer, IFN $\gamma$  is well established as a critical player of anti-tumor immunity (Street et al., 2002). Primarily secreted by CD8<sup>+</sup>CTLs, NK cells, and Th1 helper cells (Schroder et al., 2004a), IFN $\gamma$  can (1) increase cytotoxicity, effector functions and proliferation of NK cells (Biron et al., 1999), (2) increase activation,

cross presentation, cytokine signalling, maturation and co-stimulation by DCs (Schiavoni et al., 2013), (3) increase IFN $\gamma$  production, survival, activation, and effector function of CD4 $^{+}$  and CD8 $^{+}$  T cells (Bhat et al., 2017), (4) decrease Treg driven immunosuppressive activity (Overacre-Delgoffe et al., 2017), (5) enhance M1 classical macrophages' cytotoxicity (DeNardo et al., 2009), (6) reduce MDSC's immunosuppressive functions (Medina-Echeverez et al., 2014), and (7) increase antigen presentation and MHC I expression of malignant cells (Propper et al., 2003; Shankaran et al., 2001; Zhang et al., 2019). Besides being an important regulator of immune effector function and immunogenicity of the malignant cells, it also has direct antiproliferative, antiangiogenic and proapoptotic effect on malignant cells (Beatty and Paterson, 2001; Zaidi and Merlino, 2011). Phenotypically, IFN $\gamma^{-/-}$  mice (1) have significantly debilitated expansion of CD8 $^{+}$  T cells (Sercan et al., 2006), (2) reduced macrophage function in response to pathogens (Dalton et al., 1993), (3) systemically reduced MHC I and II expression (Goes et al., 1995), (4) restriction of IgG responses to IgG1 and IgG2b (Kweon et al., 1998), and (5) reduced natural killer cell activity (Dalton et al., 1993), consistent with its biological role. Thus, given the broad and extensive roles IFN $\gamma$  play during anti-tumor immune responses, IFN $\gamma^{-/-}$  and IFN $\gamma^{+/+}$  mice can be used in parallel to interrogate how differential modulation of tumor intrinsic signaling could sensitize tumors to anti-tumor immunity.

## 1.8 Experimental rationale

The host immune system is capable of eradicating malignant cells (detailed in **Section 1.3.1**) However, malignant cells can establish immunosuppressive microenvironment that (1) allows tumor evasion from immune surveillance, (2) promotes tumor progression and (3) aids resistance to cancer immunotherapy (detailed in **Section 1.3.2**). Improved understanding of how tumors shape the immune landscape to favor their growth will greatly aid in rationale design of cancer therapy. The Shc1 adaptor protein, which serves as a substrate to numerous oncogenic receptor and non-receptor tyrosine kinases in breast cancer, has been implicated in suppressing anti-tumor immune responses during breast cancer progression through unknown molecular mechanisms (detailed in **Section 1.5.3** and **1.5.3.1**). Consistent with this, increased Shc1 expression has been associated with decreased CD8 $^{+}$  T cell infiltration in human breast tumors.

Moreover, increased Shc1 phosphotyrosine signaling and its prognostic value in breast cancer patients have been previously documented. Thus, we set out to elucidate the mechanisms by which Shc1 suppresses anti-tumor immune responses and how Shc1 phosphotyrosine signaling contributes to this process using various mouse models and *in vitro* systems. Furthermore, we aimed to interrogate both transcriptional responses and protein interactomes associated with Shc1 phosphotyrosine dependent and independent signaling. We reasoned that this would allow comprehensive identification of effectors and signaling pathways downstream of tumor intrinsic Shc1 that promote immunosuppression. Based on this knowledge, we aimed (1) to reveal novel targets that may be druggable to sensitize breast cancer patients to immunotherapies and (2) to provide mechanistic insight of how RTKs and TKs that target Shc1 as substrate promote immunosuppression.

## Chapter 2: Materials and Methods

### 2.1 Animal work

#### 2.1.1 General mouse husbandry

All animal studies were approved by the Animal Resources Council at McGill University and comply with guidelines set by the Canadian Council of Animal Care.

#### 2.1.2 Generation of mouse strains

IFN $\gamma$ <sup>-/-</sup> (B6.129S7-IFN $\gamma$ <sup>tm1Ts</sup>/J; JAX stock #002287; (Dalton et al., 1993)) and CD8<sup>-/-</sup> (B6;129S2-Cd8a<sup>tm1Mak</sup>/J; JAX stock #002665; (Mak et al., 1992)) mice were purchased from JAX Laboratories and backcrossed onto an FVB background (F8). MMTV/MT (MT) and MMTV/NIC (NIC) transgenic mice have been described previously (Ursini-Siegel et al., 2008). Mice expressing a Shc1<sup>fl/fl</sup> allele harbouring tyrosine-to phenylalanine point mutations at residues 239/240 (Shc2F) and 313 (Shc313F) under the control of *Shc1* endogenous promoter have been described previously (Hardy et al., 2007). MMTV/MT/CD8<sup>-/-</sup>, MMTV/MT/Shc<sup>2F/2F</sup>/CD8<sup>-/-</sup> and MMTV/MT/Shc<sup>313F/313F</sup>/CD8<sup>-/-</sup> were generated by breeding MMTV/MT, MMTV/MT/Shc<sup>2F/2F</sup> and MMTV/MT/Shc<sup>313F/313F</sup> mice with CD8<sup>-/-</sup> (F8).

#### 2.1.3 Tail DNA extraction and genotyping

Transgenic mice were genotype at weaning and at necropsy. For each mouse, 3mm tail tissue was removed, resuspended in 500ul of tail extraction buffer (10mM Tris pH 8.0, 100mM NaCl, 10mM EDTA pH 8.0, 0.5% SDS, made with water) containing 20ug/ml proteinase K and incubated on heat block overnight at 55°C. The next day, samples were added with 170ul 5M NaCl, mixed, and spun down at maximum speed for 10 minutes. Supernatant was moved into a new tube with 900ul 95% ethanol and incubated for 15 minutes or overnight. They were subsequently spun down for 10 minutes at maximum speed and pellets were dried of any remaining ethanol. Dry pellets were resuspended in 50ul sterile PCR grade water. 1ul of each sample were used for subsequent PCR reaction. Components of PCR reaction per reaction (**Table 4**) and the primers used (**Table 5**) are listed.

**Table 4. Composition of PCR reaction for each genotype**

Components	MT	Neu	Cre	ShcKI	ShcWT	IFN $\gamma$	CD8
H <sub>2</sub> O (ul)	19.4	19.4	19.4	19.4	19.4	5.06	18.9
10X Taq polymerase buffer	2.5	2.5	2.5	2.5	2.5	1.2	2.5
MgCl <sub>2</sub> (1M)	0.5	0.5	0.5	0.5	0.5	0	0.5
10mM dNTP	0.5	0.5	0.5	0.5	0.5	0.24	0.5
Forward primer (10uM)	0.5	0.5	0.5	0.5	0.5	2.8	0.5
Reverse primer (10uM)	0.5	0.5	0.5	0.5	0.5	0.4	0.5
Third primer (10uM)						1.2	0.5
Taq (5u/ul)	0.1	0.1	0.1	0.1	0.1	0.1	0.1
DNA	1	1	1	1	1	1	1
Total volume per tube (ul)	25	25	25	25	25	12	25

**Table 5. List of primers used for PCR genotyping.**

Target	Name	Type	Primer (5'-3')
MT		Forward	GGAAGCAAGTACTTCACAAGGG
		Reverse	GGAAAGTCACTAGGAGCAGGG
Neu		Forward	TTCCGGAACCCACATCAGGCC
		Reverse	GTTTCC GCAGCAGCCTACGC
ShcKI		Forward	GGTCGCTACCATTACCAGTTGGTCTGG
		Reverse	TACCCG GTAGAATTAATTCCTCGACCG
ShcWT		Forward	CTGCAAAGGGCTTGCAAGTGTG
		Reverse	AACACCATCAAATGCCCAACTTCC
IFN $\gamma$	oIMR6218	Mutant	CCTTCTATCGCCTTCTTGACG
	oIMR8284	Wild-type	AGAAGTAAGTGGAAGGGCCCAGAAG
	oIMR8285	Common	AGGGAAACTGGGAGAGGAGAAATAT
CD8	oIMR1098	Common	GACCTGGTATGTGAAGTGTGG
	oIMR1099	Wild-type	ACATCACCGAGTTGCTGATG
	oIMR6828	Mutant	CATAGCGTTGGCTACCCGTG

#### **2.1.4 Mammary fat pad (MFP) Injections**

Mice were shaved at the injection site. Per fourth mammary fat pad, 0.5 million breast cancer cells resuspended in 30ul of sterile PBS were injected after wiping down the site of injection with chlorhexidine and making a small incision. Lidocaine was administered drop-wise at the incision site prior to it being closed with surgical clips. The clips were removed 9-10 days after the date of surgery. Carprofen was given during surgery and day after surgery and for an additional day as needed. Female virgin mice aged between 6 weeks and 12 weeks were used for injections, and the age of the mice were matched between different experimental groups. Mice were injected at both left and right fourth mammary fat pads and at least three mice (n = 6-12 tumors) per group were injected. Number of tumors involved in the experiments are indicated in the figure legends.

#### **2.1.5 Tumor monitoring**

Transgenic mice were palpated for tumor onset every week until onset. Mice were necropsied 6 to 8 weeks after date of tumor onset. Given the multi-focal and metastatic nature of the transgenic mouse models employed in these studies, mice were necropsied prior to total tumor burden reaching 6 cm<sup>3</sup> and a single tumor did not exceed 2.5 cm<sup>3</sup>. For mammary fat pad injected mice, tumor growth was monitored for biweekly via caliper measurements. Formula used to calculate the tumor size was

$$\frac{4}{3} * (3.14159) * \left(\frac{\text{longest width in cm}}{2}\right) * \left(\frac{\text{shortest width in cm}}{2}\right)^2$$

#### **2.1.6 Tumor vaccination**

For the *in vivo* immunization experiment, breast cancer cells were mitotically arrested with 225 mM mitomycin C (Abcam) for 3 hours, washed, trypsinized and injected intraperitoneally into FVB mice (1 x 10<sup>6</sup> cells per 100ul of sterile PBS) to generate an immunized cohort. Control groups were mock injected with PBS. This injection schedule was repeated 7 and 14 days later. On day 21, immunized and non-immunized mice were subjected to mammary fat pad injection with the cell line that was used for immunization.

#### **2.1.7 Immune checkpoint inhibitor treatment**

Animals were intraperitoneally injected with 100 mg of a neutralizing  $\alpha$ -PD1 antibody (clone RMP1-14, BioXCell) or its corresponding isotype control IgG (InVivoMAb Rat IgG2a, clone 2A3, BioXCell) 5 days after date of mammary fat pad injection and were repeatedly treated every 3 days thereafter. Tumour outgrowth was monitored by caliper measurements (n = 10 per group) every 3 days.

### **2.1.8 Necropsies and tissue collections**

Mouse breast tumors, spleen, and hyperplastic mammary glands were cut to appropriate size and lungs were separated into five lobes. For transgenic mice, 2-4mm of tail was collected for second round of genotyping. The tissues were held in embedding tissue cassettes and fixed in 10% buffered formalin overnight prior to being washed and resuspended in 70% ethanol. They were kept in 4°C until submission to pathology core for paraffin embedding. Paraffin embedded tissue samples were stored in 4°C.

## **2.2 Plasmid constructs and cloning**

### **2.2.1 CRISPR/Cas9 against STAT1 and STAT3**

Mouse *STAT1* and *STAT3* were targeted for CRISPR/Cas9 deletion using the CRISPR Design Tool (<http://crispr.mit.edu>): *STAT1*#1 5'-GTACGATGACAGTTTCCCCATGG-3', *STAT1*#2 5'-GGACTCCAAGTTCCTGGAGCAGG-3' within Exon 3; *STAT3*#1 5'-GGAAGTCCCGCAGCTCCATGGGG-3' within Exon 1. The gBlocks containing U6 promoter, the designed target sequence, gRNA scaffold and termination signal were purchased from IDT. Clones verified to have lost expression of STAT1 or STAT3 by immunoblot analysis were pooled for subsequent analysis (n=6). For the *STAT1* CRISPR cohort, the pooled cells were derived from two guide sequences.

### **2.2.2 BiOD and affinity purification constructs**

3XFLAG conjugated wild-type Shc1 (WT), Y239F/Y240F-Shc1 (2F), Y313F-Shc1 (313F), Y239F/Y240F/Y313F-Shc1 (3F) were amplified out from pMSCV puro retrovirus expression plasmid (clontech) using forward primer targeting NotI site (in frame with Myc-BirA; 5' CACGAGCGGCCGCAAAACAAGCTGAGT 3') and reverse primer targeting EcoRI site (3' CTGCTACTGTTCACTTTAAGCTTAAGGCCG 5'). Amplified Shc1 WT, 2F,

313F, and 3F – 3XFLAG products were inserted into pcDNA3.1(-) mycBirA-R118G-MCS plasmid (Addgene # 36047) both digested with NotI and EcoRI). MycBirA-Shc1-3XFLAG was amplified out with forward primer containing AgeI site (5'-AGCTGgcaccgtagccaccATGgaacaaaaact-3') and reverse primer containing EcoRI site (5' GCCGGAATTTCGAATTTCACTTGTCATCGTC-3'). This amplified product was inserted into pQCXIB-GFP plasmid (Clontech), where GFP was removed upon subcloning. In pMSCV puro plasmid, Shc3F-3XFLAG construct has restriction enzyme sites for Scal at nt. 741 and PstI at nt. 885 destroyed. Shc2F-3XFLAG construct has Scal at nt. 741 destroyed. Shc313F-3XFLAG has PstI at nt. 885 destroyed.

### **2.2.3 STAT3 wild-type and STAT3 mutants**

pcDNA3 STAT3 plasmid was purchased from Addgene. STAT3 cDNA was subcloned into the pMSCV hygromycin plasmid (Clontech) and pQCXIP puromycin plasmid (Clontech). Mutagenesis of tyrosine 705 to phenylalanine (Y705F), serine 727 to alanine (S727A), and serine 727 to glutamine (S727E) were done and the plasmids were sequence verified at GenScript.

### **2.2.4 Knock-down using shRNA**

HEK239T cells were transfected as follows: cells were plated in 10%FBS/DMEM growth media in 6 well plate such that at the time of transfection, cells were 90% confluent. 1hr before transfection, media was refreshed to 10%FBS/DMEM. 2ug of lentiviral shRNA plasmid was combined with packaging plasmids mix 1ug each of psPAX2 and pMD2.G (2<sup>nd</sup> generation system) to a total volume less than 30ul. 1X HBS buffer (pH 6.95; 40g NaCl, 25g HEPES, 1.85g KCl, 0.63g Na<sub>2</sub>HPO<sub>4</sub>·2H<sub>2</sub>O, 5g Dextrose, made up to 500ml with water; filter sterilized and stored at 4°C) was used to make the total volume up to 200ul for 6 well plate. Samples were vortexed for 3 seconds. 10.5ul of 2.5M CaCl<sub>2</sub> drop wise and immediately vortexed for 15 seconds and incubated in dark for 20-30min at room temperature. The mixture was carefully added to the 293T cells drop wise and put back into the tissue culture incubator. Next morning, refresh the medium (2 ml) for both phoenix and 293T. Virus was harvested at 24hrs and 36hrs and filter sterilized with 0.45um syringe filter and snap frozen or immediately used (250ul per 6 well plate infection)

with polybrene. Grb2 (Gene ID 14784) was knocked down using TRCN0000097109, TRCN0000097110, and TRCN0000097112.

## **2.3 Cell culture**

Surgically excised transgenic mice tumors were washed in ice-cold PBS, thinly chopped with surgical scissors and further minced using a McIlwain tissue chopper (Campden Instruments). Subsequently tissues were incubated with 10ml DMEM medium (supplemented with penicillin and streptomycin) containing 2.4 mg/ml Dispase (Roche; Neutral protease, grade II) and 2.4 mg/ml Collagenase B (Roche) and incubated on a 37°C shaker for 2–3 hours. Cells were washed with 1mM EDTA/PBS and centrifugation at 800 r.p.m. for 5 minutes (repeated 3 times). Cells were resuspended in 2.5% fetal bovine serum (FBS)/DMEM growth media containing mammary epithelial growth supplement (MEGS; 3 ng/ml human epidermal growth factor, 0.5 mg/ml hydrocortisone, 5 mg/ml Insulin and 0.4%v/v bovine pituitary extract) and gentamycin. For passaging cells, cells were maintained in 5% FBS/DMEM with MEGS and gentamycin. For experimental purposes, cells were seeded, and their media were changed to 1% FBS/MEGS-containing DMEM the following day with or without appropriate treatment at specified concentration and duration prior to lysis. IFN $\gamma$  (485-MI-100; R&D Systems) was used for treatments. The following inhibitors were used: JAK2/3 inhibitor INCB018424/Ruxolitinib (Selleckchem, cat# S1378) and Mek inhibitor Trametinib (Selleckchem, cat# S2673) at doses indicated.

### **2.3.1 General cell culture**

Mycoplasma test (Lonza cat# LT07-318) were carried out every time a cell vial was thawed from liquid nitrogen and prior to be used in *in vivo* experiments. Cells were not used for more than 1.5 months. Mycoplasma contaminated cells were either not used or were treated with BM-cyclin (Sigma-Aldrich, cat# 10799050001) for a week prior to being retested.

## **2.4 Flow cytometry**

### **2.4.1 Cell lines**

Surface MHC class I was measured using 0.5 mg PE-conjugated anti-mouse MHC class I antibody (H-2Db) (eBioscience, cat#12-5999-83). Per run,  $2 \times 10^6$  cells were stained for 30 minutes on ice.

#### **2.4.2 Breast tumor**

Tumors (400-500mm<sup>3</sup>) were dissociated by passing through McIlwain tissue chopper (Campden Instruments) around 7 times. Dissociated samples were collected into 50ml falcon tube with 5%FBS/DMEM media supplemented 2.4 mg/ml collagenase B (Roche) and incubate for 2hrs at 37°C on a rocker. After incubation, samples were put in 20ml of 1mM EDTA/PBS and pipetted up and down 4 times to dissociate any visible clumps. Samples were centrifuge for 7 min at 300g at room temperature. Supernatant was removed, leaving behind approximately 5ml. Jelly like layer formed on top of the cells were undisrupted. 6ml of plain DMEM containing DNase I (0.3mg/ml final concentration; Sigma) was added and incubated for 15–30 minutes on 37°C rocker. After incubation, samples were centrifuged at 300g for 7 min at 4°C. Supernatant was discarded and cells were resuspended in 10ml 1mM EDTA/PBS and pipetted up and down 3 times to dissociate any visible clumps. Cells were filtered through 70um strainer, spun down and resuspended in ice cold 10ml 2% FBS/PBS and keep on ice until staining. Spleens were homogenized in PBS using polypropylene pestles (Thomas Scientific, cat#1212M63), filtered through 70 µm mesh cell strainer and further diluted to 5ml total volume with PBS. Dissociated tumor cells ( $2 \times 10^7$ ) or spleen ( $2 \times 10^6$ ) were stained with Live/Dead Fixable Aqua 405nm (ThermoFisher, cat# L34957). Samples were blocked in Fc block CD16/CD32 (BD Biosciences, cat#553142,) and stained with fluorescently conjugated primary antibodies (**Table 6 and Table 7**) for 30 min at 4°C. Samples were analysed by LSR Fortessa Cell Analyzer (BD Biosciences) and FlowJo software. Aggregates were gated out using FSC-A versus FSC-H and SSC-A versus SSC-H, and total cells were selected. B220 was used to exclude B cells from the analysis. B220cells were further subdivided into CD8+CD69+ to determine the percentage of CD8+ CTLs and CD8+CD69+ activated CTLs. CD45+ population from live immune cells population was further gated for CD11+Gr1+ population. All percentages were reported as % of total events analysed.

**Table 6. List of antibodies and reagents used for immune panel flow cytometry**

Epitope	Fluorophore	Cat#	Company	[Ab] Tumor	[Ab] Spleen
B220	Alexa-488	557669	BD Pharmingen	0.2 µg	0.1 µg
CD8a	APC	47-0081-82	Ebioscience	0.1 µg	0.05 µg
CD69	PE	553237	BD Pharmingen	0.4 µg	0.2 µg
Gr1 (Ly6G)	Alexa-488	53-5931-82	Ebioscience	6.25 ng	2.125 ng
CD11b	APC	17-0112-81	Ebioscience	2.5 ng	1.25 ng
CD45	BV785	103149	Biolegend	0.8 µg	0.4 µg

**Table 7. List of reagents used for immune panel flow cytometry**

Reagents	Cat#	Company	[Ab] Tumor	[Ab] Spleen
Mouse Fc Block (CD16/CD32)	553142	BD Pharmingen	2 µg	1 µg
Live/Dead Fixable	L34960	Invitrogen	0.6 µl into 49.4 µl PBS	0.3 µl into 24.7 µl PBS

## 2.5 Mass spectrometry

### 2.5.1 Coomassie blue staining

To confirm efficiency of affinity purification or immunoprecipitation, purified samples were subjected to SDS PAGE for immunoblotting and Coomassie blue staining. Gel prepared for staining was fixed in 100ml solution containing 46% Methanol, 7% acetic acid and water for 1 hour. The gel was then stained in 100ml solution containing 50% methanol, 10% acetic acid, water and 0.1% Coomassie Brilliant blue-R250 for 1 hour. Gel was destained in 100ml of 5% methanol, 7.5% acetic acid for 24 hours. Second destain was done with 46% methanol, 7% acetic acid for 24 hours. Gel was wrapped in saran wrap and scanned.

### 2.5.2 BioID-MS

Cells were starved overnight (0.5%FBS/DMEM) and were subsequently treated with 50uM Biotin supplemented 10% FBS/DMEM growth media for 24 hours. Per sample, two 15cm plates worth of cells at 70% confluency were used. The next day, cells were trypsinized, washed with PBS, and spun down at 250xg for 5 minutes. For one 15cm plate, cells were lysed in 700ul RIPA lysis buffer (1% Triton X-100, 50mM Tris-HCl pH7.5, 150mM NaCl, 1mM EDTA, 1mM EGTA, 0.1% SDS) supplemented with protease inhibitor cocktail, 50U benzonase (critical to prevent any RNA binding protein contamination) and 0.5% (final concentration) sodium deoxycholate for 1 hour on ice. Vortexed every 15min for 10s to improve the lysis. Sonicated lysates at 50% amplitude 2 times 10 sec on ice. Washed with water and ethanol in between wipes. Centrifuged lysates at max for 30 min at 4°C. During the centrifugation, prepared the bead solution (equilibrating with RIPA buffer). Washed the Pierce Avidin agarose beads (30ul per pull-down; cat # 20219) three times with plain RIPA buffer without the supplements. Spun down the beads at 3000rpm for 1min and carefully removed supernatant. Washed with 1ml RIPA buffer, inverted 10 times to resuspend, spun at 3000rpm for 1min. Removed supernatant and repeated this twice. After the last spin, removed all the supernatant. Added appropriate amount of RIPA buffer so 100ul could be aliquoted per tube. Transferred supernatants from the centrifuged lysates to a new tube. Removed 6% as input control and added 6X protein loading dye. Boiled the input control for 10 min at 95°C. To the rest, added 100ul of prepared bead solution to each sample. Rotated, end-over-end for 3 hours at 4°C. Spun down the beads at 3000rpm for 1min at 4°C. Removed supernatant, added 1ml of RIPA buffer, inverted 10x, spun down. Repeated this twice. For elution for MS: washed three times with RIPA buffer, twice with LIGHT buffer (50mM Tris-HCl pH 7.5 using HPLC grade water), eluted with 150ul 50mM H<sub>3</sub>PO<sub>4</sub> (pH 1.5-2) on ice for 10 minutes. Collected the supernatant. Repeated the elution two more times. Pooled all three elutions in the same tube for final volume of approximately 500ul. Spun at max speed to remove beads and kept at -80C until shipment. Mass spectrometry experiment and analysis were carried out by Dr. Nicolas Bisson and Kevin Jacquet of University of Laval as previously described (Beigbeder et al., 2016; Jacquet et al., 2018). Myc-BirA (no biotin) and Myc-Shc1 wild-type-BirA (no biotin) were used as controls for SAINT analysis (Choi et al., 2011; Teo et al., 2014). Proteins with a SAINT score  $\geq 0.9$  were deemed genuine interactors. Criteria

for protein identifications were fixed at  $\geq 99\%$  probability to achieve an FDR  $\leq 1\%$  and required at least 1 peptide to be identified. For elution for immunoblot: at the last RIPA spin, removed supernatant, added 1ml of TAP lysis buffer (2.5ml of 1M HEPES pH 7.5, 5ml of 1M KCl, 5ml of 100% glycerol, 200ul of 0.5M EDTA, 500ul of 10% NP40 and made up with water to 50ml), inverted 10 times, spun down beads. To elute the biotinylated proteins from the beads, added 15ul of 2X-Laemmli buffer (620mg DTT, 10ml water, 4ml 1M Tris pH6.8 and 5ml 10% SDS) and 6ul of 6X loading dye and boil beads for 8min at 95°C. Vortexed to mix well, and spun down at max speed to remove beads. Bioinformatics analysis was done using ProHits Visualization tool online (Knight et al., 2017).

### **2.5.3 AP-MS**

Cells were incubated in 1% FBS/DMEM supplemented with MEGS for 24 hours. Prepared 50mM sodium orthovanadate stock (pH 10). Freshly prepared 100X pervanadate solution (7.6ml sterile water, 1.9ml 30% hydrogen peroxide, 500ul 50mM sodium orthovanadate) and let sit on ice for 10 minutes for activation. 10 minutes prior to 24-hour time point, cells were treated with the 100X pervanadate solution and put back into the tissue culture incubator for 10 minutes. A few cells detached and floated but mostly stayed adhered. Cells were lysed with buffer (50mM HEPES-NaOH pH8, 150mM NaCl, 1mM EGTA, 0.5% NP40, 2.5mM MgCl<sub>2</sub>, 10% glycerol made up with water) and 2mg of protein lysate was affinity-purified using Anti-DDDDK (FLAG) tag antibody conjugated agarose beads (Abcam cat# ab1240) for mass spectrometry. For *in vitro* validation experiments, affinity purification by FLAG-agarose beads or immunoprecipitation with anti-FLAG antibody (ThermoFisher cat# MA1-91878) were done and indicated where applicable. Mass spectrometry experiment and analysis were carried out by Dr. Nicolas Bisson and Kévin Jacquet of University of Laval as previously described (Beigbeder et al., 2016; Jacquet et al., 2018)

### **2.5.4 ProHits-vis analysis**

Dot plot and bait-bait analysis was done using ProHits-vis online tool (Knight et al., 2015). Abundance was reflected by Average Spec counts and the score was determined by BFDR. Parameters were set as follows: primary filter = 0.01, secondary filter = 0.05,

minimum abundance value of 1, maximum abundance value of 50. Control subtraction using control counts. Normalization and log transformation were not done. Hierarchical clustering was done with distance metric of Canberra and Ward's clustering type.

## 2.6 Protein analyses

### 2.6.1 Protein lysis and immunoblot

Cells were removed of media, washed with ice cold PBS, and lysed on ice using PLCy lysis buffer (50mM HEPES pH7.5, 150mM NaCl, 10% glycerol, 1% Triton x-100, 1mM EGTA pH8, 1.5mM MgCl<sub>2</sub>, 10mM NaF, 10mM NaPyrophosphate) supplemented with 5mM NaF, 1mM sodium orthovanadate, and 1000X protease inhibitor cocktail (10ul of 10mg/ml aprotinin, 10ul of 10mg/ml leupeptin, 100ul of 1mg/ml pepstatin, 1mM PMSF). After being added with either 100ul (60mm plate) to 300ul (100mm plate) of the lysis buffer, cells were scraped with a cell scrapper and collected into a 1.5ml tube and incubated on ice for 10 minutes. Samples were then vortexed for 5 seconds and spun down at maximum speed for 10 minutes in the 4°C centrifuge. Supernatants were used for protein concentration determination using Bradford reagent and spectrophotometer. The lysates were prepared into ready-to-load samples to equal concentration among samples and were supplemented with DTT (final concentration 40mM), 6X protein loading dye, and water.

**Table 8. List of antibodies used for immunoblotting**

<b>Protein</b>	<b>Dilution</b>	<b>Company</b>	<b>Cat#</b>
<b>STAT3</b>	1:3000	CST	9139
<b>Phospho-Y705 STAT3</b>	1:1000	CST	9145
<b>Phospho-S727 STAT3</b>	1:1000	CST	9134
<b>STAT1</b>	1:1000	Santa Cruz	Sc-417
<b>Phospho-Y701-STAT1</b>	1:1000	CST	9167
<b>αTubulin</b>	1:20000	Sigma Aldrich	T5168
<b>Grb2</b>	1:3000	CST	3972
<b>B2M</b>	1:15000	Abcam	ab75853

<b>FLAG</b>	1:4000	ThermoFisher	F3165
<b>MAP4k5</b>	1:1000	ThermoFisher	PA5-40649
<b>AKT</b>	1:2000	CST	9272
<b>Phospho-S473-AKT</b>	1:2000	CST	4060
<b>P38 MAPK</b>	1:2000	CST	9212
<b>Phosphor-p38MAPK</b>	1:2000	CST	9211
<b>ERK</b>	1:2000	CST	9102
<b>Phosphor-ERK</b>	1:2000	CST	9101
<b>SOCS1</b>	1:1000	CST	3950
<b>SOCS2</b>	1:1000	CST	2779
<b>SOCS3</b>	1:1000	CST	2932

### 2.6.2 ELISA

Cells were treated with PBS or IFN $\gamma$  (1ng/ml) for 24hrs. Supernatants were taken for assessment of CXCL9 protein levels using Mouse CXCL9/MIG DuoSet (DY492) ELISA kit (R&D Systems).

### 2.6.3 Immunohistochemistry (IHC)

Formalin fixed paraffin embedded (FFPE) tissues were sectioned to 0.4 $\mu$ m using Leica RM2255. Two types of antigen (ag) retrieval buffers were used depending on the antibody: Sodium Citrate Buffer (10mM Sodium Citrate in distilled water, pH 6) with 0.05% Tween 20, or TE Buffer (1.21g Tris and 0.37g EDTA in 1000ml distilled water (pH 9.0), 0.05% Tween 20). Placed the slides in a slides rack, and performed the following washes: Xylene #1, 2, 3, each 3 minutes, 50:50 Xylene:100% ethanol for 3 minutes, 100% ethanol #1, 2 each 3 minutes, 95% ethanol for 3 minutes, 70 % ethanol for 3 minutes, 50 % ethanol for 3 minutes and left in running cold tap water to rinse for 10 minutes. Filled up to level 6-7 in the pressure cooker with tap water. Added the appropriate antigen retrieval buffer to the coplin jars with the slides. Put the jars into the pressure cooker and antigen retrieval was performed at “High pressure” setting for 12 minutes. Slides were cooled down on ice for 30min and the slides were moved to the humidity chamber. Tissues were marked with wax pen. Washed the slides 2 x 5 minutes in TBS/0.05% Tween 20 + 0.025% Triton X-

100 (TBST). Incubated for 10min with avidin solution. Rinsed with TBST. Incubated for 10min with biotin solution. Rinse with TBST. Blocked with 10% BSA for 30min at room temperature. Added primary antibody (listed in **Table 9**) diluted in 2% BSA/TBS overnight at 4°C. Incubated 3 times each 5 minutes in TBST. Washed with TBS twice. Added 3% H<sub>2</sub>O<sub>2</sub> (diluted freshly from 30% H<sub>2</sub>O<sub>2</sub>) in TBS and incubate for 15min. Incubated 5 min in TBST twice. Added biotinylated secondary antibody diluted in 2% BSA/TBS at room temperature for 30 min. Incubated 5 minutes, three times in TBST. Samples were incubated in ABC (vectastatin) for 30min at room temperature and washed with TBST for 5 min 3 times. Samples were developed with DAB substrate for appropriate time (between 30 seconds and 4 minutes). 20% hematoxylin (incubate for 30 to 60 sec) was used for counterstaining and samples were placed under running tap water for 5 min to blue. Subsequently, slides were incubated for 3 min in 50% ethanol, 3 min in 70% ethanol, 3 min in 95% ethanol, 3min in 100% ethanol (#3, 4), and 3 min in xylene (#4, 5, 6), and mounted with Clearmount.

**Table 9. List of antibodies used for immunohistochemistry**

<b>Protein</b>	<b>Dilution</b>	<b>Type</b>	<b>Ag retrieval</b>	<b>Company</b>	<b>Cat#</b>
<b>STAT1a</b>	1:750	FFPE	Sodium citrate	Santa Cruz	SC-417
<b>Phospho-Y705 STAT3</b>	1:200	FFPE	TE	CST	9145
<b>CD3</b>	1:200	FFPE	Sodium citrate	Abcam	Ab16669
<b>Granzyme B</b>	1:200	FFPE	Sodium citrate	Cedarlane	Ab4059

## **2.7 RNA analyses**

### **2.7.1 RNA extraction for *in vitro* and *in vivo* studies**

For *in vitro* studies, RNA extraction was done using Trizol (ThermoFisher). Cells plated on 6 well plate were lysed using 1ml of Trizol per well and processed. Filtered tips were used at all times. For RNA-seq, either RNeasy Mini kit (cell lines) or Midi kit (tumor tissue) from Qiagen was used. *In vitro* RNA-seq: ShcWT (864, 2196, 4788, 2199), Shc2F (5372, 5835, 5376, 7706) and Shc313F (6203, 6738, 7388, 7389) cell lines were cultured in 1% FBS/MEGS media for 24 hours prior to lysis. *In vivo* RNA-seq: MT cell line (4788) that

were STAT3 null (deleted by CRISPR, clones pooled) and ectopically infected with pQCXIP empty vector (EV), STAT3 wild-type (WT), STAT3-Y705F (YF), STAT3-S727A (SA), STAT3-Y705F/S727A (DM) were injected into the mammary fat pads of syngeneic FVB mice. Tumors were taken at end point, cut into pieces and flash frozen. Flash frozen tumors of size between 300-500mm<sup>3</sup> were selected, crushed, and 4mm<sup>3</sup> pieces were homogenized for 20 seconds prior to being subjected to the RNeasy Midi kit protocol (n = 3 tumors per group; total 15 samples). RNA-seq was performed at the Genome Quebec Innovation Centre of McGill University. RNA quality was assessed by Agilent 2100 Bioanalyzer (Agilent Technologies). Libraries for RNA-seq were prepared according to strand-specific Illumina TruSeq protocols. Samples were multiplexed at four samples per lane and sequenced on an Illumina HiSeq 2000 instrument (100 bp, paired-end reads).

### **2.7.2 RNA sequencing and analysis**

RNA-seq analysis was performed as described in the published manuscript (Ahn et al., 2017) and is quoted here with modifications appropriate for this thesis: “Sequencing reads were trimmed using Trimmomatic v0.32 (Bolger et al., 2014), removing low-quality bases at the ends of reads (phred33o30) and clipping the first four bases in addition to Illumina adaptor sequences using palindrome mode. A sliding window quality trimming was performed, cutting once the average quality of a window of four bases fell below 30. Reads shorter than 30 bp after trimming were discarded. The resulting high-quality RNAseq reads were aligned to the mouse reference genome build mm10 using STAR v2.3.0e(Dobin et al., 2013). Uniquely mapped reads were quantified using featureCounts v1.4.4 and the UCSC gene annotation set. Integrative Genomics Viewer was used for visualization. Multiple quality control metrics were obtained using FASTQC v0.11.2, SAMtools(Li et al., 2009), BEDtools (Quinlan and Hall, 2010) and custom scripts. RNA-seq gene expression analysis. Global expression changes were assessed by unsupervised hierarchical clustering of samples and principal component analysis (PCA). To this end, expression levels were estimated using exonic reads mapping uniquely within the maximal genomic locus of each gene and its known isoforms. Normalization (median of ratios) and variance stabilized transformations of the data were performed using DESeq2(Love et al., 2014). Pearson’s correlation was used as the distance metric for

hierarchical clustering and average linkage as the agglomeration method. Bootstrapped hierarchical clustering was computed using the R package *pvclust* (Suzuki and Shimodaira, 2006). Differential expression analysis to identify expression changes with respect to wild-type (WT) *Shc1* controls was performed using DESeq2 (Love et al., 2014). Genes with statistically significant (adjusted P-value < 0.05) and large (fold change > 2) expression changes, expressed above a threshold (average normalized expression across samples > 100) were selected to derive gene signatures associated with each genotype. Human leukocyte antigen genes, genes with no known function and genes with no human orthologues were removed from downstream analyses. To acquire the *Shc1*-regulated gene signatures, we first compared genes that are differentially expressed between the following groups: (1) *ShcWT* versus *Shc2F* and (2) *ShcWT* versus *Shc313F*. We then compared both lists of differentially expressed genes to identify: (a) genes that are commonly differentially expressed in all *Shc2F* cell lines relative to the rest (*Shc2F*-like), (b) genes that are commonly differentially expressed in all *Shc313F* cell lines relative to the rest (*Shc313F*-like) and (c) genes that are commonly differentially expressed in both *Shc2F* and *Shc313F* cells relative to *ShcWT* cells. *STAT1* and *STAT3* gene signatures, on the other hand, were derived from previously reported validated targets. In addition, we required that mRNA levels of these across patient samples displayed a Spearman's correlation  $R > 0.1$  with *STAT1* and *STAT3* mRNA levels, respectively. All gene signatures were projected across 1,215 human breast cancers from TCGA data set using ssGSEA as described before (Barbie et al., 2009). Briefly, a score is defined to represent the degree of enrichment of a given gene set in a sample: gene expression values for each sample are rank-normalized and an enrichment score is produced using the empirical cumulative distribution functions (ECDF) of genes, with the final score computed by integrating the difference between a weighted ECDF of genes in the signature and the ECDF of the remaining genes (Barbie et al., 2009). This calculation is repeated for each signature and each sample in the data set. To compute ssGSEA scores, we used the GenePattern software implementation from the Broad Institute, ssGSEAProjection (v6) (Reich et al., 2006). We first verified that the ssGSEA scores for reduced gene signatures (containing only genes that have human orthologues) are highly correlated with the *Shc1* genotype in mice. Spearman's correlations between each

signature and expression values of specific genes (*GZMB*, *CD8A* and *PD-L1*) were then computed. For visualization purposes, patients were ranked-ordered and stratified in quartiles, and the mean expression value for each gene and each quartile was computed.”(Ahn et al., 2017)

### 2.7.3 Real time quantitative reverse transcription PCR (RT-qPCR)

RT-qPCR was performed using either goTaq SYBR Green Mix (ThermoFisher, cat# PRA6002). or Taqman MasterMix 2x (Life Technologies, Cat#4352042). Per reaction, SYBR green mix contained 0.4ul of 10uM forward primer, 0.4ul of 10uM reverse primer, 9.2ul PCR grade water, and 10ul SYBR green mix, and 1ul of appropriately diluted cDNA (between 1/5 and 1/10 diluted cDNA from 1ug RNA starting material).

**Table 10. List of mouse primers used for RT-qPCR**

Gene	Type	Direction	Primer sequence (5'-3')
<b>STAT3</b>	SYBR	Forward	CAATACCATTGACCTGCCGAT
		Reverse	GAGCGACTCAAACCTGCCCT
<b>ACTB</b>	SYBR	Forward	GGCTGTATTCCCCTCCATCG
		Reverse	CCAGTTGGTAACAATGCCATGT
<b>B2M</b>	SYBR	Forward	TGGTCTTTCTGGTGCTTGTCT
		Reverse	ATTTTTTTCCCGTTCTTCAGC
<b>CD274</b>	SYBR	Forward	GCTCCAAAGGACTTGTACGTG
		Reverse	TGATCTGAAGGGCAGCATTTC
<b>CXCL9</b>	SYBR	Forward	GGAGTTCGAGGAACCCTAGTG
		Reverse	GGGATTTGTAGTGGATCGTGC
<b>DDX60</b>	SYBR	Forward	TTCCACTGCCCAAATAGGAAAA
		Reverse	GCCAGCAACATGAGTCTTAGGAT
<b>ERAP1</b>	SYBR	Forward	TAATGGAGACTCATTCCCTTGGGA
		Reverse	AAAGTCAGAGTGCTGAGGTTTG
<b>GAPDH</b>	SYBR	Forward	AACGACCCCTTCATTGAC
		Reverse	TCCACGACATACTCAGCAC

<b>IFN<math>\gamma</math></b>	SYBR	Forward	TGTGGCCTAATTACTCATGCTC
		Reverse	ATGGAAAGGCAGAAGCAAAGT
<b>IRF9</b>	SYBR	Forward	GCCGAGTGGTGGGTAAGAC
		Reverse	GCAAAGGCGCTGAACAAAGAG
<b>MUC1</b>	SYBR	Forward	TCGTCTATTTCTTGCCCTG
		Reverse	ATTACCTGCCGAAACCTCCT
<b>IRF1</b>	SYBR	Forward	GGTTTTTGTACCAGGCGAAA
		Reverse	GATGTGAACCCTAGGCCAGA
<b>PSMB8</b>	SYBR	Forward	ATGGCGTTACTGGATCTGTGC
		Reverse	CGCGGAGAACTGTAGTGTCC
<b>TBP</b>	SYBR	Forward	ACCTTATGCTCAGGGCTTGG
		Reverse	GCCATAAGGCATCATTGGAC
<b>TAP1</b>	Taqman		Mm00443188_m1
<b>TAP2</b>	Taqman		Mm01277033_m1

## 2.8 Data availability

TCGA data used for analysis were retrieved from TCGA Research Network website (<http://cancergenome.nih.gov/>). RNA-seq data generated for Chapter 2 are deposited in the NCBI Sequence Read Archive database under the accession code SRP092760.

## 2.9 Statistics

Three independent biological replicate experiments were performed for *in vitro* studies with number of technical replicates indicated in the legend, unless specified otherwise in the legend. Data were normalized to the standard or control as appropriate. *In vivo* orthotopic tumor studies in wild-type, CD8<sup>-/-</sup> or IFN $\gamma$ <sup>-/-</sup> mice were performed with 3–6 age-matched mice (inoculated with tumor in both fourth mammary fat pads; n = 6 – 12 tumors) per group and the number of tumors is indicated in the legend. Power analysis was done using StatMate software: ten tumors per group provided 80% power to detect a difference between means of 155mm<sup>3</sup> (two-tailed; significance level of 0.05) between two groups. Significance testing between two groups were done not assuming normal distribution (nonparametric) with Wilcoxon's using GraphPad software.

## Chapter 3: Shc1 phospho-tyrosine signaling promotes immunosuppression

### 3.1 Experimental rationale

Immunotherapy has revolutionized the way cancer patients are treated today. However, critical challenges remain. First, tumor-mediated immunosuppressive mechanisms that hinder positive responses to targeted- and immune-based therapies in cancer patients need to be identified (discussed in **Section 1.3.5**). Second, biomarkers that identify patients who are responsive and non-responsive to immunotherapy pre- and post-treatment are still lacking (discussed in **Section 1.3.5**). Third, recent studies demonstrate that oncogenic tyrosine kinase signaling contributes to immunosuppression and its blockade induces anti-tumor immune responses (discussed in **Section 1.3.4**). However, due to functional redundancy and heterogeneity of the tyrosine kinome, TK inhibitors lead to acquired resistance which remains a critical challenge. Thus, mechanistic studies that inform rational combination of TK inhibitors and immunotherapeutic modalities for clinical trials are in great need (detailed in **Section 1.3.6**).

The Shc1 adaptor protein, a key converging point of many oncogenic tyrosine kinases in breast cancer, was previously identified as essential for promoting immunosuppression during breast cancer progression (Ursini-Siegel et al., 2010) (discussed in **Section 1.5.3.1**). Coincidentally, increased Shc1 expression is associated with breast cancers of poor prognosis (HER2 and TNBC subtype), and decreased CD8+ T cell presence (Ursini-Siegel et al., 2010). Furthermore, elevated phosphorylation of its tyrosines (target of numerous oncogenic kinases) are seen in breast cancer and is associated with increased relapse in breast cancer patients (discussed in **Section 1.5.3 and 1.5.4**). However, mechanisms by which tumor intrinsic Shc1 suppresses antitumor immune responses have remained poorly understood.

In Chapter 3, we investigated the mechanisms by which Shc1 suppresses CTL- and IFN $\gamma$  driven anti-tumor immune responses, and how Shc1 phosphotyrosine signaling contributes to this process. We show that Shc1 phospho-Y239/240 signaling activates STAT3 immunosuppressive signals and Shc1 phospho-Y313 signaling impairs STAT1-dependent immune surveillance in breast cancer cells. Impaired Y239/Y240-Shc1 phosphorylation selectively reduces STAT3 activation in breast tumours and sensitizing

them to immune checkpoint inhibitors and tumour vaccines. We also show that phospho-Y239/240 and phospho-Y313 dependent gene signatures created based on RNA-sequencing can stratify breast cancer patients with increased inflammation. Together, our data indicate that inhibition of phospho-Y239/240-Shc1-dependent STAT3 signalling may represent an attractive therapeutic strategy to sensitize breast tumours to immune-based therapies. Furthermore, we provide possible mechanistic insight into immunosuppression aided by RTKs and TKs that utilize Shc1 (discussed in **Section 1.3.4**).

### **3.2 Phospho-Y239/240-Shc1 signaling suppresses anti-tumor immune response**

To establish the importance of Shc1 phospho-tyrosine signaling in regulating tumor driven immunosuppression, we used mice expressing Shc1 mutant alleles harbouring tyrosine-to-phenylalanine point mutations at Y239 and Y240 (Y239F/Y240F-Shc1; termed Shc<sup>2F/2F</sup>) and Y313 (Y313F-Shc1; termed Shc<sup>313F/313F</sup>) residue, under the control of the endogenous *Shc1* promoter (Hardy et al., 2007). These mice were crossed with MMTV/MT mice (MT) to generate MT/Shc<sup>2F/2F</sup> and MT/Shc<sup>313F/313F</sup> mice. As previously reported, median ages at tumor onset of MT/Shc<sup>2F/2F</sup> mice (155 days) and MT/Shc<sup>313F/313F</sup> mice (110 days) were significantly increased compared to MT/Shc<sup>+/+</sup> mice (56 days) (**Fig. 10**) (Ursini-Siegel et al., 2008). The delayed onset was comparable to a mutant MMTV/MT mouse model where the Shc1 binding site on MT (Y250) is mutated to a phenylalanine (median age of mice at tumor onset = 143 days), reinforcing the critical importance of Shc1 phospho-tyrosine signaling in promoting MT-induced mammary gland transformation (Webster et al., 1998). Given that Y250F tumors increased recruitment of CTLs during the early stages of breast cancer (Ursini-Siegel et al., 2010), questions had remained whether CTLs contribute to the observed delay in tumor onset. Thus, the tumor onset study in MMTV/MT mice expressing Shc1 wild-type and phospho-tyrosine mutants was extended to a CD8<sup>-/-</sup> background to establish whether CTLs contributed to the delayed tumor onset in Shc1 phospho-tyrosine deficient mice. MT/Shc<sup>313F/313F</sup>/CD8<sup>-/-</sup> mice took considerably longer to generate, consistent with a previous observation that Shc<sup>313F/313F</sup> mice are born with reduced mendelian frequency (Hardy et al., 2007). Trigenic MT/Shc<sup>+/+</sup>/CD8<sup>-/-</sup> mice had a similar tumor onset as MT/Shc<sup>+/+</sup> (p=0.21 by multiple t test), consistent with a previous study (DeNardo et al., 2009). This was also the case for

MT/Shc1<sup>313F/313F</sup> ( $p=0.078$  by multiple t test). However, the absence of the CD8<sup>+</sup> T cell compartment significantly accelerated tumor onset in MT/Shc1<sup>2F/2F</sup>/CD8<sup>-/-</sup> when compared to MT/Shc1<sup>2F/2F</sup> controls, ( $p < 0.001$  by multiple t test), indicating that the delay in tumor onset from impaired Y239/240-Shc1 signaling was in part due to enhanced CTL driven anti-tumor immunity (**Fig. 10**).

In order to test the impact of tumor intrinsic phospho-Y239/240-Shc1 signaling on suppressing CTL-driven anti-tumor immune responses, we generated breast cancer cell lines from tumor bearing MT/Shc1<sup>+/+</sup> (termed ShcWT), MT/Shc1<sup>313F/313F</sup> (termed Shc313F) and MT/Shc1<sup>2F/2F</sup> mice (termed Shc2F) ( $n = 4$  tumors per genotype, total of 12 cell lines). The cell morphology observed *in vitro* was found to be heterogenous and did not stratify by genotype (**Fig. 11**). We orthotopically injected two cell lines from each genotype into the mammary fat pads of syngeneic FVB (IFN $\gamma$ <sup>+/+</sup>, CD8<sup>+/+</sup>) mice versus mice lacking the ability to mount IFN $\gamma$ - or CD8-driven anti-tumor immune responses (IFN $\gamma$ <sup>-/-</sup> and CD8<sup>-/-</sup>). For each cell line, tumor onset was unchanged between the CD8<sup>+/+</sup> and CD8<sup>-/-</sup> groups and IFN $\gamma$ <sup>+/+</sup> and IFN $\gamma$ <sup>-/-</sup> groups (**Fig. 12a-b**). The growth rate of two independent ShcWT and Shc313F tumors were marginally impacted in an immunocompetent background compared to IFN $\gamma$ <sup>-/-</sup> or CD8<sup>-/-</sup> groups, suggesting these tumors were highly immunosuppressed (**Fig. 13a-b**). Meanwhile, Shc2F expressing cells were significantly debilitated in tumor outgrowth in wild-type mice compared to in CD8<sup>-/-</sup> or IFN $\gamma$ <sup>-/-</sup> mice (**Fig. 13a-b**). These data suggested that the loss of phospho-Y239/240-Shc1 signaling in mammary tumors sensitized them to IFN $\gamma$  and CTL driven anti-tumor killing, consistent with the observations made in transgenic animals (**Fig. 10**). There were significantly increased Granzyme B<sup>+</sup> cell (**Fig. 14a**) and CD3<sup>+</sup> T cell (**Fig. 14b**) infiltration ( $p < 0.0001$  by Mann-Whitney U test) by immunohistochemical staining and evidence for increased CTL activation (CD8<sup>+</sup>CD69<sup>+</sup>) in Shc2F tumors (**Fig. 15a-b**) compared to ShcWT and Shc313F tumors by flow cytometric analysis. Given that Granzyme B is also secreted by NK cells, we cannot exclude that NK cells may also be involved in the anti-tumor immune response elicited. Interestingly, increased infiltration of CD11b<sup>+</sup>Gr1<sup>+</sup> myeloid-derived suppressor cells (MDSC) were observed in both Shc2F tumors and spleens of tumor-bearing mice (**Fig. 15a-b**), suggesting that MDSC mobilization may represent a compensatory mechanism to sustain tumor growth in the presence of an elevated anti-

tumor immune response. Histology of the tumors *in vivo* assessed by H&E staining did not stratify tumors by their phenotype (**Fig. 11**). Altogether, these data demonstrated that tumor intrinsic phospho-Y239/240-Shc1 signaling inhibits IFN $\gamma$  and CD8 driven anti-tumor immune responses to enhance tumor growth.

### **3.3 Phospho-Y313-Shc1 signaling suppresses the antigen presentation machinery**

To understand how tumor intrinsic phospho-tyrosine dependent Shc1 signaling regulates breast cancer immunosuppression, we performed RNA sequencing (RNA-seq) on four independent ShcWT, Shc2F and Shc313F cell lines (total of 12 cell lines) in culture. Differentially expressed genes were identified based on fold change greater than 2 in each cell line of given genotype, adjusted p-value smaller than 0.05 and average normalized expression across samples within each genotype bigger than 100. There were 64 differentially expressed genes with loss of Y239/240-Shc1 signaling (**Fig. 16a, Table 11**) and 98 differentially expressed genes with loss of Y313-Shc1 signaling (**Fig. 16a, Table 12**). Commonly upregulated (9 genes) or downregulated (6 genes) in Shc2F and Shc313F cells were also discovered (**Fig. 16a, Table 13**). Noticeably, there was a significant enrichment of MHC complex associated genes located on Chromosome 17 (16 out of 48 upregulated genes; 29.2%) among upregulated genes in Shc2F cells.

Our RNA-seq analysis showed that the cell lines did not stratify by their genotypes and no global transcriptomic changes unique to each genotype were induced, suggesting that Shc1 regulates transcription of a discrete set of genes (**Fig. 16b-d**). Consistent with this, clustering using a different number of genes changed the hierarchical tree, indicating that clustering was not robust between different cell lines. Interestingly, 42% of the differentially expressed genes in Shc313F cells were involved in inflammation and host defense (**Fig. 17a**). At baseline and with IFN $\gamma$  treatment, *CXCL9* (**Fig. 17b**) and components of the antigen processing and presentation (APP) machinery (*B2M*, *TAP1*, *TAP2*, *PSMB8*, *ERAP1*) were upregulated *in vitro*, consistent with the RNA-seq results (**Fig. 17c-e**). In line with this, Shc313F cells significantly upregulated surface expression of MHC class I when assessed by flow cytometry, compared to ShcWT and Shc2F cells (**Fig. 18a-b**). As a second model to support our findings with the MMTV/MT model, we

employed a Neu (HER2 in human) driven mouse model of breast cancer, MMTV/NIC (Ursini-Siegel et al., 2008). HER2 (Neu in rat), a member of EGFR family, is overexpressed in 20-30% of primary human breast cancers. In this model, an oncogenic Neu (NDL2-5; contains in-frame deletions in the extracellular domain proximal to the transmembrane domain; results in the formation of intermolecular dimers stabilized by disulfide bonds, and constitutive activation (Siegel et al., 1999)) and Cre recombinase are expressed from the same bicistronic transcript where their cDNA sequences are joined by an internal ribosome entry site (IRES). These mice were bred with Shc1<sup>fl/fl</sup> mice (MMTV/NIC/Shc1<sup>fl/fl</sup>) to delete Shc1 from the mammary epithelium. This eliminates the possibility that the stochastic nature of Cre expression under the control of the MMTV promoter will not give rise to a select population of cells expressing both oncogenic ErbB2 and Shc1 (White et al., 2004). Several APP components (*B2M*, *TAP1*, *TAP2*, *ERAP1*, *PSMB8*) were also upregulated in the absence of Shc1, specifically in the mammary epithelium (MMTV/NIC/Shc1<sup>fl/fl</sup>) (**Fig. 18c**), further supporting the observation made in the MMTV/MT model. Together, these observations were seemingly paradoxical as the loss of phospho-Y313 signaling *in vivo* failed to increase sensitivity of tumors to IFN $\gamma$  and CD8 driven anti-tumor immune responses.

On the other hand, impaired phospho-Y239/240 signaling did not significantly alter the expression of APP components or MHC class I *in vitro*, despite enhancing immune surveillance *in vivo*. In fact, *MHC B7.2* was one of the most significantly decreased genes in Shc2F cells compared to ShcWT cells by RNA-seq analysis (fold change = -4.3, adjusted p-value < 0.001) (**Table 11**). Thus, while impairing phospho-Y313 signaling could potentially increase a tumor's susceptibility to immune surveillance through enhanced expression of the APP machinery, it alone cannot overcome immunosuppression *in vivo* (**Fig. 13**). In addition, these details suggested that unknown factors derived from the tumor microenvironment (missing in tissue culture) may be necessary to trigger an immune surveillance phenotype in Shc2F cells. *IFN $\gamma$*  and *CXCL9* mRNA expression were significantly increased *in vivo* in Shc2F tumors compared to ShcWT and Shc313F tumors (**Fig. 19**), consistent with the increased CTL and Granzyme B<sup>+</sup> cell infiltration in these tumors (**Fig. 14a-b**). This was coincident with decreased expression of *SOCS2* in tumors *in vivo* but not *in vitro* as assessed by immunoblot (**Fig.**

**20a-b).** SOCS2 expressed by mononuclear phagocytes induced in response to IFN $\gamma$  has been shown to suppress adaptive anti-tumor immune responses and dendritic cell-based priming of T cells in cancer (Nirschl et al., 2017). It is possible that decreased SOCS2 levels reflect an enhanced anti-tumor immune response due to debilitated tumor intrinsic phospho-Y239/240-Shc1 signaling.

Taken together, these data suggested that although the Y313 signaling deficiency renders tumors potentially susceptible to immune surveillance *in vitro*, additional immunosuppressive mechanisms are engaged to negate this effect *in vivo*. Meanwhile, the loss of Y239/240 signaling is sufficient to render tumors susceptible to immune surveillance *in vivo*.

### **3.4 Shc1 signaling promotes STAT3 signaling and suppresses STAT1 signaling**

Given that Shc313F cells *in vitro* had significantly increased expression of IFN-responsive genes such as *CXCL9*, an IFN $\gamma$ /STAT1 inducible gene, we investigated whether the STAT1 signaling pathway was differentially induced in these cells. We observed basally elevated levels of total STAT1 (and varying phospho-Y701-STAT1 levels) in Shc313F cells compared to ShcWT and Shc2F cells, consistent with the RNA-seq data (**Fig. 21a**). Total STAT1 levels were elevated in two out of four Shc2F cell lines (**Fig. 21a-b**). However, Shc2F tumors were similarly susceptible to IFN $\gamma$  or CD8 driven immune surveillance *in vivo* regardless of their STAT1 status (high-5376 versus low-5372) (**Fig. 13a-b**). Various anti-tumor functions of STAT1 are opposed by pro-tumorigenic functions of STAT3 (Avalle et al., 2012). We observed that phosphorylation of STAT3-Y705 (a mark of STAT3 activation) was significantly reduced in all four Shc2F cell lines, while it was upregulated in Shc313F cells (**Fig. 21a-b**). In addition, phospho-S727-STAT3 levels were slightly reduced in Shc2F cells compared to ShcWT cells (**Fig. 22a-b**). To assess the extent of negative feedback activation and inducibility in response to anti-tumorigenic cytokine IFN $\gamma$  (discussed in **section 1.6.3**), STAT3 phosphorylation was measured in ShcWT, Shc2F, and Shc313F cells upon IFN $\gamma$  treatment. Shc2F cells showed reduced phosphorylation of Y705-STAT3 compared to ShcWT cells (**Fig. 22a-b**). This demonstrated that loss of phospho-Y239/240 signaling reduces the ability of breast cancer cells to also engage negative feedback loops as well. Taken together, these data

suggested that Y239/240-Shc1 signaling sustains STAT3 activation while Y313-Shc1 signaling suppresses STAT1 expression and activation in breast cancer cells.

To establish the role of tumor intrinsic Y239/240- and Y313-Shc1 signaling in regulating STAT1 signaling *in vivo*, we analyzed the ShcWT, Shc2F and Shc313F tumors at end-point for STAT1 levels (**Fig. 23**). Consistent with their enhanced immune surveillance phenotype (increased *IFN* $\gamma$  and *CXCL9* mRNA levels, activated CTL and granzyme B+ cell infiltration), Shc2F tumors showed significantly increased nuclear STAT1 positivity specifically in *IFN* $\gamma$ <sup>+/+</sup> mice compared to ShcWT and Shc313F tumors (**Fig. 23**). Interestingly, we observed that 60% of Shc2F (#5372) tumors progressively grew (PD) while 40% of the tumors regressed or stabilized in their growth rate (SD) (**Fig. 24**), suggesting the existence of two populations of cells differentially responding to the presence of an *IFN* $\gamma$ -dependent immune response (did not occur in *IFN* $\gamma$ <sup>-/-</sup> mice).

To establish the role of tumor intrinsic Y239/240- and Y313-Shc1 signaling in regulating STAT3 signaling *in vivo*, we analyzed the ShcWT, Shc2F and Shc313F tumors at end-point for phospho-Y705-STAT3 levels by immunohistochemistry. A significant reduction in phospho-Y705-STAT3 nuclear positivity was observed in Shc2F tumors compared to ShcWT and Shc313F tumors, consistent with our *in vitro* observations (**Fig. 25**). Critically, the regressing Shc2F tumors had virtually no observable phospho-Y705-STAT3 nuclear staining compared to their progressively growing counterpart (**Fig. 23, 25**). In addition, Shc2F tumors that experienced progressive growth in an *IFN* $\gamma$ <sup>+/+</sup> background had even further increased levels of STAT3 activation compared to tumors grown in *IFN* $\gamma$ <sup>-/-</sup> background. These data suggested that Shc2F tumors actively reactivates STAT3 signaling *in vivo*, specifically in an immunocompetent background to overcome immune surveillance (**Fig. 25**). Altogether, these data indicated that tumors impaired in Y239/240-Shc1 signaling fail to overcome *IFN* $\gamma$  driven immune response in part due to reduced STAT3 activation, and Shc2F tumors that successfully re-engage STAT3 activation in the presence of *IFN* $\gamma$  driven immune response can progressively grow. On the other hand, Shc313F tumors displayed elevated level of phospho-Y705-STAT3 and a concomitant increased level of STAT1, consistent with observations made *in vitro* (**Fig. 21a, 25**). Taken together, these data indicated that persistent STAT3 activation may allow tumors

to promote immunosuppression even in the face of constitutively elevated, tumor cell intrinsic STAT1 signaling.

### **3.5 STAT1 and STAT3 activation are concomitantly increased and sustained specifically with phospho-Y313-Shc1 signaling loss.**

To establish the role of tumor intrinsic STAT1 signaling in supporting immune surveillance in STAT3 low (Shc2F) or high (ShcWT, Shc313F) tumors, we used CRISPR/cas9 to delete STAT1 expression from independent cell lines across each genotype (**Fig. 26a-b**). *In vitro*, ShcWT cells induced significantly higher phospho-Y705-STAT3 expression upon IFN $\gamma$  treatment in the absence of STAT1 (**Fig. 26a-b**). This is consistent with a previous study showing that the absence of STAT1 induces prolonged STAT3 Y705 phosphorylation in MEFs (Qing and Stark, 2004). The loss of STAT1, however, did not elevate phospho-Y705-STAT3 signaling in Shc2F cells, either in the absence or presence of IFN $\gamma$  treatment, excluding the possibility that any residual STAT1 plays a role in suppressing STAT3 activation in these cells (**Fig. 26a-b**). In Shc313F cells, loss of STAT1 did not further enhance the already significantly high levels of activated STAT3, suggesting Y313 signaling engages STAT1 independent mechanisms to support persistent STAT3 activation (**Fig. 26a-b**).

To investigate the importance of STAT3 in promoting immunosuppression, we deleted STAT3 expression using CRISPR/cas9 method in ShcWT and Shc313F cells (**Fig. 27**). STAT3 absence did not alter STAT1 activity, either in the absence or presence of IFN $\gamma$ , demonstrating that persistent STAT1 activation in 313F cells is unlikely the result of heightened STAT3 activation, and that there may be other mechanisms contributing to this phenotype.

### **3.6 Y313-Shc1 signaling suppresses STAT1 to decrease expression of APP machinery and surface MHC class I**

We asked whether the increased expression of the APP machinery components and elevated surface MHC class I levels in Shc313F cells required increased STAT1. Indeed, by flow cytometry, both baseline and IFN $\gamma$  induced expression of MHC class I were STAT1 dependent in ShcWT (expression decreased by 1.3 fold in IFN $\gamma$ - and 7.0

fold in IFN $\gamma$ +) and Shc313F cells (expression decreased by 25.5 fold in IFN $\gamma$ - and 34.7 fold in IFN $\gamma$ +) (**Fig. 28a-b**). At baseline, Shc313F cells showed reduced MHC class I expression (2.6 fold; p-value = 0.008) in the absence of STAT3, suggesting that STAT3 may also contribute to increased MHC class I expression. This requires further confirmation by re-expression of STAT3 in STAT3-deleted Shc313F. In addition, elevated expression levels of the APP machinery and other IFN stimulated genes (*TAP2*, *IRF9*, *DDX60*) in Shc313F cells were also STAT1 dependent (**Fig. 29**). Altogether, this established STAT1 as a key contributor to enhanced expression of the APP machinery and surface MHC class I levels in Shc313F cells.

We also assessed the expression of *MUC1*, a known STAT3 target gene overexpressed in Shc313F cells as revealed by RNA-seq (**Table 12, Fig. 29**). *MUC1* expression was entirely dependent on STAT3 in Shc313F cells, validating our RNA-seq studies. *MUC1* has been shown to be upregulated downstream of EGFR to potentiate immunosuppression during cancer progression (Neeraja et al., 2013). Thus, *MUC1* may be one mechanism used by Shc313F cells to exert immunosuppression despite its elevated STAT1 transcriptional activity and enhanced APP machinery.

To exclude the possibility that the loss of tumor intrinsic Shc1 signaling augments production of IFN expression from the breast cancer cells themselves which would upregulate STAT1 in an autocrine manner, we performed ELISA for IFN $\alpha$ , IFN $\beta$  and IFN $\gamma$  (cytokines that induce expression of IFN inducible genes) using culture supernatants. They were undetectable in any of the cells (**Table 14**). Transcript read numbers of *IFN $\alpha$* , *IFN $\beta$*  and *IFN $\gamma$*  from RNA-seq ranged between 0 and 50 (**Table 15**). These data indicated that enhanced STAT1 expression in 313F cells is not due to autocrine IFN-dependent signaling.

### **3.7 STAT3 is critical for promoting tumor onset and growth in the presence of CTL immune response**

To assess the functional importance of STAT1 and STAT3 in regulating CTL driven anti-tumor immune responses downstream of Shc1 phospho-tyrosine signaling, we injected STAT1 or STAT3 CRISPR-deleted ShcWT, Shc2F and Shc313F cells into the

mammary fat pads of CD8<sup>+/+</sup> or CD8<sup>-/-</sup> mice. Loss in expression of STAT1 and STAT3 within tumor epithelial cells were first confirmed by IHC (**Fig. 30a, 31a**).

Next, we analyzed the impact of STAT3 loss in ShcWT and Shc313F tumors. In ShcWT tumors, the loss of STAT3 led to a significant reduction in tumor onset (25% of mammary glands tumor bearing) (**Fig. 32a-b**). Histological assessment (by H&E staining) of CD8<sup>+/+</sup> mammary glands inoculated with STAT3 deleted ShcWT cells revealed the presence of microscopic, non-palpable tumors (**Fig. 33**). The ShcWT tumors that palpated showed a similar growth rate to STAT3 proficient controls (**Fig. 32a-b**). These data suggested that STAT3 is important for the initial establishment of ShcWT tumors. For Shc313F tumors, tumor onset was unchanged, but their growth rate was reduced following the STAT3 loss (**Fig. 32a-b**). Taken together, these data showed that STAT3 is critical for breast tumor establishment and/or growth.

We extended our analysis to understand the role of STAT1 in ShcWT, Shc2F and Shc313F tumors. In Shc2F tumors, loss of STAT1 did not alter tumor onset, but accelerated tumor outgrowth in CD8<sup>+/+</sup> mice (unchanged in CD8<sup>-/-</sup> mice). This demonstrated that STAT1 is important for CTL driven immune surveillance in Shc2F tumors (**Fig. 32a-b**). In Shc313F tumors, STAT1 deficiency slightly accelerated tumor onset but did not impact tumor outgrowth. This suggested that in the presence of hyperactivated STAT3 signaling, hyperactivated STAT1 is dispensable and fails to confer an anti-tumorigenic effect. In cells such as Shc2F that were debilitated in STAT3 activation *in vitro* and *in vivo*, STAT1 conferred an anti-tumorigenic effect (**Fig. 21a-b, 22a-c, 25**). On the other hand, in ShcWT tumors, STAT1 loss did not alter tumor outgrowth. Surprisingly, it resulted in reduced tumor penetrance (40%) uniquely in CD8<sup>+/+</sup> mice (**Fig. 32a-b, 33**). This suggested that STAT1 activation in tumors with elevated STAT3 signaling (ShcWT) may also contribute to the development of breast cancer immunosuppression. This warrants further investigation by re-expression of STAT1 in these cells for assessment *in vivo*. Taken together, these results provided evidence that the STAT3 activation status of breast tumors may influence whether STAT1 plays a pro- or anti-tumorigenic role, and that Shc1 may regulate this process (**Fig. 34**).

To characterize the immune modulatory role of tumor intrinsic STAT1 and STAT3 pathways in the context of different Shc1 phospho-tyrosine signaling conditions, we first

assessed the level of CD3<sup>+</sup> T lymphocyte infiltration in the STAT1 or STAT3 CRISPR-deleted ShcWT, Shc2F and Shc313F tumors (summarized in **Fig. 43**). CD3<sup>+</sup> T cell infiltration was decreased in STAT1 deleted ShcWT, Shc2F, Shc313F tumors, with the most pronounced decrease observed in Shc2F tumors (2.1 fold, p-value = 0.021 by Mann-Whitney U test) (**Fig. 35**). These results demonstrated that CD3<sup>+</sup> T cells are recruited to the tumor in response to tumor intrinsic STAT1 signaling. Microscopic lesions of STAT3 deleted ShcWT showed increased infiltration of CD3<sup>+</sup> T cells, suggesting T cells may be either (1) suppressing the microscopic lesions from becoming palpable tumors permitted by the loss of STAT3 or (2) being recruited to promote immunosuppression and aid tumor outgrowth and dormancy.

We extended the characterization of the immune microenvironment by assessing the infiltration of Granzyme B<sup>+</sup> immune cells (indicative of anti-tumor immune responses by CTL or NK cells) (**Fig. 36**). In Shc2F tumors, STAT1 loss did not reduce the significant increase in Granzyme B<sup>+</sup> cell infiltration in Shc2F tumors, suggesting that impaired phospho-Y239/240-Shc1 signaling can elicit anti-tumor immune response by STAT1 independent mechanisms. However, STAT1 loss still accelerated tumor outgrowth in a CTL dependent manner (**Fig. 32a-b**). This suggested that Shc2F tumors may (1) elicit Granzyme B<sup>+</sup> cell infiltration to promote immune-mediated clearance independently of STAT1, and (2) rely on CTL induced STAT1 for anti-proliferative signaling during tumor outgrowth. Second hypothesis may be supported by comparing the level of Ki67<sup>+</sup> cells (marker of proliferation) between STAT1 deleted and proficient Shc2F tumors.

### **3.8 Phosphorylation status of Shc1 impacts breast tumor sensitivity to immunotherapy**

Previous studies have shown that tumors can upregulate PD-L1 expression in response to IFN $\gamma$  stimulation and bind the PD-1 immune checkpoint on effector T cells to evade anti-tumor immunity (Hillesheim et al., 2014). PD-L1 is a well-established STAT1 target gene (Bellucci et al., 2015; Garcia-Diaz et al., 2017). By RT-qPCR, we observed that Shc313F breast cancer cells had significantly increased expression of *PD-L1* compared to ShcWT and Shc2F cells *in vitro* (**Fig. 37a**), suggesting that tumor intrinsic PD-L1 expression may contribute to immunosuppression in Shc313F tumors. The

deletion of STAT1 in Shc313F cells showed significantly reduced *PD-L1* expression (1.8 fold, p-value = 0.002) to a level comparable to that of ShcWT cells (**Fig. 37a**). Interestingly, *PD-L1* mRNA expression was elevated in both Shc2F orthotopic breast tumors and MT/Shc<sup>2F/2F</sup> transgenic breast tumors (**Fig. 37b-c**). This was strictly dependent on the presence of an intact CD8+ T cell immune compartment (**Fig. 37c**).

Some retrospective clinical studies have indicated that response rates to PD-1/PD-L1 blockade therapy correlate with *PD-L1* expression (Herbst et al., 2014; Topalian et al., 2012), while some have shown no correlations (Yi et al., 2018). The level of tumor-infiltrating lymphocytes is also a key predictor of response to PD-L1 blockade therapy (Tumeh et al., 2014) and better patient outcomes during therapies (Galon et al., 2006; Mahmoud et al., 2011). Given the elevated *PD-L1* expression levels were observed with loss of phospho-tyrosine Shc1 signaling *in vivo*, we asked whether these tumors would be sensitive to PD-1/PD-L1 immune checkpoint therapy using anti-PD-1 antibody. Indeed, PD-1 immune checkpoint blockade led to reduced average tumor size at end point in ShcWT tumors (1.6 fold) and Shc2F tumors (12 fold), demonstrating that both were sensitive to PD-1 immune checkpoint blockade. On the other hand, Shc313F tumors did not show a change in average tumor size at end point (**Fig. 38a**). Taken together, these data indicated that loss of phospho-Y239/240-Shc1 signaling sensitizes breast tumors to PD-1 immune checkpoint inhibition while loss of phospho-Y313-Shc1 signaling does not.

Next, we sought ways to target the Shc313F tumors which were unresponsive to checkpoint inhibition. Unlike Shc2F tumors, Shc313F tumors were comparable to ShcWT tumors in the level of CD3+ T cell infiltration (#6203 = 0.3 fold, #6738 = 1.4 fold) (**Fig. 14b**) and Granzyme B+ cell infiltration (#6203 = 1.0 fold, #6738 = 3.7 fold) (**Fig. 15a-b**), indicating these tumors may be immune cold. Despite the fact that Shc313F tumors hyper-activate STAT3 to favor immune suppression, they also showed chronically elevated STAT1 and enhanced expression of the APP machinery. Therefore, we hypothesized that boosting the antigen specific tumor immunity may re-engage the anti-tumor immune responses in Shc313F tumors. To test this, we injected immunocompetent FVB mice with either PBS (control group) or mitotically-arrested (using antimetabolite mitomycin-c) ShcWT, Shc2F, or Shc313F breast cancer cells as vaccines (**Fig. 38b**). The mitomycin-c treatment method to prepare tumor cells as immunogens for mice

immunization have been previously described (Benjamini et al., 1977; Dai et al., 2019; He et al., 2011; Nakashima et al., 2011; Rajendrakumar et al., 2018). Immunization by vaccination was sequentially repeated three times (day 1, 7, 14). On day 21, immunized and non-immunized mice were subjected to mammary fat pad injection of the cell line that was used for immunization. Three months after tumor inoculation, 30% of immunized mice rejected ShcWT tumors, 100% of mice rejected Shc2F tumors, and 80% of mice rejected Shc313F tumors, compared to their respective non-immunized controls (100% penetrance for all tumors) (**Fig. 38b**). Cell cycle arrested tumor cells injected into a mouse may elicit an immune response through (1) their surface MHC class I-antigens recognized by the adaptive immune system and (2) cell surface markers recognized by the innate immune system. This can create either antigen specific T and B cell immune response or antigen-independent priming of innate immune response for future challenge. This method excludes induction of immunogenic cell death (Obeid et al., 2007). 70% penetrance of ShcWT tumors indicated that while some tumors primed the immune system, the majority failed to do so and at later challenge could not reject live tumor cells. Meanwhile, both Shc2F tumors and Shc313F were highly immunogenic, and the host immune system was primed to reject the live tumor cells in the mammary fat pad. Taken together, these data indicated that the inhibition of STAT3 signaling (Shc2F) or hyperactivation of STAT1 signaling (Shc313F) in mammary tumors may render tumors sensitive to vaccination based immunotherapeutic strategies. It is yet to be tested whether vaccination done therapeutically *after* tumor inoculation could improve tumor clearance. Nevertheless, these results showed that the immunosuppressive environment created with the loss of Y313-Shc1 signaling renders tumors insensitive to immune checkpoint blockade, but their elevated APP machinery and STAT1 expression may be therapeutically exploited to sensitize them to vaccination-based therapies.

### **3.9 Shc1 phospho-signaling and immune evasion in human breast cancer**

We sought to understand the clinical significance of our observations made on Shc1 phospho-tyrosine signaling in human breast cancer patients. To do so, differentially expressed genes specific to Shc2F cells (2F), Shc313F cells (313F), and common in both (DE) were generated from the RNA-seq data (**Fig. 16**). The murine genes were converted

to human orthologues, and only the subset of genes that had human orthologues were used to create Shc2F (47 out of 89 used), Shc313F (75 out of 102 used) and DE (9 out of 15 used) specific gene signatures (**Table 11-13**). We verified that the shortened gene signature of 2F, 313F and DM still accurately stratified the cell lines by their respective genotypes (**Fig. 39**).

Subsequently, single-sample Gene Set Enrichment Analysis (ssGSEA) of each signature was done in human breast cancer patients from the TCGA dataset (n=1215). The patients were stratified into quartiles (1<sup>st</sup>, 2<sup>nd</sup>, 3<sup>rd</sup> and 4<sup>th</sup>) based on low to high enrichment of each gene signature, and the *GZMB*, *CD8A* and *CD274* mRNA levels of each quartile were determined (**Fig. 40a**). Shc2F-like and Shc313F-like gene signatures positively correlated with *GZMB*, *CD8A*, and *PD-L1* levels in patients while the DE-like gene signature did not. Thus, the transcriptional changes unique to impaired phospho-Y239/240-Shc1 and phospho-Y313-Shc1 signaling stratified breast cancer patients with increased anti-tumor immune responses.

We further asked whether Shc2F- and Shc313F-like patient tumors were also altered in their STAT1 or STAT3 transcriptional programs. STAT1 and STAT3 transcription targets were curated from ChIP data in the literature (**Table 16, 17**) to generate STAT1 and STAT3 gene signatures. Supporting that the signatures manually curated were valid, there was a strong positive correlation ( $R^2$  Pearson = 0.77,  $R^2$  Spearman = 0.89) between the enrichment of STAT1 target gene transcription (measured by STAT1 ssGSEA scores of patients) and *STAT1* mRNA levels. This correlation did not exist ( $R^2$  Pearson = 0.09,  $R^2$  Spearman = 0.07) with phospho-Y705-STAT3 levels obtained from the reverse phase protein assay database (**Fig. 41a, c**). STAT3 target gene transcription (measured by STAT3 ssGSEA of patients using the STAT3 gene signature) positively correlated with both *STAT3* mRNA level and phospho-Y705-STAT3 levels as expected (**Fig. 41b, d**). Next, using the STAT1 and STAT3 gene signatures, we carried out ssGSEA on the Shc2F- and Shc313F-like patient tumors (**Fig. 40a**). Shc2F-like tumors negatively correlated ( $R = -0.16$ ) with the STAT3 transcriptional response (1<sup>st</sup> to 4<sup>th</sup> quartile) while Shc313F-like tumors positively correlated ( $R = 0.61$ ) with the STAT1 ssGSEA score (**Fig. 40a**). When patient tumors were further stratified based on STAT1<sup>low/high</sup> and STAT3<sup>low/high</sup> ssGSEA scores, we observed the greatest difference in

average expression of *GZMB* (13 fold), *CD8A* (4.3 fold) or *CD274(PD-L1)*; 2.6fold) genes between STAT1<sup>low</sup> and STAT1<sup>high</sup> groups specifically in tumors with a low STAT3 transcriptional response (**Fig. 40b**). This is supportive of the observation made in Shc2F (high STAT1, low STAT3) and Shc313F (high STAT1 and STAT3) tumors *in vivo* whereby the ability of STAT1 to induce an anti-tumor immune response in Shc2F tumors was dependent on reduced STAT3 activation (**Fig. 34**)

We sought to understand the enrichment of STAT1 or STAT3 transcriptional responses in ShcWT, Shc2F and Shc313F cell lines that were subjected to the RNA-seq analysis. To do so, we performed STAT1 and STAT3 gene signature ssGSEA on the RNA-seq transcriptome data generated from the ShcWT, Shc2F, Shc313F breast cancer cell lines (n=4 per genotype) and compared the ssGSEA scores to the STAT1/STAT3 expression and activation level obtained from immunoblot analysis (**Fig. 12a, 42**). Overall, there was a positive correlation for phospho-Y701-STAT1 and STAT1 transcriptional response ( $R^2$  Pearson = 0.62,  $R^2$  Spearman = 0.67). Positive correlation was also observed between phospho-Y705-STAT3 and STAT3 transcriptional response ( $R^2$  Pearson = 0.65,  $R^2$  Spearman = 0.60). Together, this suggested that the activation (assessed by phosphorylation) of STAT1 and STAT3 were reflected in the transcriptome of the cells. The average STAT1 ssGSEA scores of ShcWT (8329), Shc2F (9202) and Shc313F (10238) cells (n=4 per genotype) indicated the Shc313F cells scored the highest, in line with high STAT1 activation observed by immunoblot (**Fig. 12a**). Shc2F cells (#5376, #7706) that showed increased level of STAT1 and phospho-Y701-STAT1 showed slightly higher ssGSEA score (#5376 = 9837, #7706 = 9219 compared to #5372 = 8778, #5835 = 8974), suggesting that a higher STAT1 transcriptional response may be engaged in these cells as expected (**Fig. 12a, Fig. 42**). These results further highlighted the fact that STAT1 and STAT3 are key signaling pathways distinguishing Shc2F and Shc313F cells from control cells and that the activation of these transcription factors is reflected in the transcriptome of cells.

In conclusion, tumors engage Shc1 to promote STAT3 driven immunosuppression and suppress STAT1 anti-tumor killing (**Fig. 43**). Impairment of phospho-Y239/240-Shc1 signaling debilitates STAT3 signaling, allowing for robust IFN $\gamma$ , STAT1, and CTL dependent anti-tumor immune responses. This is accompanied by a further enhanced

response to anti-PD-1 checkpoint therapy and tumor vaccine treatment. Impaired phospho-Y313-Shc1 signaling upregulates expression of STAT1 regulated genes commitment with elevated STAT3 signaling in mammary tumors. However, due to significant STAT3 signaling, these tumors are immunosuppressed *in vivo* and are not responsive to anti-PD-1 checkpoint inhibition. This is circumvented in tumor vaccination strategies, demonstrating a possible node for immunotherapeutic targeting for tumors displaying high STAT1 and high STAT3 phenotypes, manifested in phospho-Y313-Shc1 deficient tumors. Thus, tumor intrinsic STAT3 signaling is the linchpin to upregulating STAT1 driven tumor killing.

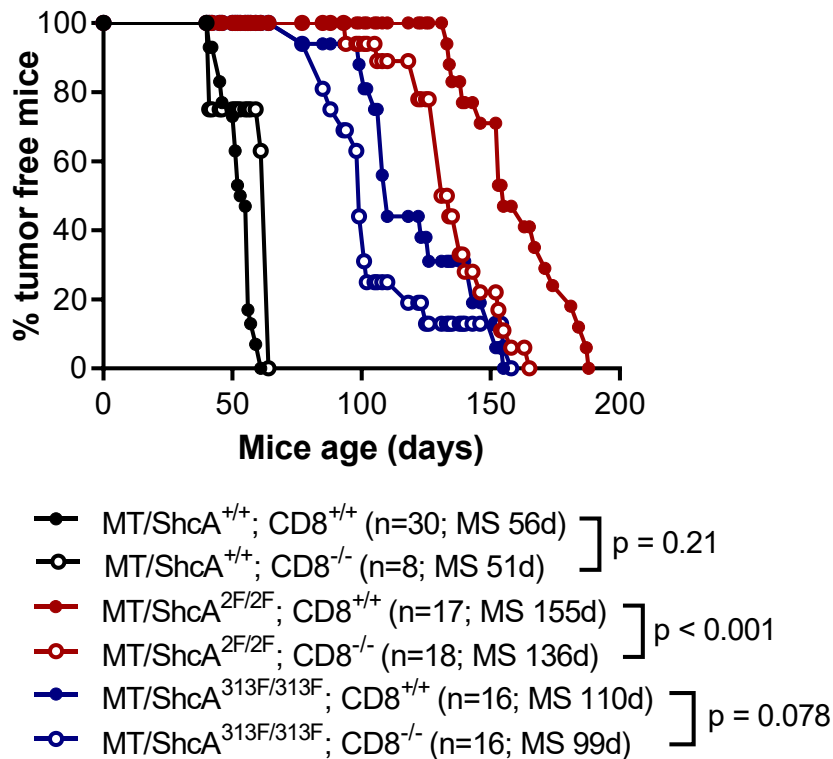


**Figure 10. Impaired phospho-Y239/240-Shc1 signaling delays breast tumor onset in a CD8+ T cell-dependent manner.**

MMTV/MT transgenic mice of the indicated genotypes were evaluated for mammary tumor onset. Percentage of tumor-free mice over time for each genotype is shown. Number (n) of mice analyzed and the median survival (MS) in days are indicated.

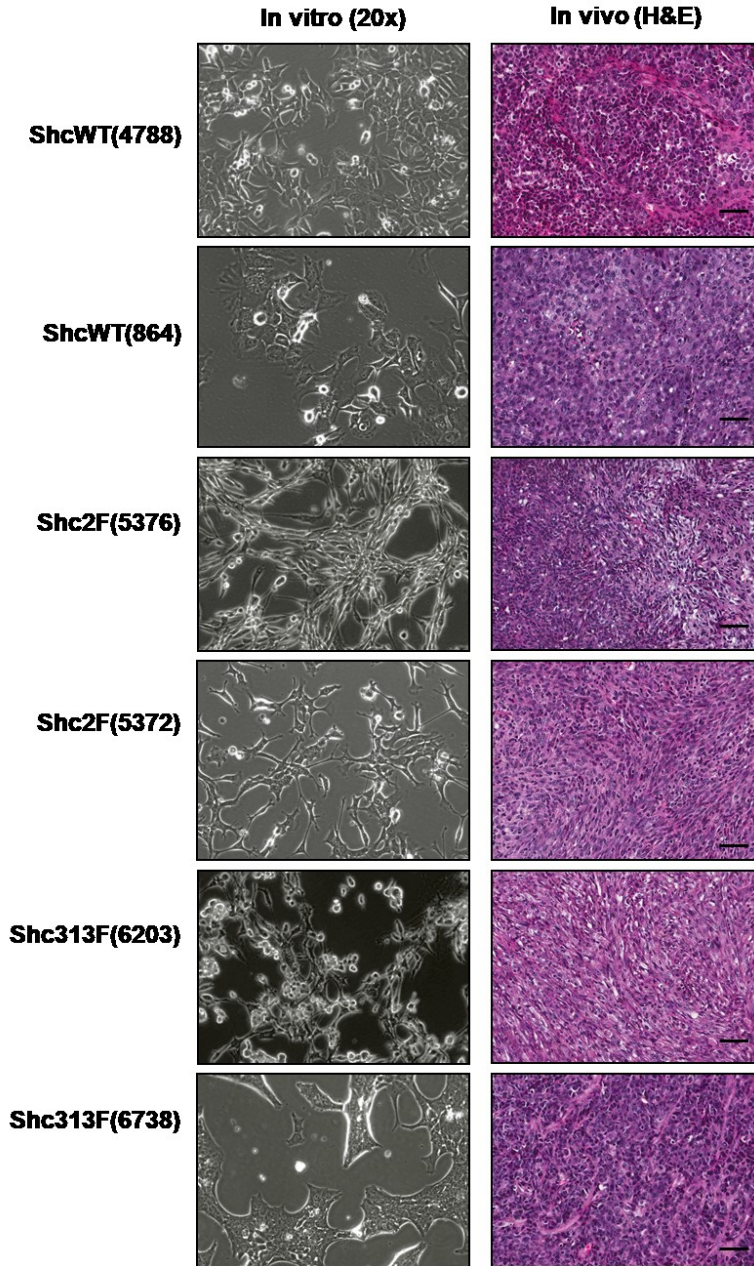


**Figure 11. Morphology of cell lines *in vitro* and histology of mammary tumors *in vivo*.**

The morphology of two independent ShcWT (864, 4788), Shc2F (5372, 5376) and Shc313F (6203, 6738) cell lines were imaged *in vitro* (left panel; 20x magnification) and their corresponding tumors that grew in immunocompetent FVB were assessed by H & E (right panel; scale bar = 50 $\mu$ m).

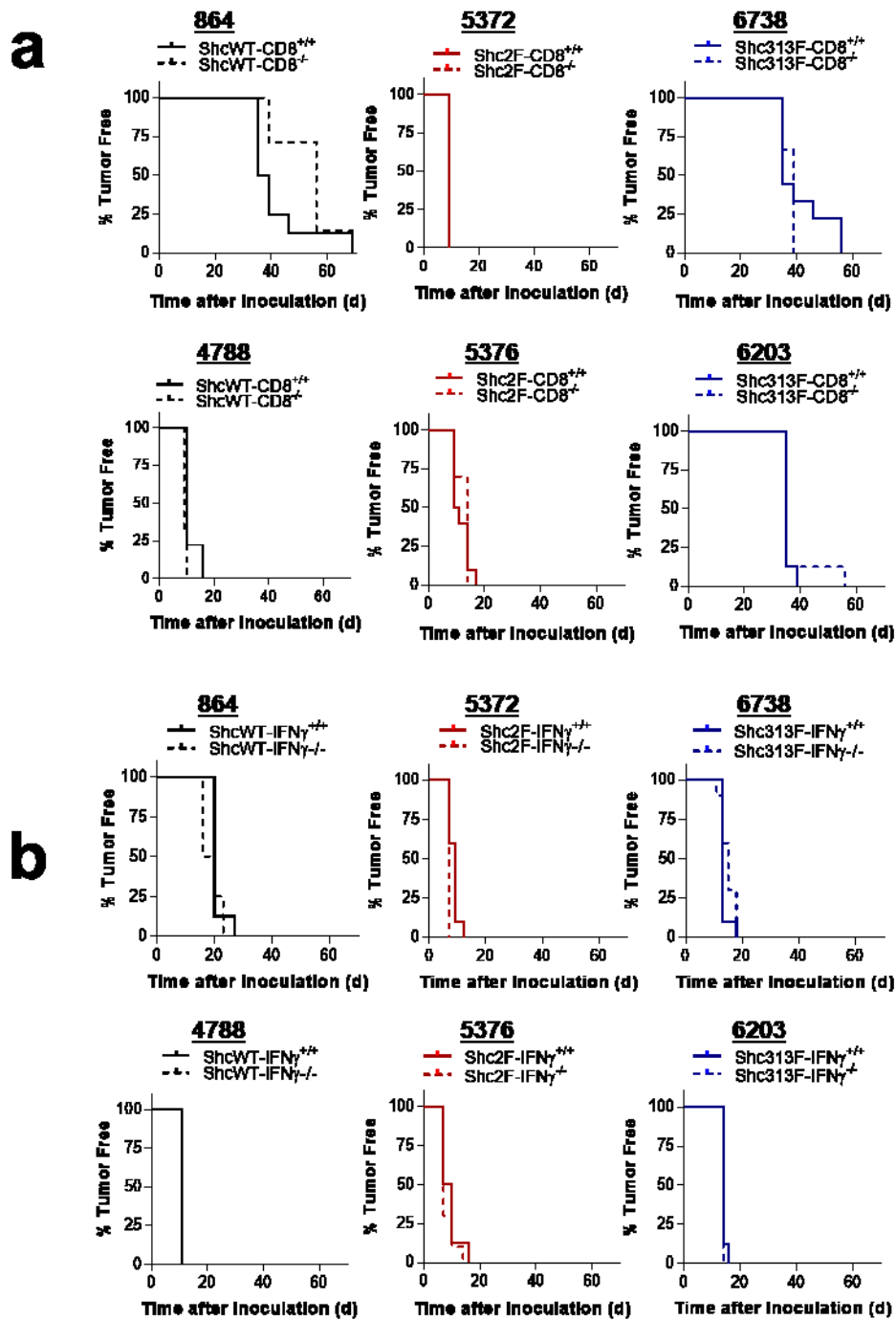


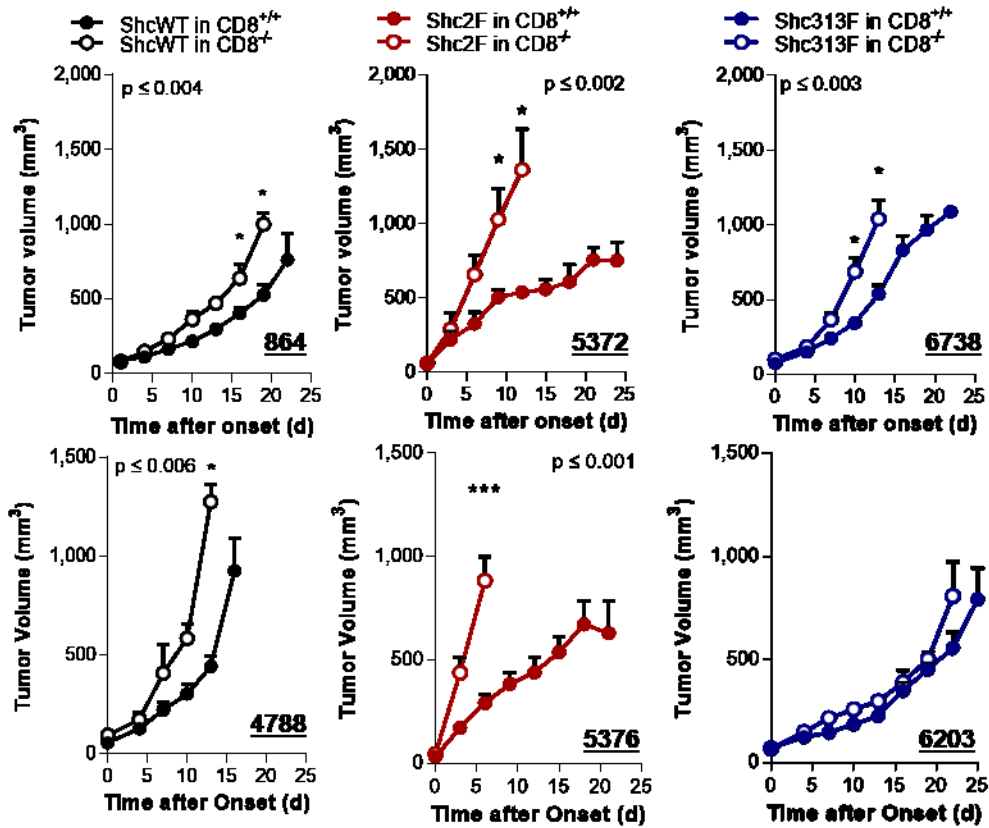
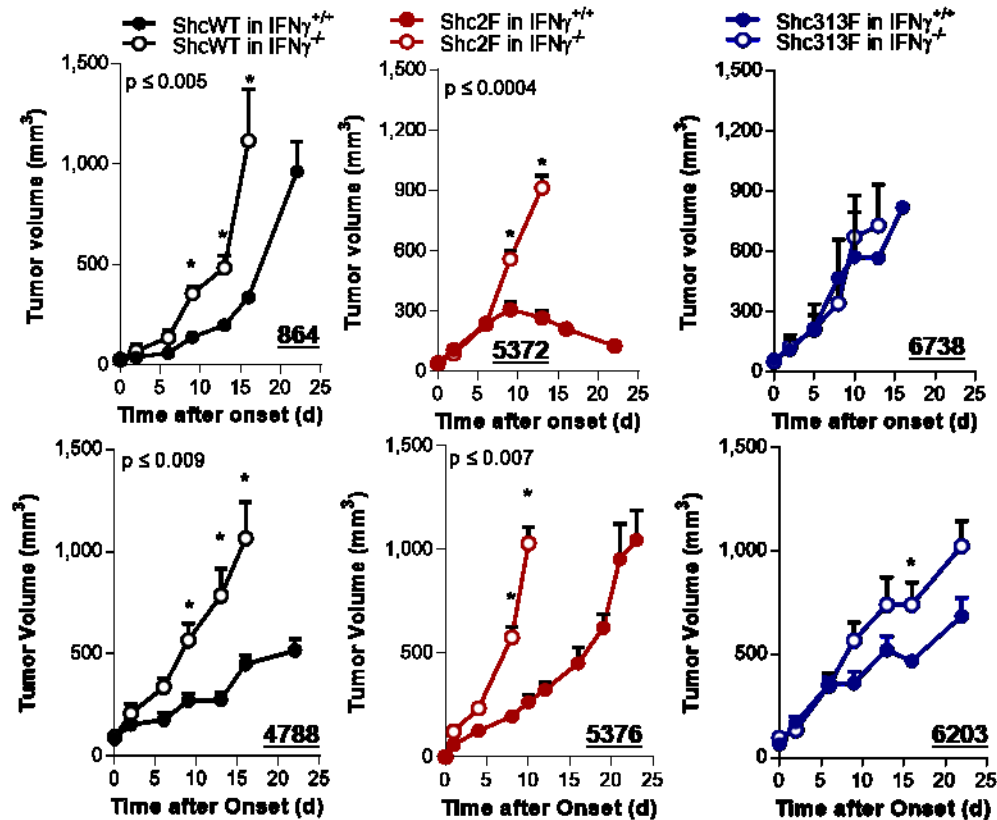
**Figure 12. Tumour onset of Shc1 wild-type and phospho-tyrosine mutant expressing cell lines *in vivo*.**

Percentage of tumor free mammary glands (by physical palpation) following injection of ShcWT (864, 4788), Shc2F (5372§, 5376) and Shc313F (6203, 6738) into fourth

mammary fat pads of **(a)** CD8<sup>+/+</sup> or CD8<sup>-/-</sup> and **(b)** IFN $\gamma$ <sup>+/+</sup> or IFN $\gamma$ <sup>-/-</sup> mice are plotted. Representative of n=7-10 tumors per group. Bold lines represent cohort of tumors injected into immune competent CD8<sup>+/+</sup> or IFN $\gamma$ <sup>+/+</sup> mice and dotted lines represent those injected into immunodeficient CD8<sup>-/-</sup> or IFN $\gamma$ <sup>-/-</sup> animals. Note that the CD8<sup>-/-</sup> and CD8<sup>+/+</sup> onset curves are completely overlapping for #5372 Shc2F tumors in **a** and #4788 ShcWT tumors in **b**.

---

---

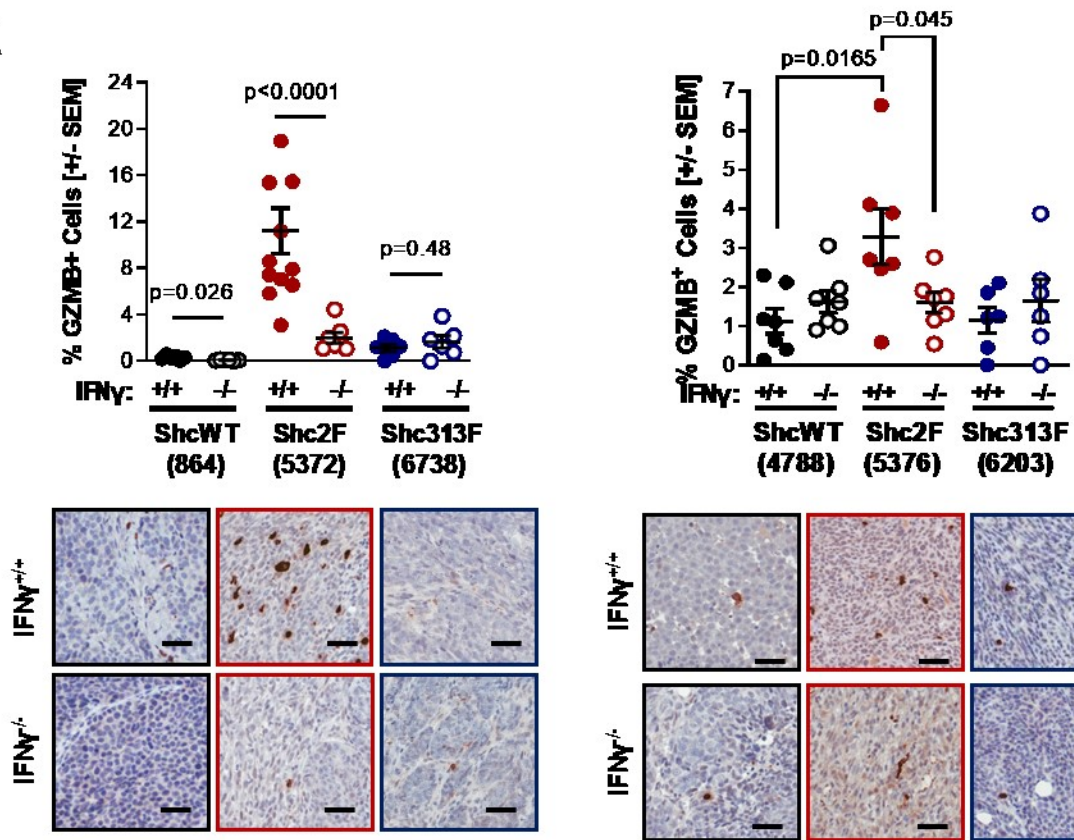
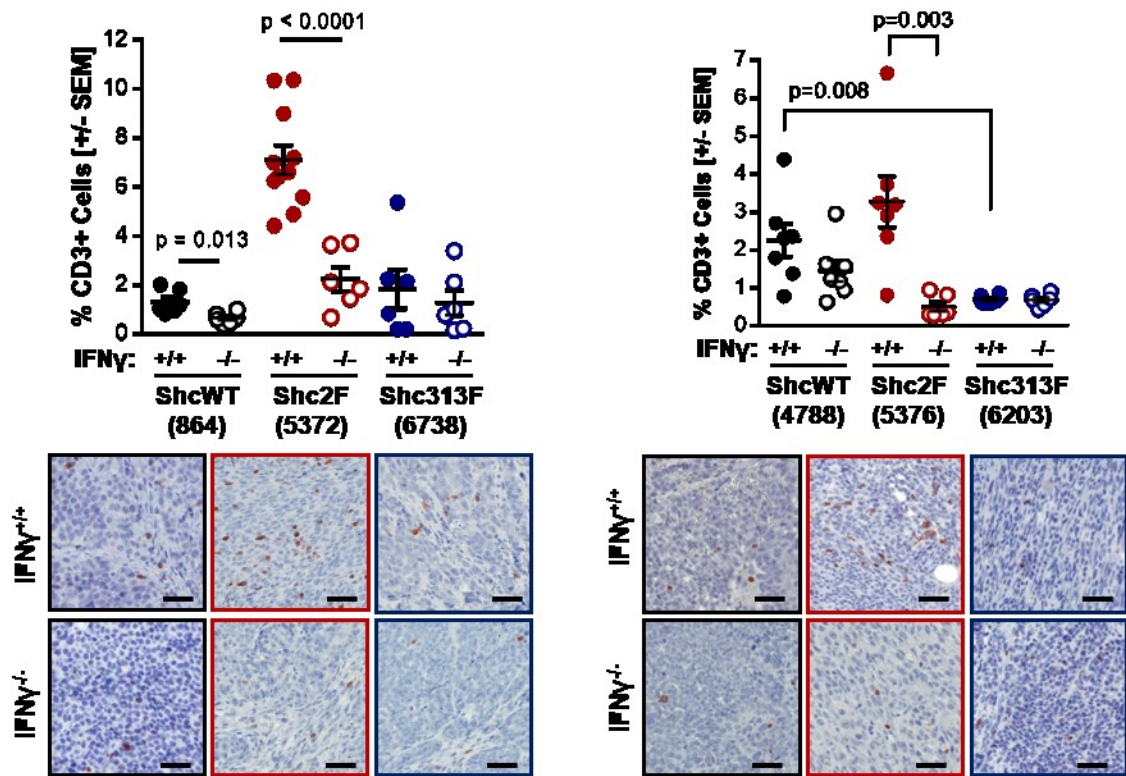
**a****b**

**Figure 13. Phospho-Y239/240-Shc1 signaling suppresses CTL and IFN $\gamma$  driven anti-tumor immunity.**

Cell lines derived from MT-driven transgenic mammary tumors that are homozygous for Shc1 wild-type (ShcWT; 864, 4788) or Shc1 Y239F/Y240F (Shc2F; 5372, 5376) or Shc1 Y313F (Shc313F; 6738, 6203) were injected into the fourth mammary fat pads of syngeneic (a, b) FVB (CD8<sup>+/+</sup>, IFN $\gamma$ <sup>+/+</sup>) and (a) CD8<sup>-/-</sup> or (b) IFN $\gamma$ <sup>-/-</sup> mice. Tumour outgrowth was measured by caliper and represented as mean tumor volume (mm<sup>3</sup>)  $\pm$  s.e.m. (n=8–12).

---

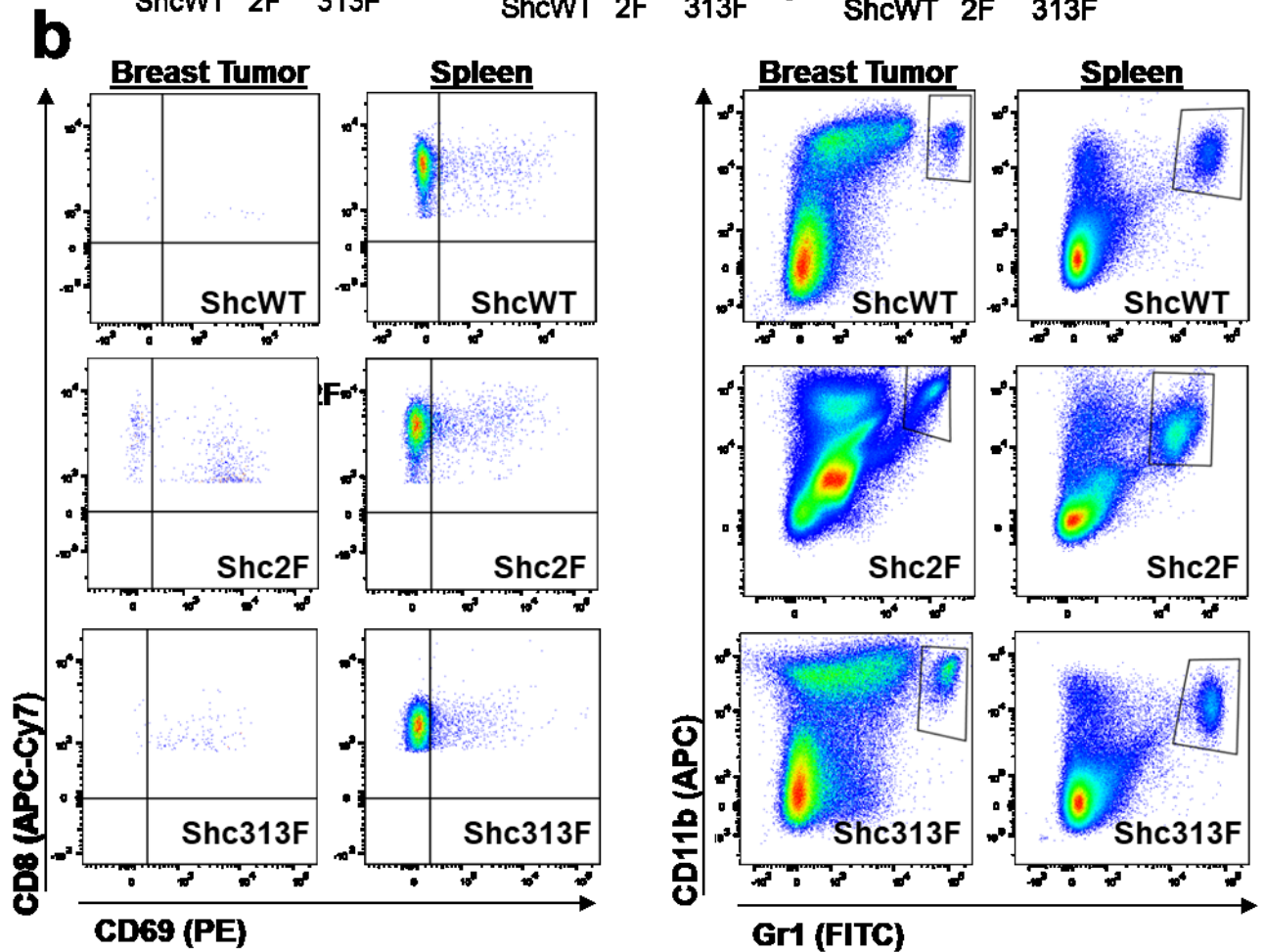
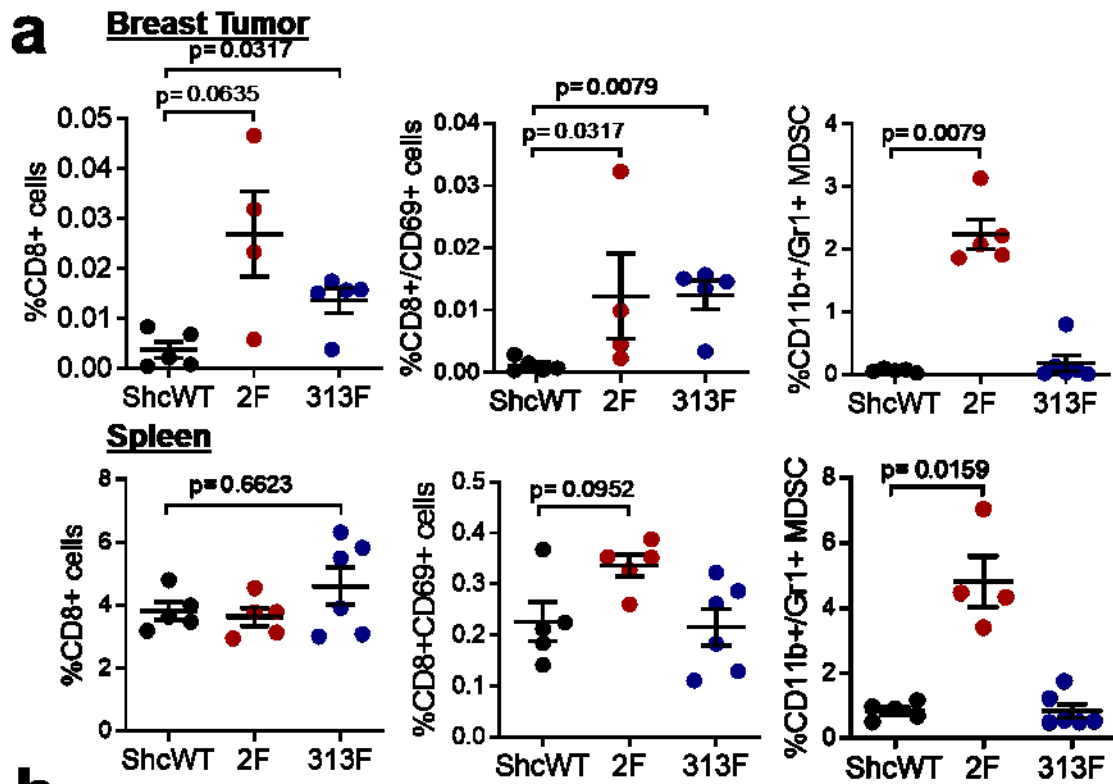
---

**a****b**

**Figure 14. Phospho-Y239/240-Shc1 signaling suppresses Granzyme B+ and CD3+ T cell infiltration.**

Immunohistochemical staining of tumor tissue (n = 6–12 per group) harvested from the indicated mice for (a) Granzyme B (GZMB) and (b) CD3 were done. The data are quantified as % GZMB+ or CD3+ T cells relative to total cells per field  $\pm$  s.e.m., and the representative images are shown at the bottom of each quantification. Scale bars = 50  $\mu$ m.

---

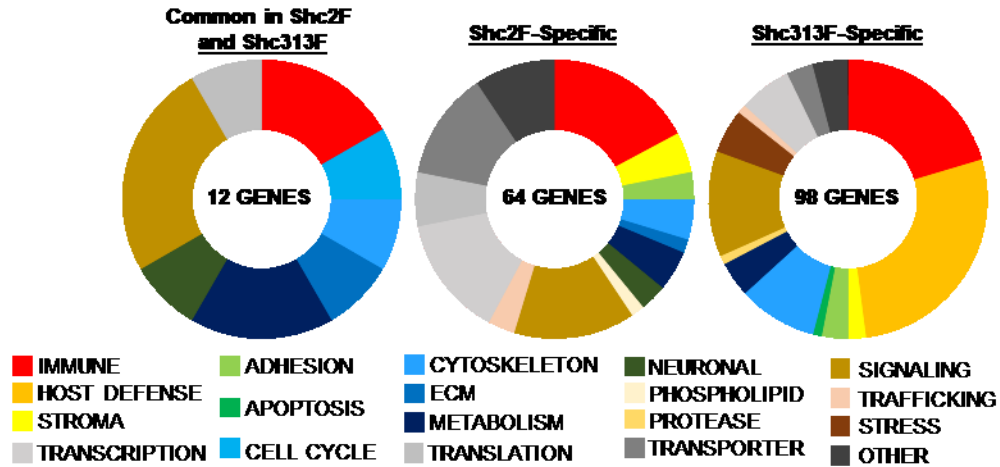
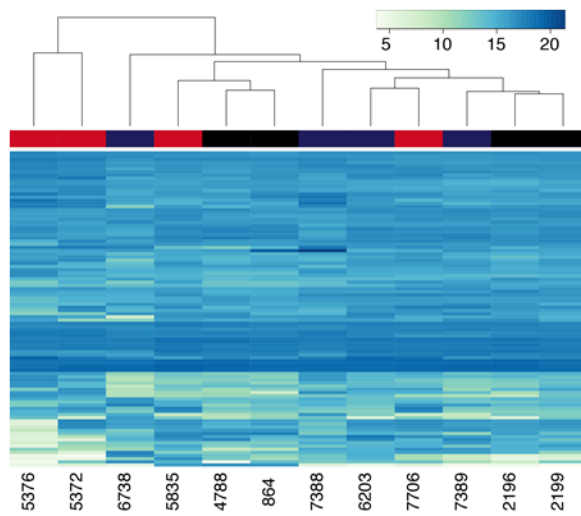
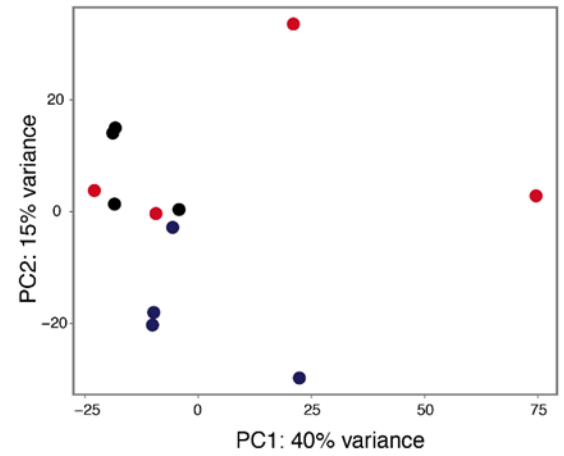
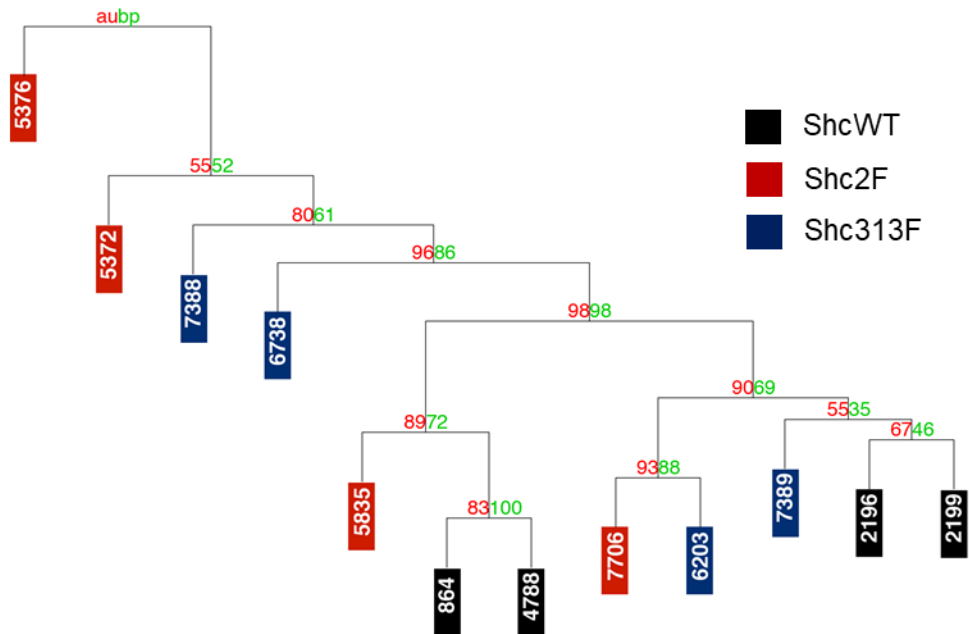


**Figure 15. Phospho-Y239/240-Shc1 signaling suppresses CTL infiltration.**

(a) Breast tumors and matching spleens from ShcWT (864), Shc2F (5372) and Shc313F (6738) tumor bearing mice in **Figure 13** were subjected to flow cytometric analysis for CD8+, CD8+/CD69+ and CD11b+/Gr1+ populations. Data are represented as % of each cell type relative to total cells analyzed  $\pm$  s.e.m. (b) Representative dot plots and gating are shown. Significance was determined by Wilcoxon's rank-sum test.

---

---

**a****b****c****d**

**Figure 16. Shc1 phospho-tyrosine signaling do not alter global transcriptome.**

RNA-sequencing was performed on ShcWT (864, 2196, 4788, 2199), Shc2F (5372, 5376, 5835, 7706) and Shc313F (6203, 6738, 7388, 7389) primary breast cancer cell lines. **(a)** Genes that were significantly differentially regulated in all four cell lines were identified and stratified into three groups: Shc2F-specific (64 genes), Shc313F-specific (98 genes) or commonly differentially expressed in Shc2F and Shc313F cells relative to ShcWT (12 genes). Pathways enriched are depicted. **(b)** Unsupervised clustering done using normalized, variant stabilized transformed data; based on 1,000 most variant genes. **(c)** principal component (PCA) analysis. **(d)** Multiscale bootstrapping of gene expression clustering, performed based on 1,000 iterations. Approximately unbiased (AU) p-value represented in red.

---

---

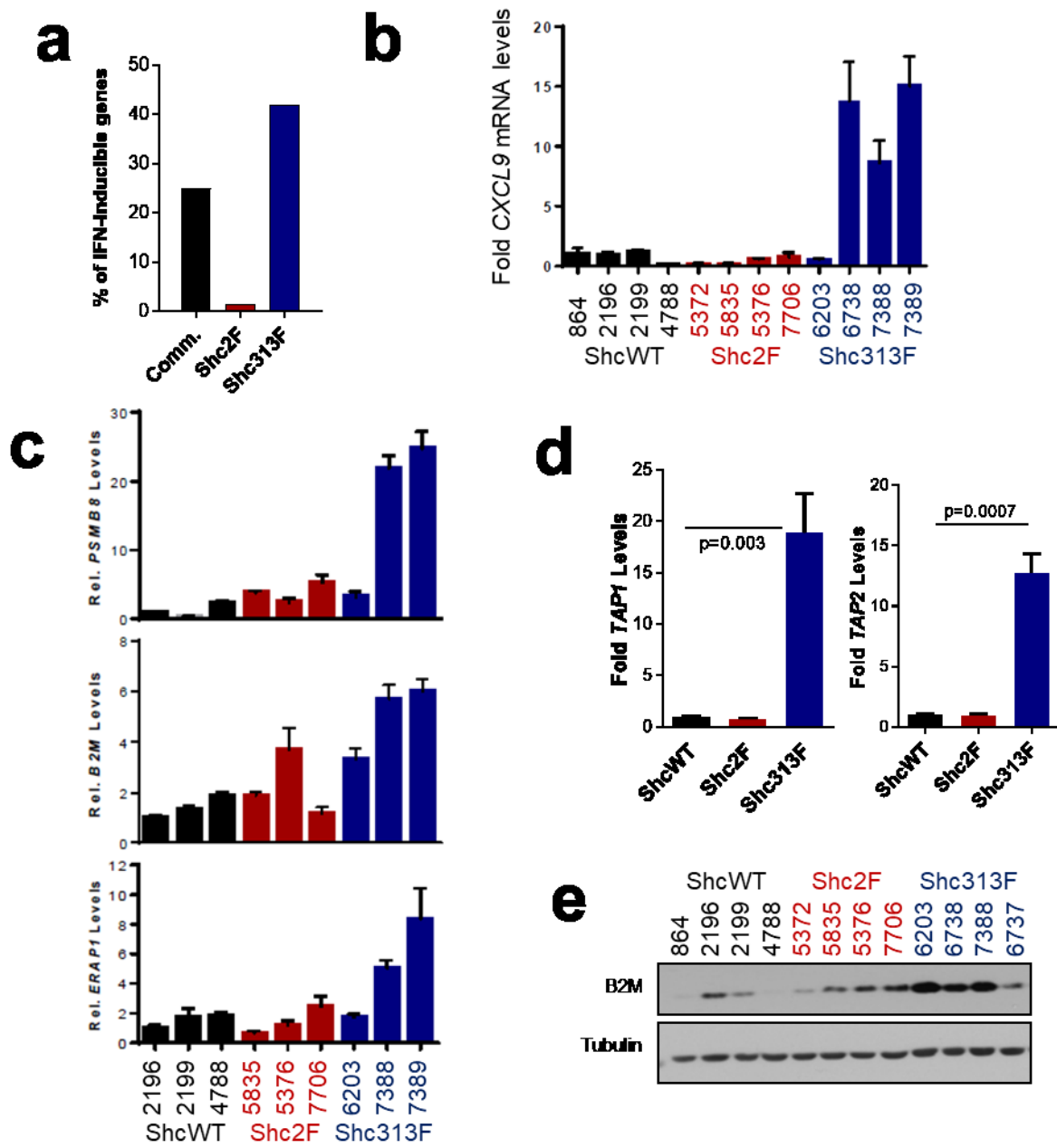


**Figure 17. Antigen processing and presentation machinery (APP) and MHC class I surface expression are increased with impaired phospho-Y313-Shc1 signaling.**

(a) Percentage of IFN-regulated genes identified by RNA-seq within each signature. (b) Average CXCL9 protein levels (ng/ml) secreted from two independent ShcWT, Shc2F and Shc313F breast cancer cells (n=5–6 supernatants per cell line) following 24hrs of PBS or IFN $\gamma$  (1ng/ml) stimulation as determined by ELISA ( $\pm$ s.d.). (c) Relative *PSMB8*, *B2m*, *ERAP1*, mRNA levels (normalized to *GAPDH*) under basal conditions in indicated

ShcWT (2196, 2199, 4788) Shc2F (5835, 5376, 7706) and Shc313F (6203, 7388, 7389) breast cancer cells. (d) Relative *TAP1* and *TAP2* mRNA level of ShcWT (864), Shc2F (5372), Shc313F (6738) cells assessed by RT-qPCR (*GAPDH* normalized). (e) Representative immunoblot analysis of the indicated breast cancer cell lines using B2M and Tubulin-specific antibodies.

---

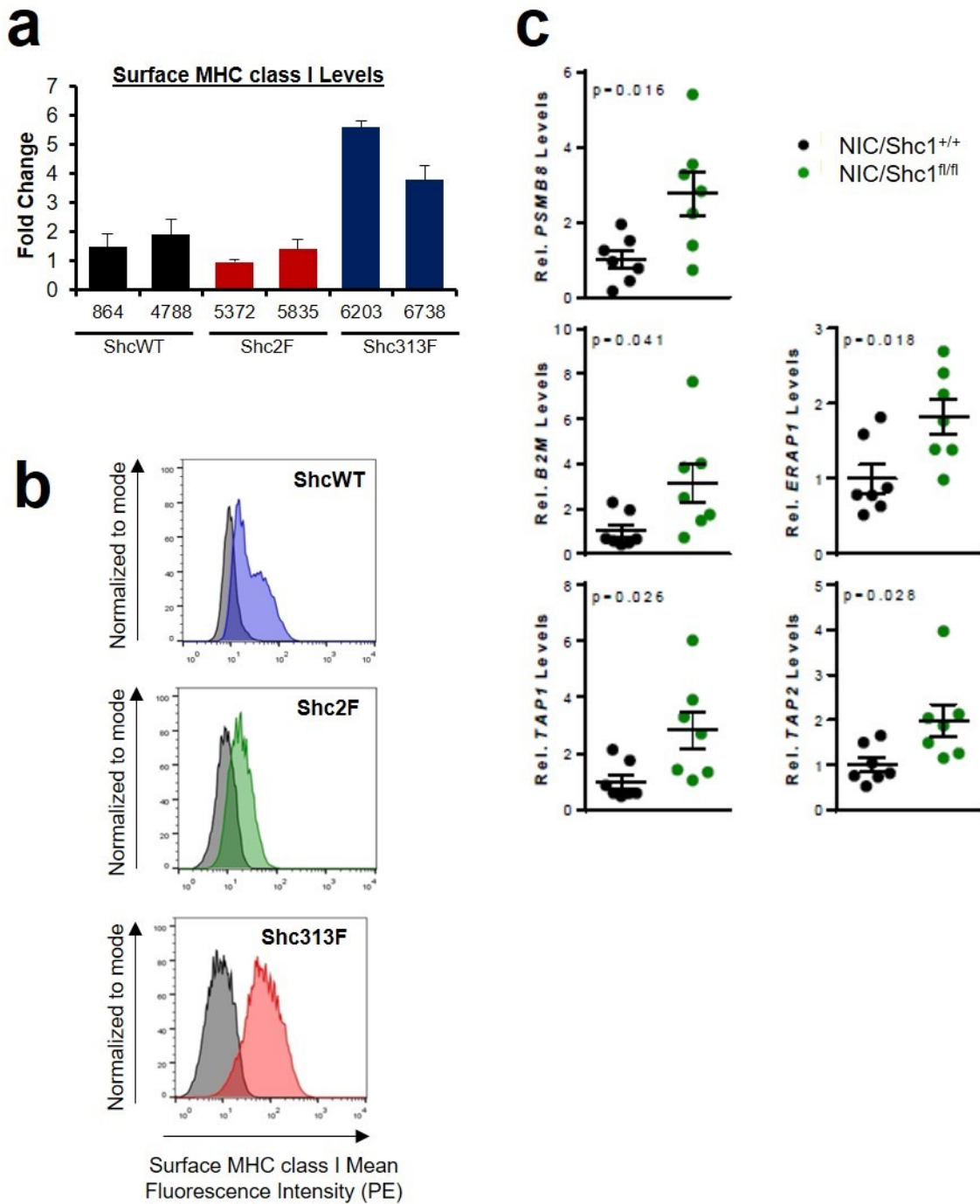


**Figure 18. Surface MHC class I is increased with loss of phospho-Y313-Shc1 signaling.**

(a) Surface MHC class I levels of independent ShcWT, Shc2F, Shc313F breast cancer cell lines as determined by flow cytometry. Shown as average fold change relative to ShcWT (864)  $\pm$  s.d. Representative of two independent experiments. (b) Representative

histograms for surface MHC class I expression levels. Unstained control in grey. (c) RT-qPCR analysis of TAP1, TAP2, ERAP1, PSMB8 and B2M mRNA levels in NIC/Shc1<sup>+/+</sup> and NIC/Shc1<sup>fl/fl</sup> *in vivo* breast tumors at end point.

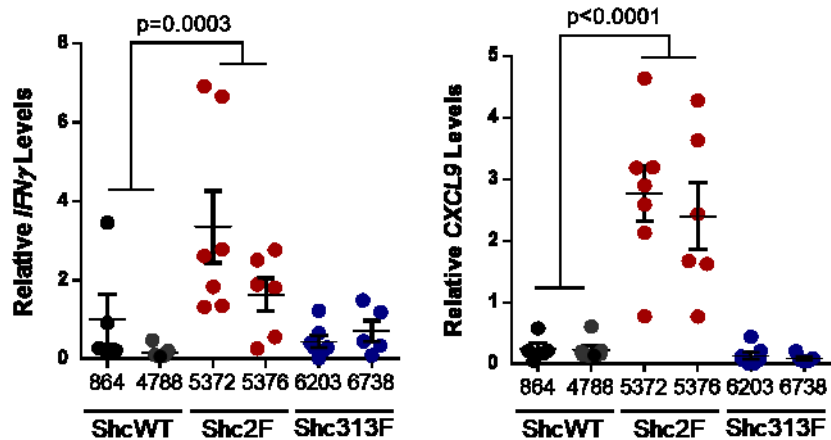


**Figure 19. Impaired phospho-Y239/240-Shc1 signaling leads to increased *IFN $\gamma$*  and *CXCL9* expression in mammary tumors.**

ShcWT, Shc2F and Shc313F cell lines (n=2 per genotype) were injected into the fourth mammary fat pads of syngeneic immunocompetent FVB mice. Tumors were analysed by RT-qPCR for relative expression of *IFN $\gamma$*  and *CXCL9* (normalized to *GAPDH*) mRNA  $\pm$  s.e.m. (n=7 tumors per group).

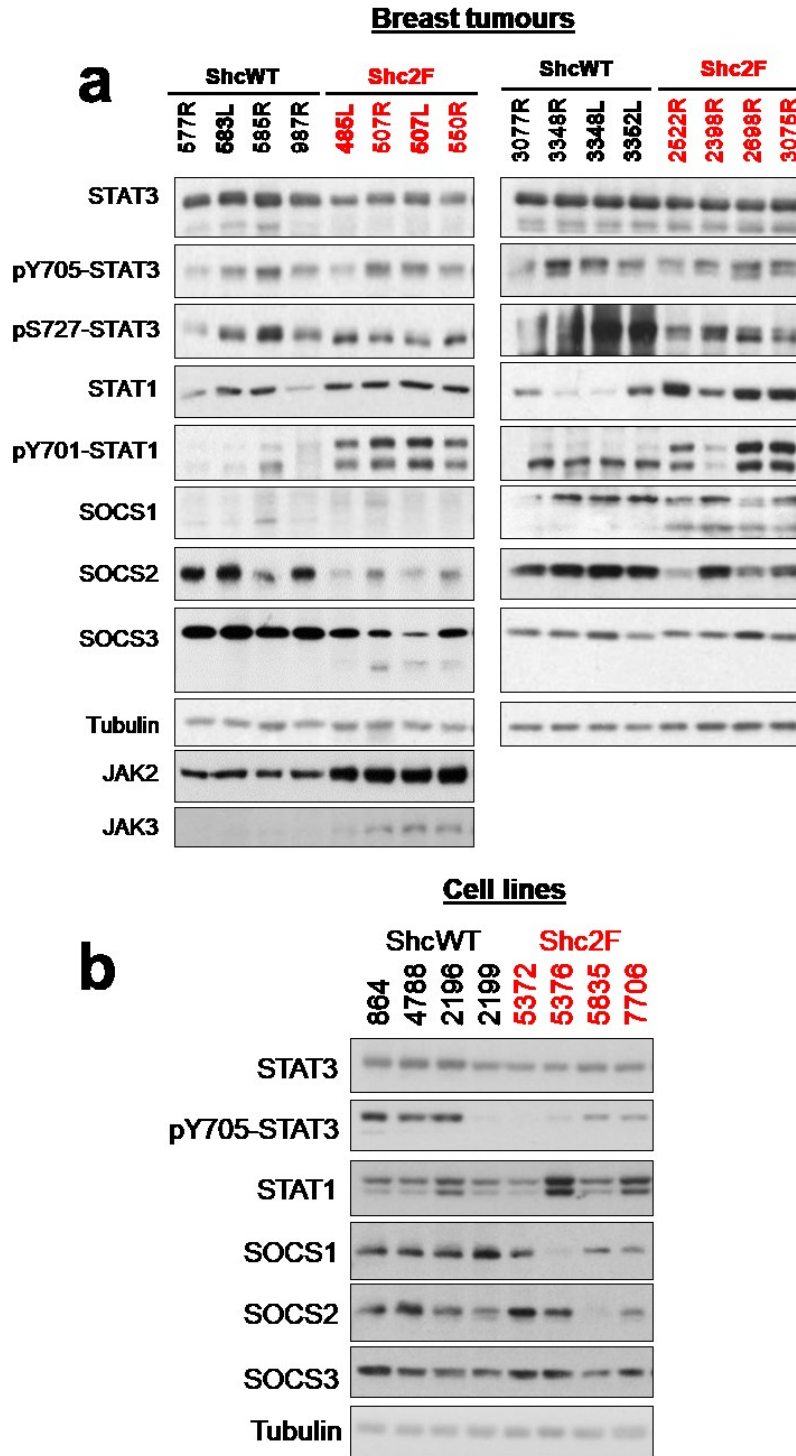


**Figure 20. STAT1 and STAT3 pathways in tumors and cell lines.**

(a) Immunoblot analysis of ShcWT (864) and Shc2F (5372) breast tumors at end point from two independent mammary fat pad injection experiments for the indicated proteins.

(b) Immunoblot analysis of primary breast cancer cell lines ShcWT (864, 4788, 2196, 2199) and Shc2F (5372, 5376, 5835, 7706) *in vitro*.

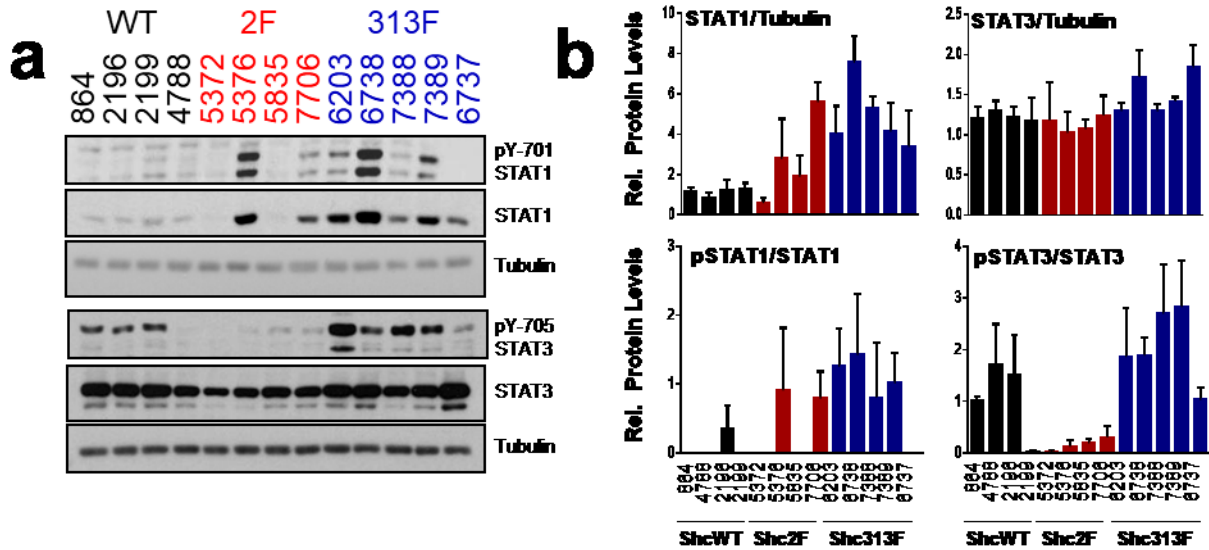


**Figure 21. Phospho-Y239/240-Shc1 signaling promotes STAT3 activation while phospho-Y313-Shc1 signaling suppresses STAT1 expression.**

(a) Immunoblot analysis of total cell lysates from ShcWT, Shc2F, and Shc313F cell lines (4-5 per genotype) using STAT1, phospho-Y701-STAT1, STAT3, phospho-Y705-STAT3 and Tubulin antibodies. (b) Densitometric quantification of immunoblots using ImageJ software. Shown as average fold change in expression levels  $\pm$ s.d. in the individual cell lines from three independent experiments.

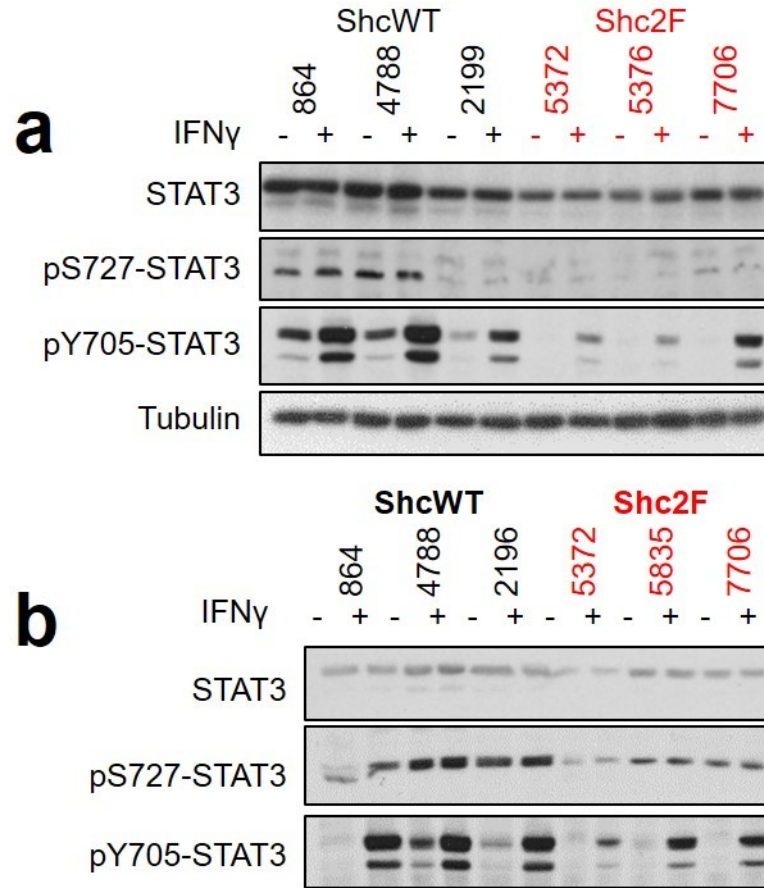


**Figure 22. STAT3 activation at baseline and with IFN $\gamma$  treatment.**

(a, b) ShcWT (864, 4788, 2199) and Shc2F (5372, 5376, 7706) were treated with IFN $\gamma$  (1ng/ml) for 45 minutes prior to being lysed for immunoblot analysis of proteins indicated. Two independent experiments are shown.

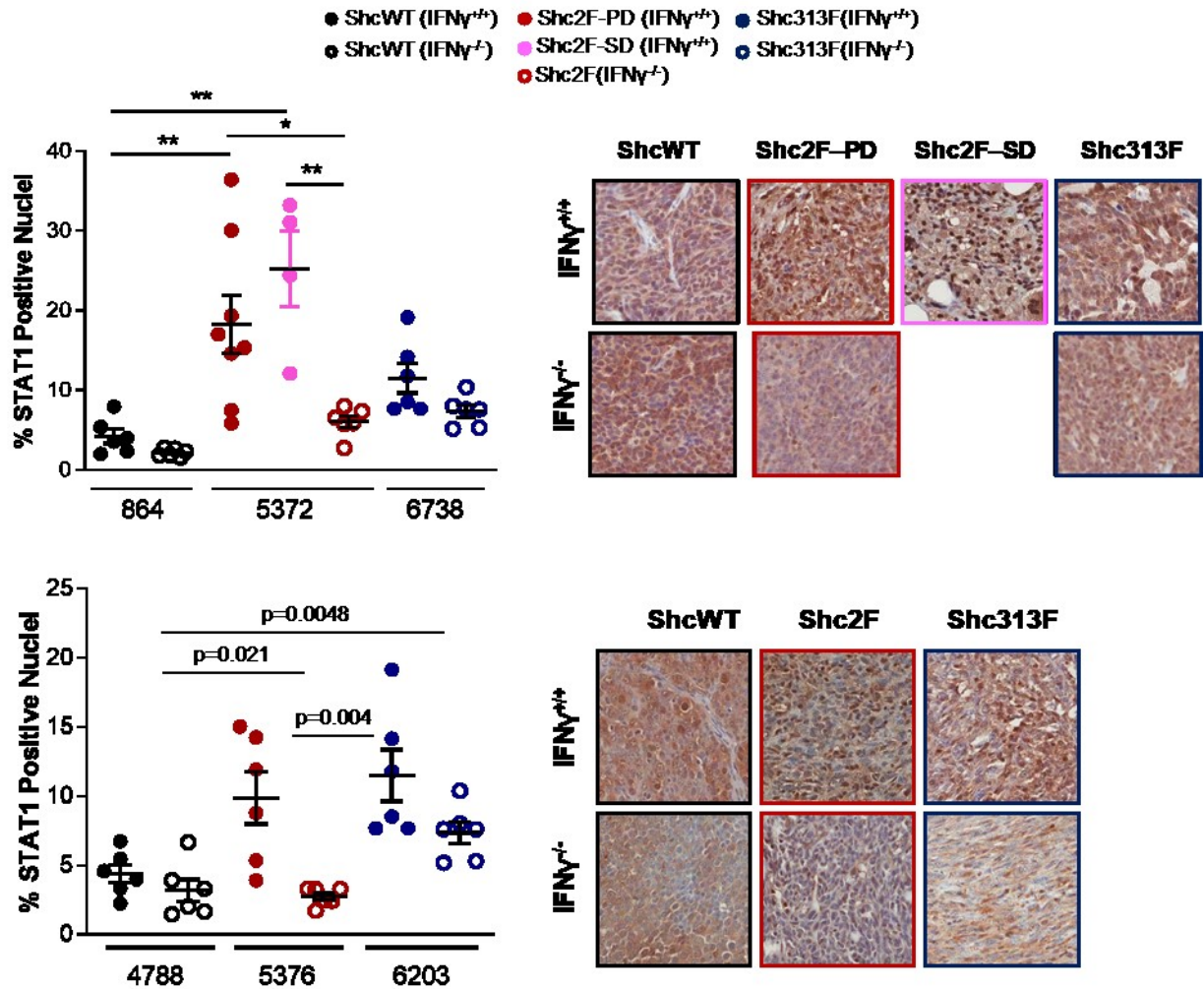


**Figure 23. Impaired phospho-Y239/240-Shc1 induces increased STAT1 signaling *in vivo* in an IFN $\gamma$  dependent manner.**

Immunohistochemical staining of ShcWT (864, 4788), Shc2F (5372, 5376), and Shc313F (6203, 6738) mammary tumors that emerged in IFN $\gamma^{+/+}$  or IFN $\gamma^{-/-}$  mice using STAT1 specific antibodies (n=6–8 tumors per genotype). The mean percentage of STAT1 stained nuclei  $\pm$  s.e.m. is shown. Shc2F tumors were stratified by progressive disease (PD) or stable disease (SD) phenotypes. Representative of two independent experiments and significance was analyzed by Wilcoxon’s rank-sum test (\*P = 0.05 and \*\*P = 0.01). (Right panel) Representative images of phospho-Y705-STAT3-stained paraffin-embedded sections (4 $\mu$ m sections). Scale bars = 50 $\mu$ m.

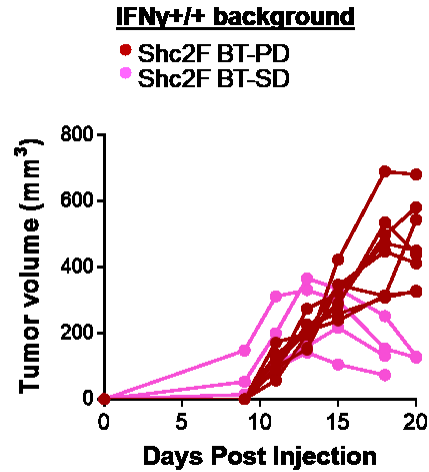


**Figure 24. Two groups of tumors arise with loss of phospho-Y239/240-Shc1 signaling.**

Growth curves for individual tumor Shc2F (#5372) mammary tumors that emerge in an immunocompetent background (IFN $\gamma$ <sup>+/+</sup>). Each line depicts the change in tumor volume of one tumor over days after injection. Represents two independent experiments. PD = progressive disease (red dot), SD = stable disease (pink dot).

---

---

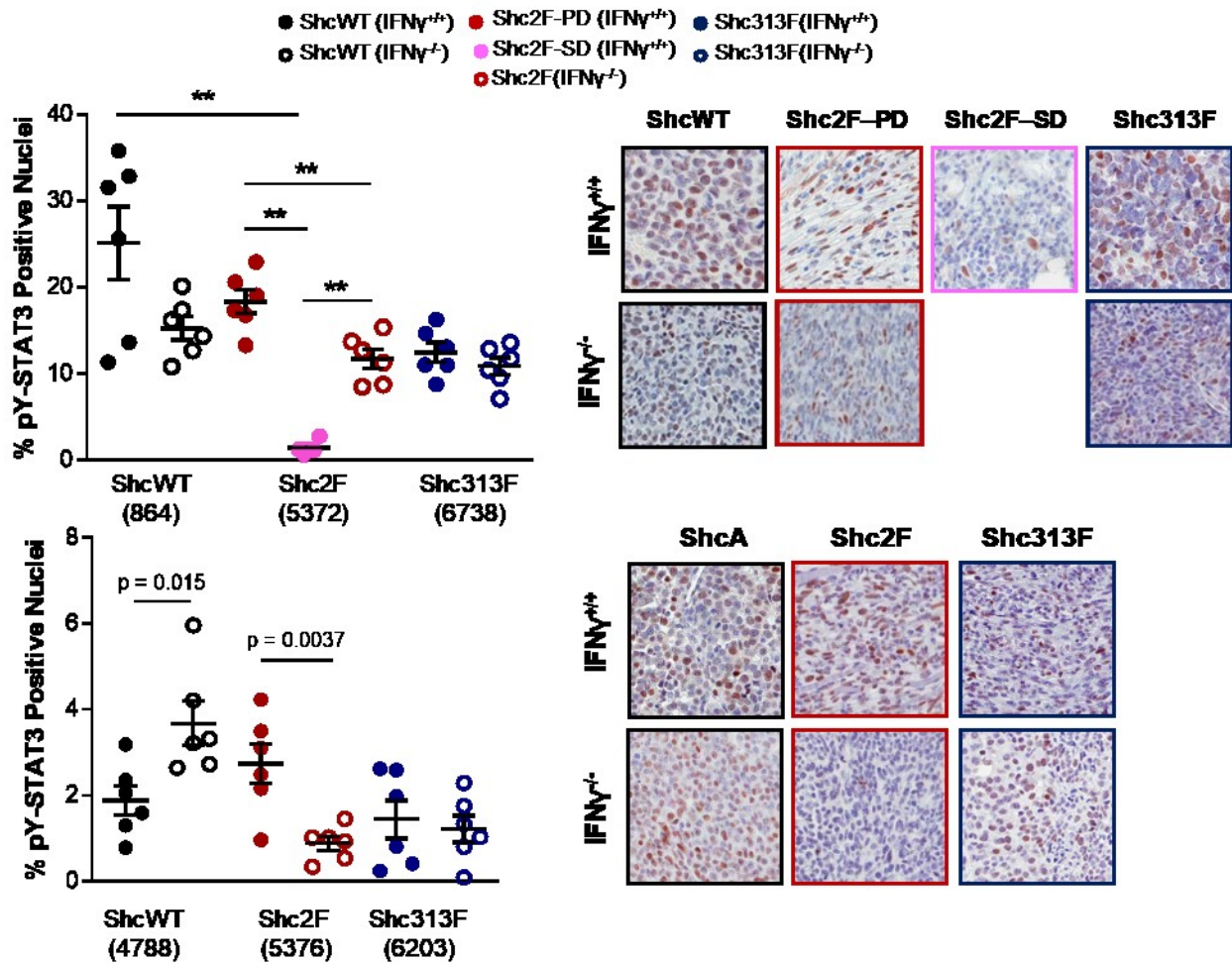


**Figure 25. Phospho-Y239/240-Shc1 promotes STAT3 signaling.**

Immunohistochemical staining of ShcWT (864, 4788), Shc2F (5372, 5376), and Shc313F (6203, 6738) mammary tumors that emerged in IFN $\gamma$ <sup>+/+</sup> or IFN $\gamma$ <sup>-/-</sup> mice using phospho-Y705-STAT3-specific antibodies (n=6–8 tumors per genotype). The mean percentage of phospho-Y705-STAT3 stained nuclei  $\pm$  s.e.m. is shown. Shc2F tumors were stratified by progressive disease (PD) or stable disease (SD) phenotypes. Representative of two independent experiments and significance was analyzed by Wilcoxon's rank-sum test (\*P = 0.05 and \*\*P = 0.01). (right panel) Representative images of phospho-Y705-STAT3-stained paraffin-embedded sections (4 $\mu$ m sections). Scale bars = 50 $\mu$ m

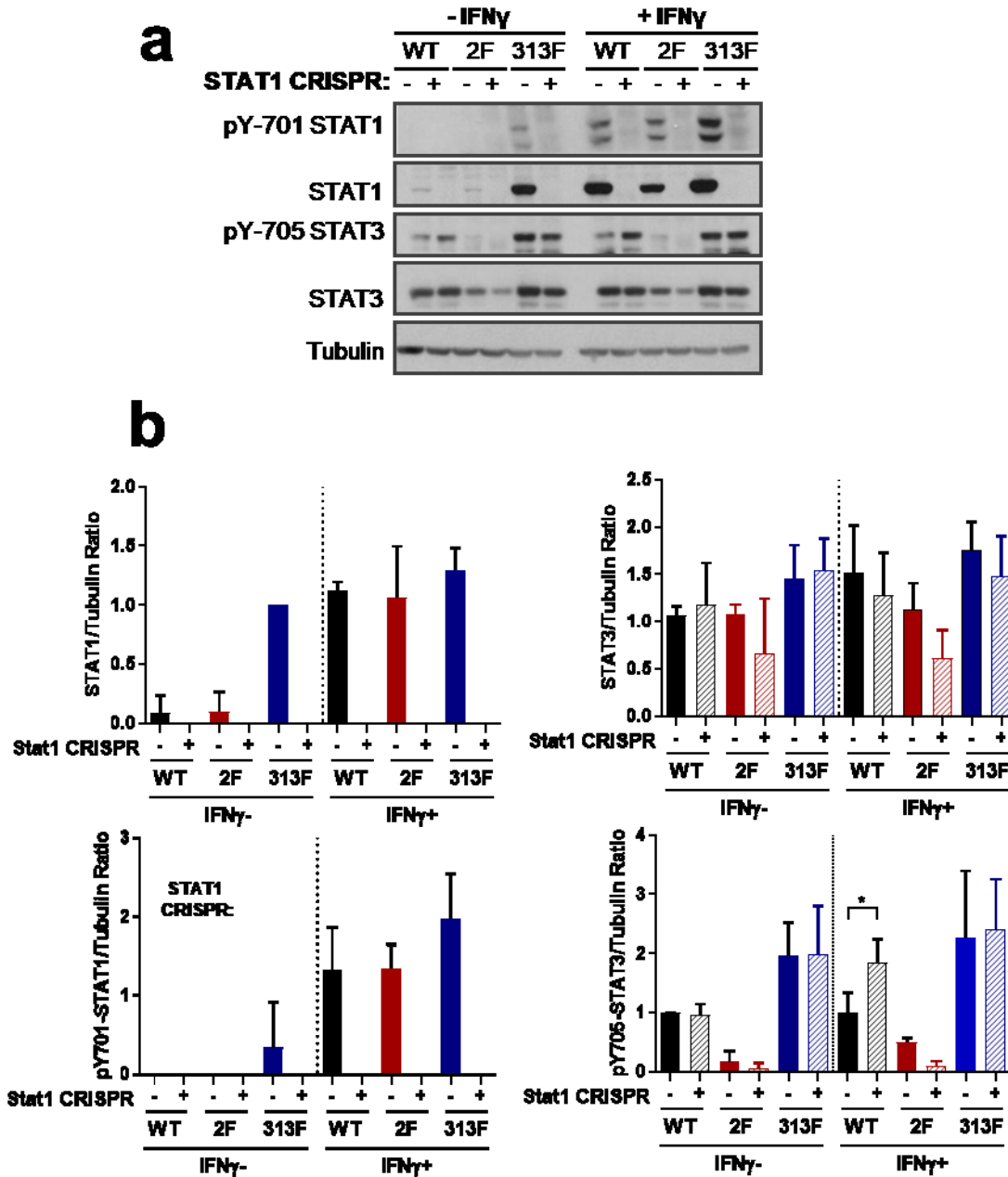


**Figure 26. STAT1 CRISPR/cas9 deletion and its impact on STAT3 activation.**

Immunoblot analysis of ShcWT (864), Shc2F (5372) and Shc313F (6738) breast cancer cell lines stably deleted of STAT1 and treated with PBS or IFN $\gamma$  (0.2 ng/ml) for 24hrs. Representative image of three independent experiments is shown.

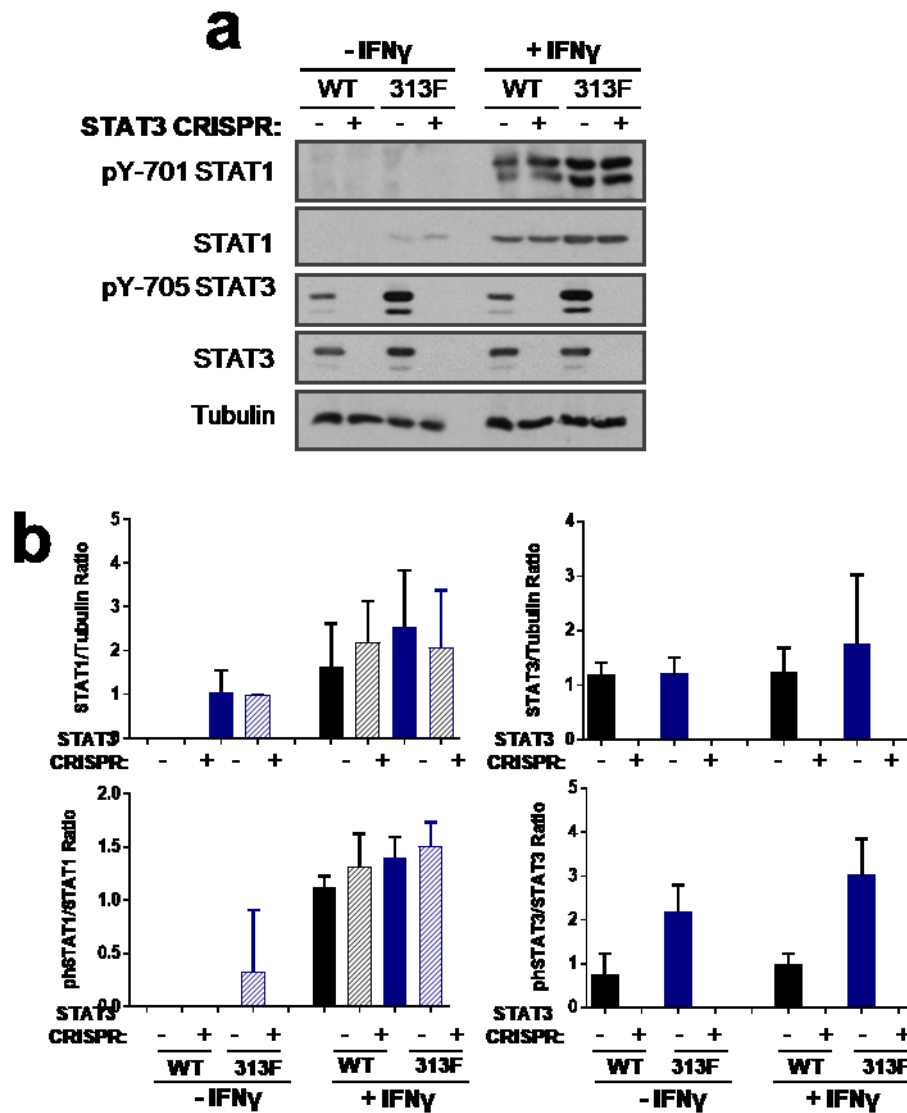


**Figure 27. STAT3 CRISPR/cas9 deletion and its impact on STAT1 activation.**

Immunoblot analysis of ShcWT (864), Shc2F (5372) and Shc313F (6738) breast cancer cell lines stably deleted of STAT3 and treated with PBS or IFN $\gamma$  (0.2 ng/ml) for 24hrs. Representative image of three independent experiments is shown.

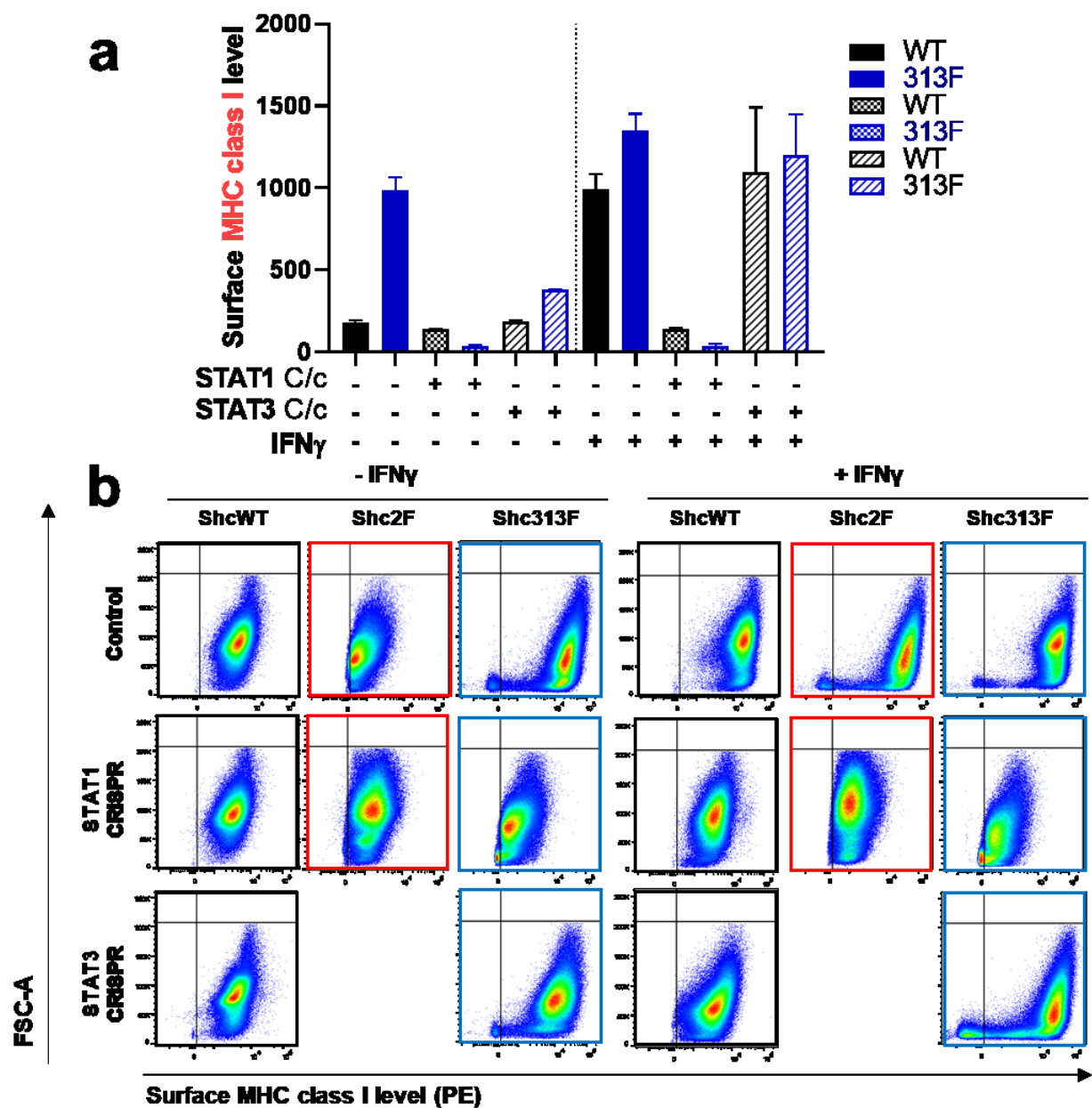


**Figure 28. Enhanced MHC class I expression due to impaired phospho-Y313-Shc1 signaling is STAT1 dependent.**

(a, b) ShcWT (864), Shc2F (5372), Shc313F (6738) cells which were deleted for STAT1 or STAT3 by CRISPR/cas9 method (C/c) as indicated were assessed for surface MHC class I expression levels by flow cytometry after 24hrs of PBS or IFN $\gamma$  treatment (0.2 ng/ml). Fluorescence from stained samples were normalized by that of unstained samples for each condition. (a) Data represented as fold change in the geometric mean  $\pm$  s.d.

relative to control cell lines for each genotype (n=6, two independent experiments). (b) Representative dot plots.

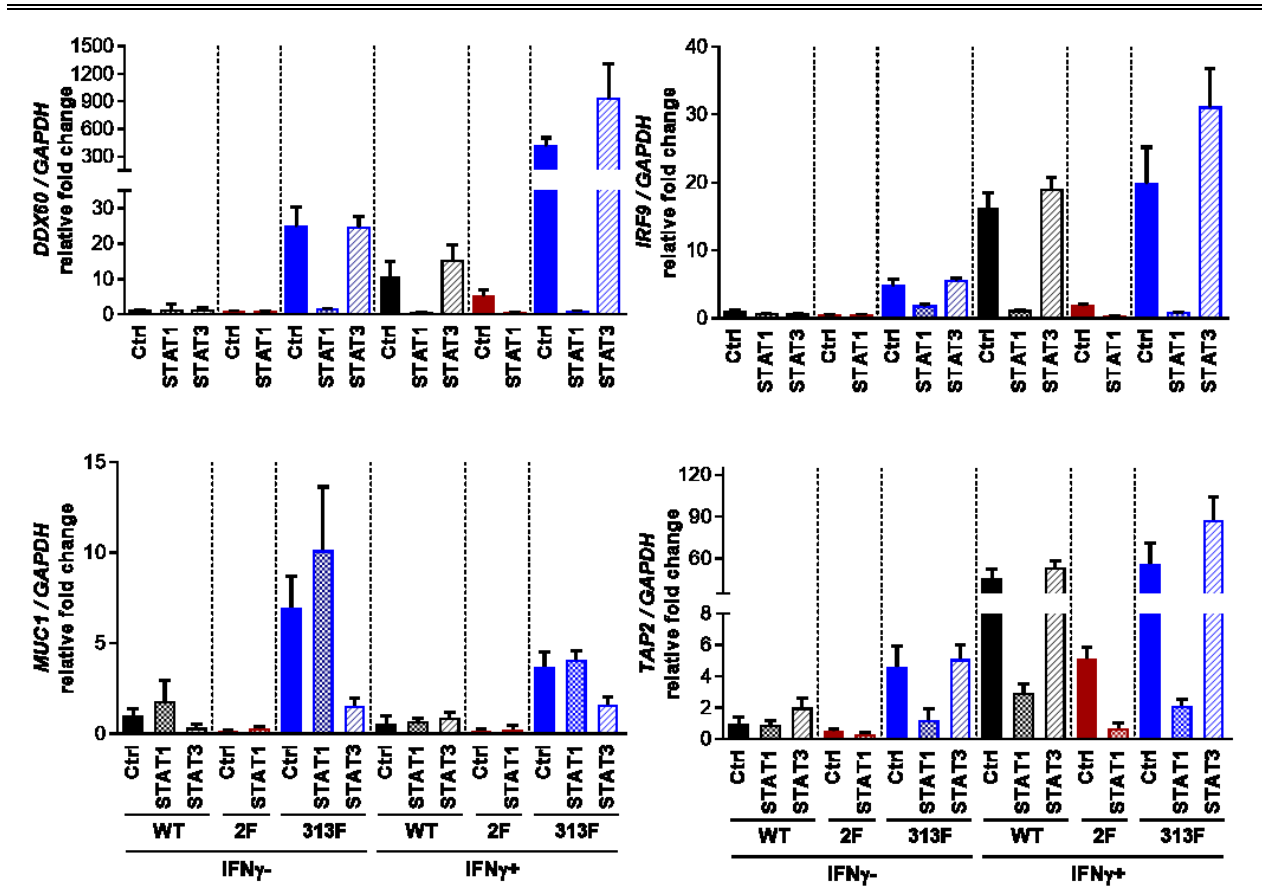


**Figure 29. IFN inducible genes upregulated upon loss of phospho-Y313-Shc1 signaling is STAT1 dependent.**

ShcWT (864), Shc2F (5372) and Shc313F (6738) breast cancer cell lines deleted for STAT1 or STAT3 by CRISPR/cas9 gene editing were treated with PBS or IFN $\gamma$  (0.2ng/ml) for 24hrs. Subsequently, RT-qPCR was performed to determine relative *IRF9*, *DDX60*, *TAP2* and *MUC1* mRNA levels, (normalized to *GAPDH* levels). The data are shown as the average fold change relative to PBS-treated ShcWT CRISPR control cells  $\pm$  s.d. (n=5 per group).

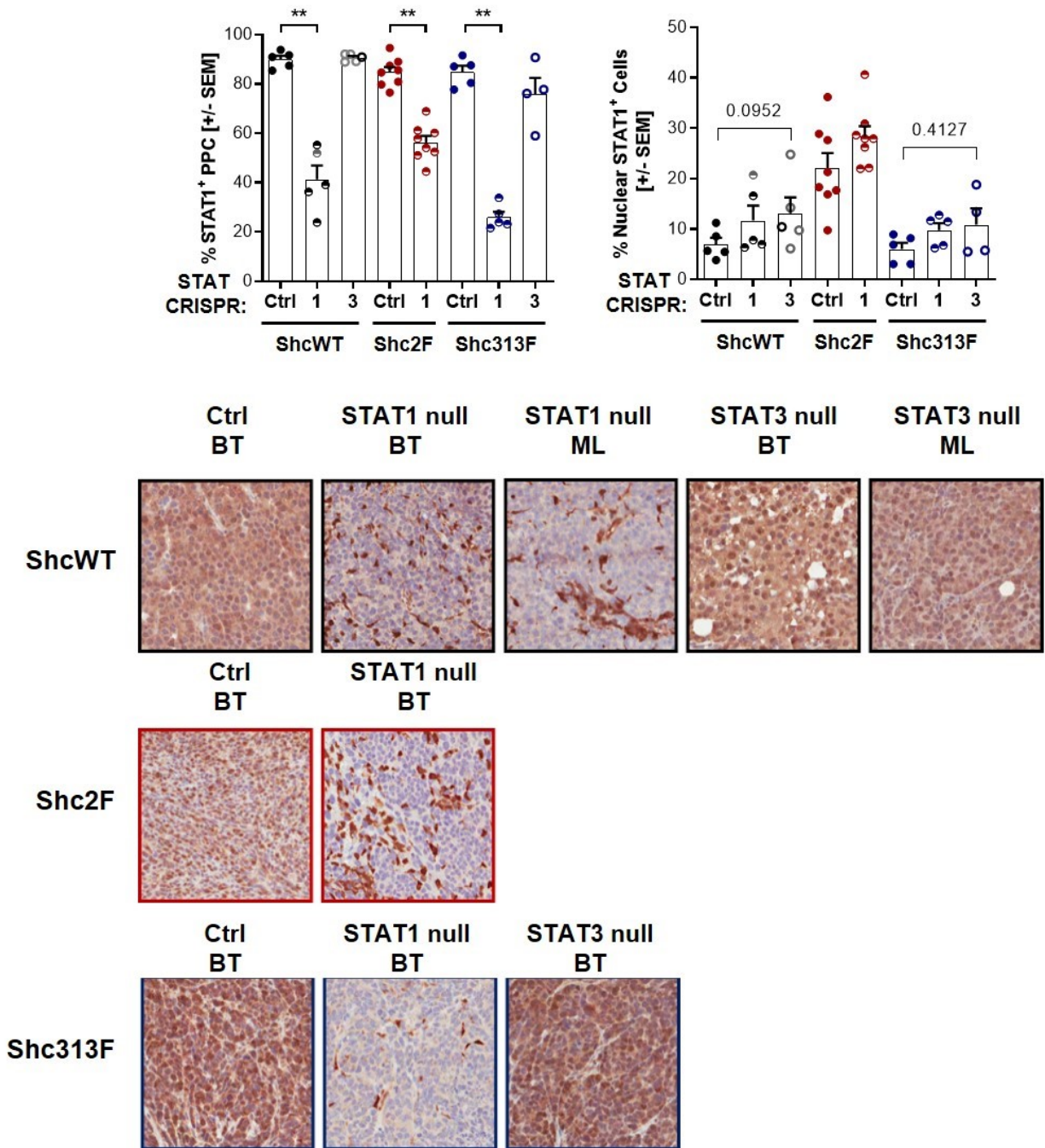


**Figure 30. Confirmation of mammary epithelial STAT1 loss in breast tumors *in vivo*.**

Control, STAT1- or STAT3- CRISPR deleted mammary tumors of ShcWT (864), Shc2F (5372), Shc313F (6738) that emerged in an immunocompetent (FVB; CD8<sup>+/+</sup>) background were analyzed for STAT1 levels by immunohistochemical staining of paraffin-embedded sections. (a) Average percentage of positive pixels (PPC) per total epithelial area ± s.e.m. (b) Average percentage of positively-stained nuclei per total epithelial area ± s.e.m.

Microscopic lesions were evaluated (grey). Significance evaluated by Wilcoxon rank-sum test (\*\*p < 0.01). (c) Representative images of immunohistochemical staining of breast tumors (BT) and microscopic lesions (ML; non-palpable) as analyzed in **a** and **b**. Both **a** and **b** are representative of 4-8 tumors. Ctrl = control.

---

---

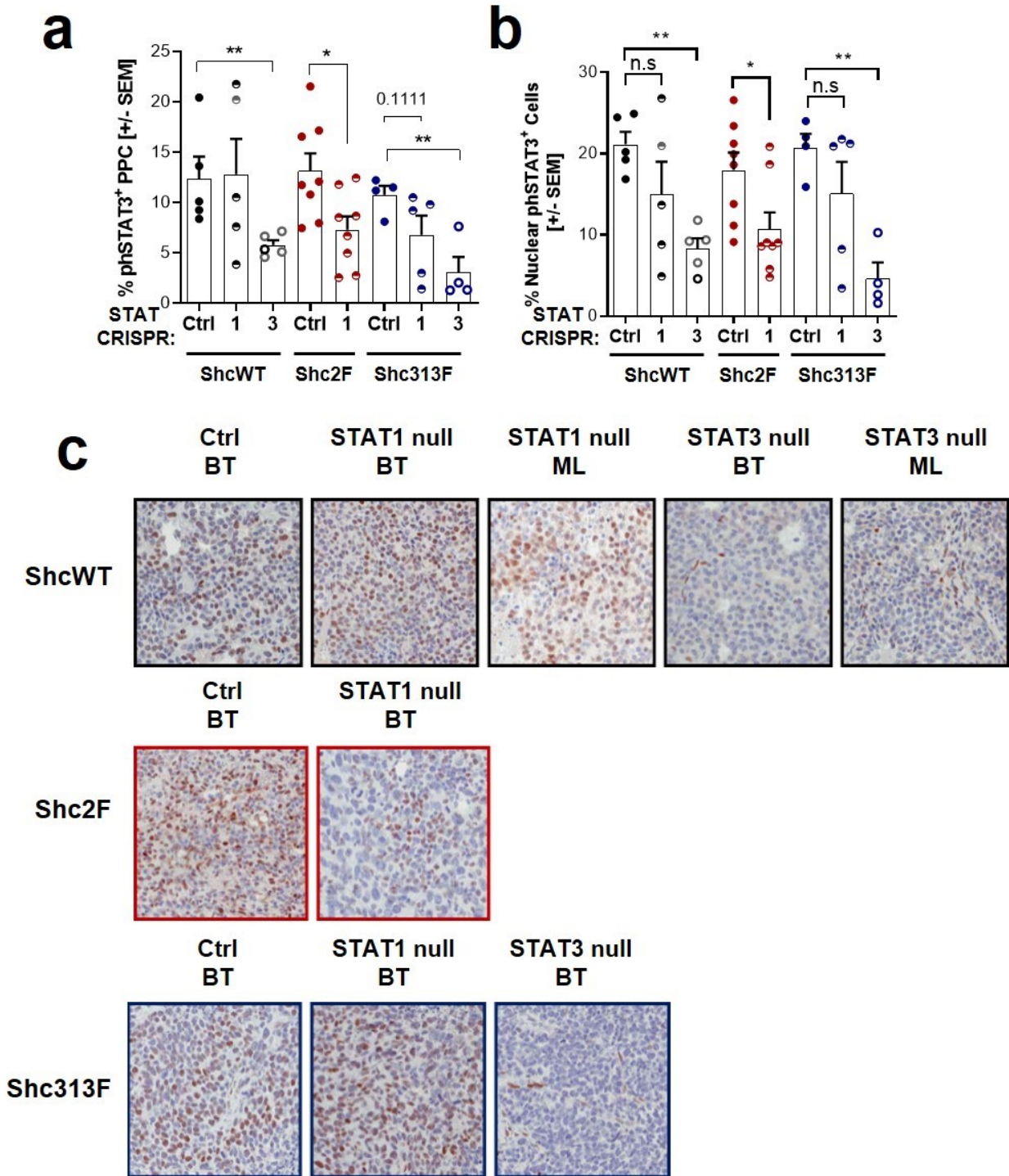


**Figure 31. Confirmation of mammary epithelial STAT3 loss in breast tumors *in vivo*.** Control, STAT1- or STAT3- CRISPR deleted mammary tumors of ShcWT (864), Shc2F (5372), Shc313F (6738) that emerged in an immunocompetent (FVB) background were

analyzed for phospho-Y705-STAT3 levels by immunohistochemical staining of paraffin-embedded sections. **(a)** Average percentage of positive pixels (PPC) per total epithelial area  $\pm$  s.e.m. **(b)** Average percentage of positively-stained nuclei per total epithelial area  $\pm$  s.e.m. Microscopic lesions were evaluated (grey). Significance evaluated by Wilcoxon rank-sum test (\*\*P < 0.01). **(c)** Representative images of immunohistochemical staining of breast tumors (BT) and microscopic lesions (ML; non-palpable) as analyzed in **a** and **b**. Both **a** and **b** are representative of 4-8 tumors. Ctrl = control.

---

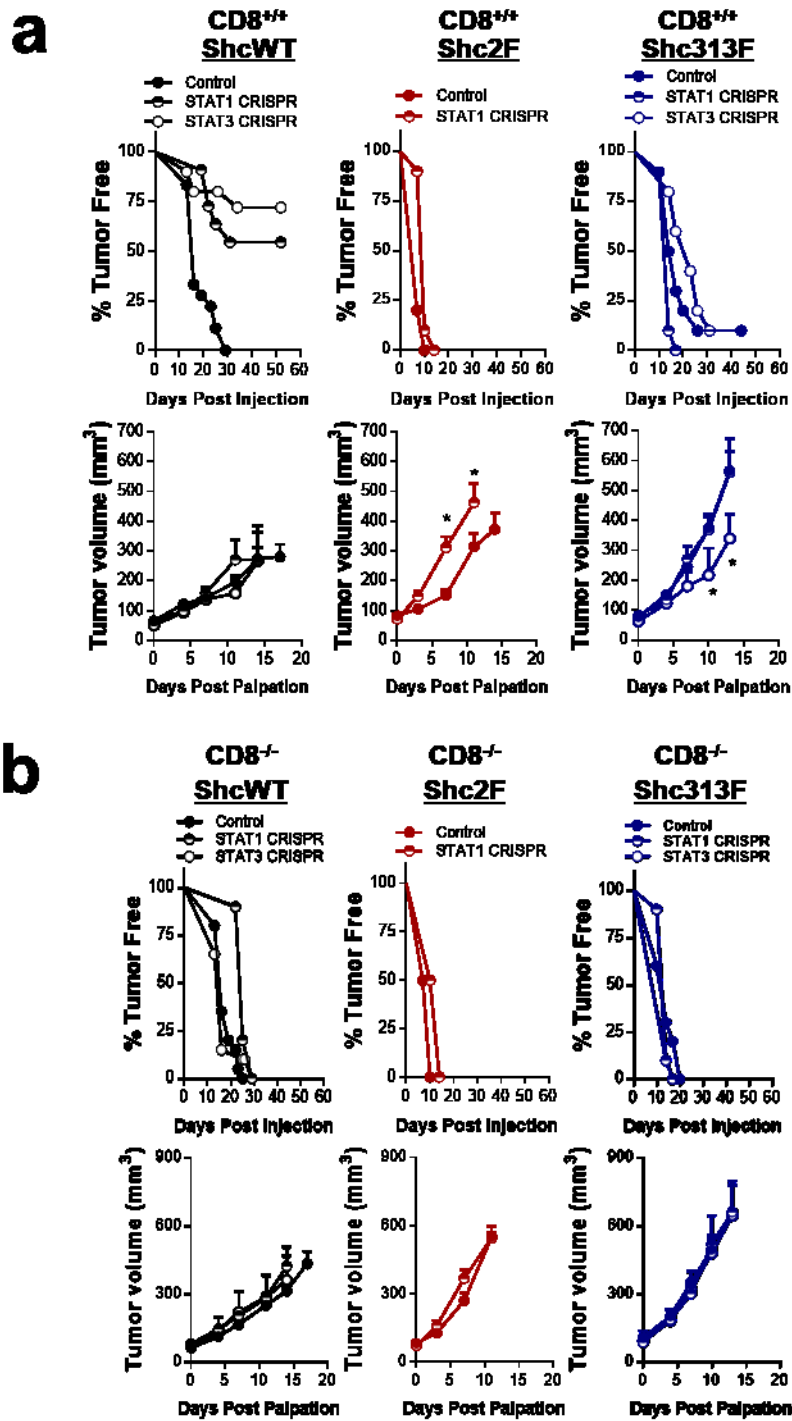
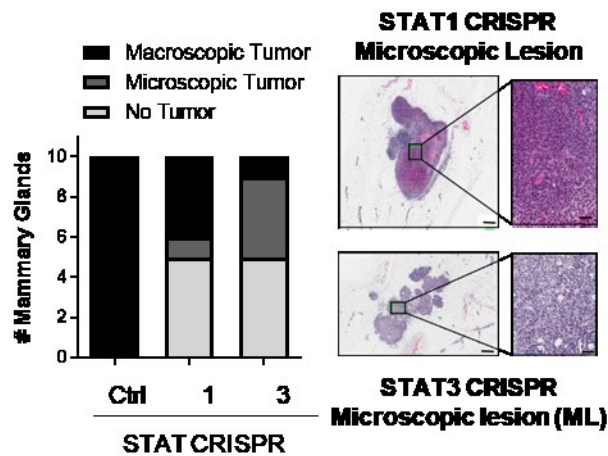


Figure 32. STAT3 promotes suppression of CTL tumor killing and STAT1 is important for CTL anti-tumor immune response upon loss of phospho-Y239/240-Shc1 signaling.

ShcWT (864), Shc2F (5372), Shc313F (6738) breast cancer cell lines deleted for STAT1 or STAT3 using CRISPR/Cas9 gene editing was injected into the fourth mammary fat pads of (a) CD8<sup>+/+</sup> or (b) CD8<sup>-/-</sup> mice. Percent tumor free glands over the days post injection were plotted (top) and tumor growth post day of tumor onset was plotted (bottom) as mean tumor volume (mm<sup>3</sup>) ± s.e.m. (n=10 tumors) (\*P=0.05 and \*\*P=0.01; one-way analysis of variance with Holm–Sidak method).



**Figure 33. STAT1 and STAT3 are both positive regulators of tumor progression in Shc1-proficient breast cancer cells in a CTL dependent manner.**

Control ShcWT (864) breast cancer cells along with its STAT1- or STAT3- deficient pooled clones were injected into the mammary fat pads of syngeneic immunocompetent CD8<sup>+/+</sup> mice. At endpoint, all animals were necropsied and the tumor burden (no tumor, unpalpable microscopic lesions or macroscopic tumors) in each mammary gland was determined by H&E staining. Representative images of microscopic lesions (ML) are shown.

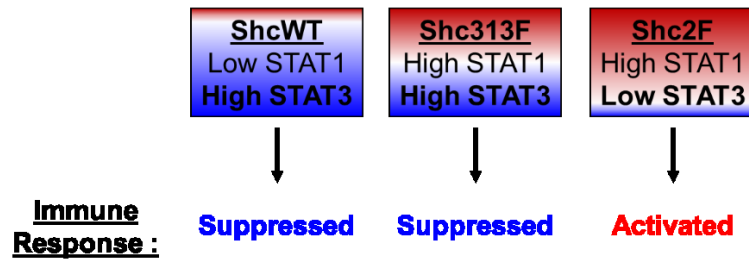
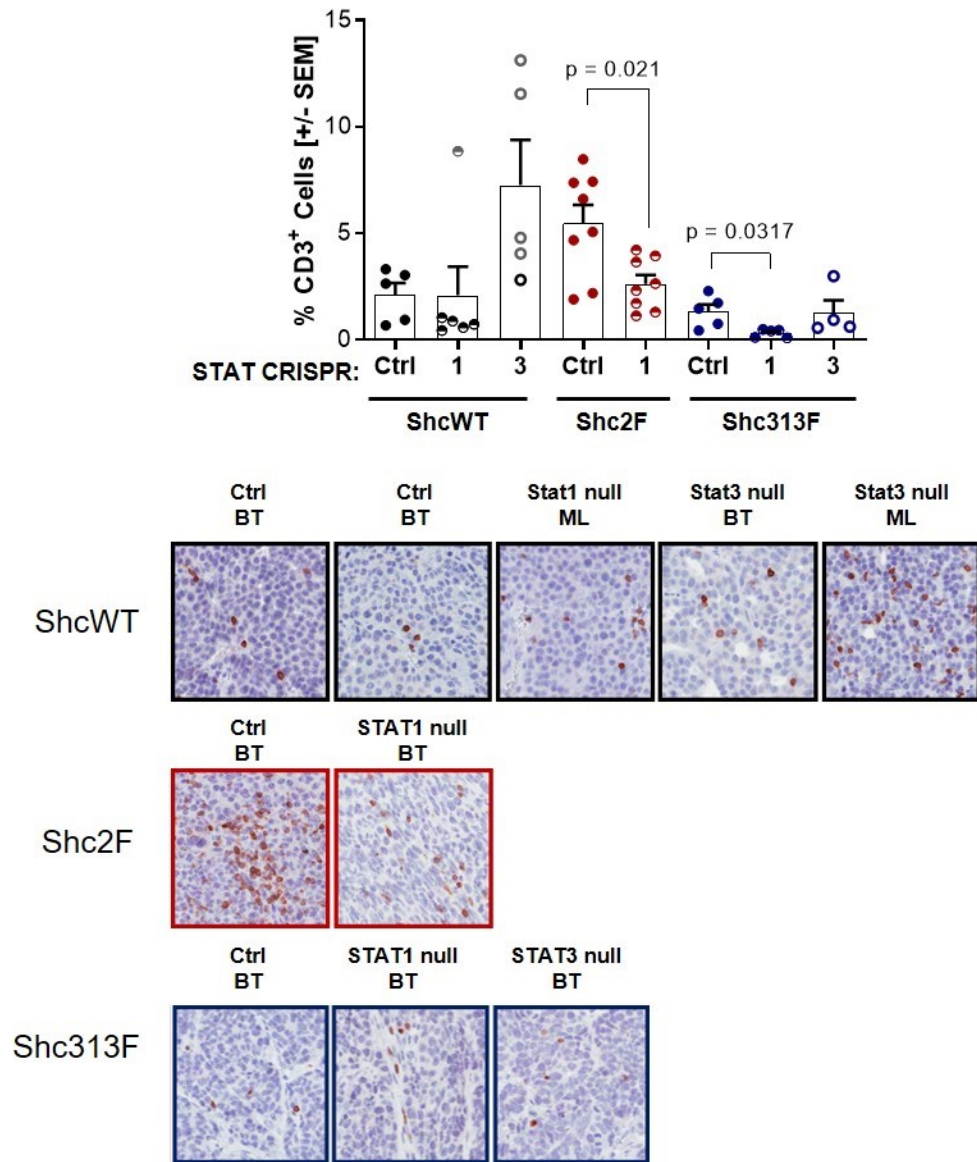
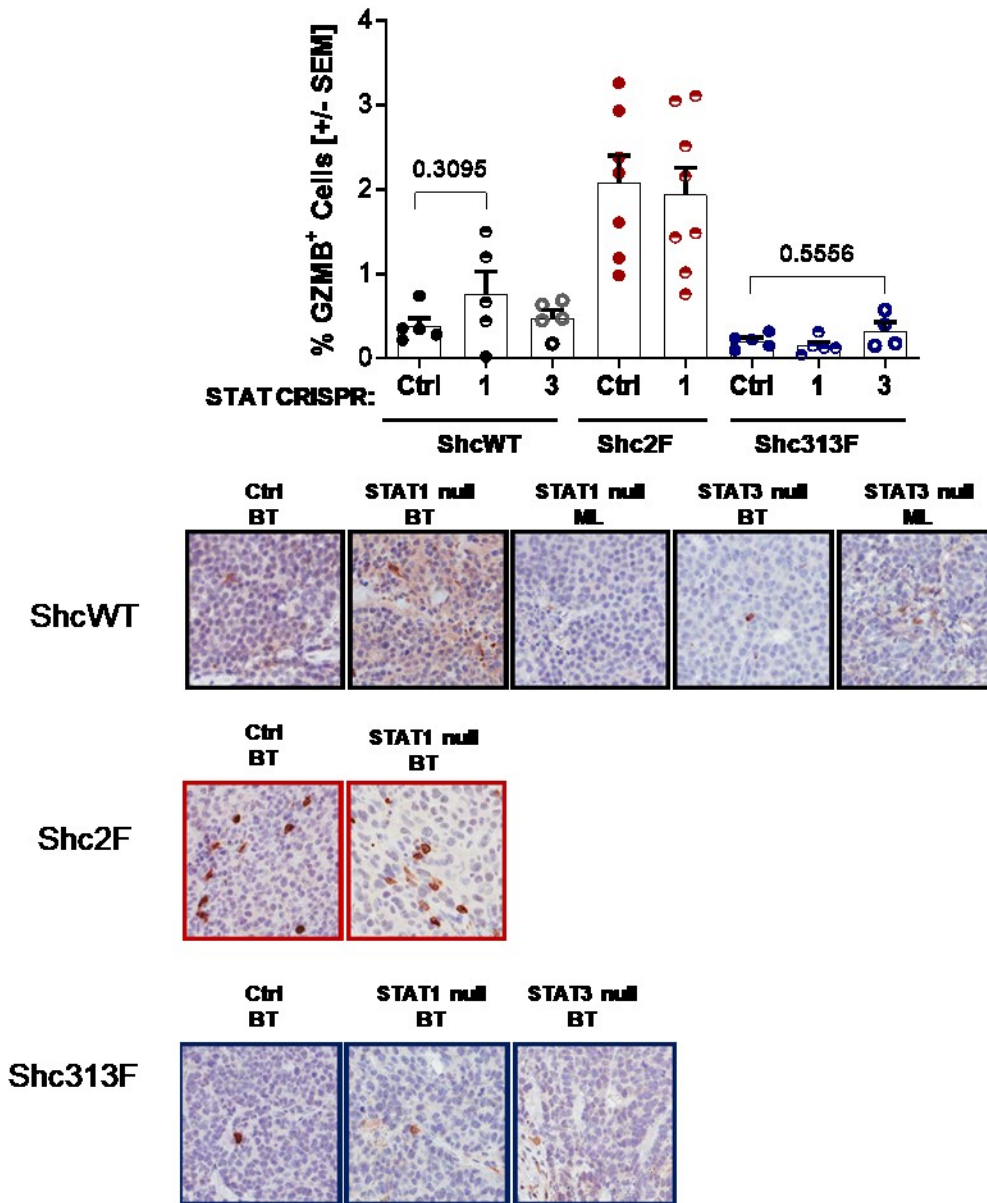


Figure 34. STAT3 activation status may dictate whether STAT1 plays pro- or anti-tumorigenic role, and Shc1 may modulates this process.

---



**Figure 35. CD3+ T cell infiltration is dependent on tumor intrinsic STAT1 activation.** Control ShcWT (864), Shc2F (5372), Shc313F (6738) tumors and their STAT1 or STAT3 deleted counterparts were assessed for CD3+ cell using immunohistochemical staining. Microscopic lesion in grey. % of positively stained cells  $\pm$  s.e.m; n=4-8 tumors. Representative images of microscopic lesions (ML) and breast tumor (BT) shown at the bottom.



**Figure 36. Increased Granzyme B+ cell infiltration in phospho-Y239/240-Shc1 deficient tumors is STAT1 independent.**

Control ShcWT (864), Shc2F (5372), Shc313F (6738) tumors and their STAT1 or STAT3 CRISPR/cas9 deleted counterparts were assessed for Granzyme B+ cell infiltration using immunohistochemical staining. Microscopic lesion is colored in grey. % of positively stained cells  $\pm$  s.e.m; n=4-8 tumors. Bottom panel: representative images of microscopic lesions (ML) and breast tumor (BT) in top panel.

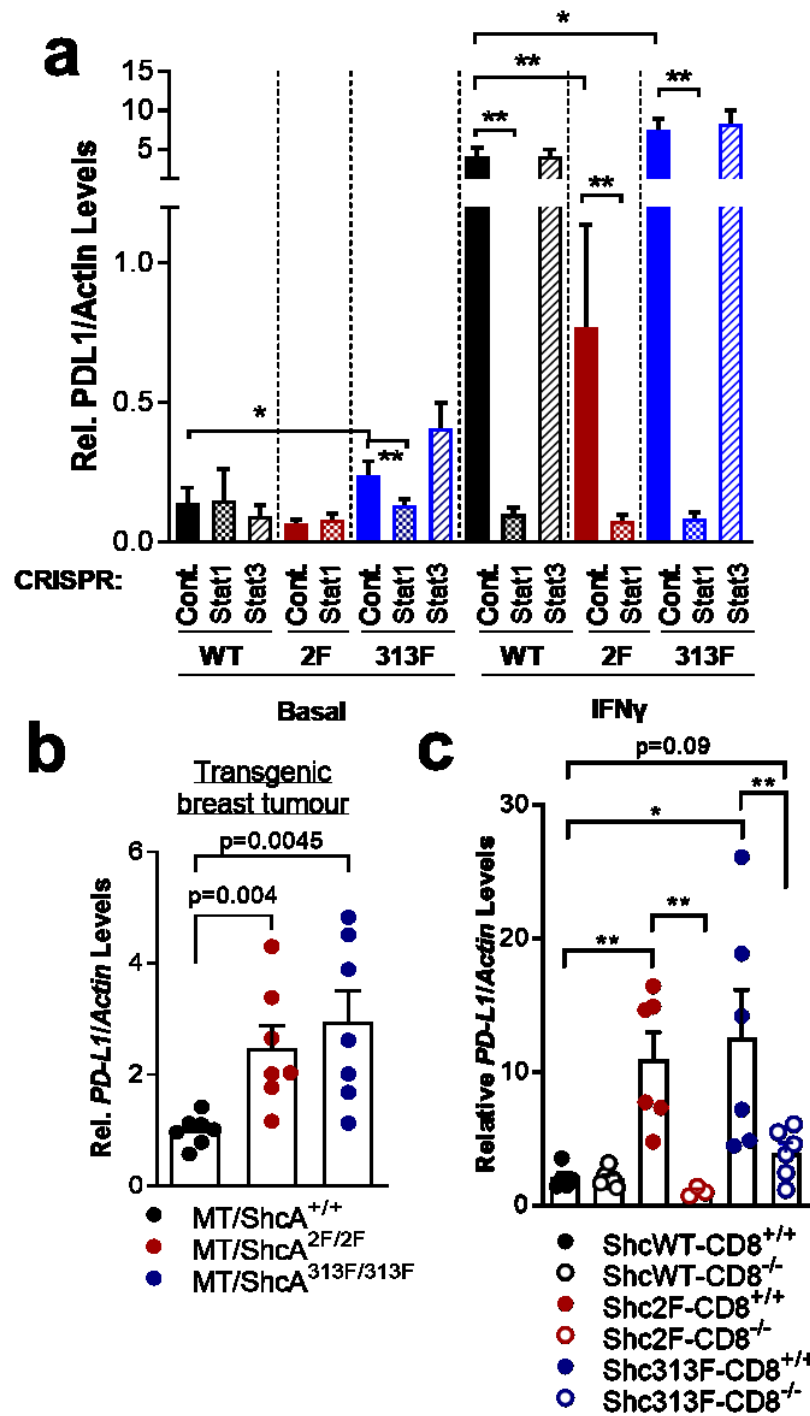
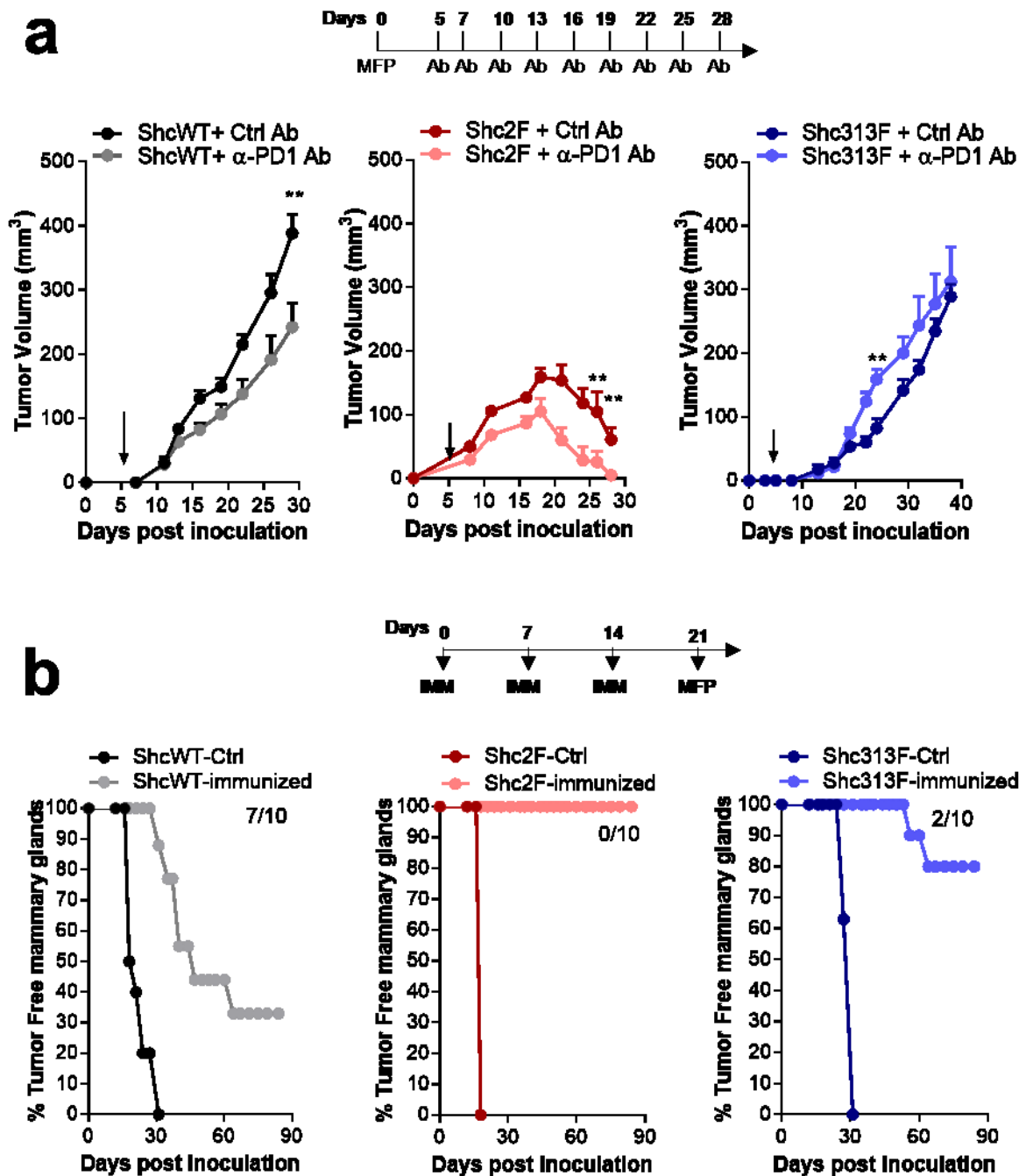


Figure 37. Loss of phospho-tyrosine Shc1 signaling leads to increased *PD-L1* expression.

(a) Control, STAT1- or STAT3-deleted cells of ShcWT (864), Shc2F (5372), Shc313F (6738) were cultured for 24hrs with PBS or IFN $\gamma$  (0.2ng/ml) and relative *PD-L1* mRNA levels were determined by RT-qPCR (normalized to *Actb* levels). Mean  $\pm$  s.d. (b) Relative *PD-L1* mRNA levels (normalized to *Actb*) were assessed by RT-qPCR in mammary tumors derived from MT/Shc1<sup>+/+</sup>, MT/Shc<sup>2F/2F</sup> and MT/Shc<sup>313F/313F</sup> transgenic mice (n=7 tumors per genotype)  $\pm$  s.e.m. (c) Relative *PD-L1* mRNA levels (normalized to *Actb*) were assessed by RT-qPCR in mammary tumors from CD8<sup>+/+</sup> and CD8<sup>-/-</sup> mice injected with breast cancer cells of the indicated genotypes: ShcWT (864), Shc2F (5372) and Shc313F (6738). Mean  $\pm$  s.e.m. n=6 tumors each (\*P=0.05 and \*\*P=0.01; unpaired two-tailed Student's t-test for a and Wilcoxon's rank-sum test for b and c).

---

---



**Figure 38. Loss of phospho-Y239/240-Shc1 signaling sensitizes tumors to immune checkpoint inhibition and tumor vaccination, while loss of phospho-Y313-Shc1 signaling sensitizes tumors to tumor vaccination.**

(a) ShcWT (864), Shc2F (5372) and Shc313F (6738) breast cancer cells were injected into mammary fat pads of immunocompetent FVB mice. On day 5, mice were treated

intraperitoneally with 100mg anti-PD-1 antibody or IgG isotype control, and every 3 days thereafter (n=10 tumors per group). Data are represented as mean tumor volume  $\pm$  s.e.m. (b) FVB mice received three intraperitoneal immunizing (IMM) injections (days 0, 7 and 14) with PBS or mitomycin C-treated breast cancer cells of the indicated genotypes (ShcWT 864, Shc2F 5372 or Shc313F 6738). On day 21, mammary fat pad (MFP) injections were performed with breast cancer cells of the same genotype used for vaccination (n=9–11 mice each). Significance was determined using multiple t-test with Holm–Sidak method (\*p=0.05 and \*\*P=0.01).

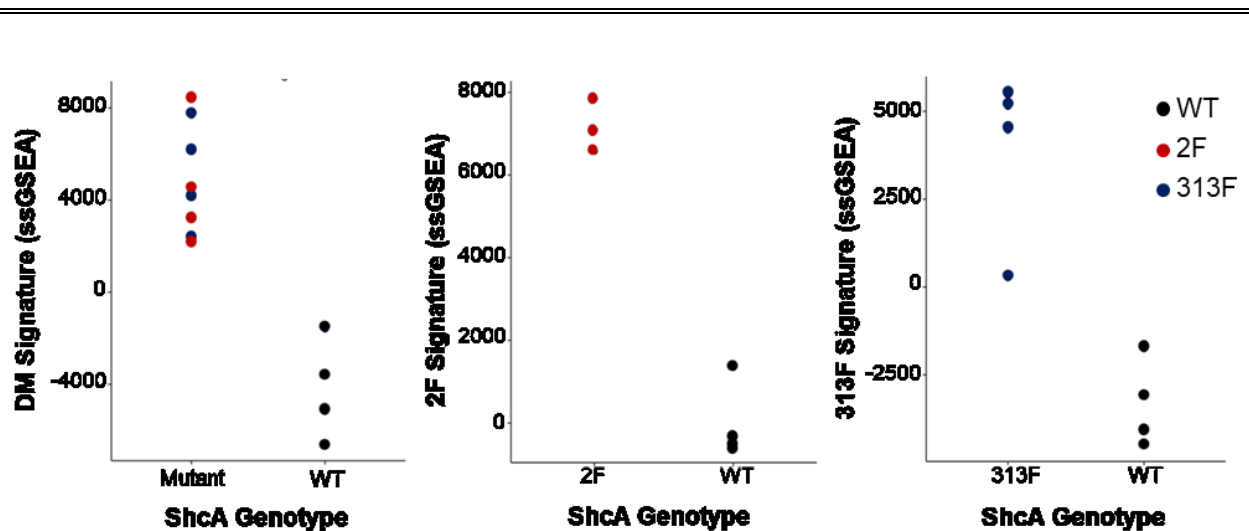


**Figure 39. Shortened DM, 2F and 313F gene signatures used for breast cancer patient TCGA analysis accurately predict their respective Shc1 genotypes in cell lines.**

Using the shortened gene list, we created Shc2F (47 out of 89 used), Shc313F (75 out of 102 used) and DE (9 out of 15 used) specific gene signatures (**Table 11-13**) which were used to stratify the TCGA human breast cancer dataset (n=1215). Subsequently, the shortened gene signature was used to obtain ssGSEA scores of ShcWT, Shc2F and Shc313F cell lines.

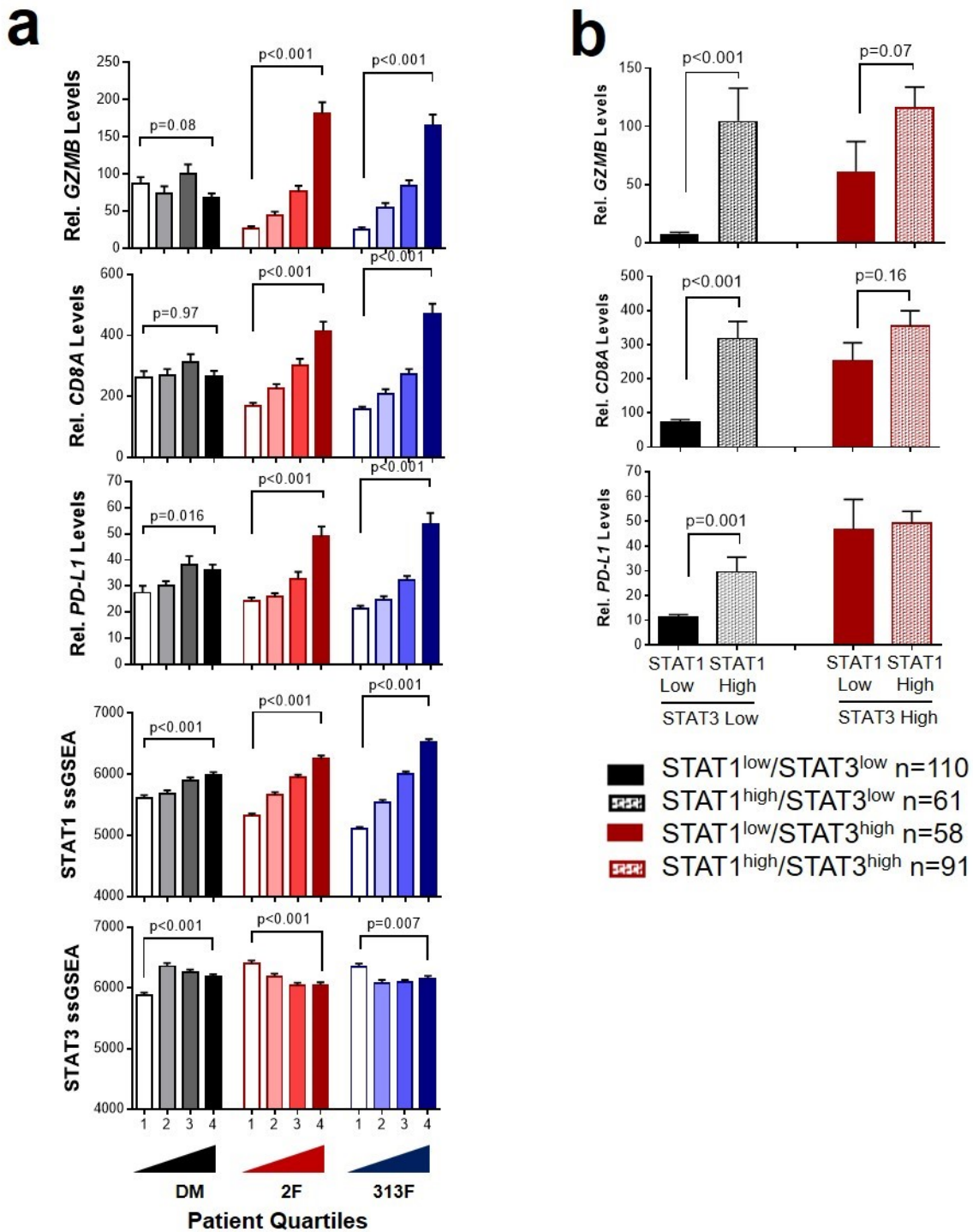


**Figure 40. Relevance of Shc1 gene signature in human breast cancer patients.**

Breast tumors from TCGA RNA-sequencing data (n=1,215) were stratified into quartiles from low to high enrichment (rank ordered by ssGSEA) of gene signatures unique to

Shc2F (2F), Shc313F (313F) and common to Shc2F and Shc313F (DM). (a) Average *GZMB*, *CD8A* and *PD-L1* mRNA levels were evaluated in each patient quartile. Data are shown as average expression levels  $\pm$  s.e.m. The average STAT1 and STAT3 ssGSEA scores were determined for tumors in each quartile. (b) Tumors (n=320) were stratified by STAT1 low/high (1<sup>st</sup>/4<sup>th</sup> quartile) and by STAT3 low/high (1<sup>st</sup>/4<sup>th</sup> quartile) based on ssGSEA scores and their relative *GZMB*, *CD8A* and *PD-L1* expression levels are plotted ( $\pm$  s.e.m.). The number of tumors included in each group indicated above the graph. Significance was determined unpaired two-tailed Student's t-test.

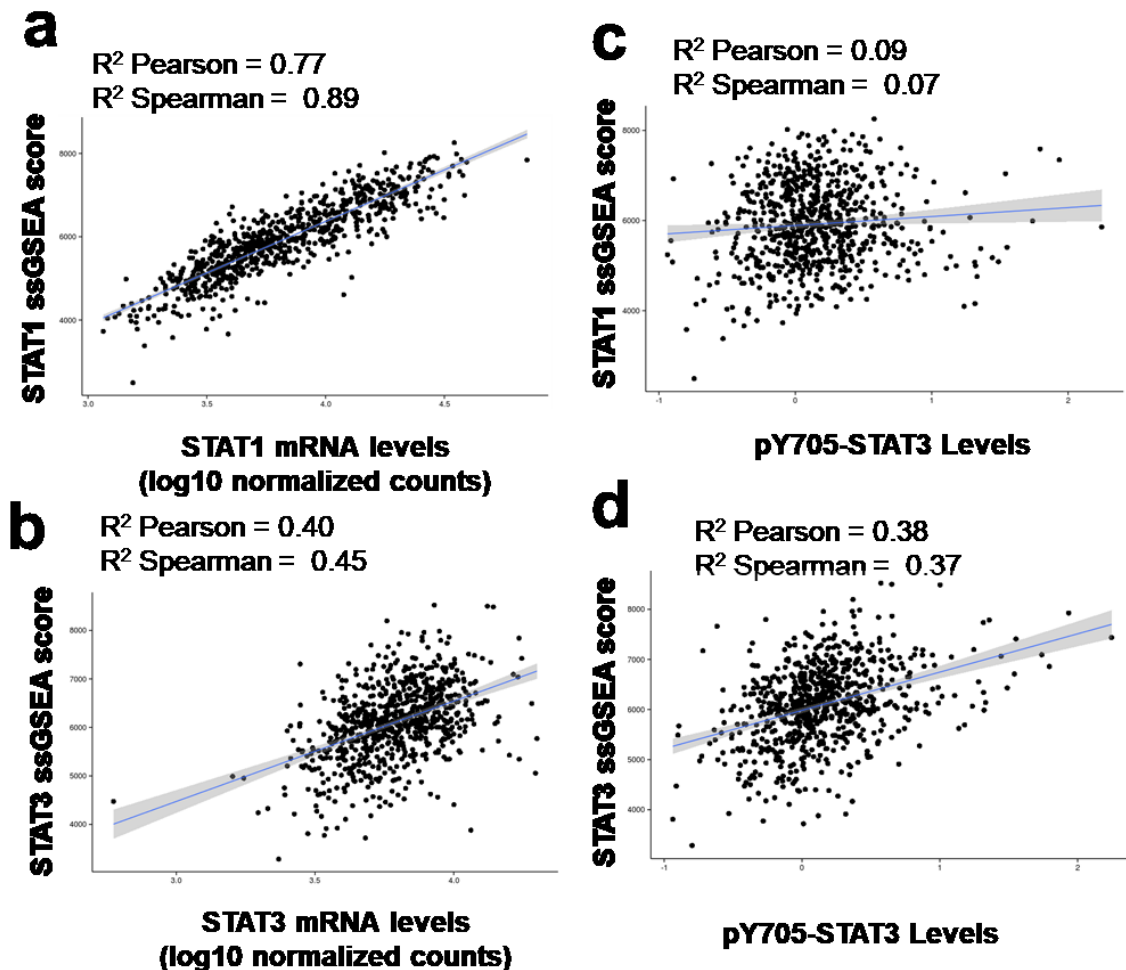


Figure 41. Positive correlation between STAT1, STAT3, phospho-Y705-STAT3 expression and their target gene transcription.

(a, b) STAT1 and STAT3 mRNA levels were evaluated in TCGA human breast tumors dataset (n=1,215) and correlated to their STAT1 and STAT3 transcriptional target gene signature (measured by ssGSEA score). (c, d) Steady state phospho-Y705-STAT3 protein levels (determined by reverse phase protein analysis) was correlated with the STAT1 or STAT3 gene signature in a subset of TCGA human breast tumors (N=747).

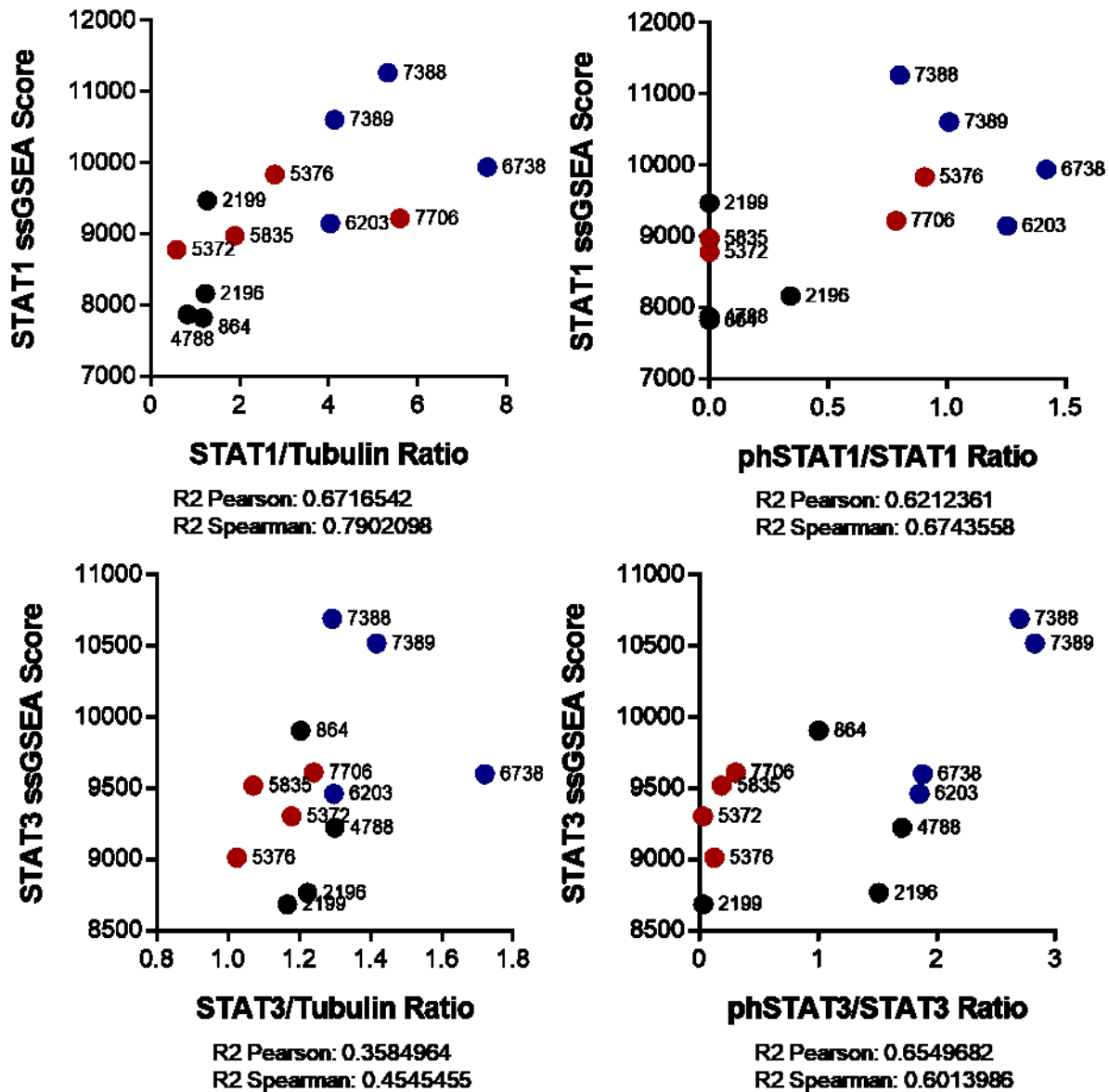


Figure 42. STAT1 and STAT3 activation status in mouse breast cancer cell lines correlate with the level of respective transcriptional target genes.

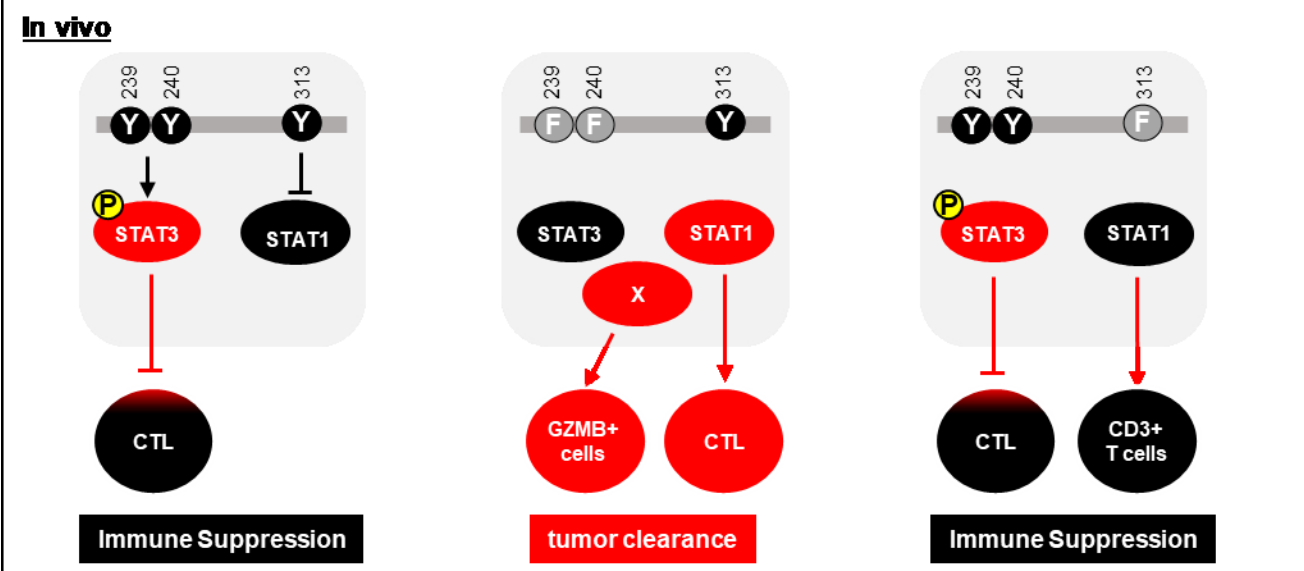
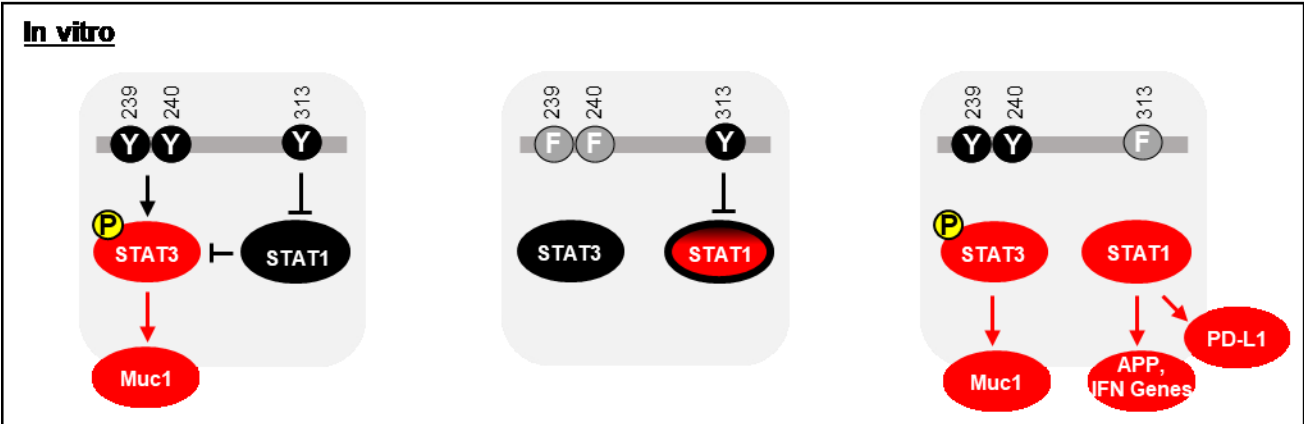
ShcWT (861, 2196, 2199, 4788; black), Shc2F (5372, 5835, 7706, 5376; red) and Shc313F (6203, 6738, 7389, 7388; blue) cells were analyzed for STAT1, tubulin, phospho-Y701-STAT1, STAT3, phospho-Y705-STAT3 level by immunoblotting (quantified in **Fig. 12**). The ratio between proteins indicated in each cell line was compared against STAT1 or STAT3 ssGSEA scores on the transcriptome (RNA-seq result) of each cell lines.

---

**pY high**

**pY239/240 deficient**

**pY313 deficient**



**Summary of STAT1 and STAT3 roles in vitro and in vivo**

<p><b>STAT1</b></p> <ul style="list-style-type: none"> <li>• does not promote T cell recruitment</li> <li>• dispensable for Gzmb+ cell recruitment</li> <li>• <b>Suppresses STAT3 activation in vitro but not in vivo</b></li> </ul> <p><b>STAT3</b></p> <ul style="list-style-type: none"> <li>• <b>inhibits T cell recruitment</b></li> <li>• <b>Required to evade CTL dependent suppression of onset</b></li> </ul>	<p><b>STAT1</b></p> <ul style="list-style-type: none"> <li>• <b>promotes T cell recruitment</b></li> <li>• <b>Required to for CTL dependent suppression of growth</b></li> <li>• dispensable for Gzmb+ cell recruitment</li> <li>• Does not suppress STAT3 activation in vitro</li> <li>• <b>promotes STAT3 activation (either tumor or stroma) in vivo</b></li> </ul>	<p><b>STAT1</b></p> <ul style="list-style-type: none"> <li>• <b>promotes T cell recruitment</b></li> <li>• dispensable for Gzmb+ cell recruitment</li> <li>• Does not regulate STAT3 activation in vitro or in vivo</li> <li>• Dispensable for CTL mediated tumor clearance</li> </ul> <p><b>STAT3</b></p> <ul style="list-style-type: none"> <li>• does not inhibit T cell recruitment</li> <li>• <b>helps evade CTL dependent suppression of growth and onset</b></li> </ul>
--	--	--

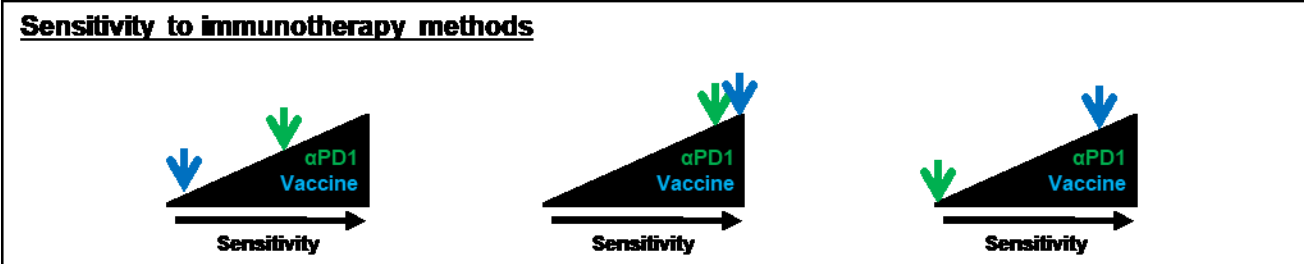


**Figure 43. Schematic diagram of Shc1 driven immunosuppression and impact on immunotherapy.**

Tumors engage Shc1 to promote STAT3 driven immunosuppression and suppress STAT1 anti-tumor killing. Impairment of phospho-Y239/240-Shc1 signaling debilitates STAT3 signaling, allowing for robust IFN $\gamma$ , STAT1, and CTL dependent anti-tumor immune responses. This is accompanied by a further enhanced response to anti-PD-1 checkpoint therapy and tumor vaccine treatment. Impaired phospho-Y313-Shc1 signaling leads to an increased STAT1-dependent upregulation of the antigen processing and presentation machinery along with increased IFN $\gamma$  transcriptional responses. This is concomitant with a parallel increased in STAT3 signaling *in vitro*. However, due to significant STAT3 signaling, tumors are immunosuppressed *in vivo* and are not responsive to anti-PD-1 checkpoint inhibition. This is circumvented in tumor vaccination strategies, which rely on an elevated STAT1 response, demonstrating a possible node for immunotherapeutic targeting for tumors displaying a high STAT1 and high STAT3 phenotype manifested by Y313-Shc1 deficient tumors. Thus, tumor intrinsic STAT3 signaling is the linchpin to upregulating STAT1 driven tumor killing.

**Table 11. Differentially regulated genes in Shc2F (n=4 cell lines) by RNA-seq.**

Upregulated in Shc2F		Downregulated in Shc2F	
mouse	human	mouse	human
<b>Pls3</b>	PLS3	<b>2610035D17Rik</b>	
<b>ERVFRD-1</b>		<b>AB339817</b>	
<b>C4orf33</b>		<b>AK051008</b>	
<b>AB344666</b>		<b>AK138383</b>	
<b>Mir100hg</b>		<b>AK208354</b>	
<b>Slc37a2</b>	SLC37A2	<b>AK210533</b>	
<b>Slco2a1</b>	SLCO2A1	<b>Anxa9</b>	ANXA9
<b>Plod2</b>	PLOD2	<b>Aph1b</b>	APH1B
<b>Efnb2</b>	EFNB2	<b>Aph1c</b>	
<b>Tsku</b>	TSKU	<b>BC019819</b>	

<b>Tnfrsf23</b>		<b>BC023719</b>	
<b>Fosb</b>	FOSB	<b>C920025E04Rik</b>	
<b>Rps18</b>	RPS18	<b>Cdh13</b>	CDH13
<b>C10orf10</b>		<b>Col11a2</b>	COL11A2
<b>Klra2</b>	KLRA1	<b>Cyp46a1</b>	CYP46A1
<b>Nipal1</b>	NIPAL1	<b>Fgfr1</b>	FGFRL1
<b>AK079527</b>		<b>Gm8909</b>	
<b>Abcb1a</b>	ABCB1	<b>H2-Q1</b>	HLA-A
<b>Abcb1b</b>		<b>H2-Q10</b>	
<b>EPHB2</b>	EPHB2	<b>H2-Q2</b>	
<b>NOCT</b>	CCRN4L	<b>H2-Q6</b>	
<b>Fosl1</b>	FOSL1	<b>H2-Q7</b>	
<b>AK205190</b>		<b>H2-T10</b>	
<b>Zbtb7c</b>	ZBTB7C	<b>Il17rb</b>	IL17RB
<b>Nol4</b>	NOL4	<b>Lifr</b>	LIFR
<b>Ltbp1</b>	LTBP1	<b>Lmx1b</b>	LMX1B
<b>Sema6b</b>	SEMA6B	<b>Lpcat2</b>	LPCAT2
<b>Rps28</b>	RPS28	<b>Med12l</b>	MED12L
<b>Rps2</b>		<b>MHC B7.2</b>	
<b>Zfp960</b>		<b>Prepl</b>	PRELP
<b>H2-T22</b>		<b>Scin</b>	SCIN
<b>H2-T23</b>		<b>Slc38a3</b>	SLC38A3
<b>G7e</b>		<b>Slc6a2</b>	SLC6A2
<b>Vars</b>	VARS	<b>Tbc1d16</b>	TBC1D16
<b>Rps2</b>	RPS2	<b>Tfap2b</b>	TFAP2B
<b>H2-T9</b>	HLA-F	<b>Trpv4</b>	TRPV4
<b>hmga1</b>		<b>Wdr5b</b>	WDR5B
<b>hmga1</b>		<b>Zfp40</b>	
<b>Hmga1</b>	HMGA1		
<b>DYNLT1</b>	DYNLT1		

<b>Tmem181b-ps</b>			
<b>EVA1C</b>			
<b>CDHR1</b>	CDHR1		
<b>Hmga1-rs1</b>			
<b>AK005678</b>			
<b>BC098228</b>			
<b>Rspo3</b>	RSPO3		
<b>hmga2</b>	HMGA2		
<b>Hmga2-ps1</b>			
<b>AK155734</b>			
<b>Slc21a2</b>			

**Table 12. Differentially regulated genes in Shc313F (n=4 cell lines) by RNA-seq.**

<b>Upregulated in Shc313F</b>		<b>Downregulated in Shc313F</b>	
<b>mouse</b>	<b>human</b>	<b>mouse</b>	<b>human</b>
<b>2010002M12Rik</b>		<b>Krt14</b>	KRT14
<b>6030419C18Rik</b>		<b>Espn</b>	ESPN
<b>A330035P11Rik</b>		<b>Frmd7</b>	FRMD7
<b>Adamts2</b>	ADAMTS2	<b>Lama3</b>	LAMA3
<b>AI607873</b>		<b>Lmo7</b>	LMO7
<b>Aif1l</b>	AIF1L	<b>Eva1a</b>	
<b>AK053109</b>		<b>Tex2</b>	TEX2
<b>Ank2</b>	ANK2	<b>2610018G03Rik</b>	MST4
<b>Apol9a</b>		<b>Efhd1</b>	EFHD1
<b>Apol9b</b>		<b>Fam83g</b>	FAM83G
<b>Bach2</b>	BACH2	<b>Fgfbp1</b>	FGFBP1
<b>Bst2</b>	BST2	<b>Gna15</b>	GNA15
<b>Cd1d1</b>	CD1D	<b>Gnai1</b>	GNAI1
<b>Clic6</b>	CLIC6	<b>Ppfia3</b>	PPFIA3

<b>Cml2</b>		<b>Casz1</b>	CASZ1
<b>Cmpk2</b>	CMPK2	<b>Nr1h5</b>	
<b>Cmtm3</b>	CMTM3	<b>Sema5a</b>	SEMA5A
<b>Coro2b</b>	CORO2B	<b>Slc5a10</b>	SLC5A10
<b>Dcdc2a</b>			
<b>Ddah1</b>	DDAH1		
<b>Ddit3</b>	DDIT3		
<b>Ddx60</b>	DDX60		
<b>Dhx58</b>	DHX58		
<b>Eif2ak2</b>	EIF2AK2		
<b>Epsti1</b>	EPSTI1		
<b>Flrt2</b>	FLRT2		
<b>Fndc1</b>	FNDC1		
<b>Gadd45a</b>	GADD45A		
<b>Gadd45g</b>	GADD45G		
<b>Gbp2</b>	GBP2		
<b>Gbp3</b>	GBP3		
<b>Gbp7</b>	GBP7		
<b>Gdpd3</b>	GDPD3		
<b>Gm11149</b>			
<b>Golm1</b>	GOLM1		
<b>Gria4</b>	GRIA4		
<b>Helz2</b>			
<b>Ifi203</b>			
<b>Ifi204</b>			
<b>Ifi44</b>	IFI44		
<b>Ifi47</b>			
<b>Ifih1</b>	IFIH1		
<b>Ifit1</b>	IFIT1		
<b>Igtp</b>			

<b>Irf7</b>	IRF7		
<b>Irf9</b>	IRF9		
<b>Irgm1</b>	IRGM		
<b>Irgm2</b>			
<b>Isg15</b>	ISG15		
<b>Mnda</b>	MNDA		
<b>Mndal</b>			
<b>MUC1</b>	MUC1		
<b>Mx2</b>	MX2		
<b>Ncam1</b>	NCAM1		
<b>Nexn</b>	NEXN		
<b>Oas1a</b>	OAS1		
<b>Oas1b</b>			
<b>Oas1g</b>			
<b>Oas1l</b>	OASL		
<b>Olfml3</b>			
<b>Parp12</b>	PARP12		
<b>Pea15a</b>	PEA15		
<b>Pear1</b>	PEAR1		
<b>Psmb8</b>	PSMB8		
<b>Ptprn</b>	PTPRN		
<b>Rmdn2</b>			
<b>Rsad2</b>	RSAD2		
<b>Rtp4</b>	RTP4		
<b>Sdc3</b>	SDC3		
<b>Sftpd</b>	SFTPD		
<b>Sipa1l2</b>	SIPA1L2		
<b>Slfn2</b>			
<b>Soga2</b>			
<b>STAT1</b>	STAT1		

<b>Tgtp1</b>			
<b>Tnfsf10</b>	TNFSF10		
<b>Trim21</b>	TRIM21		
<b>Trim34b</b>			
<b>Usp18</b>	USP18		
<b>Wisp1</b>	WISP1		
<b>Xaf1</b>	XAF1		
<b>Zbp1</b>	ZBP1		
<b>Zfp467</b>	ZNF467		
<b>Zfp612</b>	ZNF23		

**Table 13. Differentially regulated genes in both Shc2F and Shc313F by RNA-seq.**

<b>Commonly upregulated in Shc2F and Shc313F cells</b>		<b>Commonly downregulated in Shc2F and Shc313F cells</b>	
<b>Mouse</b>	<b>Human</b>	<b>Mouse</b>	<b>Human</b>
<b>Agpat4</b>	AGPAT4	<b>1700003D09Rik</b>	
<b>Apcdd1</b>	APCDD1	<b>C130021I20Rik</b>	
<b>Cd1d2</b>		<b>Col9a1</b>	COL9A1
<b>Cxzc5</b>	CXXC5	<b>Ppp1r1b</b>	PPP1R1B
<b>Gm4349</b>		<b>Rps3a1</b>	
<b>Gng11</b>	GNG11	<b>Tmod4</b>	TMOD4
<b>Ifi202b</b>			
<b>Slfn8</b>	SLFN11		
<b>Stbd1</b>	STBD1		

**Table 14. IFN $\alpha$ , IFN $\beta$ , and IFN $\gamma$  protein levels detected by ELISA in the supernatants of ShcWT, Shc2F and Shc313F cells in culture (n=3-4 wells per cell line).**

	Cells	IFN $\alpha$ (pg/ml) average	IFN $\alpha$ (pg/ml) std dev	IFN $\beta$ (pg/ml) average	IFN $\beta$ (pg/ml) std dev	IFN $\gamma$ (pg/ml) average	IFN $\gamma$ (pg/ml) std dev
<b>ShcWT</b>	864	0	0	12.53	1.57	0	0
	4788	0	0	8.12	0.55	0	0
	2196	0	0	14.31	0.56	0	0
	2199	0	0	6.24	0.4	0	0
<b>Shc2F</b>	5372	0	0	9.24	0.69	0	0
	5835	0	0	9.21	1.04	0	0
	7706	0	0	16.45	0.8	0	0
	7707	0	0	9.62	0.64	0	0
<b>Shc313F</b>	6203	0	0	11.79	1.11	0	0
	6738	0	0	11.33	0.93	0	0
	7388	0	0	10.27	1.9	0	0
	7389	0	0	23.52	3.52	0	0

Std dev= standard deviation

**Table 15. Number of reads of IFN genes in ShcWT, Shc2F and Shc313F cells based on RNA-seq analysis.**

Gene	ShcWT				Shc2F				Shc313F			
	864	2196	2199	4788	5372	5376	5835	7706	6203	6738	7388	7389
<b>Ifna1</b>	0	0	0	0	0	0	0	0	0	0	0	0
<b>Ifna2</b>	0	0	0	0	0	0	0	0	0	0	0	0
<b>Ifna4</b>	0	2	0	0	0	0	0	2	2	2	5	4
<b>Ifna5</b>	0	0	0	0	0	0	0	0	0	0	0	0
<b>Ifna6</b>	0	0	0	0	0	0	0	0	0	0	0	0

<b>Ifna7</b>	0	0	0	0	0	0	0	0	0	0	0	0
<b>Ifna9</b>	0	0	0	0	0	0	0	0	0	0	0	0
<b>Ifna14</b>	0	0	0	0	0	0	0	0	0	0	0	0
<b>Ifnb1</b>	0	0	1	0	0	0	2	0	0	6	7	15
<b>IFN<math>\gamma</math></b>	0	0	0	0	0	0	0	0	0	0	0	0

**Table 16. List of STAT1 target genes that define the STAT1 ssGSEA signature.**

<b>Gene</b>	<b>Score*</b>	<b>References**</b>
<b>STAT1</b>	1	(Bhinge et al., 2007; Chawla et al., 2013; QIAGEN, 2015; Satoh and Tabunoki, 2013)
<b>PARP14</b>	0.83059951	(Bhinge et al., 2007)
<b>CXCL10</b>	0.79534805	(Satoh and Tabunoki, 2013)
<b>PARP9</b>	0.79338464	(Bhinge et al., 2007; Satoh and Tabunoki, 2013; TFsearcher, 2015)
<b>TAP1</b>	0.78190277	(Satoh and Tabunoki, 2013; TFsearcher, 2015)
<b>GBP5</b>	0.75997402	(Satoh and Tabunoki, 2013)
<b>MX1</b>	0.71665641	(Satoh and Tabunoki, 2013)
<b>DTX3L</b>	0.71112409	(Bhinge et al., 2007; Satoh and Tabunoki, 2013; TFsearcher, 2015)
<b>GBP1</b>	0.71097103	(Satoh and Tabunoki, 2013)
<b>NLRC5</b>	0.68864493	(Wang et al., 2010)
<b>AIM2</b>	0.68719323	(Satoh and Tabunoki, 2013)
<b>ZBP1</b>	0.68547864	(QIAGEN, 2015)
<b>TAP2</b>	0.6848176	(Satoh and Tabunoki, 2013)
<b>BATF2</b>	0.68213951	(Bhinge et al., 2007; Satoh and Tabunoki, 2013)
<b>IDO1</b>	0.67601428	(Satoh and Tabunoki, 2013)
<b>CXCL9</b>	0.67269701	(Satoh and Tabunoki, 2013)
<b>PSMB9</b>	0.65108485	(Satoh and Tabunoki, 2013)

<b>IRF9</b>	0.64794506	(Chawla et al., 2013; Satoh and Tabunoki, 2013; TFsearcher, 2015; Wang et al., 2010)
<b>PLSCR1</b>	0.64664812	(Bhinge et al., 2007; Chawla et al., 2013; Satoh and Tabunoki, 2013)
<b>APOL6</b>	0.63641934	(Bhinge et al., 2007; Satoh and Tabunoki, 2013)
<b>CCRN4L</b>	0.63529631	(Satoh and Tabunoki, 2013; Wang et al., 2010)
<b>APOL1</b>	0.62604301	(Satoh and Tabunoki, 2013)
<b>IFI27</b>	0.6189761	(Satoh and Tabunoki, 2013; TFsearcher, 2015)
<b>TRIM21</b>	0.58228556	(Satoh and Tabunoki, 2013)
<b>IRF1</b>	0.57598741	(Satoh and Tabunoki, 2013; Wang et al., 2010),(Bhinge et al., 2007; Chawla et al., 2013)
<b>NMI</b>	0.56423296	(Satoh and Tabunoki, 2013; TFsearcher, 2015)
<b>PSMB8</b>	0.55738005	(Satoh and Tabunoki, 2013; TFsearcher, 2015)
<b>PDCD1LG2</b>	0.54932666	(Satoh and Tabunoki, 2013; Wang et al., 2010)
<b>RTP4</b>	0.53875957	(TFsearcher, 2015)
<b>CIITA</b>	0.4689531	(Satoh and Tabunoki, 2013)
<b>BRCA2</b>	0.45651856	(Bhinge et al., 2007; Satoh and Tabunoki, 2013)
<b>APOL3</b>	0.44997339	(Satoh and Tabunoki, 2013)
<b>CXCL13</b>	0.44906025	(QIAGEN, 2015; Satoh and Tabunoki, 2013)
<b>WIPF1</b>	0.44532865	(Satoh and Tabunoki, 2013; Wang et al., 2010)
<b>IFI35</b>	0.43718503	(Bhinge et al., 2007; Satoh and Tabunoki, 2013; TFsearcher, 2015)
<b>BST2</b>	0.43643893	(Bhinge et al., 2007; Satoh and Tabunoki, 2013)
<b>TMEM140</b>	0.43144908	(Satoh and Tabunoki, 2013; TFsearcher, 2015)
<b>LGALS3BP</b>	0.42831041	(Satoh and Tabunoki, 2013; TFsearcher, 2015)
<b>IDO2</b>	0.42663042	(Satoh and Tabunoki, 2013)
<b>IFI16</b>	0.38574132	(Bhinge et al., 2007; Chawla et al., 2013; Satoh and Tabunoki, 2013)
<b>IL15RA</b>	0.36595285	(QIAGEN, 2015; Satoh and Tabunoki, 2013)

<b>MTHFD2</b>	0.34958656	(Bhinge et al., 2007; Satoh and Tabunoki, 2013; Wang et al., 2010)
<b>TOP1</b>	0.34441541	(Satoh and Tabunoki, 2013; Wang et al., 2010)
<b>KIF2A</b>	0.34239429	(QIAGEN, 2015; Satoh and Tabunoki, 2013; Wang et al., 2010)
<b>PML</b>	0.33822912	(Satoh and Tabunoki, 2013; Wang et al., 2010)
<b>MFHAS1</b>	0.33226027	(Wang et al., 2010)
<b>IRF7</b>	0.325158	(Chawla et al., 2013; Satoh and Tabunoki, 2013)
<b>BCAT1</b>	0.32212846	(Satoh and Tabunoki, 2013)
<b>ERAP1</b>	0.32094206	(TFsearcher, 2015)
<b>EZH2</b>	0.3108083	(Satoh and Tabunoki, 2013; Wang et al., 2010)
<b>CAND1</b>	0.29682544	(TFsearcher, 2015; Wang et al., 2010)
<b>GBP2</b>	0.28108758	(Satoh and Tabunoki, 2013; TFsearcher, 2015)
<b>SETX</b>	0.27760148	(QIAGEN, 2015; Wang et al., 2010)
<b>CASP7</b>	0.26854694	(Satoh and Tabunoki, 2013; Wang et al., 2010)
<b>PHEX</b>	0.26788217	(Satoh and Tabunoki, 2013)
<b>RAP1A</b>	0.26093333	(Satoh and Tabunoki, 2013; Wang et al., 2010),(Bhinge et al., 2007)
<b>IL10RB</b>	0.24953463	(Satoh and Tabunoki, 2013)
<b>NUP210</b>	0.23707301	(Wang et al., 2010),(Bhinge et al., 2007)
<b>DNMT3B</b>	0.2259721	(Satoh and Tabunoki, 2013)
<b>GLRX</b>	0.22103016	(Wang et al., 2010)
<b>COPG</b>	0.21878909	(Satoh and Tabunoki, 2013),(Bhinge et al., 2007)
<b>CCDC60</b>	0.21652676	(Satoh and Tabunoki, 2013)
<b>UHMK1</b>	0.21045863	(Satoh and Tabunoki, 2013; Wang et al., 2010)
<b>CLIC2</b>	0.20880268	(Satoh and Tabunoki, 2013),(Bhinge et al., 2007)
<b>HM13</b>	0.18924991	(Satoh and Tabunoki, 2013; Wang et al., 2010),(Bhinge et al., 2007)
<b>CYP1B1</b>	0.18806773	(Satoh and Tabunoki, 2013; Wang et al., 2010)
<b>UEVLD</b>	0.16493473	(Satoh and Tabunoki, 2013; Wang et al., 2010)

<b>TRIM25</b>	0.16334499	(Satoh and Tabunoki, 2013)
<b>NCOA7</b>	0.1570198	(Satoh and Tabunoki, 2013; Wang et al., 2010)
<b>FYN</b>	0.15238024	(Satoh and Tabunoki, 2013)
<b>CSF1</b>	0.14813757	(Satoh and Tabunoki, 2013; Wang et al., 2010)
<b>APAF1</b>	0.14155321	(Satoh and Tabunoki, 2013; Wang et al., 2010)
<b>USP3</b>	0.13756893	(Wang et al., 2010)
<b>RDX</b>	0.13545045	(QIAGEN, 2015; Satoh and Tabunoki, 2013; Wang et al., 2010)
<b>ZNF473</b>	0.13393581	(Satoh and Tabunoki, 2013; Wang et al., 2010),(Bhinge et al., 2007)
<b>IRF2</b>	0.13307439	(Chawla et al., 2013; Satoh and Tabunoki, 2013; Wang et al., 2010)
<b>IPO8</b>	0.12870036	(Satoh and Tabunoki, 2013; Wang et al., 2010),(Bhinge et al., 2007)
<b>GFM1</b>	0.12783804	(Satoh and Tabunoki, 2013; Wang et al., 2010),(Bhinge et al., 2007)
<b>KLF3</b>	0.12780589	(Chawla et al., 2013; Satoh and Tabunoki, 2013; Wang et al., 2010)
<b>ATMIN</b>	0.12195655	(QIAGEN, 2015; Wang et al., 2010)
<b>RDH10</b>	0.11789259	(Satoh and Tabunoki, 2013; Wang et al., 2010)
<b>IMPAD1</b>	0.11617159	(Satoh and Tabunoki, 2013; Wang et al., 2010)
<b>NOX4</b>	0.11604627	(Satoh and Tabunoki, 2013; Wang et al., 2010)
<b>BAZ2A</b>	0.11316689	(Satoh and Tabunoki, 2013; Wang et al., 2010),(Bhinge et al., 2007)
<b>UBP1</b>	0.11201484	(Chawla et al., 2013; Satoh and Tabunoki, 2013; Wang et al., 2010)
<b>CCDC6</b>	0.11092008	(Satoh and Tabunoki, 2013; Wang et al., 2010)
<b>UBR1</b>	0.11078076	(Bhinge et al., 2007; Satoh and Tabunoki, 2013; Wang et al., 2010)
<b>MORC3</b>	0.10306528	(Satoh and Tabunoki, 2013; Wang et al., 2010)

<b>HRH1</b>	0.1013663	(Sato and Tabunoki, 2013; Wang et al., 2010)
-------------	-----------	--

\*The frequency with which relative expression levels of each gene are comparable with STAT1 mRNA levels in individual breast tumors from the TCGA RNA-seq dataset (n=1215).

**Table 17. List of STAT3 target genes that define the STAT3 ssGSEA signature.**

<b>Gene</b>	<b>Score*</b>	<b>References**</b>
<b>STAT3</b>	1	(Chawla et al., 2013; Dauer et al., 2005; Ehret et al., 2001; TFsearcher, 2015)
<b>IL6ST</b>	0.43835358	(Oh et al., 2009; TFsearcher, 2015)
<b>NFKB1</b>	0.41621436	(Chawla et al., 2013)
<b>FOSL2</b>	0.41340799	(Chawla et al., 2013; Dauer et al., 2005)
<b>SLC4A7</b>	0.35683991	(Dauer et al., 2005)
<b>UGCG</b>	0.33030354	(Dauer et al., 2005; Oh et al., 2009)
<b>MCL1</b>	0.30895228	(Alvarez et al., 2005; Oh et al., 2009; QIAGEN, 2015)
<b>PFKFB3</b>	0.30336005	(Dauer et al., 2005)
<b>JAK2</b>	0.27602273	(Alvarez et al., 2005; Dauer et al., 2005)
<b>FEM1C</b>	0.27566194	(Dauer et al., 2005)
<b>SAMD4A</b>	0.27486799	(Dauer et al., 2005)
<b>AKAP2</b>	0.26924854	(Dauer et al., 2005)
<b>AKAP12</b>	0.26716036	(Dauer et al., 2005; Oh et al., 2009)
<b>STOM</b>	0.25314173	(Dauer et al., 2005)
<b>ICAM1</b>	0.25181764	(Dauer et al., 2005)
<b>ABCA1</b>	0.25120452	(Dauer et al., 2005)
<b>FLNB</b>	0.25015441	(Dauer et al., 2005)
<b>MBNL2</b>	0.2470801	(Dauer et al., 2005; TFsearcher, 2015)
<b>SERPINA3</b>	0.2463125	(Dauer et al., 2005; Ehret et al., 2001; Oh et al., 2009; TFsearcher, 2015)
<b>TGFB2</b>	0.24187624	(Snyder et al., 2008)
<b>SOD2</b>	0.22952525	(Dauer et al., 2005)

<b>THBS1</b>	0.2255324	(Dauer et al., 2005; Oh et al., 2009)
<b>BCL6</b>	0.21904633	(Alvarez et al., 2005; Chawla et al., 2013; Dauer et al., 2005)
<b>C3</b>	0.20114834	(Dauer et al., 2005)
<b>FGL2</b>	0.19811681	(Snyder et al., 2008)
<b>TEK</b>	0.19164484	(Snyder et al., 2008)
<b>THBD</b>	0.19113941	(Dauer et al., 2005; Paz et al., 2004)
<b>MUC1</b>	0.18890754	(Oh et al., 2009)
<b>NPC1</b>	0.18613671	(Dauer et al., 2005; Oh et al., 2009)
<b>LAMA3</b>	0.17806808	(Dauer et al., 2005)
<b>GFPT2</b>	0.17546918	(Dauer et al., 2005)
<b>LDLR</b>	0.17146452	(Dauer et al., 2005; Oh et al., 2009)
<b>PPAP2B</b>	0.16594436	(Dauer et al., 2005)
<b>PELI2</b>	0.16552106	(Dauer et al., 2005)
<b>CCND2</b>	0.16316837	(Paz et al., 2004)
<b>FGB</b>	0.1544856	(Dauer et al., 2005)
<b>LBP</b>	0.15409878	(Dauer et al., 2005; Ehret et al., 2001)
<b>AGT</b>	0.14964365	(Dauer et al., 2005; Oh et al., 2009)
<b>A2M</b>	0.14909279	(Ehret et al., 2001; Oh et al., 2009)
<b>TRIB1</b>	0.14849039	(Marie et al., 2012)
<b>SLC2A14</b>	0.14756321	(Dauer et al., 2005)
<b>MMP2</b>	0.13652352	(Oh et al., 2009; QIAGEN, 2015)
<b>SOCS3</b>	0.13617275	(Dauer et al., 2005; Ehret et al., 2001; Oh et al., 2009) (Alvarez et al., 2005; Przanowski et al., 2014; QIAGEN, 2015)
<b>ATF3</b>	0.13325996	(Chawla et al., 2013; Dauer et al., 2005; Oh et al., 2009)
<b>SLC2A3</b>	0.12961652	(Dauer et al., 2005; Oh et al., 2009)
<b>FOS</b>	0.12886529	(Chawla et al., 2013; Ehret et al., 2001; Oh et al., 2009)
<b>FGG</b>	0.12710997	(Dauer et al., 2005; Ehret et al., 2001)
<b>ZFP36</b>	0.12528609	(Dauer et al., 2005)

<b>KLF11</b>	0.1048312	(Chawla et al., 2013)
<b>PLOD2</b>	0.10282667	(Dauer et al., 2005)
<b>IL6</b>	0.10095934	(QIAGEN, 2015) (Przanowski et al., 2014)

\*The frequency with which relative expression levels of each gene are comparable with STAT1 mRNA levels in individual breast tumors from the TCGA RNA-seq dataset (n=1215).

---

## **Chapter 4: Shc1 phospho-tyrosine dependent interactors that mediate immunosuppression**

### **4.1 Experimental rationale**

Our work presented in Chapter 3 has highlighted the role of Shc1 phosphotyrosine signaling in balancing STAT1 and STAT3 pathways to suppress anti-tumor immunity in favor of breast cancer progression. However, the molecular mechanism by which Shc1 phosphotyrosines directly regulate STAT1 expression and STAT3 activation remained unclear. Furthermore, the existence of other signaling cascades that may confer the ability of tumor intrinsic Shc1 to promote immunosuppression have not been investigated. While previous studies have explored Shc1 interactomes on a large scale (Liu and McGlade, 1998; Patterson et al., 1996; Thomas et al., 1995; Zheng et al., 2013), no studies have defined a comprehensive Shc1 interactome uniquely dependent on phospho-Y239/240 or phospho-Y313 in the context of breast cancer. Thus, we set out to investigate the phospho-tyrosine dependent and independent interactors of Shc1 that mediate breast cancer immunosuppression using affinity purification (AP) and BioID proximity labeling (BioID) approaches, each followed by mass spectrometry (AP-MS and BioID-MS). This two-pronged approach allowed us to identify and validate Map4k5 as a possible novel interactor of Shc1 that merits further investigation. Furthermore, the results will serve as important resource to further explore Shc1 signaling in regulating immunosuppression.

### **4.2 Identification of Shc1 phospho-tyrosine dependent and independent interactome**

In the BioID method, an *E. coli* derived mutant form of biotin ligase (BirA-R118G; termed BirA\*) is fused to a protein of interest. BirA\*, generating a highly reactive biotinoyl-5'-AMP intermediate that promiscuously reacts with accessible lysine side chains of proteins in proximity to the protein of interest (estimated to be approximately 10nm) (Roux et al., 2018). This leads to formation of a covalent amide bond between biotin and the lysine side chain (Varnaite and MacNeill, 2016). The BioID method allows capturing of (1) insoluble cellular structures as harsh lysis conditions are allowed, (2) transient or weak interactors, (3) direct and indirect interactors within a signaling complex, and (4)

interactions that occur over a period of time (Roux et al., 2018). On the other hand, AP-MS method captures stable interactors in the soluble fraction (cytoplasm and nucleoplasm; excludes interactors in the membrane or those bound tightly to DNA) that are both direct and indirect within a signaling complex, capturing a snapshot of protein associations in their cellular context (Gingras et al., 2007; Gingras and Raught, 2012; Lavalley-Adam et al., 2013; Roux et al., 2018). AP-MS and BioID-MS methods have been used together to identify novel interactomes (Lambert et al., 2015). Thus, we reasoned that using AP-MS and BioID-MS in parallel allows for a two-pronged approach to capture multiple Shc1 interactors.

ShcWT breast cancer cells (#4788) were ectopically infected with empty vector control (control), wild-type Shc1 (termed WT), Y239F/Y240F-Shc1 (termed 2F) Y313F-Shc1 (termed 313F), and Y239F/Y240F/Y313F-Shc1 (termed 3F) all of which were FLAG tagged at the C-terminus and conjugated to Myc-tagged BirA\* at the N-terminus (**Fig. 44**).

For the BioID studies, control, WT, 2F, and 313F cells were serum-starved overnight and pulsed with 10% FBS growth media supplemented with exogenous biotin for 24 hours prior to being lysed and affinity purified using avidin conjugated agarose beads. The ability of Shc1 conjugated BirA\* enzyme to successfully biotinylated proteins was first verified using Streptavidin-HRP immunoblot on input and pull-down samples (**Fig. 45a**). Comparable expression of each construct was verified using a Myc-tag immunoblot (**Fig. 45b**). To confirm proper Shc1 signaling, input and pulled-down samples were probed by immunoblot for Grb2, a well-established phospho-Y239/240 and Y313-Shc1 interactor (**Fig. 45b**) (Ravichandran, 2001). Mutation of all three tyrosines (3F) abolished Grb2 binding (**Fig. 45b**). While Y313F-Shc1 engaged Grb2 comparably to WT, a significant reduction in Grb2 interaction was observed in Y239/240F-Shc1, suggesting that Grb2 predominantly engages Shc1 through phospho-Y239/240 residues in this model (**Fig. 45b**), in line with the literature (Ravichandran, 2001).

Using BioID-MS, 167 unique Shc1 binding partners were captured (SAINT score = 0.9) (**Fig. 46a-b**). Three technical replicates were analyzed, and nonspecific interactions were eliminated using CRAPome analysis (Mellacheruvu et al., 2013) and SAINT. A Number of known Shc1 interactors were identified, including Ptpn11 (313F dependent), Asap2 (phospho-Y239/240 dependent), Ptpn12 and Shcbp1 (tyrosine

independent or requires either one of the tyrosines) (Zheng et al., 2013). In addition, we discovered interactors of Shc1 that were previously not reported based on BioGRID analysis (Stark et al., 2006). They included Y239/240- (23 proteins), Y313- (5 proteins), and all three tyrosines- (34 proteins) dependent interactors of Shc1. We also identified proteins that interacted with Shc1 (1) independently of the tyrosines or require either phospho-Y239/240 or Y313 (42 proteins), (2) uniquely when phospho-Y239/240 were lost (4 proteins) (3) uniquely when Y313 was lost (55 proteins). These data suggested that each Shc1 tyrosine phosphorylation site allows for the formation of unique signaling complexes. Interestingly, we observed a high number of interactors that uniquely bound Shc1 upon loss of Y313 phosphorylation (313F), distinct from what we observed upon loss of Y239/240. This may suggest (1) Shc1313F is included in more diverse signaling complexes and/or (2) Y313 may regulate signaling events or conformational changes that promote downregulation, re-localization, degradation of signaling complexes. Altogether, BioID method identified known and novel Shc1 interacting proteins. In addition, our BioID-MS studies further identified STAT3 as a Shc1 interacting protein, requiring all three Shc1 phospho-tyrosine residues. This further substantiates the importance of the Shc1 tyrosine phosphorylation sites in regulating the STAT3 pathway.

In order to capture all the Shc1 interactors, we used AP-MS and BioID-MS in parallel as a two-pronged approach. Both studies were carried out using the same constructs and cells (**Fig. 44, 47a-b**). To maximize the chance of capturing phospho-tyrosine dependent interactors, WT, 2F and 313F cells were treated with or without sodium orthovanadate (pan tyrosine phosphatase inhibitor) for 10 minutes prior to being subjected for affinity purification with agarose beads (conjugated to anti-FLAG monoclonal antibody). Using AP-MS, 76 unique Shc1 binding partners were captured – 91 less interactors than BioID-MS had captured. This is consistent with observations made by previous studies using both approaches in parallel (Couzens et al., 2013; Varnaite and MacNeill, 2016), and suggestive of the broader reach of BioID method in capturing signaling complexes. A number of previously validated Shc1 interactors (AP2A2, LRRK1, EGFR, ErbB2, Gab1, PIK3R1, Ptpn11, and Inpp1 (Gagnon et al., 2003; Zheng et al., 2013)) were identified in our MS experiments to be Y313 dependent interactors. Previously known Shc1 interactors Grb2 and Arhgef5 (Zheng et al., 2013) were identified

as Y230/240 dependent interactors. Thus, we have provided insight into the Y239/240 or Y313 dependency of known Shc1 interactors.

To understand which biological processes were enriched in each interactome, we used STRING online tool (Szklarczyk et al., 2015) to analyze the interactors identified in AP-MS and BioID-MS (**Table 18**). Numerous processes previously linked to Shc1 were identified (e.g. endocytosis, MAP kinase activity regulation, cytoskeleton organization), as expected.

We observed that 16 proteins were commonly identified in both AP-MS (21% of interactors) and BioID-MS (2% of interactors) experiments (**Table 19**). Thus, the methods captured considerably different Shc1 signaling complexes. In addition, some of these interactors showed discrepancy in requirement of specific tyrosine residues for binding (**Table 19**). For instance, By BioID, Grb2 bound Shc1 via Y239/240 or Y313. By AP, it required Y239/240 at baseline but bound Y239/240 or Y313 with sodium orthovanadate ( $\text{Na}_3\text{VO}_4$ ) treatment. Thus, at maximally phosphorylated state induced by  $\text{Na}_3\text{VO}_4$ , Y313 could compensate for the absence of Y239/240 to interact with Grb2. This is consistent with previous reports that Shc1 can use either Y239/240 or Y313 to engage Shc1, but with preference to Y239/240 (Ravichandran et al., 1995) (**Fig. 45b-c, 46a-b, 47a-b**). Taken together, we have successfully identified both previously known and unknown interactors of Shc1 and defined which Shc1 tyrosines are required for these interactions using two mass spectrometry approaches.

### **4.3 Map4k5 and Grb2 as Shc1 interactor that mediates immunosuppression**

To identify the molecular interactors of Shc1 that promote immunosuppression, we focused our attention on those that were identified by both BioID-MS and AP-MS methods (**Table 19**). We reasoned that they would be most likely to be true Shc1 interactors. Two candidates Grb2 and Map4k5 were initially selected as potential Shc1 downstream effectors that regulate immunosuppression.

Grb2 has been shown to bind Gab2 which in turn recruits STAT3, leading to phosphorylation of Y705-STAT3 (Ni et al., 2007). Gab2 is a well-established recruiter of p85 regulatory subunit of PI3K, which in turn activates the AKT pathway (Wohrle et al., 2009). In our model, Impaired phospho-Y239/240-Shc1 signaling led to a significant

reduction of AKT phosphorylation (T308 and S473) at steady state (**Fig. 48a**) and following EGF induction (**Fig. 49**). Noticeably, Shc2F cells had a baseline elevated ERK phosphorylation, and EGF induced ERK phosphorylation that were comparable to ShcWT cells (**Fig. 49**). This suggests that the reduced phospho-S727-STAT3 (target of ERK) seen in Shc2F cells is unlikely due to lack of ERK activation. Our BioID immunoblot (**Fig. 45b-c**), AP-MS data (**Fig. 47a**) and subsequent AP validation experiments (**Fig. 50**) established that Grb2-Shc1 interaction depends on Y239/240. Thus, we hypothesized that phospho-Y239/240-Shc1 interacts with a Grb2/Gab2/PI3K complex to regulate STAT3 phosphorylation (**Fig. 48b**).

We chose Map4k5 for two reasons. First, Map4k5 (a.k.a. GCKR, KHS1) is a member of the Ste1 serine/threonine kinase family (Wang et al., 2016) that is activated by TNF $\alpha$  to phosphorylate JNK (Chin et al., 1999; Shi et al., 1999; Shi and Kehrl, 1997). It is well established that JNK signaling in response to TNF leads to transcription of c-Jun, AP1, and ATF2, ultimately allowing transcription of inflammatory cytokines (e.g. IL-6), synergy with IFNs, and regulation of immune response (Sedger and McDermott, 2014). TNF $\alpha$ -induced JNK activation has been shown to phosphorylate S727-STAT3 (Lim and Cao, 1999a). Immunoblot results done on tumors from *in vivo* (**Fig. 20a**) and cells *in vitro* (**Fig. 21a**) of our breast cancer model demonstrated that Y239/240-Shc1 signaling potentiates phosphorylation of S727-STAT3. Thus, we hypothesized that Map4k5 may regulate immunosuppression downstream of Shc1 through STAT3 phosphorylation (**Fig. 51**). Second, Map4k5 has been also shown to engage the consensus SH3 binding motif of CrkL, Crk-I, and Crk-II (Shi et al., 2000). Crk-Shc1 interaction was detected in WT (average spectral count = 6), 2F (average spectral count = 4) and 313F (average spectral count = 7), suggesting that either tyrosine can be used for the interaction (slightly reduced with the loss of Y239/240) or that the interaction is tyrosine independent (**Fig. 46a-b**). The Map4k5-Shc1 interaction required Y239/240 or Y313 by BioID-MS, but only required Y239/240 by AP-MS (**Fig. 46, 47, Table 19**). Thus, we hypothesized that Map4k5 may bind Crk in our model. Importantly, Crk has been shown to specifically bind Y239/240-Shc1 downstream of TGF $\beta$  signaling to promote migration of breast cancer cells (Northey et al., 2012), further supporting the hypothesis that Crk and Map4k5 may form complex with Shc1 through phospho-Y239/240. Strikingly, Crk has been shown to suppress anti-

tumor immune responses against primary and metastatic tumors in a 4T1 mouse model of breast cancer, and the deletion of Crk elicits anti-tumor immunity (e.g. increased CD3+ T cell infiltration, CD8+ T cell infiltration, granzyme B+ expression, IFN $\gamma$  presence, CXCL9 expression, CD11b+ cell infiltration), reminiscent of Shc2F tumors (Kumar et al., 2017). Thus, we hypothesized that Shc1-Y239/240 may form a Crk/Map4k5 signaling complex to promote immunosuppression, in part through STAT3 activation (**Fig. 51**).

We also considered the possibility that Shc1-Y239/240 may form Grb2/Map4k5 signaling complex to promote immunosuppression (**Fig. 51**). Grb2, a well-established direct interactor of Shc1, also possesses two SH3 domains, similarly to Crk. Map4k5 appeared in the same category as Grb2 in both AP-MS and BioID-MS experiments (**Table 19**). Thus, this supported the idea that Map4k5 may be a true and novel downstream effector of Shc1 through Grb2.

#### **4.4 Loss of Grb2 leads to STAT3 activation**

To interrogate whether Grb2 regulates STAT3 phosphorylation and activations, Grb2 was knocked-down using shRNAs (**Fig. 52**). Significant increase in phospho-Y705-STAT3 levels and unchanged phospho-S727-STAT3 levels were observed in four different ShcWT cell lines (864, 4788, 2199, 2196) (**Fig. 52**). These data suggested that Grb2 negatively regulates phospho-Y705-STAT3 either through Shc1 or through other signaling interactors. Meanwhile, it suggested S727-STAT3 phosphorylation may be regulated separately.

#### **4.5 Map4k5 is a novel Shc1 interactor**

We also sought to validate the Map4k5-Shc1 interaction observed by AP-MS and BioID-MS experiments (**Fig. 46a-b, 47a**). Therefore, AP and BioID pull-down experiments were repeated and followed by immunoblotting for Map4k5. Using BioID, Map4k5 was biotinylated by Shc1-WT, 2F, 313F, 3F, regardless of their tyrosine status (**Fig. 53a-d**), validating the BioID-MS result. By AP, the Map4k5-Shc1 interaction was impaired by the loss of Y239/240 phosphorylation, in line with the AP-MS results, and indicated that Map4k5-Shc1 interaction preferentially occurs through Y239/240 of Shc1 (**Fig. 50a-c**). Interestingly, ectopic expression of ShcWT, Shc2F, Shc313F, Shc3F increased Map4k5

levels in MT breast cancer cells as detected in the input lanes of the affinity purification experiments (**Fig. 53a-d**). This suggested that Shc1 likely regulates Map4k5 expression either transcriptionally or post-transcriptionally.

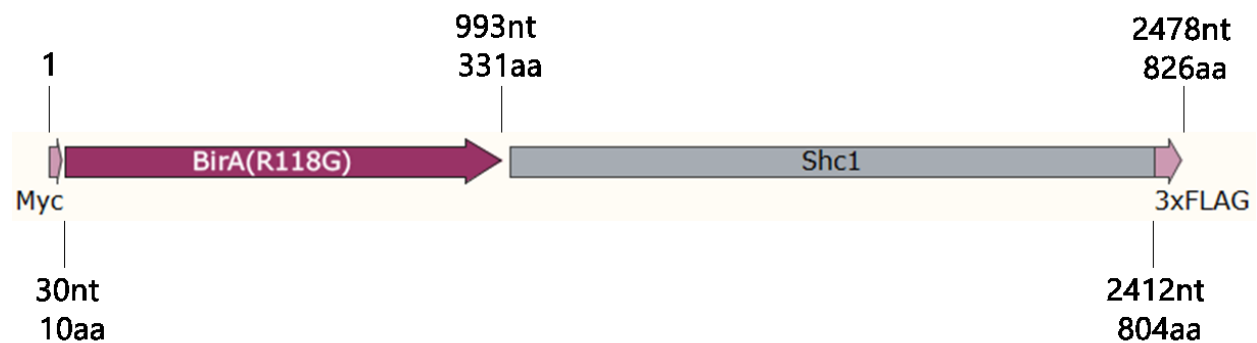
To support our hypothesis that Map4k5 is recruited to Shc1 through Grb2 (**Fig. 51**), we asked if Grb2 and Map4k5 share the same requirement for their interaction with Shc1. By BioID, Grb2-Shc1 interaction highly depended on Y239/240 (**Fig. 45b-c**) while Map4k5-Shc1 interaction did not as indicated by the Map4k5 biotinylation regardless of the the Shc1 phosphotyrosine status (**Fig. 53a-d**). Given BioID-MS revealed Grb2 was biotinylated as long as either Y239/240 or Y313 was functional, the threshold for positive identification in BioID-MS may be lower than that of the BioID-immunoblot. By AP, both Map4k5 and Grb2 required Y239/240 at baseline (**Fig. 50a-c**). Upon Na<sub>3</sub>VO<sub>4</sub> treatment, both Map4k5 and Grb2 engaged Shc1 independently of Y239/240 (**Fig. 50a-c**). Taken together, our AP and BioID data support that Map4k5 comes into proximity or forms a complex with Shc1 preferentially through Y239/240, possibly using Grb2 or other scaffolds.

During our validation experiments, we encountered considerable challenge with the commercially available anti-Map4k5 antibody to obtain consistent results and interpretation. Frequently, probing for Map4k5 in the total lysate input control was far less efficient than in the pulled-down fraction unlike with Grb2 which was detected equally efficiently in both fractions. This suggested that Map4k5 is significantly less abundant in cells compared to Grb2. Between twelve independent ShcWT, Shc2F, Shc313F cell lines previously RNA-sequenced, the normalized mRNA read counts ranged between 5,080 and 8,111 for Map4k5 (average 6,121) while they ranged between 6,065 and 23,552 for Grb2 (average 15,328). Taken together, we have provided evidence supporting Map4k5 as a novel Shc1 interactor that preferentially binds on phospho-Y239/240 residues of Shc1, although it does not exclude that Map4k5 can also bind the phospho-Y313 residue.

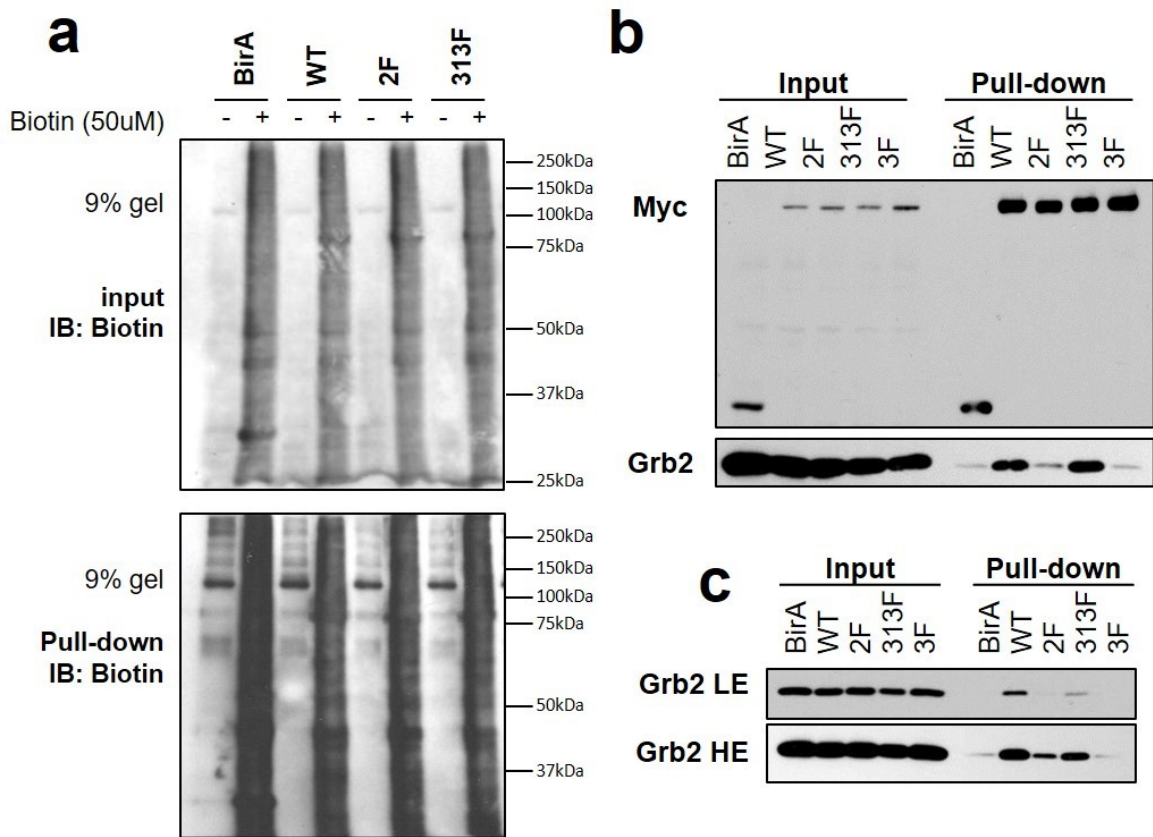
#### **4.6 MEK pathway and JAK2/3 phosphorylates S727- and Y705-STAT3**

Given the well established role of ERK in phosphorylating S727 downstream of growth factor receptor pathways and JAK2/3 in phosphorylating Y705-STAT3 downstream of cytokine signaling (**Table 3**), we employed MEK and JAK2/3 kinase

inhibitors to ask whether these pathways regulate STAT3 activation in our MT model. First, ShcWT cell lines (864) were treated with a JAK2/3 inhibitor Tofacitinib. Tofacitinib led to a significant reduction in phosphorylation of Y705 but not S727 of STAT3, suggesting that a considerable amount of Y705-STAT3 phosphorylation is through JAK2/3 pathway in these cells (**Fig. 54a**). Reduction in phosphorylation of Y705 did not alter S727 phosphorylation, demonstrating that S727 phosphorylation is independent of Y705 phosphorylation in this treatment setting. Treatment of ShcWT cells (4788) with Trametinib, a MEK inhibitor, led to a significant reduction in phospho-S727-STAT3 levels, suggesting that significant portion of S727-STAT3 phosphorylation in ShcWT cells is due to ERK signaling (**Fig. 54b**). Downregulation of phospho-S727-STAT3 did not alter phospho-Y705-STAT3 level in this treatment setting. Taken together, these results suggested S727 and Y705 of STAT3 are regulated in our model in part by the MEK/ERK and JAK2/3 pathways, respectively.

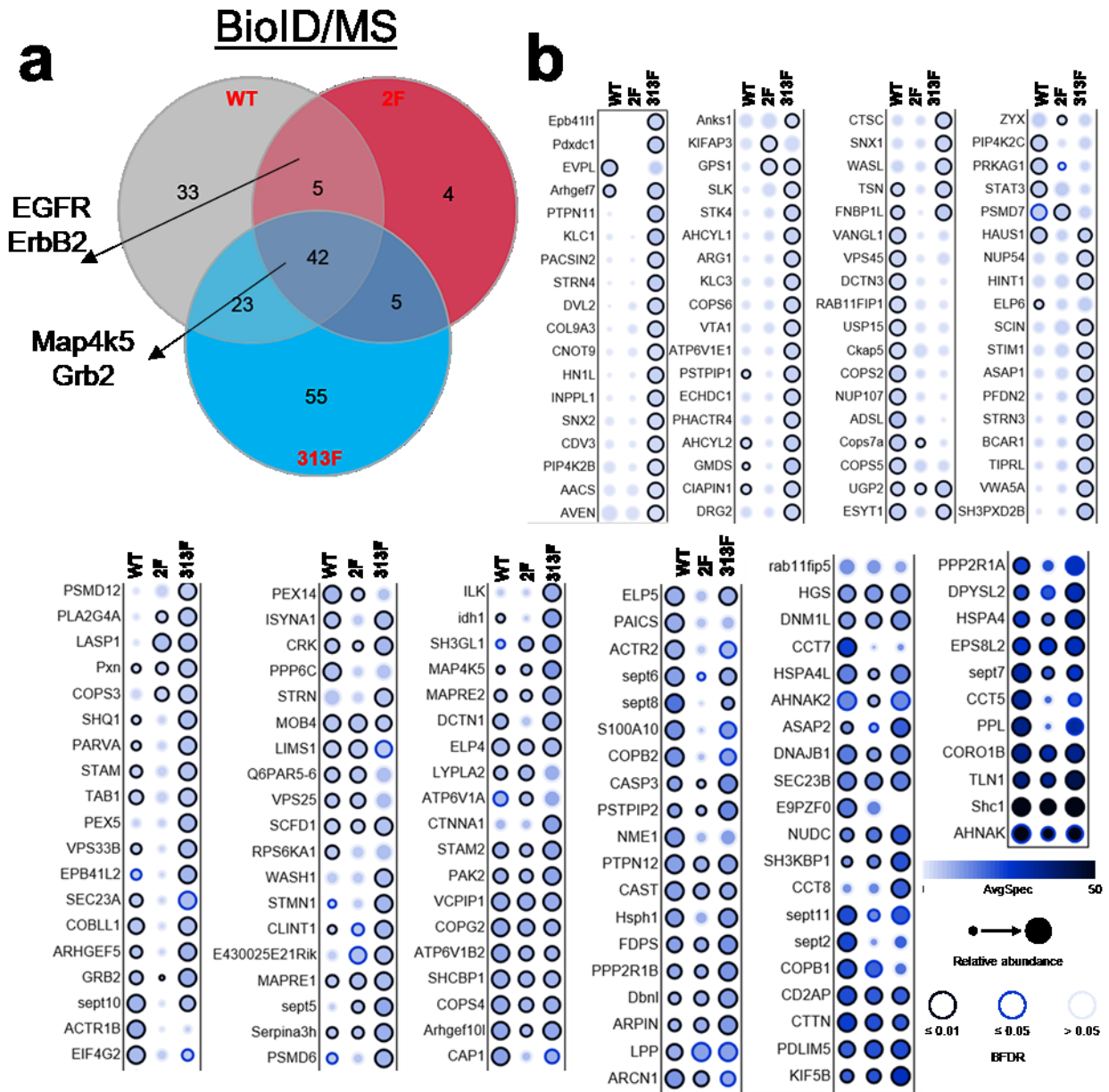


**Figure 44. Schematic of Myc-BirA-Shc1-3xFLAG constructs used in the study.**  
aa, amino acids. nt, nucleotide.



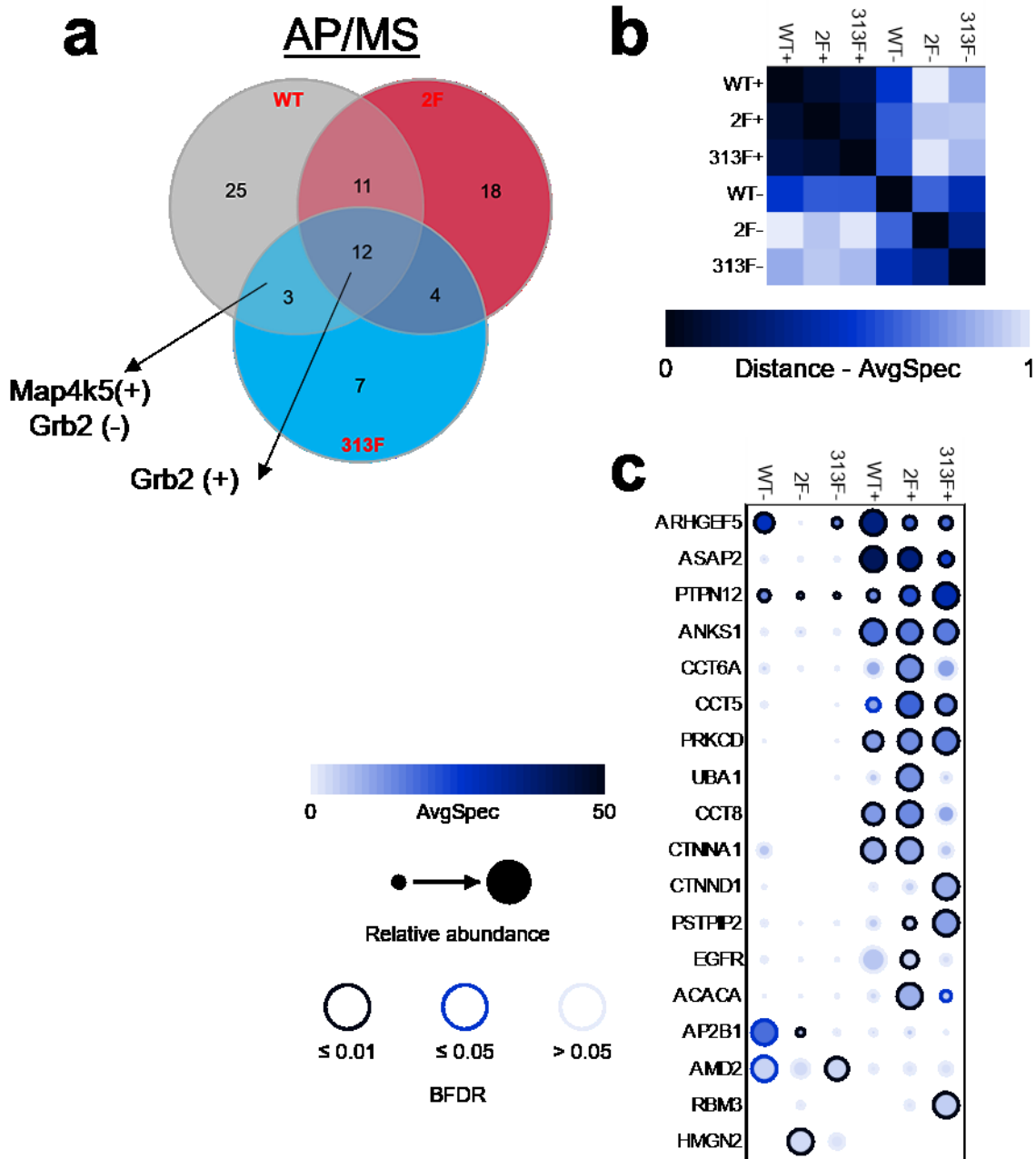
**Figure 45. Validation of BioID constructs.**

(a) Myc-BirA empty vector control, and myc-BirA conjugated WT, 2F, 313F Shc1 constructs were expressed in ShcWT (4788) cells and incubated with or without 50uM Biotin for 24hrs prior to being lysed, affinity-purified, and immunoblotted (IB) for biotinylated proteins both in input and pull-down fraction. (b) ShcWT 4788 cells and (c) ShcWT 864 were infected with myc-BirA empty vector control, and myc-BirA conjugated Shc1 WT, 2F, 313F, and 3F constructs and incubated in 50uM biotin for 24hrs prior to being lysed, affinity-purified, and immunoblotted myc tag and Grb2 protein in both input and pull-down fraction. LE = low exposure, HE = high exposure



**Figure 46. BioID/MS interactome of Shc1.**

(a) Schematic diagram of BioID/MS and IP/MS results with indication of which fraction Grb2, and Map4k5 were discovered in. (b) Dot plot as analyzed by ProHits-viz. AvgSpec = average spectral counts. BFDR (Bayesian false discovery rate) describes confidence proximity interactions



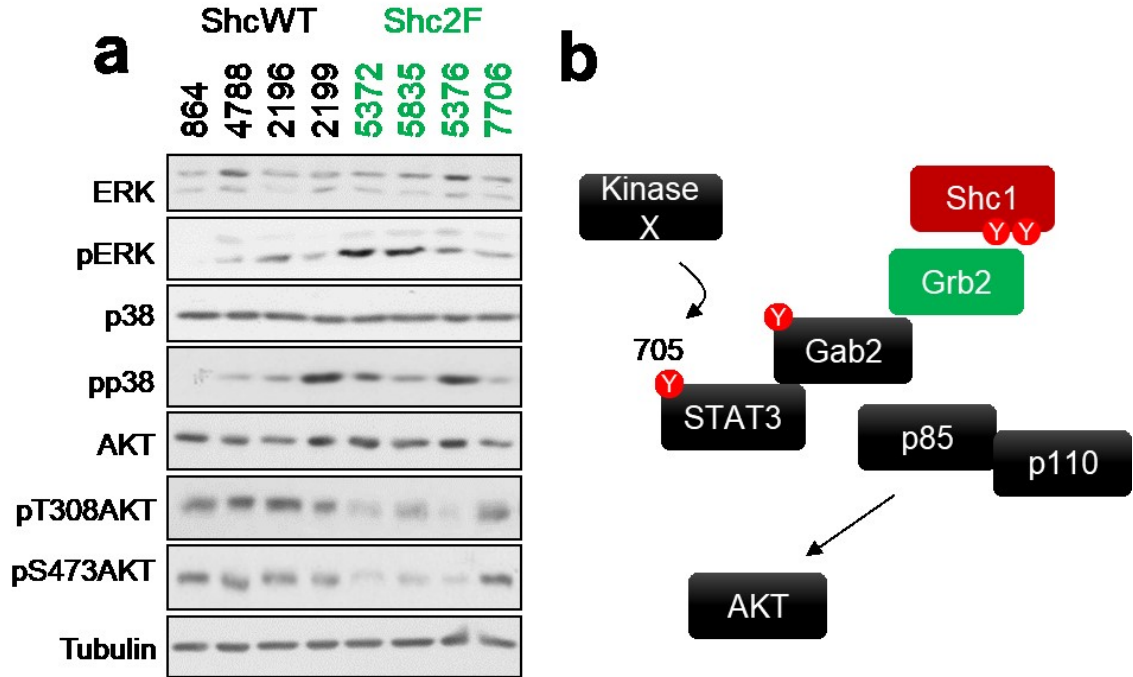


**Figure 48. AKT activation is impaired with loss of phospho-Y239/240-Shc1 signaling.**

(a) ShcWT (864, 4788, 2196, 2199) and Shc2F (5372, 5835, 5376, 7706) cells were assessed for steady state activation of the AKT and MAPK pathways. (b) Model for Shc1/Grb2/Gab2 driven STAT3 regulation.

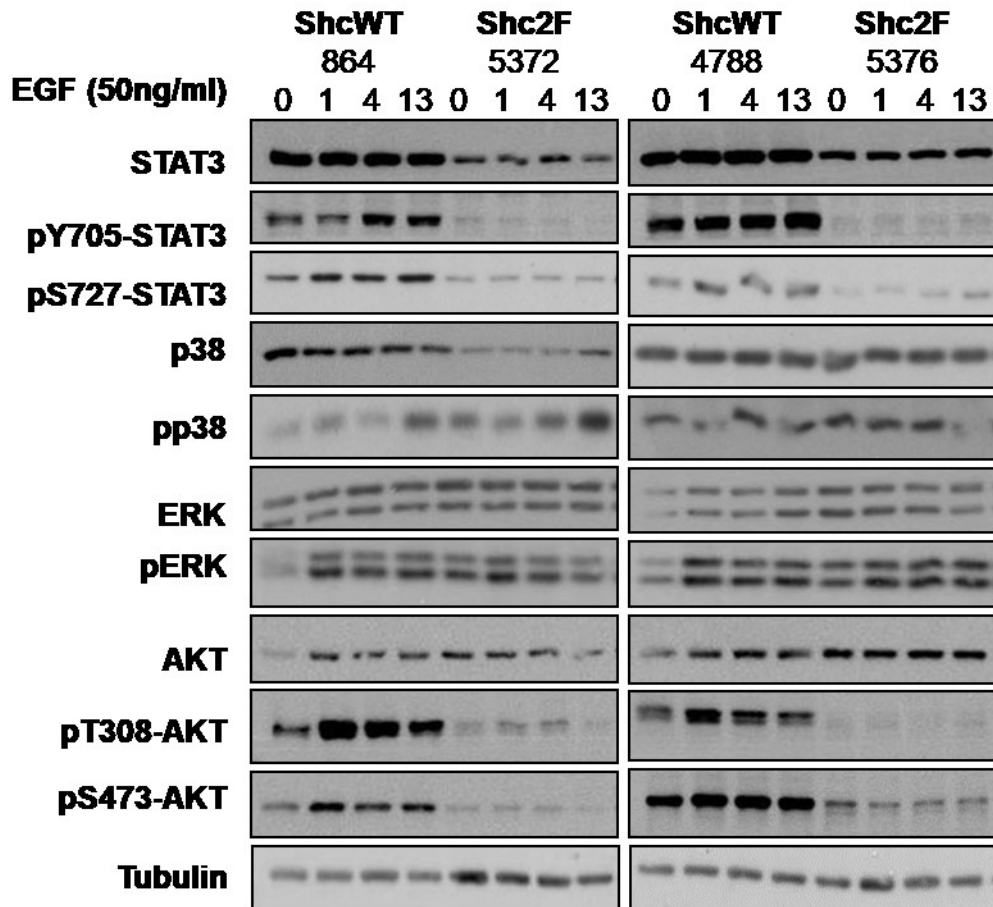


**Figure 49. EGF induced AKT activation is debilitated in phospho-Y239/240-Shc1 impaired cells.**

ShcWT (864 or 4788) and Shc2F (5372 or 5376) cells were starved overnight in 0.5%FBS/DMEM and stimulated with EGF (50ng/ml) for the indicated duration before being lysed and immunoblotted for indicated MAPK and AKT pathway proteins.

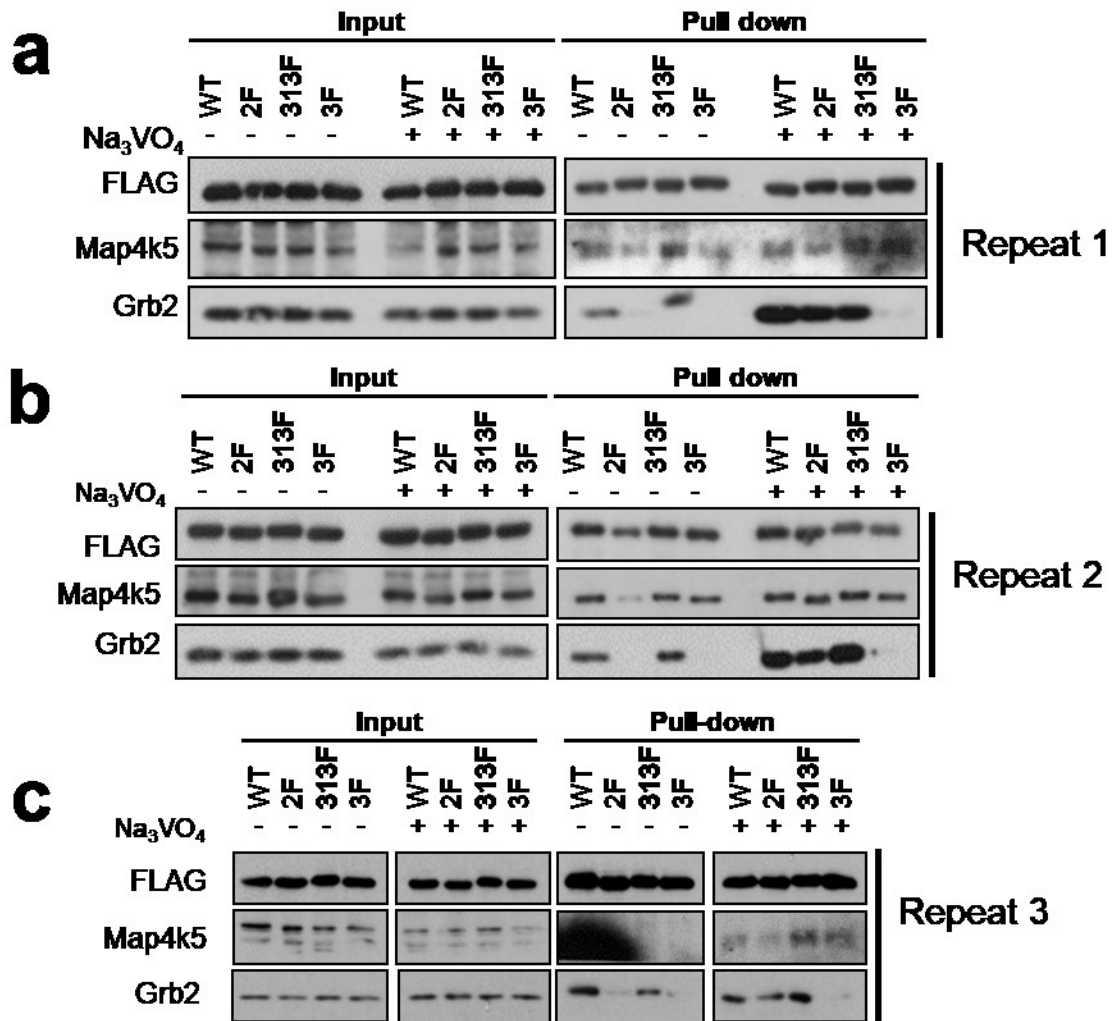


**Figure 50. Grb2 and Map4k5 interaction with Shc1 affinity purification.**

WT, 2F, 313F, 3F cells (ShcWT 864 parent) were treated with or without Na<sub>3</sub>VO<sub>4</sub> for 10 minutes prior to being lysed, (a, b) Affinity-purified using FLAG agarose beads or (c) Immunoprecipitated using anti-FLAG antibody. All were immunoblotted for FLAG, Map4k5, and Grb2. Three biological repeats are shown.

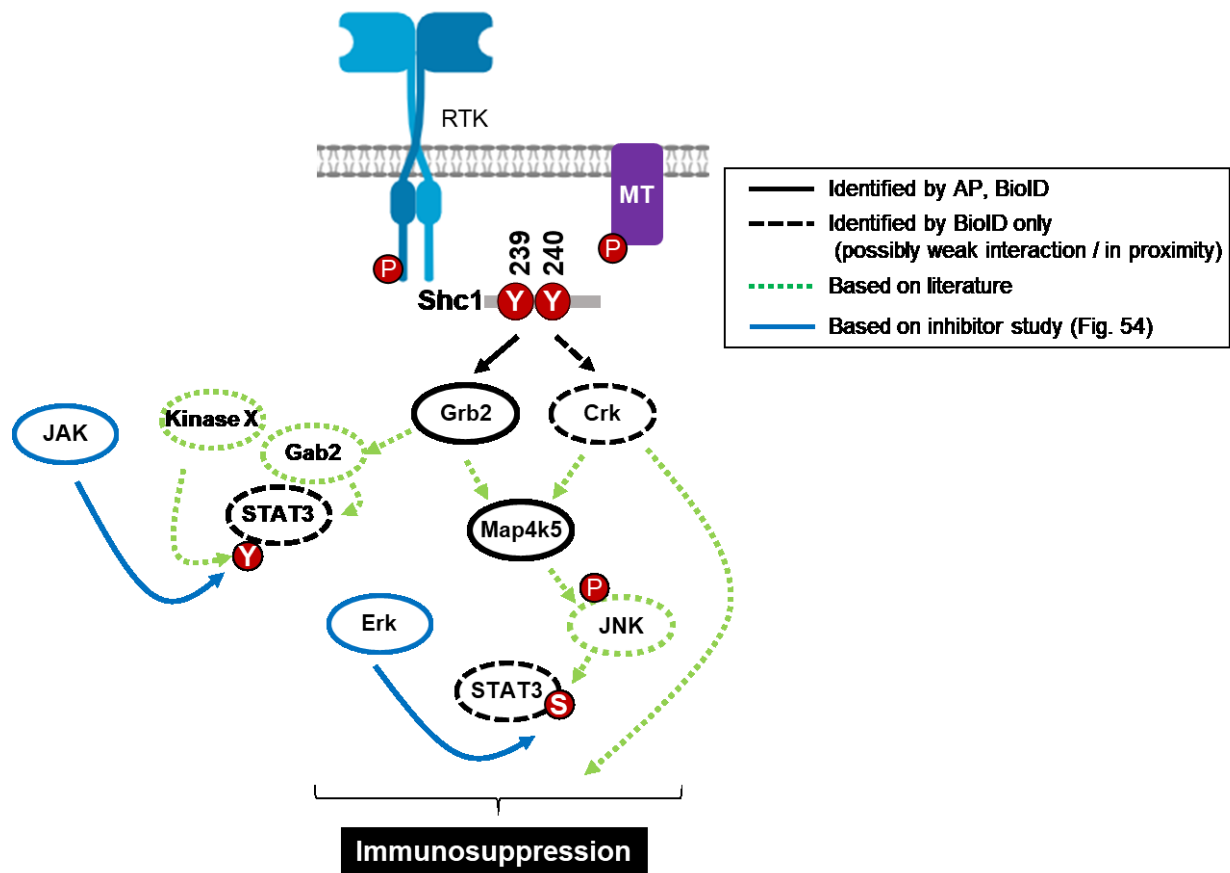
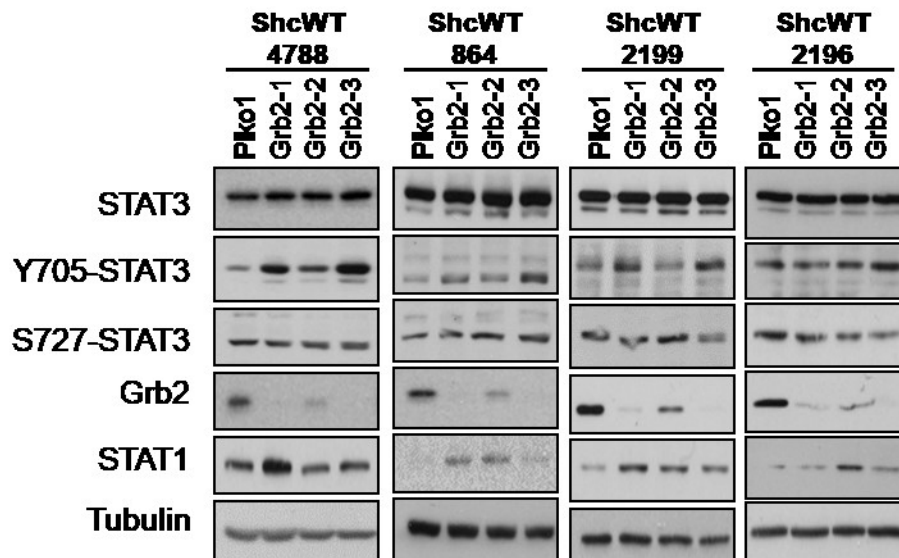


Figure 51. Predicted model of how Map4k5 promotes immunosuppression in cancer.



**Figure 52. ShRNA induced knock-down of Grb2.**

MMTV/MT derived primary cell lines (4788, 864, 2199, 2196) were infected with pLKO.1 control and Grb2 (#1-3 shRNA) and immunoblotted for the indicated proteins

---

---

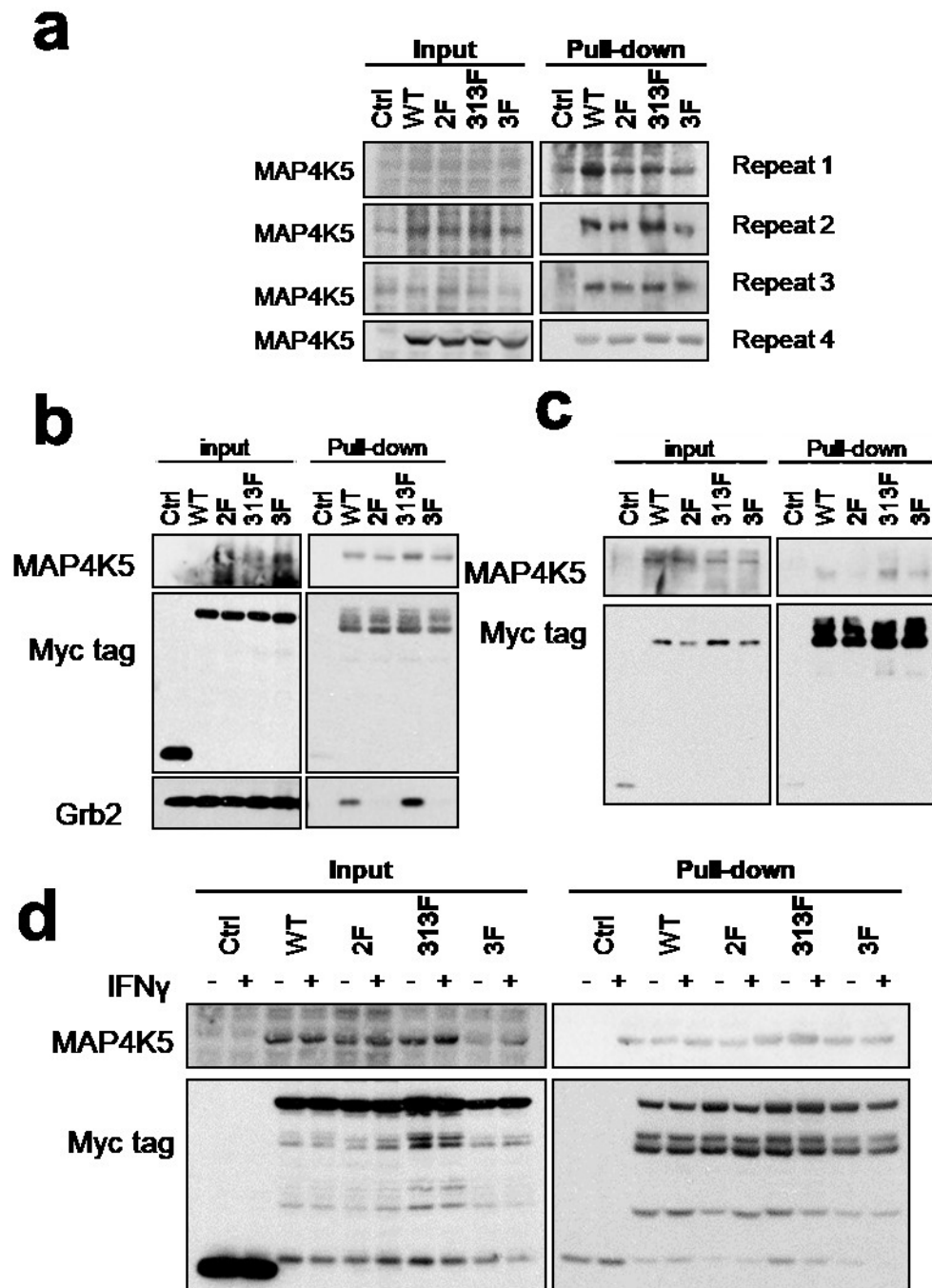


**Figure 53. Map4k5 engages Shc1 independently of phospho-tyrosine in BioID assay.**

(a-c) MT cells expressing Shc1-WT, 2F, 313F, 3F fused with myc-BirA\* constructs were incubated in 50uM Biotin for 24 hrs and affinity purified using avidin-agarose beads. Immunoblot analysis of input and pull-down fractions are shown. (d) MT cells expressing

Shc1-WT, 2F, 313F, 3F fused with myc-BirA\* constructs were incubated in 50uM Biotin for 24 hrs in the presence of PBS or IFN $\gamma$  (1ng/ml) and were subsequently affinity purified using avidin-agarose beads. Immunoblot analysis of input and pull-down fractions are shown.

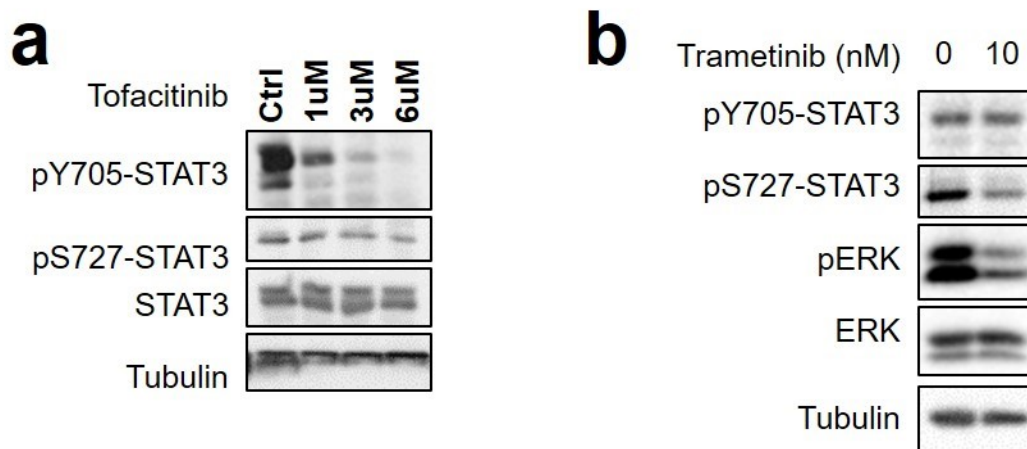


**Figure 54. ERK and JAK2/3 phosphorylate STAT3.**

(a) ShcWT (864) cells were treated with JAK2/3 inhibitor tofacitinib at the indicated dose for 20hrs prior to being lysed for immunoblot analysis. (b) ShcWT (4788) cells were treated with MEK inhibitor Trametinib for 21hrs at the indicated dose in 2.5%FBS/MEGS media and immunoblotted for the indicated proteins.

**Table 18. STRING analysis results for each condition (top two GO terms are shown)**

Shc1	GO	Term	OGC / BGC	FDR
<b>AP-MS</b>				
<b>WT-</b>	0006898	receptor-mediated endocytosis	5/173	7.86E-06
	0031623	receptor internalization	3/56	0.00054
<b>WT+</b>	0032268	regulation of cellular protein metabolic process	22/2443	1.91E-06
	0043405	regulation of MAP kinase activity	10/304	1.91E-06

<b>2F-</b>	0006898	receptor-mediated endocytosis	3/173	0.022
	0072583	clathrin-dependent endocytosis	2/19	0.022
<b>2F+</b>	1903827	regulation of cellular protein localization	12/484	5.62E-08
	0071495	cellular response to endogenous stimulus	15/997	5.75E-08
<b>313F-</b>	N/A*			
<b>313F+</b>	0051054	positive regulation of DNA metabolic process	7/223	6.82E-07
	1904851	positive regulation of establishment of protein localization to telomere	4/10	6.82E-07
<b>BioID-MS</b>				
<b>WT</b>	0016192	vesicle-mediated transport	23/1020	7.16E-07
	0044087	regulation of cellular component biogenesis	21/863	7.16E-07
<b>2F</b>	0044087	regulation of cellular component biogenesis	14/863	3.07E-05
	0051179	Localization	28/4315	0.00016
<b>313F</b>	0007010	cytoskeleton organization	26/916	9.47E-09
	0009987	cellular process	106/12459	9.47E-09

\* biological function clustering could not be done. OGC, observed gene count. BGC, background gene count. FDR, false discovery rate. GO, gene ontology. – or + indicate the presence or absence of Na<sub>3</sub>VO<sub>4</sub> treatment.

**Table 19. List of 16 proteins discovered in both BioID-MS and AP-MS. Indicated are the tyrosines requirements for interaction.**

	<b>BioID-MS</b>	<b>AP-MS (-/+ Na<sub>3</sub>VO<sub>4</sub>)</b>
<b>Grb2**</b>	Y independent or either one sufficient	Y239/240(-), Y independent (+)
<b>Map4k5**</b>	Y independent or either one sufficient	Y239/240(+)
<b>Pstpip2</b>	Y independent or either one sufficient	Y independent (+)
<b>Ptpn12</b>	Y independent or either one sufficient	Y independent (-/+)

<b>Sept7</b>	Y independent or either one sufficient	Y239/240/313(+)
<b>NME2</b>	Y239/240/313	Y239/240/313(+)
<b>PPP2R1A</b>	Y239/240/313	2F (+)
<b>Cct7</b>	Y239/240/313	313F (+)
<b>Cct5</b>	Y239/240/313, Y313 (0.7*)	Y independent (+)
<b>Asap2</b>	Y239/240	Y independent (-/+)
<b>Arhgef5</b>	Y239/240	Y239/240(-), Y independent (+)
<b>Anks1a</b>	313F	2F (-), Y independent (+)
<b>Cct8</b>	313F	Y independent (+)
<b>Ctnna1</b>	313F	Y313(+)
<b>Inpp1</b>	313F	Y313(+)
<b>Ptpn11</b>	313F	Y313(+)

\* Identified when SAINT score of 0.7 used. Rest are identified by SAINT score of 0.9.

\*\* Selected for further investigation.

## Chapter 5: Mechanism of STAT3 driven immunosuppression

### 5.1 Experimental rationale

Our work presented in Chapter 3 highlighted the importance of STAT3 phosphorylation and activation downstream of phospho-Y239/240-Shc1 to suppress the CTL/IFN $\gamma$ -driven anti-tumor immunity and the sensitivity to immune-based therapies in mice. The canonical STAT3 gene transcription upon stimuli involves phosphorylation of Y705 of STAT3 monomer which stably engages the R603 within SH2 domain of another STAT3 monomer, resulting in STAT3 dimerization (Bromberg et al.). This dimer can enter the nucleus to bind DNA and activate transcription of STAT3 targets. The phosphorylation of S727 has been shown to enhance homodimerization and DNA binding for maximal transcriptional activity. Unlike the role of Y705, the role of S727-STAT3 has remained controversial in the literature (Dimri et al., 2017; Zhang et al., 2001). We observed that ShcWT and Shc2F tumor tissues (progressively growing) from immunocompetent mice had comparable phospho-Y705-STAT3 levels by immunoblot and IHC (**Fig. 19a, 21**). Interestingly however, Shc2F tumors expressed decreased level of phospho-S727-STAT3, concomitant with significant increase in phospho-Y701-STAT1 levels (**Fig. 19a**). Additionally, immunoblot analysis of the cell lines *in vitro* showed Shc2F cells expressed both lower phospho-Y705-STAT3 and phospho-S727-STAT3 compared to ShcWT cells (**Fig. 22a-c**). These data suggested that Y239/240-Shc1 promotes both Y705- and S727-STAT3 phosphorylation and raised the question of whether S727-STAT3 contributes to immunosuppression downstream of Y239/240-Shc1. Furthermore, emerging evidence in the literature indicates a possible role of S727 in regulating pro-tumorigenic pathways independently of Y705 (detailed in **Section 1.6.1.2**). Therefore, we set out to define the functional role of both Y705 and S727-STAT3 phosphorylation in suppressing anti-tumor immune responses. Through combined use of RNA-seq and mice models, we have highlighted the importance of both Y705 and S727 in regulating IFN $\gamma$  dependent anti-tumor immune responses during breast cancer progression.

### 5.2 Phospho-Y705 and phospho-S727 STAT3 signaling suppresses IFN $\gamma$ driven anti-tumor immunity

STAT3 CRISPR/cas9 deleted ShcWT cells (4788) were ectopically infected with an empty vector control (null), STAT3 wild-type (WT), STAT3 tyrosine-to-phenylalanine mutant (Y705F; YF), STAT3 serine-to-alanine mutant (S727A; SA), STAT3 serine-to-glutamate phospho-mimetic mutant (S727E; SE), or a STAT3 tyrosine and serine double mutant (Y705F/S727A; termed DM). The successful STAT3 re-expression and Y705 and S727 phosphorylation were verified by immunoblot (**Fig. 55a-b**). The Y705 phosphorylation was upregulated in S727A mutant expressers compared to the wild-type STAT3 expressing STAT3-CRISPR deleted cells. This is consistent with previous studies reporting that the S727 site negatively regulates the phosphorylation of Y705 of STAT3 (Chung et al., 1997b; Chung et al., 1997c; Gartsbein et al., 2006; Tian and An, 2004). Nuclear phosphatase TC45 (TCPTP) may be involved as suggested by one group (Wakahara et al., 2012). SOCS3, a well established STAT3 target gene (Bluyssen et al., 2010), was verified for its expression in the wild-type and mutant STAT3 expressing cells to demonstrate phenotypes consistent with the literature (**Fig. 55c**).

To investigate the functional role of differentially phosphorylated STAT3 in suppressing IFN $\gamma$  driven tumor clearance, WT, YF, SA, SE and DM STAT3 expressing cells, along with the null control, were injected into the mammary fat pads of syngeneic IFN $\gamma^{+/+}$  or IFN $\gamma^{-/-}$  mice (**Fig. 56a-c**). In IFN $\gamma^{-/-}$  mice, no statistically significant growth differences were observed between the null and WT ( $p = 0.93$ ), YF ( $p = 0.069$ ), SA ( $p = 0.24$ ), SE ( $p = 0.14$ ) or DM ( $p = 0.076$ ) (**Fig. 56a**). As previously observed, loss of STAT3 significantly reduced the tumor growth ( $p < 0.001$ ) in the presence of intact IFN $\gamma$  signaling (**Fig. 56b**). Re-expression of STAT3-WT allowed enhanced tumor growth in IFN $\gamma^{+/+}$  mice ( $p = 0.003$ ) which became comparable to that in IFN $\gamma^{-/-}$  mice, indicating that wild-type STAT3 is necessary and sufficient to overcome IFN $\gamma$  driven anti-tumor immune responses (**Fig. 56b-c**). STAT3 null and STAT3-Y705F expressing tumors showed significantly reduced growth capabilities in IFN $\gamma^{+/+}$  compared to IFN $\gamma^{-/-}$  mice, demonstrating that Y705-STAT3 plays a critical role in suppressing IFN $\gamma$  driven anti-tumor immune responses (**Fig. 56c**). In IFN $\gamma^{+/+}$  mice, STAT3-S727A expressing tumors showed increased growth (2.9 fold at end point) compared to STAT3-Y705F expressing tumors, but decreased growth (0.7 fold at end point) compared to the wild-type STAT3 expressing tumors (**Fig. 56c**). Furthermore, STAT3-S727A expressing tumors growing in IFN $\gamma^{+/+}$  and

IFN $\gamma$ <sup>-/-</sup> mice showed pronounced difference in outgrowth capabilities (2.9 fold at end point,  $p = 0.008$  using Holm-Sidak multiple t-test method), indicating that S727-STAT3 signaling contributes to suppressing IFN $\gamma$  dependent anti-tumor immune response (**Fig. 56c**). Together, these data suggested that both Y705 and S727 are important in regulating tumor driven immune suppression to IFN $\gamma$ .

To delineate the impact of differential phospho-Y705 or phospho-S727 STAT3 signaling on the transcriptome, we performed RNA-seq on null, WT, YF, SA, DM-STAT3 expressing breast tumors excised at end point from the IFN $\gamma$ <sup>+/+</sup> mice (**Fig. 56d**). Thus, we identified differentially expressed genes unique to each STAT3 activation status, as well as those that overlap between different STAT3 activation status in mammary tumors. The differentially expressed genes are currently being investigated and validated. To establish the proper STAT3 activity in tumors, the expression of SOCS3 mRNA in tumor tissues were verified by RT-qPCR (**Fig. 57**). The SOCS3 mRNA expression pattern was comparable between the cell lines and the tumor tissues (**Fig. 55c, 57**), and they were in line with the well characterized SOCS3 expression pattern by the STAT3 wild-type and mutants (Yang et al., 2010), suggesting that STAT3 wild-type and mutant proteins behave as expected. Thus, we have identified genes (stroma and tumor derived) uniquely regulated by differentially activated STAT3 from breast tumor cells.

### **5.3 STAT3 localization and phosphorylation status**

To understand how STAT3 phosphorylation status differentially impacts immunosuppression in our model, localization pattern of STAT3 wild-type and mutants to the nucleus and cytoplasm was assessed by cellular fractionation (**Fig. 58**). We reasoned that its cellular localization would reflect whether differentially activated STAT3 confer its immune regulatory phenotype predominantly as a transcription factor or as a cytoplasmic signaling protein. STAT3 CRISPR/cas9 deleted ShcWT cells (4788) were infected with an empty vector control (null), STAT3 wild-type (WT), Y705F-STAT3 (YF), S727A-STAT3 (SA), and Y705F/S727A-STAT3 (DM). By cytoplasmic and nuclear fractionation, STAT3 localized to the nucleus regardless of the mutation status compared to the null control (**Fig. 58**). These findings should be further confirmed by co-immunofluorescence assay of STAT3 and DAPI. Nevertheless, this is consistent with the previous report that

unphosphorylated STAT3 can localize to the nucleus (Yue et al., 2010) and in the absence of Y705 phosphorylation (Meyer et al., 2002; Yang et al., 2005; Yang et al., 2010) (discussed in **section 1.6.1.2**). Taken together, we provide evidence that at least *in vitro*, STAT3 localizes to the nucleus regardless of the mutations and that they may promote immunosuppression through regulating transcription.

#### **5.4 Summary**

In this thesis, we defined for the first time the molecular mechanism of Shc1 driven breast cancer immune suppression. We demonstrate that tumor intrinsic Shc1 signaling engages the Y239/240 phospho-site to positively regulate STAT3 activation while Y313 phosphorylation negatively regulate STAT1 expression and activation in breast cancer cells. Using CRISPR/Cas9 gene deletion method, we provide evidence that STAT3 is a critical suppressor of a CTL- and IFN $\gamma$ -mediated anti-tumor immune response, and that STAT3 is a molecular player bifurcating the pro- and anti-tumorigenic functions of STAT1 during breast cancer progression. Thus, we have provided the first functional evidence that post-translational modifications of adaptor proteins are required to potentiate breast cancer immunosuppression. To expand our understanding of Shc1 signaling partners that modulate immunosuppression, we assessed Shc1 phospho-tyrosine independent and dependent interactors of Shc1 by BioID-MS and AP-MS. From this we identified Map4k5 as a Shc1 interactor. Furthermore, we explored how differential STAT3 activation by phosphorylation at Y705 or S727 regulated IFN $\gamma$ -mediated anti-tumor immune responses in orthotopic mouse models of breast cancer and demonstrated that both phosphorylation sites contribute to immunosuppression.

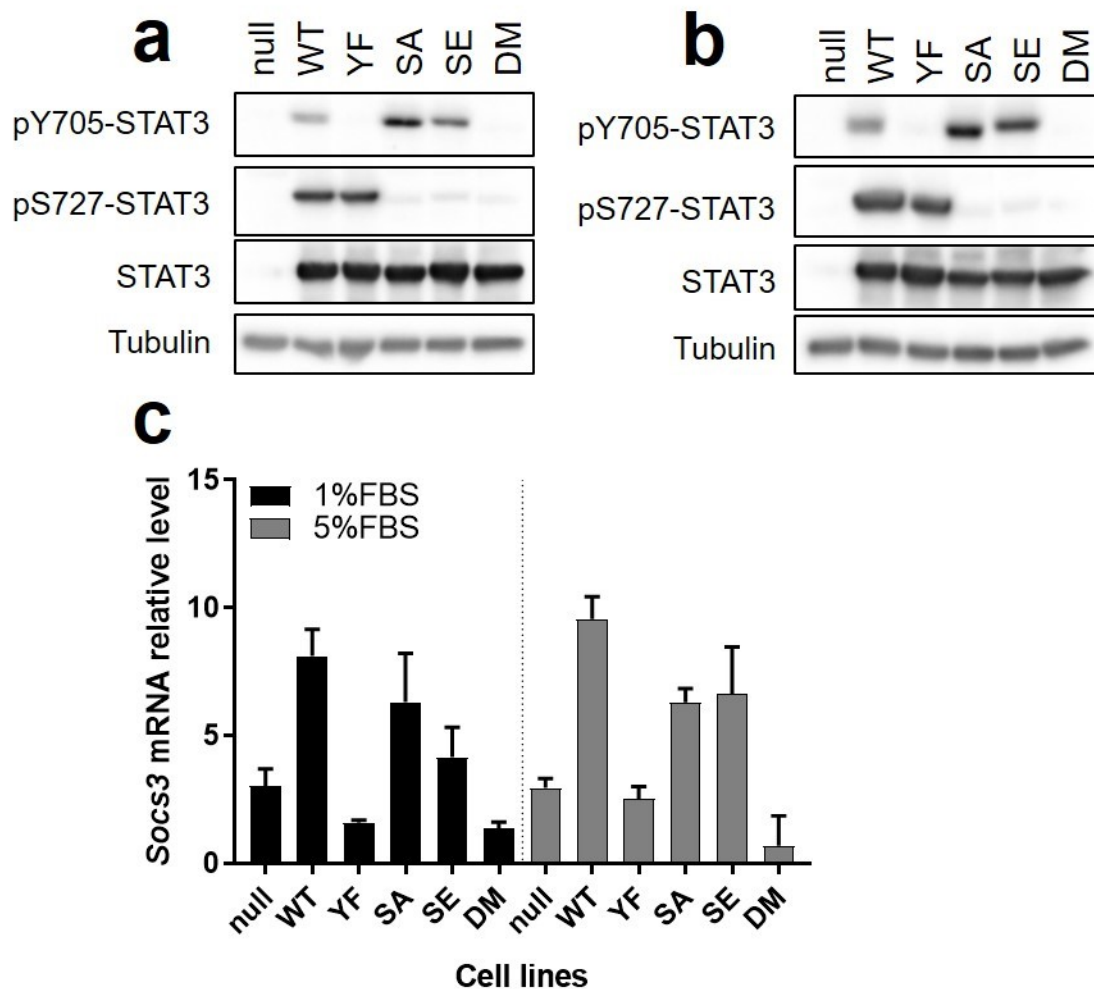


**Figure 55. STAT3 wild-type and mutant models successfully generated.**

ShcWT (4788) cells deleted of STAT3 by CRISPR/Cas9 were ectopically infected with empty vector (null), STAT3 wild-type (WT), or Y705F (YF), S727F (SA), S727E (SE), Y705F/S727A (DM) mutants. Immunoblot was carried out to verify proper expression of the STAT3 construct in (a) 1%FBS/MEGS growth media or (b) 5% FBS/MEGS growth media. (c) Cells were assessed for SOCS3 mRNA level by RT-qPCR to validate a target gene of STAT3 known to be affected by differential phosphorylation of STAT3. mean  $\pm$  s.d.

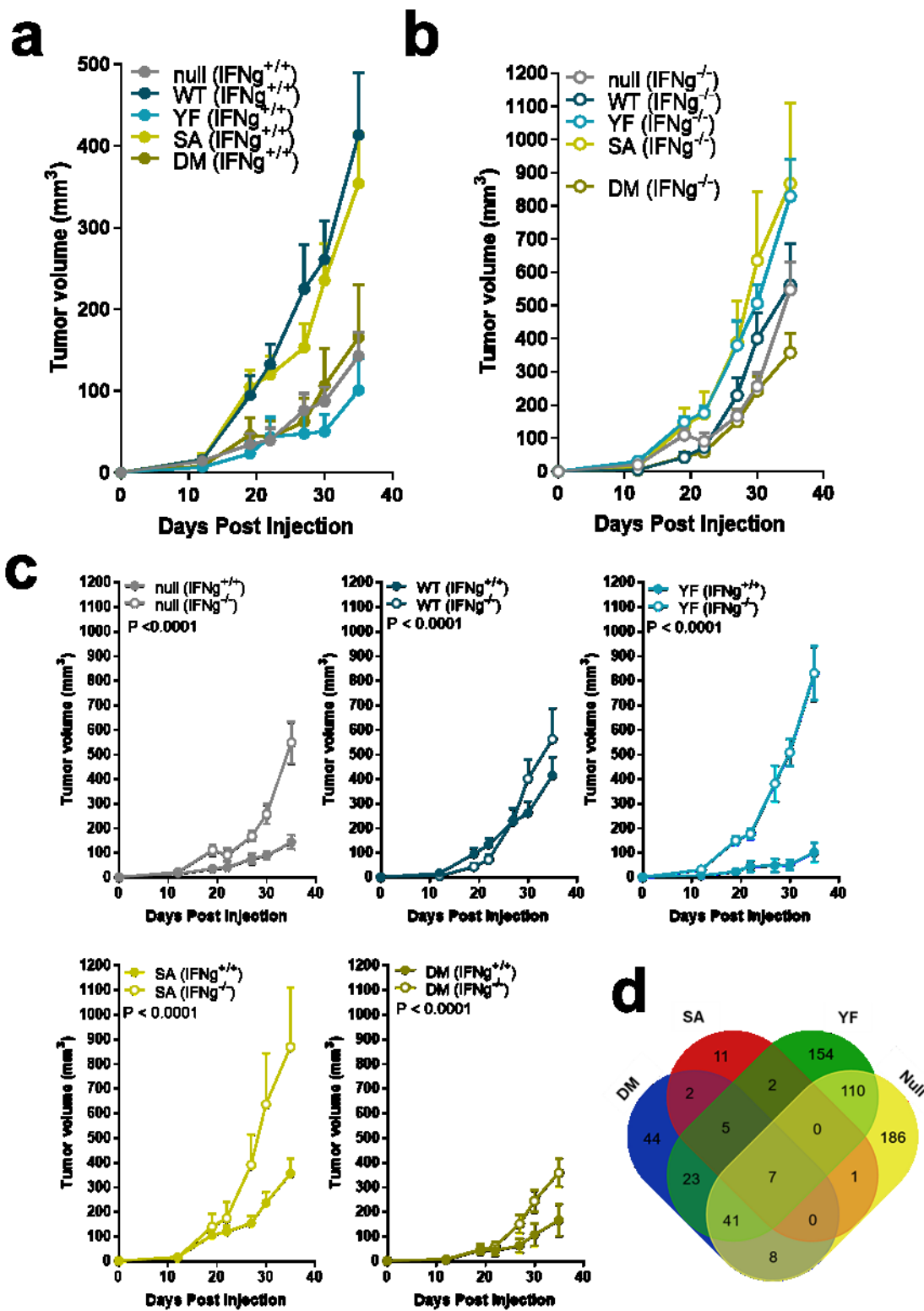
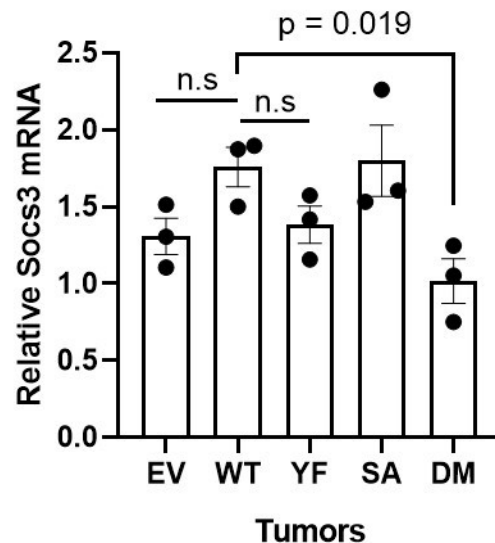


Figure 56. Phospho-Y705-STAT3 and phospho-S727-STAT3 signaling suppresses IFN $\gamma$  driven anti-tumor immune response.

STAT3 CRISPR/cas9 deleted cells were infected with pQCXIP STAT3 wild-type (WT), Y705F (YF), S727A (SA), and Y705F/S727 (DM) were injected into the mammary fat pad of syngeneic (a) IFN $\gamma^{+/+}$  or (b) IFN $\gamma^{-/-}$  mice. (c) The same outgrowth curve from (a) and (b) are plotted for individual cell line. Tumour outgrowth was measured by caliper and represented as mean tumor volume (mm<sup>3</sup>)  $\pm$  s.e.m. (n=6–12) (d) RNA-seq analysis was done on the breast tumors (n=3 / type) retrieved from IFN $\gamma^{+/+}$  mice. Fold change > 2 and p.adj < 0.05. Shown is the Venn diagram of differentially expressed genes. Statistical analysis for a, b, c was done using two-way ANOVA and Bonferroni correction.



**Figure 57. Level of SOCS3 expression *in vivo*.**

STAT3 null, WT, YF, SA, DM expressing tumors were excised at end point and analyzed by RT-qPCR for relative SOCS3 mRNA level. Data were normalized by GAPDH mRNA. Significance evaluated by two tailed, parametric, unpaired t-test. Represents average of n=2 technical replicate of 3 tumors per group.

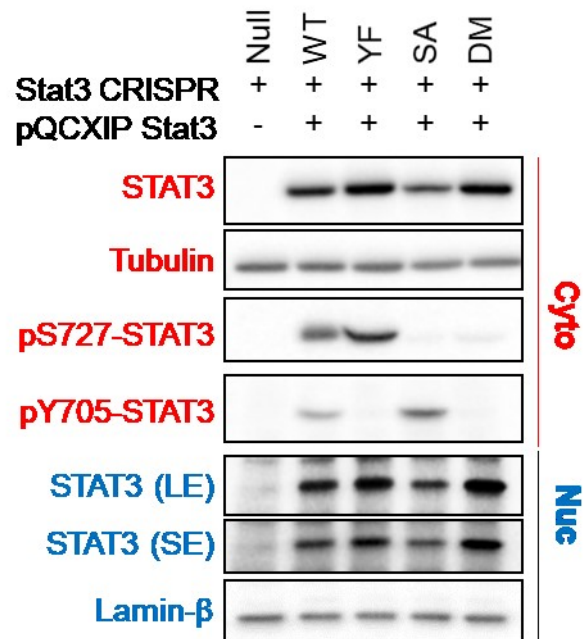


**Figure 58. STAT3 localizes to nucleus regardless of its phosphorylation status.**

Nuclear and cytoplasmic fractionation was carried out on STAT3 null or STAT3 WT, Y705F, S727A and Y705F/S727A (DM) expressing ShcWT 4788 (STAT3 null by CRISPR; re-expression vector pQCXIP). LE = long exposure. SE = short exposure.

## Chapter 6: Discussion and future directions

### 6.1 Mechanism of STAT3 activation by phospho-Y239/240-Shc1 signaling to promote immunosuppression.

We show that phospho-Y239/240-Shc1 signaling suppresses anti-tumor immune responses in part by STAT3 dependent mechanisms. The ability of the p52 Shc1 isoform to potentiate STAT3 activation *in vitro* was previously shown (Sato et al., 2002). Here we provide strong evidence that phospho-Y239/240-Shc1 signaling is the potentiator of STAT3 signaling and immunosuppression. We saw enrichment of MDSCs and increased T cell infiltration in phospho-Y239/240-Shc1 deficient tumors. This is consistent with the observation made in a MMTV/MT breast cancer mouse model where mammary epithelial specific loss of STAT3 led to increased infiltration of tumor associated macrophages while increasing T cell infiltration (Jones et al., 2015). Critically, we highlight the importance of a STAT3-Y239/240-Shc1 signaling axis in suppressing CTL-driven immune responses using both transgenic and orthotopic mouse models. There was a significant delay in tumor onset with loss of phospho-Y239/240-Shc1 signaling in MMTV/MT breast cancer model compared to controls (by 110 days) and this was partially rescued in the absence of a CTL compartment (accelerated by 19 days). Thus, while CTL driven immune responses were important in delaying the tumor onset of Shc2F tumors, there was still a significant delay due to CTL independent causes. For instance, we have not excluded the possibility that loss of Y239/240-Shc1 signaling also elicits NK and NKT cell mediated tumor clearance. This can be tested using neutralizing antibodies against asialo-GM1 or NK1.1 *in vivo* (Chiossone et al., 2018). We can also apply the CIBERSORT method on the TCGA RNA-seq dataset of breast cancer patients that showed enrichment of 2F specific gene signature to ask whether 2F signature enrichment is associated with increased infiltration of NK, NKT, and CTLs in patients (Newman et al., 2015). Importantly, tumor intrinsic Y239/240-Shc1 signaling has been shown to promote tumor progression through enhancing angiogenesis (Ursini-Siegel et al., 2008) and survival pathways (Webster et al., 1998), which likely contributed to the delayed onset.

There are other mechanisms by which phospho-Y239/240-Shc1 signaling may regulate immunosuppression. First, Shc2F cells showed significant upregulation of transcription factors *HMGA1* (2.8 fold, p.adj = 0.0004) and *HMGA2* (2.6 fold, p.adj = 0.017)

by RNA-seq. While HMGA2 has been shown to promote invasion and metastasis in breast cancer (Sun et al., 2013), in part through TGF $\beta$  driven activation (Thuault et al., 2006), both HMGA1 and HMGA2 act as damage associated molecular pattern (DAMP) molecules when released into the tumor microenvironment upon cell death, ultimately recruiting innate immune cells to further promote inflammation (Kang et al., 2014). Thus, enhanced anti-tumor killing immune responses may further synergize with released HMGA2 in breast cancer cells in response to reduced tumor intrinsic Shc1 signaling. Second, VEGF-A which promotes angiogenesis has been shown to induce accumulation of immature DC, MDSCs, Tregs, and suppress T cell infiltration (Chen and Hurwitz, 2018; Voron et al., 2014). In the MT and ErbB2 driven mouse models of breast cancer, phospho-Y239/240-Shc1 signaling has been shown to promote angiogenesis and its loss leads to reduced micro vessel density as a result of decreased VEGF production (Ursini-Siegel et al., 2008). Thus, this may have contributed to reduced immune suppression. Whether VEGF-A plays a role downstream of Y239/240-Shc1 to suppress anti-tumor immune response in our model could be substantiated by verifying the level of VEGF-A in the tumors using ELISA and repeating the *in vivo* experiment (in CD8<sup>+/+</sup> and CD8<sup>-/-</sup> mice) using Shc2F cells ectopically transfected with VEGF-A. Third, we show preliminary data that phosphorylation of Y705-STAT3 in our breast cancer cell lines is partly mediated by JAK kinase activity. These results must be first further substantiated by specific knockdown of JAK1, JAK2, and JAK3 (targets of tofacitinib). Phosphorylation of JAKs (marking activation) in Shc2F and ShcWT cells should be also compared. It is unclear how Y239/240-Shc1 may regulate JAK activation. One possibility is that phospho-Y239/240-Shc1 may activate signaling cascades that transcriptionally and translationally upregulate expression of genes responsible for JAK activation (e.g. cytokines, cytokine receptors), which in turn activate STAT3. Shc1 phospho-tyrosine signaling has been previously shown to stimulate translation through promoting AKT pathway (Im et al., 2014). Thus, it will be interesting to examine the translationally-regulated cytokines and cytokine receptors by polysome profiling followed by RNA-seq. This may also reveal other proteins involved in regulating tumor-host interaction and immunosuppression by Y239/240-Shc1 signaling that were not detected by our RNA-seq experiment.

## 6.2 Mechanism of phospho-Y313-Shc1 signaling driven suppression of STAT1 signaling

We report that phospho-Y313-Shc1 signaling suppresses STAT1 expression, STAT1 activation, expression of the APP machinery and IFN/STAT1 responsive genes (e.g. *Ifit1bl2*, *Ifit1*, *Ifih1*, *Ifi44*, *IRF9*, *IRF7*, *Ifi47*, *Ifi204*, *Ifi203*). In addition, persistent STAT1 and STAT3 activation led to increased expression of immunosuppressive proteins such as PD-L1 and MUC1, respectively. While heightened STAT1 expression did not confer pro- or anti-tumorigenic properties to Shc313F tumors *in vivo* as shown by STAT1 CRISPR-deleted tumor injections, STAT3 was critical for both Shc313F (STAT1 high) and ShcWT (STAT1 low) tumors to suppress CTL-mediated tumor clearance. We propose that STAT3 is important for dictating whether or not STAT1 can elicit anti-tumorigenic functions. Furthermore, phospho-Y313-Shc1 signaling deficient tumors demonstrated resistance to anti-PD-1 checkpoint inhibitor treatment but were sensitive to tumor vaccine treatment compared to ShcWT tumors. Taken together, we have highlighted the importance of Y313-Shc1 phosphorylation site in regulating tumor immune suppression.

It has yet to be determined how the loss of phospho-Y313-Shc1 signaling induces STAT1 expression and phosphorylation. A study by Chakraborty *et al.*, combined with our observations, may provide a critical explanation for this phenomenon (Chakraborty *et al.*, 2014). They showed that the overexpression of wild-type EGFR creates two distinct and mutually exclusive modes of signaling (Chakraborty *et al.*, 2014). At baseline, EGFR signaling recruits TBK1 kinase and activates the IRF3 transcription factor, leading to the expression of IFN responsive genes (e.g. *Ifit1*) (Chakraborty *et al.*, 2014), a phenotype also seen in Shc313F cells. Upon ligand-mediated activation, canonical ERK and AKT pathways are engaged through EGFR-Shc1 signaling complex (Chakraborty *et al.*, 2014). The study did not delve into the status of Shc1 phosphorylation. Interestingly, our AP-MS study of Shc1 mutants showed that the phosphorylation of Y313 is important for Shc1 to engage EGFR and ERBB2 (**Fig. 47**). TBK1 or IRF3 did not pull-down in any of our MS studies. Thus, it is plausible that the loss in phospho-Y313-Shc1 allows EGFR to predominantly engage TBK1/IRF3 complexes in lieu of Shc1, leading to the upregulation of STAT1 and IFN inducible genes. We can further explore by validating that Shc313F has reduced EGFR interaction compared to ShcWT through immunoprecipitating

Shc313F and ShcWT signaling complexes and probing for EGFR. We can immunoprecipitate EGFR and probe for TBK1 and Shc1 in ShcWT and Shc313F expressing cells to recapitulate what Chakraborty *et al.* saw using our cell lines. Additionally, TBK1 phosphorylation can be verified in ShcWT and Shc313F cells. Taken together, these data will substantiate the hypothesis that the loss in phospho-Y313-Shc1 allows EGFR to predominantly engage TBK1/IRF3 complexes in lieu of Shc1, ultimately upregulating STAT1.

### 6.3 Shc1 Interactome

We have characterized distinct Shc1 signaling complexes that are regulated by Y239/240 and Y313 phosphorylation in breast cancer cells using BioID-MS and AP-MS. We highlighted that these two motifs, in line with our observation made in suppressing anti-tumor immune responses through STAT3 and STAT1 pathways *in vivo*, serve as separate and distinct platforms of signaling complex formation. Numerous interactors we identified were previously known as Shc1 binders (e.g. AP2A2, LRRK1, EGFR, ErbB2, Gab1, PIK3R1, Ptpn11, and Inpp1) in the literature while some were novel (e.g. Map4k5). We then further investigated Grb2 and Map4k5 that were phospho-Y239/240-Shc1 dependent interactors of Shc1 in hopes of elucidating signaling pathways downstream of Shc1 relevant in regulating immunosuppression in breast cancer. Importantly, the potential interactors identified through the MS studies can serve as foundations for future exploration of Shc1 signaling.

We interrogated the possibility of Grb2 positively regulating STAT3 activation downstream of Shc1. Knock-down of Grb2 paradoxically led to increased phospho-Y705-STAT3 levels, an observation previously seen in one study (Zhang *et al.*, 2003a). Phospho-S727-STAT3 level did not change, suggesting that phospho-S727-STAT3 may be regulated independently of Grb2. Zhang *et al.* argued that STAT3 and Grb2 (through SH2 domain) likely compete for the Y1068 and Y1086 residues within EGFR, negatively regulating the phosphorylation of Y705-STAT3 by suppressing the ability of STAT3 to interact with EGFR (Zhang *et al.*, 2003a). This is further supported by the findings that EGFR interacts with STAT3 (Olayioye *et al.*, 1999; Park *et al.*, 1996) and this interaction has been shown to be through Y1068 and Y1086 of EGFR (Shao *et al.*, 2003; Xia *et al.*,

2002). We have observed by AP and BioID that the loss of Y239/240-Shc1 reduces Grb2 binding. It is plausible that this increases the availability of Grb2 for competitive binding to the STAT3 binding site within EGFR, resulting in overall reduction in STAT3 phosphorylation in Shc2F cells. However, the work by Zhang *et al.* did not investigate whether Shc1-Grb2 interaction played a role in their phenotype. In fact, Grb2 has also been shown to positive regulate STAT3 activation. PEAK1, a Lyn tyrosine kinase substrate, has been shown to specifically bind and use Grb2 to promote STAT3 activation (Croucher *et al.*, 2013). Grb2 in complex with SHP2 also competes with SOCS3 to bind the leptin receptor, ultimately promoting STAT3 activation (Bjorbak *et al.*, 2000; Tups *et al.*, 2012). Given the multi-faceted role of Grb2 in signal transduction independently of Shc1 (Ijaz *et al.*, 2018), knocking down Grb2 in ShcWT cells likely showed the combined effects of Shc1 dependent and independent Grb2 pathways that regulate STAT3. Thus, based on our data and the literature, we cannot yet exclude the possibility that Shc1-Grb2 interaction directly potentiates STAT3 activation.

Using BioID and AP, we provide preliminary evidence to support that Map4k5 is a novel Shc1 interactor. It is yet unclear whether Crk or Grb2 mediate this interaction. Three lines of investigation must be further pursued to define the hypothesized role of Map4k5/Crk/Shc1 signaling cascade on promoting immunosuppression (**Fig. 51**). First, to overcome the challenge encountered with the commercially available anti-Map4k5 antibody that interfered with consistent results, we could use HA tagged Map4k5 to test whether Map4k5 interacts with Shc1 in a phospho-tyrosine independent (in line with the BioID-MS result) or dependent manner (in line with the AP-MS result). This HA-Map4k5 construct would also be useful to test the hypothesis that both Shc1/Crk/Map4k5 or Shc1/Grb2/Map4k5 complexes are formed in breast cancer cells in a phospho-Y239/240-Shc1 dependent manner (**Fig. 51**). Second, Map4k5 CRISPR-deleted or shRNA knocked-down ShcWT cells are needed to assess the changes in STAT3 activity compared to controls to establish whether Map4k5 regulates STAT3 activation. Third, if indeed Map4k5/Crk/Shc1 complexes are formed, we could inject (1) Map4k5, (2) Crk or (3) Map4k5/Crk double CRISPR-deleted breast cancer cells into the mammary fat pads of CD8<sup>+/+</sup> and CD8<sup>-/-</sup>. If our hypothesis is correct, we would observe enhanced CTL driven anti-tumor immune responses in all three cohorts. We can re-express (1) Map4k5 or (2)

Crk or (3) both Map4k5 and Crk into the Map4k5/Crk double CRISPR-deleted cells. Only when both Map4k5 and Crk are re-expressed would the CTL driven anti-tumor immune response be reversed. Together, these experiments would establish whether a Shc1/Crk/Map4k5 signaling cascade plays a role in immune suppression.

Phosphorylation of S727-STAT3 in ShcWT cells was shown to be in part due to MEK pathway using trametinib. Given Shc2F cells have a baseline elevated and EGF induced ERK phosphorylation that were comparable to ShcWT (**Fig. 49**), the reduced S727-STAT3 phosphorylation observed in Shc2F is likely not through the MEK/ERK pathway. Multiple Serine/Threonine kinases have been linked to regulating phosphorylation of S727-STAT3 (**Table 3**). Of the Serine/Threonine kinases identified from our BioID-MS experiment, RSK1 (all pY dependent), and Tab1 (phospho-Y239/240 dependent) have been previously implicated in regulating STAT3 activation. RSK1, which is dependent on all phospho-Y239/240/313 sites to engage Shc1 by BioID-MS, had been shown to phosphorylate MITF to suppress PIAS3 (a STAT3 negative regulator) in response to IL-6/gp130 activation (Sonnenblick et al., 2004). It would be interesting to first validate the RSK1-Shc1 interaction and verify the level of MITF phosphorylation in Shc2F cells. Tab1, which appeared as a phospho-Y239/240 dependent interactor by BioID-MS has been shown to constitutively engage and phosphorylate Tak1 which has been shown to phosphorylate S727 upon TGF $\beta$  stimulation (Doerks et al., 2002; Kishimoto et al., 2000) or IL-6 stimulation (Kojima et al., 2005). It may be of interest to verify the level of Tak1 phosphorylation in ShcWT and Shc2F cells. mTORC1 has been previously shown to directly phosphorylate STAT3 S727 (Dodd et al., 2015). Given the reduced AKT signaling upon loss of Y239/240-Shc1 signaling, which would lead to reduced mTORC1 activation (Saxton and Sabatini, 2017), it will be of interest to characterize the mTORC1 kinase activity in Shc2F cells.

Surprisingly, well known Y705-STAT3 phosphorylating tyrosine kinases such as Src family kinases or JAK that have previously shown to interact with Shc1 were not discovered in either of our MS studies (Mishra and Kumar, 2014; Sato et al., 2002; Wills and Jones, 2012). Neither did we find known negative regulators of STAT3 pathways such as SOCS1 (FA et al., 2010) or SOCS5 (Linossi et al., 2013), both of which have been reported to bind Shc1. Linossi *et al.* showed that Y317-Shc1 (equivalent to Y313 in

mouse) binds the SH2 domain of SOCS5. This was done using surface plasmon resonance and was validated through an immunoprecipitation condition where in 293T cells were first transfected with molecularly tagged Shc1 and SOCS5, followed by treatment with proteasome inhibitor and sodium pervanadate. For our MS conditions, we neither used proteasome inhibitor nor ectopically overexpressed SOCS5. Thus, the endogenous SOCS5 expression level may have been too low for identification of SOCS5 as a Shc1 interactor by MS. These studies were conducted using overexpression of the bait proteins, contrary to our system, which interrogated binding to endogenous proteins. In addition, for AP-MS, undetected previously known interactors are possibly transient or weak Shc1 binders, which may preclude our ability to capture them by AP. For the BioID-MS, some interactors may have been excluded from the analysis due to the control Myc-BirA\* being able to significantly biotinylate those proteins, which is one of the pitfalls of BioID assay. It is also possible that at their interacting surface with Shc1, BirA on Shc1 did not have access to any lysine residues to biotinylate. Some biotinylated interactors may have been degraded before 24 hours, evading their capture. We cannot preclude the possibility that Myc-BirA and FLAG fusion prevented some of the interactors from engaging Shc1 efficiently. However, our group had previously shown that known interactors of the Shc1 PTB domain, tyrosines or SH2 domain were not impacted by the Myc-BirA\* and FLAG fusion, and that no gross changes in protein folding were likely occurring (Ha et al., 2018b).

While the kinases and phosphatases from the MS experiments are reasonable candidates to investigate, it is possible that there are other scaffold proteins that indirectly link Shc1 to STAT3 phosphorylation. It is also possible the Y239/240 phosphorylation engages multiple pathways through multiple downstream effectors that converge on STAT3 activation, and modulation of one of them in ShcWT cells may not be sufficient to implicate its role in Shc1 driven STAT3 activation. This may also explain the profound reduction in STAT3 activation in Shc2F cells as these cells are homozygous for Y239/240F. In future investigations, CRISPR/Cas9 gRNA library screen or shRNA screen against these kinases will be useful to further define the critical players in STAT3 phosphorylation and regulation.

## 6.4 Shc1 and immunotherapy

While checkpoint inhibitors have been used to treat various cancers resulting in a high response rate, large proportion of patients still remains resistant or refractory to these therapies (Sade-Feldman et al., 2018). This begs the question as to why some tumors are responsive and others are not, and what molecular mechanisms are involved. This has emerged as a pressing question in immune checkpoint therapy and immunotherapy, and studies guiding the rational design of combination therapies are needed. Here we showed that differential phosphorylation of the Shc1 adaptor protein may serve as a biomarker to predict sensitivity to immunotherapies. Using pre-clinical models of breast cancer, we have implicated the Shc1 pathway as a mechanism by which breast cancers create distinct tumor microenvironments with differential responsiveness to two types of immunotherapy, including vaccination and immune checkpoint inhibitors.

Currently, no Y239/240/313 mutations have been found in patient tumors, and no drugs can specifically inhibit a tyrosine motif within an adaptor protein (let alone be delivered to all tumor cells *in vivo*). However, our model, through mimicking a condition where all tumors are inhibited with tyrosine kinase inhibitors specifically to reduce phospho-Y239/240 or phospho-Y313 signaling, demonstrates a proof of principle that adaptor proteins can regulate tumor driven immunosuppression. It will be clinically relevant to investigate the phosphorylation status of Shc1 upon receptor and non-receptor tyrosine kinases inhibition over short and long term to understand whether there is a preferred inhibition of phosphorylation at phospho-Y239/240 or phospho-Y313 by certain treatments. Our results suggest that cells primed to re-engage STAT3 signaling would overcome TK inhibition.

Numerous inhibitors of RTKs that recruit and phosphorylate Shc1 have been shown to elicit anti-tumor immune responses, consistent with our observations made with tumors deficient of Shc1 phospho-tyrosine signaling. Sunitinib which targets VEGFR, PDGFR $\alpha$ , Ret and Kit – all of which recruit Shc1 – has been shown to elicit CTL driven anti-tumor immune responses partially through suppression of the STAT3 signaling pathway in renal cell carcinoma (Xin et al., 2009). Mutation or overexpression of EGFR (recruits Shc1), in NSCLC have been shown to promote immunosuppression, and its inhibition (e.g. gefitinib, erlotinib) restores MHC class I expression, reduces PD-L1

expression or upregulates expression of NKG2D ligands for NK cell tumor killing (Liang et al., 2018). A high-throughput immune oncology screen identified the EGFR inhibitor Erlotinib as a potent enhancer of antigen specific CTL tumor cell killing (Lizotte et al., 2018). They further showed that Erlotinib treatment synergizes with anti-PD-1 checkpoint inhibition to suppress colon cancer growth (Lizotte et al., 2018). Cabozantinib (blocks RET and MET; both recruit Shc1) has been shown to increase MHC class I (H-2Db) and Fas expression in colon cancer cell lines (Kwilas et al., 2014). Given that Shc1 serves as a substrate for these targeted RTKs (**Fig. 5, section 1.4 and 1.5.4**), our observations may provide mechanistical insight into how targeting these RTKs elicits anti-tumor immune responses and sensitizes tumors to immunotherapeutic modalities. It also argues that our observations made with Shc1 in breast cancer may extend to other solid cancer models, warranting further investigation into the role of Shc1 phospho-tyrosine signaling in other types of cancers in immune suppression.

While these results indicate TK inhibitors are promising agents to reverse immunosuppression in combination with checkpoint inhibitors, inhibitors of TKs that use Shc1 as substrate such as sorafenib (VEGFR, PDGFR, c-RAF inhibitor), dasatinib (Src kinases, Abl inhibitor), tofacitinib (JAK inhibitor), imatinib (c-Abl, Bcr-Abl, c-kit, PDGFR inhibitor) in certain context have also shown to suppress anti-tumorigenic functions of various immune cells in different types of cancers (Nishioka et al., 2011). Possibly, this may contribute to the lack of efficacy of these agents in treating breast cancer (Polk et al., 2018). Thus, it will be critical to test and choose TK inhibitors that simultaneously alleviate tumor intrinsic immune suppression and elicit anti-tumor immune response in combination with immunotherapeutic modalities (Kwilas et al., 2015)

Another emerging strategy in immunotherapy is therapeutic cancer vaccination (Hu et al., 2018). Technological advancement in next-generation sequencing and development of bioinformatics algorithms have made testing of the personalized cancer vaccination feasible, and several recent studies have brought significant promise (Hundal et al., 2019; Keskin et al., 2019; Schumacher and Schreiber, 2015). In our study, we have captured the differential responses to tumor vaccination strategies *in vivo* based on differential phosphorylation status of Shc1. Multiple points need further investigations. First, while the adaptive immune system develops memory through antigen-specific

immune responses, innate immunity has been proposed to develop heightened reactivity to stimuli in a non-specific short-lived manner (Boraschi and Italiani, 2018; Netea et al., 2011; Sun et al., 2014), using, for instance, epigenetic mechanisms (Kamada et al., 2018). Thus, we do not know whether the vaccination trained cells require adaptive and/or innate immunity to generate enhanced immune responses in Shc313F cells. It is also unclear if the enhanced APP machinery and IFN inducible gene expression in Shc313F cells were responsible for enhanced responsiveness to tumor vaccination. To test this, the tumor vaccination study can be repeated using STAT1 null versus wild-type Shc313F cells. Second, it may be interesting to address whether the differential response to tumor vaccination depended on the quality or quantity of tumor specific neo-antigens. To answer this, we can perform whole exome sequencing on the Shc1 wild-type and mutant cell lines to identify tumor cell specific mutations and use MHC binding prediction software specific for mouse to identify MHC binding neoantigens as previously done (Laumont et al., 2018; Matsushita et al., 2012), or perform immunopeptidomic (MHC class I associated peptides) mass spectrometry analysis to identify the quality of neoantigens expressed on the cell surface (Schuster et al., 2018).

Another challenge in neoantigen vaccine development is the selection of adjuvants for optimal stimulation of the host immune system delivered with the neoantigen vaccine (Hu et al., 2018). What type of soluble immunostimulatory factors are secreted with loss of phospho-Y239/240-Shc1 signaling? Could combination with these factors activate or prime the naïve antigen specific T cells and the professional APCs? It may be informative to characterize the secretomes of ShcWT, Shc2F and Shc313F breast cancer cells to understand the distinguishing cytokine or chemokine profiles between them (Patel et al., 2014; Shin et al., 2019).

Identifying signaling pathway dependency, redundancy, homeostasis (e.g. unfolded protein response, protein degradation) and signaling heterogeneity in tumors will guide cancer treatment strategies (Yaffe and VanHook, 2017). There exists a window of opportunity in combinatorial targeting of tumor signaling cascades through the use of small molecule inhibitors and boosting anti-tumor immune responses. We first need to answer which TK inhibitors can selectively elicit anti-tumor immune responses while suppressing oncogenic pathways within malignant cells. This can be addressed by

barcoding mass cytometry by time-of-flight (CyTOF) of both tumors and various immune cells (local and systemic level) with or without treatment (mono or combination) to study how the phosphoproteome of both populations are altered. Here, the phosphorylation status of Shc1 at Y239/240, Y313 and STAT3 phospho-Y705 and phospho-S727, phospho-Y701-STAT1 can serve as readouts.

## 6.5 STAT3 and immunosuppression

Multiple scenarios exist for S727 phosphorylation in the regulation of STAT3 driven immunosuppressive signals. First, it may ensure overall maximal transcription of STAT3 target (Wen et al., 1995) or allow STAT3 homodimers to effectively bind the DNA (Zhang et al., 1995). Mutating the S727 leads to reduced level of promoter activity and reduced number of transcripts (e.g. *SOCS3*) (Wakahara et al., 2012). These data suggest that S727 phosphorylation may affect quantitative aspects of STAT3 transcription. Second, it may alter the transcription of certain target genes, adding selectivity and specificity to STAT3 transcriptional responses. This could be postulated from the fact that the assessment of total STAT3 or phospho-S727-STAT3 bound to *SOCS3*, *CDCA1*, *CD14* promoters over 24 hours of IL-6 stimulation do not show the same pattern (Yang et al., 2010). Yang *et al.* also reported that the loss of S727-STAT3 phosphorylation alone significantly reduces K140 dimethylation of DNA bound STAT3 upon IL-6 treatment, and that the dimethylation event can positively or negatively regulate transcription of different STAT3 target genes (Yang et al., 2010). Thus, it will be of interest to determine how S727-STAT3 phosphorylation regulates immunosuppression through differential gene transcription.

We defined the impact of differential phosphorylation of STAT3 on the global transcriptome of tumors *in vivo* by RNA-seq. The results cannot distinguish the contribution of stromal and immune compartment from that of the tumor where there is overlap, and the direct and indirect STAT3 driven gene regulation cannot be distinguished. To address these issues, chromatin-immunoprecipitation RNA-seq (ChIP-seq) can be performed on the tumor cells in culture and *in vivo* to exhaustively answer which part of the genome it bound due to differential phosphorylation. Furthermore, some of the interesting targets known to be directly regulated by STAT3 can be analyzed by ChIP

assays, the condition for which have been optimized. It was previously reported that in hepatocytes, 41%-89% of the orthologous promoters bound by well conserved transcription factors in human were not bound by the same protein in the mouse within 5kb of the transcription start site (Odom et al., 2007). In addition, when both orthologous genes were bound by the same transcription factors, two-thirds of the binding sites do not align (Odom et al., 2007). This emphasizes that genes whose promoters have been discovered to bind differentially phosphorylated STAT3 in mouse may be significantly lacking in predictability for how STAT3 would bind genes in human cells. This suggests that ChIP-seq analysis should be done in human and mouse breast cancer models in parallel to easily identify the most critical and relevant transcriptionally regulated STAT3 target genes.

Our *in vivo* studies demonstrated the importance of both phospho-Y705-STAT3 and phospho-S727-STAT3 signaling in suppressing IFN $\gamma$  driven anti-tumor immunity. In ShcWT cells, reduced Y705 phosphorylation by JAK2/3 inhibition did not alter S727 phosphorylation, similar to what was seen in one study (Huang et al., 2014). This suggests that tyrosine and serine phosphorylation of STAT3 are regulated separately, and that tyrosine phosphorylation is not a necessary step for serine phosphorylation. Interestingly, a study in melanocytes has shown that STAT3 is phosphorylated on S727 in the absence of Y705 phosphorylation and that in primary lesions of acral lentiginous melanoma S727 phosphorylation precedes Y705 phosphorylation in the early stages of melanoma progression (Sakaguchi et al., 2012). Selective upregulation of phosphorylation at S727 was seen in tumor initiating cells to enable their survival in suspension (Liu et al., 2016). In hepatocarcinoma, increased S727 phosphorylation is observed in adenoma and late stages of HCC compared to normal tissues, while Y705 phosphorylation is detected mainly in HCC (Miyakoshi et al., 2014). Based on these reports and our observation, it will be important to investigate how differential phosphorylation status of STAT3 tyrosine and serine modulates STAT3 transcription targets and how this confers STAT3 the ability to inhibit the IFN $\gamma$  anti-tumor immune responses. Performing ChIP-Seq on these cells will indicate how the phosphorylation of tyrosine or serine differentially regulate STAT3 transcription targets in the presence or absence of IFN $\gamma$ . It was previously reported that unphosphorylated STAT3 can bind

regulatory regions of STAT3 target genes (Timofeeva et al., 2013) and that tyrosine phosphorylation or dimerization is not required for STAT3 import into the nucleus(Liu et al., 2005) as extensively discussed in **Section 1.6.1.3**. This is contradicted by another report showing that phosphorylation of tyrosine is required for nuclear import (Huang et al., 2014). Future experiments will be important to tease out what holds true in our model system and how they are implicated in blocking IFN $\gamma$  driven anti-tumor immune responses.

## Chapter 7: References

- Ahn, R., Sabourin, V., Bolt, A. M., Hébert, S., Totten, S., De Jay, N., Festa, M. C., Young, Y. K., Im, Y. K., Pawson, T., *et al.* (2017). The Shc1 adaptor simultaneously balances Stat1 and Stat3 activity to promote breast cancer immune suppression. *Nature communications* 8, 14638.
- Ahn, R., Sabourin, V., Ha, J. R., Cory, S., Maric, G., Im, Y. K., Hardy, W. R., Zhao, H., Park, M., Hallett, M., *et al.* (2013). The ShcA PTB Domain Functions as a Biological Sensor of Phosphotyrosine Signaling during Breast Cancer Progression. *Cancer Res* 73, 4521-4532.
- Akbay, E. A., Koyama, S., Carretero, J., Altabef, A., Tchaicha, J. H., Christensen, C. L., Mikse, O. R., Cherniack, A. D., Beauchamp, E. M., Pugh, T. J., *et al.* (2013). Activation of the PD-1 pathway contributes to immune escape in EGFR-driven lung tumors. *Cancer discovery* 3, 1355-1363.
- Akira, S., Nishio, Y., Inoue, M., Wang, X. J., Wei, S., Matsusaka, T., Yoshida, K., Sudo, T., Naruto, M., and Kishimoto, T. (1994). Molecular cloning of APRF, a novel IFN-stimulated gene factor 3 p91-related transcription factor involved in the gp130-mediated signaling pathway. *Cell* 77, 63-71.
- Ali, H. R., Provenzano, E., Dawson, S. J., Blows, F. M., Liu, B., Shah, M., Earl, H. M., Poole, C. J., Hiller, L., Dunn, J. A., *et al.* (2014). Association between CD8+ T-cell infiltration and breast cancer survival in 12,439 patients. *Annals of oncology : official journal of the European Society for Medical Oncology / ESMO* 25, 1536-1543.
- Alvarez, J. V., Febbo, P. G., Ramaswamy, S., Loda, M., Richardson, A., and Frank, D. A. (2005). Identification of a Genetic Signature of Activated Signal Transducer and Activator of Transcription 3 in Human Tumors. *Cancer Res* 65, 5054-5062.
- Arany, I., Faisal, A., Nagamine, Y., and Safirstein, R. L. (2008). p66shc inhibits pro-survival epidermal growth factor receptor/ERK signaling during severe oxidative stress in mouse renal proximal tubule cells. *J Biol Chem* 283, 6110-6117.
- Atkins, M. B., and Tannir, N. M. (2018). Current and emerging therapies for first-line treatment of metastatic clear cell renal cell carcinoma. *Cancer Treat Rev* 70, 127-137.
- Avalle, L., Pensa, S., Regis, G., Novelli, F., and Poli, V. (2012). STAT1 and STAT3 in tumorigenesis: A matter of balance. *Jak-Stat* 1, 65-72.
- Banerji, S., Cibulskis, K., Rangel-Escareno, C., Brown, K. K., Carter, S. L., Frederick, A. M., Lawrence, M. S., Sivachenko, A. Y., Sougnez, C., Zou, L., *et al.* (2012). Sequence analysis of mutations and translocations across breast cancer subtypes. *Nature* 486, 405-409.
- Barbie, D. A., Tamayo, P., Boehm, J. S., Kim, S. Y., Moody, S. E., Dunn, I. F., Schinzel, A. C., Sandy, P., Meylan, E., Scholl, C., *et al.* (2009). Systematic RNA interference reveals that oncogenic KRAS-driven cancers require TBK1. *Nature* 462, 108-112.
- Beatty, G., and Paterson, Y. (2001). IFN-gamma-dependent inhibition of tumor angiogenesis by tumor-infiltrating CD4+ T cells requires tumor responsiveness to IFN-gamma. *J Immunol* 166, 2276-2282.

- Beigbeder, A., Velot, L., James, D. A., and Bisson, N. (2016). Sample Preparation for Mass Spectrometry Analysis of Protein-Protein Interactions in Cancer Cell Lines and Tissues. *Methods in molecular biology* 1458, 339-347.
- Beigel, F., Friedrich, M., Probst, C., Sotlar, K., Goke, B., Diegelmann, J., and Brand, S. (2014). Oncostatin M mediates STAT3-dependent intestinal epithelial restitution via increased cell proliferation, decreased apoptosis and upregulation of SERPIN family members. *PLoS One* 9, e93498.
- Bellucci, R., Martin, A., Bommarito, D., Wang, K., Hansen, S. H., Freeman, G. J., and Ritz, J. (2015). Interferon-gamma-induced activation of JAK1 and JAK2 suppresses tumor cell susceptibility to NK cells through upregulation of PD-L1 expression. *Oncoimmunology* 4, e1008824.
- Benjamini, E., Fong, S., Erickson, C., Leung, C. Y., Rennick, D., and Scibienski, R. J. (1977). Immunity to Lymphoid Tumors Induced in Syngeneic Mice by Immunization with Mitomycin C-Treated Cells. *The Journal of Immunology* 118, 685-693.
- Beurel, E., and Jope, R. S. (2008). Differential regulation of STAT family members by glycogen synthase kinase-3. *J Biol Chem* 283, 21934-21944.
- Bhat, P., Leggatt, G., Waterhouse, N., and Frazer, I. H. (2017). Interferon-gamma derived from cytotoxic lymphocytes directly enhances their motility and cytotoxicity. *Cell death & disease* 8, e2836.
- Bhingre, A. A., Kim, J., Euskirchen, G. M., Snyder, M., and Iyer, V. R. (2007). Mapping the chromosomal targets of STAT1 by Sequence Tag Analysis of Genomic Enrichment (STAGE). *Genome Res* 17, 910-916.
- Bhullar, K. S., Lagaron, N. O., McGowan, E. M., Parmar, I., Jha, A., Hubbard, B. P., and Rupasinghe, H. P. V. (2018). Kinase-targeted cancer therapies: progress, challenges and future directions. *Mol Cancer* 17, 48.
- Biron, C. A., Nguyen, K. B., Pien, G. C., Cousens, L. P., and Salazar-Mather, T. P. (1999). Natural killer cells in antiviral defense: function and regulation by innate cytokines. *Annu Rev Immunol* 17, 189-220.
- Bjorbak, C., Lavery, H. J., Bates, S. H., Olson, R. K., Davis, S. M., Flier, J. S., and Myers, M. G., Jr. (2000). SOCS3 mediates feedback inhibition of the leptin receptor via Tyr985. *J Biol Chem* 275, 40649-40657.
- Blaikie, P. A., Fournier, E., Dilworth, S. M., Birnbaum, D., Borg, J. P., and Margolis, B. (1997). The role of the Shc phosphotyrosine interaction/phosphotyrosine binding domain and tyrosine phosphorylation sites in polyoma middle T antigen-mediated cell transformation. *J Biol Chem* 272, 20671-20677.
- Blyussen, H. A. R., Rastmanesh, M. M., Tilburgs, C., Jie, K., Wesseling, S., Goumans, M.-J., Boer, P., Joles, J. A., and Braam, B. (2010). IFN $\gamma$ -dependent SOCS3 expression inhibits IL-6-induced STAT3 phosphorylation and differentially affects IL-6 mediated transcriptional responses in endothelial cells, Vol 299).

- Bodelon, C., Oh, H., Chatterjee, N., Garcia-Closas, M., Palakal, M., Sherman, M. E., Pfeiffer, R. M., Geller, B. M., Vacek, P. M., Weaver, D. L., *et al.* (2017). Association between breast cancer genetic susceptibility variants and terminal duct lobular unit involution of the breast. *International Journal of Cancer* *140*, 825-832.
- Boero, S., Morabito, A., Banelli, B., Cardinali, B., Dozin, B., Lunardi, G., Piccioli, P., Lastraioli, S., Carosio, R., Salvi, S., *et al.* (2015). Analysis of in vitro ADCC and clinical response to trastuzumab: possible relevance of FcγR3A/FcγR2A gene polymorphisms and HER-2 expression levels on breast cancer cell lines. *J Transl Med* *13*, 324.
- Bolger, A. M., Lohse, M., and Usadel, B. (2014). Trimmomatic: a flexible trimmer for Illumina sequence data. *Bioinformatics* *30*, 2114-2120.
- Bombonati, A., and Sgroi, D. C. (2011). The molecular pathology of breast cancer progression. *J Pathol* *223*, 307-317.
- Bonaventura, P., Shekarian, T., Alcazer, V., Valladeau-Guilemond, J., Valsesia-Wittmann, S., Amigorena, S., Caux, C., and Depil, S. (2019). Cold Tumors: A Therapeutic Challenge for Immunotherapy. *Front Immunol* *10*, 168.
- Boraschi, D., and Italiani, P. (2018). Innate Immune Memory: Time for Adopting a Correct Terminology. *Front Immunol* *9*, 799-799.
- Boulton, T. G., Stahl, N., and Yancopoulos, G. D. (1994). Ciliary neurotrophic factor/leukemia inhibitory factor/interleukin 6/oncostatin M family of cytokines induces tyrosine phosphorylation of a common set of proteins overlapping those induced by other cytokines and growth factors. *J Biol Chem* *269*, 11648-11655.
- Braumuller, H., Wieder, T., Brenner, E., Assmann, S., Hahn, M., Alkhaled, M., Schilbach, K., Essmann, F., Kneilling, M., Griessinger, C., *et al.* (2013). T-helper-1-cell cytokines drive cancer into senescence. *Nature* *494*, 361-365.
- Braunstein, J., Brutsaert, S., Olson, R., and Schindler, C. (2003). STATs Dimerize in the Absence of Phosphorylation. *Journal of Biological Chemistry* *278*, 34133-34140.
- Breit, A., Besik, V., Solinski, H. J., Muehlich, S., Glas, E., Yarwood, S. J., and Gudermann, T. (2015). Serine-727 phosphorylation activates hypothalamic STAT-3 independently from tyrosine-705 phosphorylation. *Molecular endocrinology (Baltimore, Md)* *29*, 445-459.
- Bromberg, J. F., Wrzeszczynska, M. H., Devgan, G., Zhao, Y., Pestell, R. G., Albanese, C., and Darnell, J. E., Jr. Stat3 as an Oncogene. *Cell* *98*, 295-303.
- Buchert, M., Burns, C. J., and Ernst, M. (2016). Targeting JAK kinase in solid tumors: emerging opportunities and challenges. *Oncogene* *35*, 939-951.
- Buerger, C., Nagel-Wolfrum, K., Kunz, C., Wittig, I., Butz, K., Hoppe-Seyler, F., and Groner, B. (2003). Sequence-specific peptide aptamers, interacting with the intracellular domain of the epidermal growth factor receptor, interfere with Stat3 activation and inhibit the growth of tumor cells. *J Biol Chem* *278*, 37610-37621.

Burke, F., Smith, P. D., Crompton, M. R., Upton, C., and Balkwill, F. R. (1999). Cytotoxic response of ovarian cancer cell lines to IFN-gamma is associated with sustained induction of IRF-1 and p21 mRNA. *Br J Cancer* *80*, 1236-1244.

Burstein, M. D., Tsimelzon, A., Poage, G. M., Covington, K. R., Contreras, A., Fuqua, S. A., Savage, M. I., Osborne, C. K., Hilsenbeck, S. G., Chang, J. C., *et al.* (2015). Comprehensive genomic analysis identifies novel subtypes and targets of triple-negative breast cancer. *Clin Cancer Res* *21*, 1688-1698.

Butti, R., Das, S., Gunasekaran, V. P., Yadav, A. S., Kumar, D., and Kundu, G. C. (2018). Receptor tyrosine kinases (RTKs) in breast cancer: signaling, therapeutic implications and challenges. *Mol Cancer* *17*, 34.

Campbell, K. S., Ogris, E., Burke, B., Su, W., Auger, K. R., Druker, B. J., Schaffhausen, B. S., Roberts, T. M., and Pallas, D. C. (1994). Polyoma middle tumor antigen interacts with SHC protein via the NPTY (Asn-Pro-Thr-Tyr) motif in middle tumor antigen. *Proceedings of the National Academy of Sciences* *91*, 6344-6348.

Cantin, E., Tanamachi, B., Openshaw, H., Mann, J., and Clarke, K. (1999). Gamma Interferon (IFN- $\gamma$ ) Receptor Null-Mutant Mice Are More Susceptible to Herpes Simplex Virus Type 1 Infection than IFN- $\gamma$  Ligand Null-Mutant Mice. *Journal of Virology* *73*, 5196-5200.

Cao, X., Tay, A., Guy, G. R., and Tan, Y. H. (1996). Activation and association of Stat3 with Src in v-Src-transformed cell lines. *Molecular and cellular biology* *16*, 1595-1603.

Carbognin, E., Betto, R. M., Soriano, M. E., Smith, A. G., and Martello, G. (2016). Stat3 promotes mitochondrial transcription and oxidative respiration during maintenance and induction of naive pluripotency. *EMBO J* *35*, 618-634.

Casey, S. C., Tong, L., Li, Y., Do, R., Walz, S., Fitzgerald, K. N., Gouw, A. M., Baylot, V., Gutgemann, I., Eilers, M., and Felsher, D. W. (2016). MYC regulates the antitumor immune response through CD47 and PD-L1. *Science* *352*, 227-231.

Cato, A. C., Henderson, D., and Ponta, H. (1987). The hormone response element of the mouse mammary tumour virus DNA mediates the progestin and androgen induction of transcription in the proviral long terminal repeat region. *The EMBO journal* *6*, 363-368.

Ceresa, B. P., and Pessin, J. E. (1996). Insulin stimulates the serine phosphorylation of the signal transducer and activator of transcription (STAT3) isoform. *J Biol Chem* *271*, 12121-12124.

Chakraborty, S., Li, L., Puliappadamba, V. T., Guo, G., Hatanpaa, K. J., Mickey, B., Souza, R. F., Vo, P., Herz, J., Chen, M. R., *et al.* (2014). Constitutive and ligand-induced EGFR signalling triggers distinct and mutually exclusive downstream signalling networks. *Nature communications* *5*, 5811.

Chan, S. R., Rickert, C. G., Vermi, W., Sheehan, K. C., Arthur, C., Allen, J. A., White, J. M., Archambault, J., Lonardi, S., McDevitt, T. M., *et al.* (2014). Dysregulated STAT1-SOCS1 control of JAK2 promotes mammary luminal progenitor cell survival and drives ERalpha(+) tumorigenesis. *Cell Death Differ* *21*, 234-246.

- Chang, Q., Bournazou, E., Sansone, P., Berishaj, M., Gao, S. P., Daly, L., Wels, J., Theilen, T., Granitto, S., Zhang, X., *et al.* (2013). The IL-6/JAK/Stat3 feed-forward loop drives tumorigenesis and metastasis. *Neoplasia* 15, 848-862.
- Chatterjee-Kishore, M., van Den Akker, F., and Stark, G. R. (2000). Adenovirus E1A down-regulates LMP2 transcription by interfering with the binding of stat1 to IRF1. *J Biol Chem* 275, 20406-20411.
- Chawla, K., Tripathi, S., Thommesen, L., Laegreid, A., and Kuiper, M. (2013). TFcheckpoint: a curated compendium of specific DNA-binding RNA polymerase II transcription factors. *Bioinformatics* 29, 2519-2520.
- Chen, D. S., and Hurwitz, H. (2018). Combinations of Bevacizumab With Cancer Immunotherapy. *Cancer J* 24, 193-204.
- Chen, G., Gupta, R., Petrik, S., Laiko, M., Leatherman, J. M., Asquith, J. M., Daphtary, M. M., Garrett-Mayer, E., Davidson, N. E., Hirt, K., *et al.* (2014). A feasibility study of cyclophosphamide, trastuzumab, and an allogeneic GM-CSF-secreting breast tumor vaccine for HER2+ metastatic breast cancer. *Cancer Immunol Res* 2, 949-961.
- Cheng, F., Lienlaf, M., Wang, H. W., Perez-Villaruel, P., Lee, C., Woan, K., Rock-Klotz, J., Sahakian, E., Woods, D., Pinilla-Ibarz, J., *et al.* (2014). A novel role for histone deacetylase 6 in the regulation of the tolerogenic STAT3/IL-10 pathway in APCs. *J Immunol* 193, 2850-2862.
- Cheng, F., Wang, H.-W., Cuenca, A., Huang, M., Ghansah, T., Brayer, J., Kerr, W. G., Takeda, K., Akira, S., Schoenberger, S. P., *et al.* (2003). A Critical Role for Stat3 Signaling in Immune Tolerance. *Immunity* 19, 425-436.
- Cheon, H., and Stark, G. R. (2009). Unphosphorylated STAT1 prolongs the expression of interferon-induced immune regulatory genes. *Proc Natl Acad Sci U S A* 106, 9373-9378.
- Chiang, C. L.-L., Coukos, G., and Kandalaft, L. E. (2015). Whole Tumor Antigen Vaccines: Where Are We? *Vaccines (Basel)* 3, 344-372.
- Chin, A. I., Shu, J., Shan Shi, C., Yao, Z., Kehrl, J. H., and Cheng, G. (1999). TANK potentiates tumor necrosis factor receptor-associated factor-mediated c-Jun N-terminal kinase/stress-activated protein kinase activation through the germinal center kinase pathway. *Mol Cell Biol* 19, 6665-6672.
- Chiossone, L., Dumas, P. Y., Vienne, M., and Vivier, E. (2018). Natural killer cells and other innate lymphoid cells in cancer. *Nat Rev Immunol* 18, 671-688.
- Choi, H., Larsen, B., Lin, Z. Y., Breikreutz, A., Mellacheruvu, D., Fermin, D., Qin, Z. S., Tyers, M., Gingras, A. C., and Nesvizhskii, A. I. (2011). SAINT: probabilistic scoring of affinity purification-mass spectrometry data. *Nature methods* 8, 70-73.
- Chung, C. D., Liao, J., Liu, B., Rao, X., Jay, P., Berta, P., and Shuai, K. (1997a). Specific inhibition of Stat3 signal transduction by PIAS3. *Science* 278, 1803-1805.

- Chung, J., Uchida, E., Grammer, T. C., and Blenis, J. (1997b). STAT3 serine phosphorylation by ERK-dependent and -independent pathways negatively modulates its tyrosine phosphorylation. *Molecular and Cellular Biology* 17, 6508-6516.
- Chung, J., Uchida, E., Grammer, T. C., and Blenis, J. (1997c). STAT3 serine phosphorylation by ERK-dependent and -independent pathways negatively modulates its tyrosine phosphorylation. *Molecular and Cellular Biology* 17, 6508-6516.
- Cimino-Mathews, A., Thompson, E., Taube, J. M., Ye, X., Lu, Y., Meeker, A., Xu, H., Sharma, R., Lecksell, K., Cornish, T. C., *et al.* (2016). PD-L1 (B7-H1) expression and the immune tumor microenvironment in primary and metastatic breast carcinomas. *Hum Pathol* 47, 52-63.
- Concha-Benavente, F., and Ferris, R. (2015). JAK2 inhibition prevents NK-released IFN $\gamma$ -mediated PD-L1 upregulation and enhances cetuximab mediated ADCC of HNC cells (TUM2P.1014). *The Journal of Immunology* 194, 69.11.
- Cordon-Cardo, C., and Prives, C. (1999). At the crossroads of inflammation and tumorigenesis. *J Exp Med* 190, 1367-1370.
- Corredor, G., Wang, X., Zhou, Y., Lu, C., Fu, P., Syrigos, K., Rimm, D. L., Yang, M., Romero, E., Schalper, K. A., *et al.* (2019). Spatial Architecture and Arrangement of Tumor-Infiltrating Lymphocytes for Predicting Likelihood of Recurrence in Early-Stage Non-Small Cell Lung Cancer. *Clin Cancer Res* 25, 1526-1534.
- Courapied, S., Sellier, H., de Carne Trecesson, S., Vigneron, A., Bernard, A. C., Gamelin, E., Barre, B., and Coqueret, O. (2010). The cdk5 kinase regulates the STAT3 transcription factor to prevent DNA damage upon topoisomerase I inhibition. *J Biol Chem* 285, 26765-26778.
- Coussens, L. M., Raymond, W. W., Bergers, G., Laig-Webster, M., Behrendtsen, O., Werb, Z., Caughey, G. H., and Hanahan, D. (1999). Inflammatory mast cells up-regulate angiogenesis during squamous epithelial carcinogenesis. *Genes and Development* 13, 1382-1397.
- Coussens, L. M., Tinkle, C. L., Hanahan, D., and Werb, Z. (2000). MMP-9 supplied by bone marrow-derived cells contributes to skin carcinogenesis. *Cell* 103, 481-490.
- Couzens, A. L., Knight, J. D., Kean, M. J., Teo, G., Weiss, A., Dunham, W. H., Lin, Z. Y., Bagshaw, R. D., Sicheri, F., Pawson, T., *et al.* (2013). Protein interaction network of the mammalian Hippo pathway reveals mechanisms of kinase-phosphatase interactions. *Sci Signal* 6, rs15.
- Croucher, D. R., Hochgrafe, F., Zhang, L., Liu, L., Lyons, R. J., Rickwood, D., Tactacan, C. M., Browne, B. C., Ali, N., Chan, H., *et al.* (2013). Involvement of Lyn and the atypical kinase Sgk269/PEAK1 in a basal breast cancer signaling pathway. *Cancer Res* 73, 1969-1980.
- Dai, X., Park, J. J., Du, Y., Kim, H. R., Wang, G., Errami, Y., and Chen, S. (2019). One-step generation of modular CAR-T cells with AAV-Cpf1. *Nature methods* 16, 247-254.
- Dalton, D. K., Pitts-Meek, S., Keshav, S., Figari, I. S., Bradley, A., and Stewart, T. A. (1993). Multiple defects of immune cell function in mice with disrupted interferon-gamma genes. *Science* 259, 1739-1742.

- Dankort, D., Maslikowski, B., Warner, N., Kanno, N., Kim, H., Wang, Z., Moran, M. F., Oshima, R. G., Cardiff, R. D., and Muller, W. J. (2001). Grb2 and Shc adapter proteins play distinct roles in Neu (ErbB-2)-induced mammary tumorigenesis: implications for human breast cancer. *Molecular and Cellular Biology* 21, 1540-1551.
- Darnell, J., Kerr, I., and Stark, G. (1994). Jak-STAT pathways and transcriptional activation in response to IFNs and other extracellular signaling proteins. *Science* 264, 1415-1421.
- Dauer, D. J., Ferraro, B., Song, L., Yu, B., Mora, L., Buettner, R., Enkemann, S., Jove, R., and Haura, E. B. (2005). Stat3 regulates genes common to both wound healing and cancer. *Oncogene* 24, 3397-3408.
- David, M., Wong, L., Flavell, R., Thompson, S. A., Wells, A., Larner, A. C., and Johnson, G. R. (1996). STAT Activation by Epidermal Growth Factor (EGF) and Amphiregulin: REQUIREMENT FOR THE EGF RECEPTOR KINASE BUT NOT FOR TYROSINE PHOSPHORYLATION SITES OR JAK1. *Journal of Biological Chemistry* 271, 9185-9188.
- Davol, P. A., Bagdasaryan, R., Eifenbein, G. J., Maizel, A. L., and Frackelton, A. R. (2003). Shc Proteins Are Strong, Independent Prognostic Markers for Both Node-Negative and Node-Positive Primary Breast Cancer. *Cancer Res* 63, 6772-6783.
- Decker, T., and Kovarik, P. (2000). Serine phosphorylation of STATs. *Oncogene* 19, 2628-2637.
- Demaria, M., Giorgi, C., Lebedzinska, M., Esposito, G., D'Angeli, L., Bartoli, A., Gough, D. J., Turkson, J., Levy, D. E., Watson, C. J., *et al.* (2010). A STAT3-mediated metabolic switch is involved in tumour transformation and STAT3 addiction. *Aging (Albany NY)* 2, 823-842.
- DeNardo, D. G., Andreu, P., and Coussens, L. M. (2010). Interactions between lymphocytes and myeloid cells regulate pro- versus anti-tumor immunity. *Cancer Metastasis Rev* 29, 309-316.
- DeNardo, D. G., Barreto, J. B., Andreu, P., Vasquez, L., Tawfik, D., Kolhatkar, N., and Coussens, L. M. (2009). CD4 + T Cells Regulate Pulmonary Metastasis of Mammary Carcinomas by Enhancing Protumor Properties of Macrophages. *Cancer Cell* 16, 91-102.
- Denkert, C., von Minckwitz, G., Darb-Esfahani, S., Lederer, B., Heppner, B. I., Weber, K. E., Budczies, J., Huober, J., Klauschen, F., Furlanetto, J., *et al.* (2018). Tumour-infiltrating lymphocytes and prognosis in different subtypes of breast cancer: a pooled analysis of 3771 patients treated with neoadjuvant therapy. *The Lancet Oncology* 19, 40-50.
- Dhar, K., Rakesh, K., Pankajakshan, D., and Agrawal, D. K. (2013). SOCS3 promotor hypermethylation and STAT3-NF-κB interaction downregulate SOCS3 expression in human coronary artery smooth muscle cells, Vol 304).
- Dilworth, S. M. (1995). Polyoma virus middle T antigen: meddler or mimic? *Trends in microbiology* 3, 31-35.
- Dilworth, S. M., Brewster, C. E. P., Jones, M. D., Lanfrancone, L., Pelicci, G., and Pelicci, P. G. (1994). Transformation by polyoma virus middle T-antigen involves the binding and tyrosine phosphorylation of Shc. *Nature* 367, 87-90.

Dimberg, A., Karlberg, I., Nilsson, K., and Oberg, F. (2003). Ser727/Tyr701-phosphorylated Stat1 is required for the regulation of c-Myc, cyclins, and p27Kip1 associated with ATRA-induced G0/G1 arrest of U-937 cells. *Blood* 102, 254-261.

Dimri, S., Sukanya, and De, A. (2017). Approaching non-canonical STAT3 signaling to redefine cancer therapeutic strategy. *Integrative Molecular Medicine* 4.

Dobin, A., Davis, C. A., Schlesinger, F., Drenkow, J., Zaleski, C., Jha, S., Batut, P., Chaisson, M., and Gingeras, T. R. (2013). STAR: ultrafast universal RNA-seq aligner. *Bioinformatics* 29, 15-21.

Dodd, K. M., Yang, J., Shen, M. H., Sampson, J. R., and Tee, A. R. (2015). mTORC1 drives HIF-1alpha and VEGF-A signalling via multiple mechanisms involving 4E-BP1, S6K1 and STAT3. *Oncogene* 34, 2239-2250.

Doerks, T., Copley, R. R., Schultz, J., Ponting, C. P., and Bork, P. (2002). Systematic identification of novel protein domain families associated with nuclear functions. *Genome Res* 12, 47-56.

Domoszlai, T., Martincuks, A., Fahrenkamp, D., Schmitz-Van de Leur, H., Kuster, A., and Muller-Newen, G. (2014). Consequences of the disease-related L78R mutation for dimerization and activity of STAT3. *J Cell Sci* 127, 1899-1910.

Dunn, G. P., Bruce, A. T., Ikeda, H., Old, L. J., and Schreiber, R. D. (2002). Cancer immunoediting: from immunosurveillance to tumor escape. *Nat Immunol* 3, 991-998.

Dunn, G. P., Koebel, C. M., and Schreiber, R. D. (2006). Interferons, immunity and cancer immunoediting. *Nat Rev Immunol* 6, 836-848.

Dunn, G. P., Old, L. J., and Schreiber, R. D. (2004). The immunobiology of cancer immunosurveillance and immunoediting. *Immunity* 21, 137-148.

Durbin, J. E., Hackenmiller, R., Simon, M. C., and Levy, D. E. (1996). Targeted Disruption of the Mouse Stat1 Gene Results in Compromised Innate Immunity to Viral Disease. *Cell* 84, 443-450.

Dvorak, H. F. (1986). Tumors: Wounds That Do Not Heal. *New England Journal of Medicine* 315, 1650-1659.

Ehret, G. B., Reichenbach, P., Schindler, U., Horvath, C. M., Fritz, S., Nabholz, M., and Bucher, P. (2001). DNA binding specificity of different STAT proteins. Comparison of in vitro specificity with natural target sites. *J Biol Chem* 276, 6675-6688.

Eyob, H., Ekiz, H. A., Derose, Y. S., Waltz, S. E., Williams, M. A., and Welm, A. L. (2013). Inhibition of ron kinase blocks conversion of micrometastases to overt metastases by boosting antitumor immunity. *Cancer discovery* 3, 751-760.

FA, M., V, C., S, I., and G., F. (2010). SOCS1, a novel interaction partner of p53 controlling oncogene-induced senescence. *Aging (Albany NY)* 2, 445-452.

Fagiani, E., Giardina, G., Luzi, L., Cesaroni, M., Quarto, M., Capra, M., Germano, G., Bono, M., Capillo, M., Pelicci, P., and Lanfrancone, L. (2007). RaLP, a new member of the Src homology and collagen family, regulates cell migration and tumor growth of metastatic melanomas. *Cancer Res* 67, 3064-3073.

- Fantin, V. R., Loboda, A., Paweletz, C. P., Hendrickson, R. C., Pierce, J. W., Roth, J. A., Li, L., Gooden, F., Korenchuk, S., Hou, X. S., *et al.* (2008). Constitutive Activation of Signal Transducers and Activators of Transcription Predicts Vorinostat Resistance in Cutaneous T-Cell Lymphoma. *Cancer Res* *68*, 3785-3794.
- Feng, Y., Spezia, M., Huang, S., Yuan, C., Zeng, Z., Zhang, L., Ji, X., Liu, W., Huang, B., Luo, W., *et al.* (2018). Breast cancer development and progression: Risk factors, cancer stem cells, signaling pathways, genomics, and molecular pathogenesis. *Genes Dis* *5*, 77-106.
- Figuroa, J. D., Pfeiffer, R. M., Patel, D. A., Linville, L., Brinton, L. A., Gierach, G. L., Yang, X. R., Papatomas, D., Visscher, D., Mies, C., *et al.* (2014). Terminal duct lobular unit involution of the normal breast: implications for breast cancer etiology. *Journal of the National Cancer Institute* *106*, dju286.
- Finlayson, C. A., Chappell, J., Leitner, J. W., Goalstone, M. L., Garrity, M., Nawaz, S., Ciaraldi, T. P., and Draznin, B. (2003). Enhanced insulin signaling via Shc in human breast cancer. *Metabolism - Clinical and Experimental* *52*, 1606-1611.
- Fluck, M. M., and Schaffhausen, B. S. (2009). Lessons in signaling and tumorigenesis from polyomavirus middle T antigen. *Microbiology and molecular biology reviews* : MMBR *73*, 542-563, Table of Contents.
- Flynn, D. C. (2001). Adaptor proteins. *Oncogene* *20*, 6270.
- Foster, B. M., Zaidi, D., Young, T. R., Mobley, M. E., and Kerr, B. A. (2018). CD117/c-kit in Cancer Stem Cell-Mediated Progression and Therapeutic Resistance. *Biomedicines* *6*, 31.
- Frackelton, A. R., Jr., Lu, L., Davol, P. A., Bagdasaryan, R., Hafer, L. J., and Sgroi, D. C. (2006). p66 Shc and tyrosine-phosphorylated Shc in primary breast tumors identify patients likely to relapse despite tamoxifen therapy. *Breast Cancer Res* *8*, R73.
- Fu, N., Lindeman, G. J., and Visvader, J. E. (2014). Chapter Five - The Mammary Stem Cell Hierarchy. In *Current Topics in Developmental Biology*, M. Rendl, ed. (Academic Press), pp. 133-160.
- Fu, X.-Y., and Zhang, J.-J. (1993). Transcription factor p91 interacts with the epidermal growth factor receptor and mediates activation of the c-fos gene promoter. *Cell* *74*, 1135-1145.
- Fung-Leung, W. P., Schilham, M. W., Rahemtulla, A., Kundig, T. M., Vollenweider, M., Potter, J., van Ewijk, W., and Mak, T. W. (1991). CD8 is needed for development of cytotoxic T cells but not helper T cells. *Cell* *65*, 443-449.
- Gabrilovich, D. I., Ostrand-Rosenberg, S., and Bronte, V. (2012). Coordinated regulation of myeloid cells by tumours. *Nat Rev Immunol* *12*, 253-268.
- Gagnon, A., Artemenko, Y., Crapper, T., and Sorisky, A. (2003). Regulation of endogenous SH2 domain-containing inositol 5-phosphatase (SHIP2) in 3T3-L1 and human preadipocytes. *J Cell Physiol* *197*, 243-250.

Galon, J., Costes, A., Sanchez-Cabo, F., Kirilovsky, A., Mlecnik, B., Lagorce-Pages, C., Tosolini, M., Camus, M., Berger, A., Wind, P., *et al.* (2006). Type, density, and location of immune cells within human colorectal tumors predict clinical outcome. *Science* *313*, 1960-1964.

Galvagni, F., Pennacchini, S., Salameh, A., Rocchigiani, M., Neri, F., Orlandini, M., Petraglia, F., Gotta, S., Sardone, G. L., Matteucci, G., *et al.* (2010). Endothelial cell adhesion to the extracellular matrix induces c-Src-dependent VEGFR-3 phosphorylation without the activation of the receptor intrinsic kinase activity. *Circ Res* *106*, 1839-1848.

Garcia-Diaz, A., Shin, D. S., Moreno, B. H., Saco, J., Escuin-Ordinas, H., Rodriguez, G. A., Zaretsky, J. M., Sun, L., Hugo, W., Wang, X., *et al.* (2017). Interferon Receptor Signaling Pathways Regulating PD-L1 and PD-L2 Expression. *Cell Rep* *19*, 1189-1201.

Gartsbein, M., Alt, A., Hashimoto, K., Nakajima, K., Kuroki, T., and Tennenbaum, T. (2006). The role of protein kinase C delta activation and STAT3 Ser727 phosphorylation in insulin-induced keratinocyte proliferation. *J Cell Sci* *119*, 470-481.

Gingras, A. C., Gstaiger, M., Raught, B., and Aebersold, R. (2007). Analysis of protein complexes using mass spectrometry. *Nat Rev Mol Cell Biol* *8*, 645-654.

Gingras, A. C., and Raught, B. (2012). Beyond hairballs: The use of quantitative mass spectrometry data to understand protein-protein interactions. *FEBS Lett* *586*, 2723-2731.

Giordano, V., De Falco, G., Chiari, R., Quinto, I., Pelicci, P. G., Bartholomew, L., Delmastro, P., Gadina, M., and Scala, G. (1997). Shc mediates IL-6 signaling by interacting with gp130 and Jak2 kinase. *J Immunol* *158*, 4097-4103.

Goel, S., DeCristo, M. J., Watt, A. C., BrinJones, H., Sceneay, J., Li, B. B., Khan, N., Ubellacker, J. M., Xie, S., Metzger-Filho, O., *et al.* (2017). CDK4/6 inhibition triggers anti-tumour immunity. *Nature* *548*, 471-475.

Goes, N., Sims, T., Urmson, J., Vincent, D., Ramassar, V., and Halloran, P. F. (1995). Disturbed MHC regulation in the IFN-gamma knockout mouse. Evidence for three states of MHC expression with distinct roles for IFN-gamma. *J Immunol* *155*, 4559-4566.

Goodman, A. M., Kato, S., Bazhenova, L., Patel, S. P., Frampton, G. M., Miller, V., Stephens, P. J., Daniels, G. A., and Kurzrock, R. (2017). Tumor Mutational Burden as an Independent Predictor of Response to Immunotherapy in Diverse Cancers. *Mol Cancer Ther* *16*, 2598-2608.

Gotoh, N., Tojo, A., and Shibuya, M. (1996). A novel pathway from phosphorylation of tyrosine residues 239/240 of Shc, contributing to suppress apoptosis by IL-3. *Embo j* *15*, 6197-6204.

Gotoh, N., Toyoda, M., and Shibuya, M. (1997). Tyrosine phosphorylation sites at amino acids 239 and 240 of Shc are involved in epidermal growth factor-induced mitogenic signaling that is distinct from Ras/mitogen-activated protein kinase activation. *Mol Cell Biol* *17*, 1824-1831.

Gough, D. J., Corlett, A., Schlessinger, K., Wegrzyn, J., Lerner, A. C., and Levy, D. E. (2009). Mitochondrial STAT3 supports Ras-dependent oncogenic transformation. *Science* *324*, 1713-1716.

- Gough, D. J., Koetz, L., and Levy, D. E. (2013). The MEK-ERK pathway is necessary for serine phosphorylation of mitochondrial STAT3 and Ras-mediated transformation. *PLoS One* *8*, e83395.
- Grandis, J. R., Drenning, S. D., Chakraborty, A., Zhou, M. Y., Zeng, Q., Pitt, A. S., and Tweardy, D. J. (1998). Requirement of Stat3 but not Stat1 activation for epidermal growth factor receptor-mediated cell growth In vitro. *J Clin Invest* *102*, 1385-1392.
- Greulich, H., Chen, T. H., Feng, W., Janne, P. A., Alvarez, J. V., Zappaterra, M., Bulmer, S. E., Frank, D. A., Hahn, W. C., Sellers, W. R., and Meyerson, M. (2005). Oncogenic transformation by inhibitor-sensitive and -resistant EGFR mutants. *PLoS medicine* *2*, e313.
- Gudjonsson, T., Adriance, M. C., Sternlicht, M. D., Petersen, O. W., and Bissell, M. J. (2005). Myoepithelial cells: their origin and function in breast morphogenesis and neoplasia. *J Mammary Gland Biol Neoplasia* *10*, 261-272.
- Guy, C. T., Cardiff, R. D., and Muller, W. J. (1992). Induction of mammary tumors by expression of polyomavirus middle T oncogene: a transgenic mouse model for metastatic disease. *Molecular and Cellular Biology* *12*, 954-961.
- Ha, J. R., Ahn, R., Smith, H. W., Sabourin, V., Hebert, S., Cepeda Canedo, E., Im, Y. K., Kleinman, C., Muller, W. J., and Ursini-Siegel, J. (2018a). Integration of distinct ShcA signaling complexes promotes breast tumor growth and tyrosine kinase inhibitor resistance. *Mol Cancer Res*.
- Ha, J. R., Ahn, R., Smith, H. W., Sabourin, V., Hebert, S., Cepeda Canedo, E., Im, Y. K., Kleinman, C. L., Muller, W. J., and Ursini-Siegel, J. (2018b). Integration of Distinct ShcA Signaling Complexes Promotes Breast Tumor Growth and Tyrosine Kinase Inhibitor Resistance. *Mol Cancer Res* *16*, 894-908.
- Ha, J. R., Siegel, P. M., and Ursini-Siegel, J. (2016). The Tyrosine Kinome Dictates Breast Cancer Heterogeneity and Therapeutic Responsiveness. *J Cell Biochem* *117*, 1971-1990.
- HAAN, S., KORTYLEWSKI, M., BEHRMANN, I., MÜLLER-ESTERL, W., HEINRICH, P. C., and SCHAPER, F. (2000). Cytoplasmic STAT proteins associate prior to activation. *Biochemical Journal* *345*, 417-421.
- Haines, E., Saucier, C., and Claing, A. (2014). The adaptor proteins p66Shc and Grb2 regulate the activation of the GTPases ARF1 and ARF6 in invasive breast cancer cells. *J Biol Chem*.
- Hanahan, D., and Weinberg, R. A. (2011). Hallmarks of cancer: the next generation. *Cell* *144*, 646-674.
- Hannesdottir, L., Tymoszuk, P., Parajuli, N., Wasmer, M. H., Philipp, S., Daschil, N., Datta, S., Koller, J. B., Tripp, C. H., Stoitzner, P., *et al.* (2013). Lapatinib and doxorubicin enhance the Stat1-dependent antitumor immune response. *Eur J Immunol*.
- Hardy, W. R., Li, L., Wang, Z., Sedy, J., Fawcett, J., Frank, E., Kucera, J., and Pawson, T. (2007). Combinatorial ShcA Docking Interactions Support Diversity in Tissue Morphogenesis. *Science* *317*, 251-256.

- Haura, E. B., Turkson, J., and Jove, R. (2005). Mechanisms of disease: Insights into the emerging role of signal transducers and activators of transcription in cancer. *Nat Clin Pract Oncol* 2, 315-324.
- Hazan-Halevy, I., Harris, D., Liu, Z., Liu, J., Li, P., Chen, X., Shanker, S., Ferrajoli, A., Keating, M. J., and Estrov, Z. (2010). STAT3 is constitutively phosphorylated on serine 727 residues, binds DNA, and activates transcription in CLL cells. *Blood* 115, 2852-2863.
- He, X., Wang, J., Dou, J., Yu, F., Cai, K., Li, X., Zhang, H., and Gu, N. (2011). Antitumor efficacy induced by a B16F10 tumor cell vaccine treated with mitoxantrone alone or in combination with reserpine and verapamil in mice. *Exp Ther Med* 2, 911-916.
- Heindl, A., Sestak, I., Naidoo, K., Cuzick, J., Dowsett, M., and Yuan, Y. (2018). Relevance of Spatial Heterogeneity of Immune Infiltration for Predicting Risk of Recurrence After Endocrine Therapy of ER+ Breast Cancer. *Journal of the National Cancer Institute* 110.
- Heninger, E., Krueger, T. E., and Lang, J. M. (2015). Augmenting antitumor immune responses with epigenetic modifying agents. *Front Immunol* 6, 29.
- Herbeuval, J. P., Lelievre, E., Lambert, C., Dy, M., and Genin, C. (2004). Recruitment of STAT3 for production of IL-10 by colon carcinoma cells induced by macrophage-derived IL-6. *J Immunol* 172, 4630-4636.
- Herbst, R. S., Soria, J. C., Kowanetz, M., Fine, G. D., Hamid, O., Gordon, M. S., Sosman, J. A., McDermott, D. F., Powderly, J. D., Gettinger, S. N., *et al.* (2014). Predictive correlates of response to the anti-PD-L1 antibody MPDL3280A in cancer patients. *Nature* 515, 563-567.
- Hillesheim, A., Nordhoff, C., Boergeling, Y., Ludwig, S., and Wixler, V. (2014). beta-catenin promotes the type I IFN synthesis and the IFN-dependent signaling response but is suppressed by influenza A virus-induced RIG-I/NF-kappaB signaling. *Cell communication and signaling : CCS* 12, 29.
- Ho, H. H., and Ivashkiv, L. B. (2006). Role of STAT3 in type I interferon responses. Negative regulation of STAT1-dependent inflammatory gene activation. *J Biol Chem* 281, 14111-14118.
- Hodgson, J. G., Malek, T., Bornstein, S., Hariono, S., Ginzinger, D. G., Muller, W. J., and Gray, J. W. (2005). Copy number aberrations in mouse breast tumors reveal loci and genes important in tumorigenic receptor tyrosine kinase signaling. *Cancer Res* 65, 9695-9704.
- Hollern, D. P., and Andrechek, E. R. (2014). A genomic analysis of mouse models of breast cancer reveals molecular features of mouse models and relationships to human breast cancer. *Breast Cancer Res* 16, R59-R59.
- Hu, Z., Ott, P. A., and Wu, C. J. (2018). Towards personalized, tumour-specific, therapeutic vaccines for cancer. *Nat Rev Immunol* 18, 168-182.
- Huang, G., Yan, H., Ye, S., Tong, C., and Ying, Q. L. (2014). STAT3 phosphorylation at tyrosine 705 and serine 727 differentially regulates mouse ESC fates. *Stem cells* 32, 1149-1160.
- Huang, Y., Li, T., Sane, D. C., and Li, L. (2004). IRAK1 serves as a novel regulator essential for lipopolysaccharide-induced interleukin-10 gene expression. *J Biol Chem* 279, 51697-51703.

Hudson, J., Ha, J. R., Sabourin, V., Ahn, R., La Selva, R., Livingstone, J., Podmore, L., Knight, J., Forrest, L., Beauchemin, N., *et al.* (2014). p66ShcA Promotes Breast Cancer Plasticity by Inducing an Epithelial-to-Mesenchymal Transition. *Mol Cell Biol* **34**, 3689-3701.

Hudson, J. D., Shoaibi, M. A., Maestro, R., Carnero, A., Hannon, G. J., and Beach, D. H. (1999). A proinflammatory cytokine inhibits p53 tumor suppressor activity. *J Exp Med* **190**, 1375-1382.

Hundal, J., Kiwala, S., Feng, Y. Y., Liu, C. J., Govindan, R., Chapman, W. C., Uppaluri, R., Swamidass, S. J., Griffith, O. L., Mardis, E. R., and Griffith, M. (2019). Accounting for proximal variants improves neoantigen prediction. *Nature genetics* **51**, 175-179.

Huynh, L., Kusnadi, A., Park, S. H., Murata, K., Park-Min, K.-H., and Ivashkiv, L. B. (2016). Opposing regulation of the late phase TNF response by mTORC1-IL-10 signaling and hypoxia in human macrophages. *Scientific reports* **6**, 31959.

Ijaz, M., Wang, F., Shahbaz, M., Jiang, W., Fathy, A. H., and Nesa, E. U. (2018). The Role of Grb2 in Cancer and Peptides as Grb2 Antagonists. *Protein Pept Lett* **24**, 1084-1095.

Im, Y. K., La Selva, R., Gandin, V., Ha, J. R., Sabourin, V., Sonenberg, N., Pawson, T., Topisirovic, I., and Ursini-Siegel, J. (2014). The ShcA adaptor activates AKT signaling to potentiate breast tumor angiogenesis by stimulating VEGF mRNA translation in a 4E-BP-dependent manner. *Oncogene*.

Im, Y. K., Najyb, O., Gravel, S. P., McGuirk, S., Ahn, R., Avizonis, D. Z., Chenard, V., Sabourin, V., Hudson, J., Pawson, T., *et al.* (2018). Interplay between ShcA Signaling and PGC-1alpha Triggers Targetable Metabolic Vulnerabilities in Breast Cancer. *Cancer Res* **78**, 4826-4838.

Iqbal, N., and Iqbal, N. (2014). Human Epidermal Growth Factor Receptor 2 (HER2) in Cancers: Overexpression and Therapeutic Implications. *Molecular biology international* **2014**, 852748-852748.

Ishihara, H., Sasaoka, T., Ishiki, M., Takata, Y., Imamura, T., Usui, I., Langlois, W. J., Sawa, T., and Kobayashi, M. (1997). Functional importance of Shc tyrosine 317 on insulin signaling in Rat1 fibroblasts expressing insulin receptors. *J Biol Chem* **272**, 9581-9586.

Ishihara, H., Sasaoka, T., Wada, T., Ishiki, M., Haruta, T., Usui, I., Iwata, M., Takano, A., Uno, T., Ueno, E., and Kobayashi, M. (1998). Relative involvement of Shc tyrosine 239/240 and tyrosine 317 on insulin induced mitogenic signaling in rat1 fibroblasts expressing insulin receptors. *Biochem Biophys Res Commun* **252**, 139-144.

Ito, N., Eto, M., Nakamura, E., Takahashi, A., Tsukamoto, T., Toma, H., Nakazawa, H., Hirao, Y., Uemura, H., Kagawa, S., *et al.* (2007). STAT3 polymorphism predicts interferon-alfa response in patients with metastatic renal cell carcinoma. *J Clin Oncol* **25**, 2785-2791.

Jacquet, K., Banerjee, S. L., Chartier, F. J. M., Elowe, S., and Bisson, N. (2018). Proteomic Analysis of NCK1/2 Adaptors Uncovers Paralog-specific Interactions That Reveal a New Role for NCK2 in Cell Abscission During Cytokinesis. *Molecular & cellular proteomics : MCP* **17**, 1979-1990.

Johnson, D. E., O'Keefe, R. A., and Grandis, J. R. (2018). Targeting the IL-6/JAK/STAT3 signalling axis in cancer. *Nat Rev Clin Oncol* **15**, 234-248.

Johnston, S. J., and Cheung, K.-L. (2018). Endocrine Therapy for Breast Cancer: A Model of Hormonal Manipulation. *Oncology and Therapy* 6, 141-156.

Jones, L. M., Broz, M. L., Ranger, J. J., Ozcelik, J., Ahn, R., Zuo, D., Ursini-Siegel, J., Hallett, M., Krummel, M., and Muller, W. J. (2015). Stat3 establishes an immunosuppressive microenvironment during the early stages of breast carcinogenesis to promote tumor growth and metastasis. *Cancer Res*.

Jones, N., Hardy, W. R., Friese, M. B., Jorgensen, C., Smith, M. J., Woody, N. M., Burden, S. J., and Pawson, T. (2007). Analysis of a Shc family adaptor protein, ShcD/Shc4, that associates with muscle-specific kinase. *Mol Cell Biol* 27, 4759-4773.

Kamada, R., Yang, W., Zhang, Y., Patel, M. C., Yang, Y., Ouda, R., Dey, A., Wakabayashi, Y., Sakaguchi, K., Fujita, T., *et al.* (2018). Interferon stimulation creates chromatin marks and establishes transcriptional memory. *Proceedings of the National Academy of Sciences* 115, E9162-E9171.

Kang, J. W., Park, Y. S., Lee, D. H., Kim, J. H., Kim, M. S., Bak, Y., Hong, J., and Yoon, D. Y. (2012). Intracellular interaction of interleukin (IL)-32alpha with protein kinase Cepsilon (PKCepsilon) and STAT3 protein augments IL-6 production in THP-1 promonocytic cells. *J Biol Chem* 287, 35556-35564.

Kang, R., Chen, R., Zhang, Q., Hou, W., Wu, S., Cao, L., Huang, J., Yu, Y., Fan, X. G., Yan, Z., *et al.* (2014). HMGB1 in health and disease. *Molecular aspects of medicine* 40, 1-116.

Kario, E., Marmor, M. D., Adamsky, K., Citri, A., Amit, I., Amariglio, N., Rechavi, G., and Yarden, Y. (2005). Suppressors of cytokine signaling 4 and 5 regulate epidermal growth factor receptor signaling. *J Biol Chem* 280, 7038-7048.

Keskin, D. B., Anandappa, A. J., Sun, J., Tirosh, I., Mathewson, N. D., Li, S., Oliveira, G., Giobbie-Hurder, A., Felt, K., Gjini, E., *et al.* (2019). Neoantigen vaccine generates intratumoral T cell responses in phase Ib glioblastoma trial. *Nature* 565, 234-239.

Kharma, B., Baba, T., Matsumura, N., Kang, H. S., Hamanishi, J., Murakami, R., McConechy, M. M., Leung, S., Yamaguchi, K., Hosoe, Y., *et al.* (2014). STAT1 drives tumor progression in serous papillary endometrial cancer. *Cancer Res* 74, 6519-6530.

Khodarev, N., Ahmad, R., Rajabi, H., Pitroda, S., Kufe, T., McClary, C., Joshi, M. D., MacDermid, D., Weichselbaum, R., and Kufe, D. (2010). Cooperativity of the MUC1 oncoprotein and STAT1 pathway in poor prognosis human breast cancer. *Oncogene* 29, 920-929.

Kim, D. J., Tremblay, M. L., and Digiovanni, J. (2010). Protein tyrosine phosphatases, TC-PTP, SHP1, and SHP2, cooperate in rapid dephosphorylation of Stat3 in keratinocytes following UVB irradiation. *PLoS One* 5, e10290.

Kim, H. J., and Cantor, H. (2014). The path to reactivation of antitumor immunity and checkpoint immunotherapy. *Cancer Immunol Res* 2, 926-936.

Kim, J., Modlin, R. L., Moy, R. L., Dubinett, S. M., McHugh, T., Nickoloff, B. J., and Uyemura, K. (1995). IL-10 production in cutaneous basal and squamous cell carcinomas. A mechanism for evading the local T cell immune response. *The Journal of Immunology* 155, 2240-2247.

Kishimoto, K., Matsumoto, K., and Ninomiya-Tsuji, J. (2000). TAK1 Mitogen-activated Protein Kinase Kinase Kinase Is Activated by Autophosphorylation within Its Activation Loop. *Journal of Biological Chemistry* 275, 7359-7364.

Klint, P., Kanda, S., and Claesson-Welsh, L. (1995). Shc and a Novel 89-kDa Component Couple to the Grb2-Sos Complex in Fibroblast Growth Factor-2-stimulated Cells. *Journal of Biological Chemistry* 270, 23337-23344.

Klover, P. J., Muller, W. J., Robinson, G. W., Pfeiffer, R. M., Yamaji, D., and Hennighausen\*, L. (2010). Loss of STAT1 from Mouse Mammary Epithelium Results in an Increased Neu-Induced Tumor Burden. *Neoplasia* 12, 899-905.

Knight, J. D., Liu, G., Zhang, J. P., Pasculescu, A., Choi, H., and Gingras, A. C. (2015). A web-tool for visualizing quantitative protein-protein interaction data. *Proteomics* 15, 1432-1436.

Knight, J. D. R., Choi, H., Gupta, G. D., Pelletier, L., Raught, B., Nesvizhskii, A. I., and Gingras, A.-C. (2017). ProHits-viz: a suite of web tools for visualizing interaction proteomics data. *Nature methods* 14, 645.

Kojima, H., Sasaki, T., Ishitani, T., Iemura, S., Zhao, H., Kaneko, S., Kunimoto, H., Natsume, T., Matsumoto, K., and Nakajima, K. (2005). STAT3 regulates Nemo-like kinase by mediating its interaction with IL-6-stimulated TGFbeta-activated kinase 1 for STAT3 Ser-727 phosphorylation. *Proc Natl Acad Sci U S A* 102, 4524-4529.

König, L., Mairinger, F. D., Hoffmann, O., Bittner, A.-K., Schmid, K. W., Kimmig, R., Kasimir-Bauer, S., and Bankfalvi, A. (2019). Dissimilar patterns of tumor-infiltrating immune cells at the invasive tumor front and tumor center are associated with response to neoadjuvant chemotherapy in primary breast cancer. *BMC Cancer* 19, 120.

Koromilas, A. E., and Sexl, V. (2013). The tumor suppressor function of STAT1 in breast cancer. *Jak-Stat* 2, e23353.

Kretzschmar, A. K., Dinger, M. C., Henze, C., Brocke-Heidrich, K., and Horn, F. (2004). Analysis of Stat3 (signal transducer and activator of transcription 3) dimerization by fluorescence resonance energy transfer in living cells. *Biochem J* 377, 289-297.

Kroemer, G., Senovilla, L., Galluzzi, L., Andre, F., and Zitvogel, L. (2015). Natural and therapy-induced immunosurveillance in breast cancer. *Nat Med* 21, 1128-1138.

Kumar, S., Davra, V., E. Obr, A., Geng, K., L. Wood, T., and Birge, R. B. (2017). Crk adaptor protein promotes PD-L1 expression, EMT and immune evasion in a murine model of triple-negative breast cancer. *Oncoimmunology*, e1376155.

Kweon, M. N., Fujihashi, K., VanCott, J. L., Higuchi, K., Yamamoto, M., McGhee, J. R., and Kiyono, H. (1998). Lack of orally induced systemic unresponsiveness in IFN-gamma knockout mice. *J Immunol* 160, 1687-1693.

Kwilas, A. R., Ardiani, A., Donahue, R. N., Aftab, D. T., and Hodge, J. W. (2014). Dual effects of a targeted small-molecule inhibitor (cabozantinib) on immune-mediated killing of tumor cells and immune tumor microenvironment permissiveness when combined with a cancer vaccine. *J Transl Med* 12, 294.

- Kwilas, A. R., Donahue, R. N., Tsang, K. Y., and Hodge, J. W. (2015). Immune consequences of tyrosine kinase inhibitors that synergize with cancer immunotherapy. *Cancer Cell Microenviron* 2.
- Lai, K.-M. V., and Pawson, T. (2000). The ShcA phosphotyrosine docking protein sensitizes cardiovascular signaling in the mouse embryo. In *Genes & Development*, pp. 1132-1145.
- Laird, A. D., Li, G., Moss, K. G., Blake, R. A., Broome, M. A., Cherrington, J. M., and Mendel, D. B. (2003). Src Family Kinase Activity Is Required for Signal Transducer and Activator of Transcription 3 and Focal Adhesion Kinase Phosphorylation and Vascular Endothelial Growth Factor Signaling *in Vivo* and for Anchorage-dependent and -independent Growth of Human Tumor Cells. *Molecular Cancer Therapeutics* 2, 461-469.
- Lambert, J. P., Tucholska, M., Go, C., Knight, J. D., and Gingras, A. C. (2015). Proximity biotinylation and affinity purification are complementary approaches for the interactome mapping of chromatin-associated protein complexes. *J Proteomics* 118, 81-94.
- Landry, M., Pomerleau, V., and Saucier, C. (2016). Non-canonical dynamic mechanisms of interaction between the p66Shc protein and Met receptor. *Biochem J* 473, 1617-1627.
- Lapidus, R. G., Nass, S. J., and Davidson, N. E. (1998). The Loss of Estrogen and Progesterone Receptor Gene Expression in Human Breast Cancer. *J Mammary Gland Biol Neoplasia* 3, 85-94.
- Laumont, C. M., Vincent, K., Hesnard, L., Audemard, É., Bonneil, É., Laverdure, J.-P., Gendron, P., Courcelles, M., Hardy, M.-P., Côté, C., *et al.* (2018). Noncoding regions are the main source of targetable tumor-specific antigens. *Science translational medicine* 10, eaau5516.
- Lavallee-Adam, M., Rousseau, J., Domecq, C., Bouchard, A., Forget, D., Faubert, D., Blanchette, M., and Coulombe, B. (2013). Discovery of cell compartment specific protein-protein interactions using affinity purification combined with tandem mass spectrometry. *J Proteome Res* 12, 272-281.
- Lee, H., Pal, S. K., Reckamp, K., Figlin, R. A., and Yu, H. (2011). STAT3: a target to enhance antitumor immune response. *Curr Top Microbiol Immunol* 344, 41-59.
- Lee, M. S., Igawa, T., and Lin, M. F. (2004). Tyrosine-317 of p52(Shc) mediates androgen-stimulated proliferation signals in human prostate cancer cells. *Oncogene* 23, 3048-3058.
- Lehmann, B. D., Bauer, J. A., Chen, X., Sanders, M. E., Chakravarthy, A. B., Shyr, Y., and Pietenpol, J. A. (2011). Identification of human triple-negative breast cancer subtypes and preclinical models for selection of targeted therapies. *J Clin Invest* 121, 2750-2767.
- Lemmon, M. A., and Schlessinger, J. (2010). Cell signaling by receptor tyrosine kinases. *Cell* 141, 1117-1134.
- Li, H., Handsaker, B., Wysoker, A., Fennell, T., Ruan, J., Homer, N., Marth, G., Abecasis, G., Durbin, R., and Genome Project Data Processing, S. (2009). The Sequence Alignment/Map format and SAMtools. *Bioinformatics (Oxford, England)* 25, 2078-2079.
- Li, X., Gruosso, T., Zuo, D., Omeroglu, A., Meterissian, S., Guiot, M. C., Salazar, A., Park, M., and Levine, H. (2019). Infiltration of CD8(+) T cells into tumor cell clusters in triple-negative breast cancer. *Proc Natl Acad Sci U S A* 116, 3678-3687.

- Liang, H., Liu, X., and Wang, M. (2018). Immunotherapy combined with epidermal growth factor receptor-tyrosine kinase inhibitors in non-small-cell lung cancer treatment. *Onco Targets Ther* 11, 6189-6196.
- Lim, C. P., and Cao, X. (1999a). Serine phosphorylation and negative regulation of Stat3 by JNK. *J Biol Chem* 274, 31055-31061.
- Lim, C. P., and Cao, X. (1999b). Serine Phosphorylation and Negative Regulation of Stat3 by JNK. *Journal of Biological Chemistry* 274, 31055-31061.
- Lin, C.-H., Yu, M.-C., Chiang, C.-C., Bien, M.-Y., Chien, M.-H., and Chen, B.-C. (2013). Thrombin-induced NF- $\kappa$ B activation and IL-8/CXCL8 release is mediated by c-Src-dependent Shc, Raf-1, and ERK pathways in lung epithelial cells. *Cell Signal* 25, 1166-1175.
- Lin, E. Y., Jones, J. G., Li, P., Zhu, L., Whitney, K. D., Muller, W. J., and Pollard, J. W. (2003). Progression to Malignancy in the Polyoma Middle T Oncoprotein Mouse Breast Cancer Model Provides a Reliable Model for Human Diseases. *The American Journal of Pathology* 163, 2113-2126.
- Lin, G. S., Chen, Y. P., Lin, Z. X., Wang, X. F., Zheng, Z. Q., and Chen, L. (2014). STAT3 serine 727 phosphorylation influences clinical outcome in glioblastoma. *International journal of clinical and experimental pathology* 7, 3141-3149.
- Linossi, E. M., Chandrashekar, I. R., Kolesnik, T. B., Murphy, J. M., Webb, A. I., Willson, T. A., Kedzierski, L., Bullock, A. N., Babon, J. J., Norton, R. S., *et al.* (2013). Suppressor of Cytokine Signaling (SOCS) 5 utilises distinct domains for regulation of JAK1 and interaction with the adaptor protein Shc-1. *PLoS One* 8, e70536.
- Lippi, G., Mattiuzzi, C., and Montagnana, M. (2017). BRCA population screening for predicting breast cancer: for or against? *Ann Transl Med* 5, 275-275.
- Liu, B. A., Engelmann, B. W., and Nash, P. D. (2012a). High-throughput analysis of peptide-binding modules. *Proteomics* 12, 1527-1546.
- Liu, C. C., Lin, S. P., Hsu, H. S., Yang, S. H., Lin, C. H., Yang, M. H., Hung, M. C., and Hung, S. C. (2016). Suspension survival mediated by PP2A-STAT3-Col XVII determines tumour initiation and metastasis in cancer stem cells. *Nature communications* 7, 11798.
- Liu, J., Chen, B., Lu, Y., Guan, Y., and Chen, F. (2012b). JNK-dependent Stat3 phosphorylation contributes to Akt activation in response to arsenic exposure. *Toxicological sciences : an official journal of the Society of Toxicology* 129, 363-371.
- Liu, L., McBride, K. M., and Reich, N. C. (2005). STAT3 nuclear import is independent of tyrosine phosphorylation and mediated by importin- $\alpha$ 3. *Proc Natl Acad Sci U S A* 102, 8150-8155.
- Liu, S. K., and McGlade, C. J. (1998). Gads is a novel SH2 and SH3 domain-containing adaptor protein that binds to tyrosine-phosphorylated Shc. *Oncogene* 17, 3073-3082.
- Liu, Y., Zhang, X., Yang, B., Zhuang, H., Guo, H., Wei, W., Li, Y., Chen, R., Li, Y., and Zhang, N. (2018). Demethylation-Induced Overexpression of Shc3 Drives c-Raf-Independent Activation of MEK/ERK in HCC. *Cancer Res* 78, 2219-2232.

Lizotte, P. H., Hong, R. L., Luster, T. A., Cavanaugh, M. E., Taus, L. J., Wang, S., Dhaneshwar, A., Mayman, N., Yang, A., Kulkarni, M., *et al.* (2018). A High-Throughput Immune-Oncology Screen Identifies EGFR Inhibitors as Potent Enhancers of Antigen-Specific Cytotoxic T-lymphocyte Tumor Cell Killing. *Cancer Immunol Res* 6, 1511-1523.

Loeffler, S., Fayard, B., Weis, J., and Weissenberger, J. (2005). Interleukin-6 induces transcriptional activation of vascular endothelial growth factor (VEGF) in astrocytes in vivo and regulates VEGF promoter activity in glioblastoma cells via direct interaction between STAT3 and Sp1. *Int J Cancer* 115, 202-213.

Loi, S., Sirtaine, N., Piette, F., Salgado, R., Viale, G., Van Eenoo, F., Rouas, G., Francis, P., Crown, J. P., Hitre, E., *et al.* (2013). Prognostic and predictive value of tumor-infiltrating lymphocytes in a phase III randomized adjuvant breast cancer trial in node-positive breast cancer comparing the addition of docetaxel to doxorubicin with doxorubicin-based chemotherapy: BIG 02-98. *J Clin Oncol* 31, 860-867.

Lotti, L. V., Lanfrancone, L., Migliaccio, E., Zompetta, C., Pelicci, G., Salcini, A. E., Falini, B., Pelicci, P. G., and Torrisi, M. R. (1996). Src proteins are localized on endoplasmic reticulum membranes and are redistributed after tyrosine kinase receptor activation. *Molecular and Cellular Biology* 16, 1946-1954.

Love, M. I., Huber, W., and Anders, S. (2014). Moderated estimation of fold change and dispersion for RNA-seq data with DESeq2. *Genome Biol* 15, 550.

Lu, D., Liu, L., Ji, X., Gao, Y., Chen, X., Liu, Y., Liu, Y., Zhao, X., Li, Y., Li, Y., *et al.* (2015). The phosphatase DUSP2 controls the activity of the transcription activator STAT3 and regulates TH17 differentiation. *Nat Immunol* 16, 1263-1273.

Lu, L., Zhu, F., Zhang, M., Li, Y., Drennan, A. C., Kimpara, S., Rumball, I., Selzer, C., Cameron, H., Kellicut, A., *et al.* (2018). Gene regulation and suppression of type I interferon signaling by STAT3 in diffuse large B cell lymphoma. *Proceedings of the National Academy of Sciences* 115, E498-E505.

Ma, J. F., Sanchez, B. J., Hall, D. T., Tremblay, A. K., Di Marco, S., and Gallouzi, I. E. (2017). STAT3 promotes IFN $\gamma$ /TNF $\alpha$ -induced muscle wasting in an NF- $\kappa$ B-dependent and IL-6-independent manner. *EMBO Mol Med* 9, 622-637.

Maglione, J. E., Moghanaki, D., Young, L. J. T., Manner, C. K., Ellies, L. G., Joseph, S. O., Nicholson, B., Cardiff, R. D., and MacLeod, C. L. (2001). Transgenic Polyoma Middle-T Mice Model Premalignant Mammary Disease. *Cancer Res* 61, 8298-8305.

Mahmoud, S., Paish, E., Powe, D., Macmillan, R., Grainge, M., Lee, A., Ellis, I., and Green, A. (2011). Tumor-infiltrating CD8 $^{+}$  lymphocytes predict clinical outcome in breast cancer. *J Clin Oncol* 29, 1949 - 1955.

Mahmoud, S. M., Lee, A. H., Paish, E. C., Macmillan, R. D., Ellis, I. O., and Green, A. R. (2012). The prognostic significance of B lymphocytes in invasive carcinoma of the breast. *Breast Cancer Res Treat* 132, 545-553.

- Mak, T. W., Rahemtulla, A., Schilham, M., Koh, D. R., and Fung-Leung, W. P. (1992). Generation of mutant mice lacking surface expression of CD4 or CD8 by gene targeting. *J Autoimmun* 5 *Suppl* A, 55-59.
- Makhoul, I., Atiq, M., Alwbari, A., and Kieber-Emmons, T. (2018). Breast Cancer Immunotherapy: An Update. *Breast Cancer (Auckl)* 12, 1178223418774802.
- Marie, C. S., Verkerke, H. P., Paul, S. N., Mackey, A. J., and Petri, W. A., Jr. (2012). Leptin protects host cells from *Entamoeba histolytica* cytotoxicity by a STAT3-dependent mechanism. *Infection and immunity* 80, 1934-1943.
- Maritano, D., Sugrue, M. L., Tininini, S., Dewilde, S., Strobl, B., Fu, X., Murray-Tait, V., Chiarle, R., and Poli, V. (2004). The STAT3 isoforms alpha and beta have unique and specific functions. *Nat Immunol* 5, 401-409.
- Marzec, M., Zhang, Q., Goradia, A., Raghunath, P. N., Liu, X., Paessler, M., Wang, H. Y., Wysocka, M., Cheng, M., Ruggeri, B. A., and Wasik, M. A. (2008). Oncogenic kinase NPM/ALK induces through STAT3 expression of immunosuppressive protein CD274 (PD-L1, B7-H1). *Proc Natl Acad Sci U S A* 105, 20852-20857.
- Matsushita, H., Vesely, M. D., Koboldt, D. C., Rickert, C. G., Uppaluri, R., Magrini, V. J., Arthur, C. D., White, J. M., Chen, Y. S., Shea, L. K., *et al.* (2012). Cancer exome analysis reveals a T-cell-dependent mechanism of cancer immunoediting. *Nature* 482, 400-404.
- Medina-Echeverez, J., Haile, L. A., Zhao, F., Gamrekelashvili, J., Ma, C., Metais, J. Y., Dunbar, C. E., Kapoor, V., Manns, M. P., Korangy, F., and Greten, T. F. (2014). IFN-gamma regulates survival and function of tumor-induced CD11b<sup>+</sup> Gr-1<sup>high</sup> myeloid derived suppressor cells by modulating the anti-apoptotic molecule Bcl2a1. *Eur J Immunol* 44, 2457-2467.
- Meissl, K., Macho-Maschler, S., Muller, M., and Strobl, B. (2015). The good and the bad faces of STAT1 in solid tumours. *Cytokine*.
- Mellacheruvu, D., Wright, Z., Couzens, A. L., Lambert, J. P., St-Denis, N. A., Li, T., Miteva, Y. V., Hauri, S., Sardi, M. E., Low, T. Y., *et al.* (2013). The CRAPome: a contaminant repository for affinity purification-mass spectrometry data. *Nature methods* 10, 730-736.
- Meraz, M. A., White, J. M., Sheehan, K. C. F., Bach, E. A., Rodig, S. J., Dighe, A. S., Kaplan, D. H., Riley, J. K., Greenlund, A. C., Campbell, D., *et al.* (1996). Targeted Disruption of the Stat1 Gene in Mice Reveals Unexpected Physiologic Specificity in the JAK-STAT Signaling Pathway. *Cell* 84, 431-442.
- Mertens, C., Zhong, M., Krishnaraj, R., Zou, W., Chen, X., and Darnell, J. E., Jr. (2006). Dephosphorylation of phosphotyrosine on STAT1 dimers requires extensive spatial reorientation of the monomers facilitated by the N-terminal domain. *Genes Dev* 20, 3372-3381.
- Mestas, J., and Hughes, C. C. W. (2004). Of Mice and Not Men: Differences between Mouse and Human Immunology. *The Journal of Immunology* 172, 2731-2738.
- Meyer, T., Gavenis, K., and Vinkemeier, U. (2002). Cell type-specific and tyrosine phosphorylation-independent nuclear presence of STAT1 and STAT3. *Experimental cell research* 272, 45-55.

- Meyer Zu Horste, G., Przybylski, D., Schramm, M. A., Wang, C., Schnell, A., Lee, Y., Sobel, R., Regev, A., and Kuchroo, V. K. (2018). Fas Promotes T Helper 17 Cell Differentiation and Inhibits T Helper 1 Cell Development by Binding and Sequestering Transcription Factor STAT1. *Immunity* *48*, 556-569 e557.
- Migliaccio, E., Giorgio, M., and Pelicci, P. G. (2006). Apoptosis and aging: role of p66Shc redox protein. *Antioxidants & redox signaling* *8*, 600-608.
- Migliaccio, E., Mele, S., Salcini, A. E., Pelicci, G., Lai, K.-M. V., Superti-Furga, G., Pawson, T., Di Fiore, P. P., Lanfrancone, L., and Pelicci, P. G. (1997). Opposite effects of the p52shc/p46shc and p66shc splicing isoforms on the EGF receptor-MAP kinase-fos signalling pathway. *EMBO J* *16*, 706-716.
- Milanesi, L., Petrillo, M., Sepe, L., Boccia, A., D'Agostino, N., Passamano, M., Di Nardo, S., Tasco, G., Casadio, R., and Paoletta, G. (2005). Systematic analysis of human kinase genes: a large number of genes and alternative splicing events result in functional and structural diversity. *BMC Bioinformatics* *6 Suppl 4*, S20-S20.
- Mishra, J., and Kumar, N. (2014). Adapter protein SHC regulates JANUS kinase 3 phosphorylation. *Journal of Biological Chemistry*.
- Miyakoshi, M., Yamamoto, M., Tanaka, H., and Ogawa, K. (2014). Serine 727 phosphorylation of STAT3: an early change in mouse hepatocarcinogenesis induced by neonatal treatment with diethylnitrosamine. *Mol Carcinog* *53*, 67-76.
- Motzer, R. J., Penkov, K., Haanen, J., Rini, B., Albiges, L., Campbell, M. T., Venugopal, B., Kollmannsberger, C., Negrier, S., Uemura, M., *et al.* (2019). Avelumab plus Axitinib versus Sunitinib for Advanced Renal-Cell Carcinoma. *New England Journal of Medicine* *380*, 1103-1115.
- Mukhopadhyay, S., Shah, M., Xu, F., Patel, K., Tuder, R. M., and Sehgal, P. B. (2008). Cytoplasmic provenance of STAT3 and PY-STAT3 in the endolysosomal compartments in pulmonary arterial endothelial and smooth muscle cells: implications in pulmonary arterial hypertension. *American journal of physiology Lung cellular and molecular physiology* *294*, L449-468.
- Muntasell, A., Cabo, M., Servitja, S., Tusquets, I., Martínez-García, M., Rovira, A., Rojo, F., Albanell, J., and López-Botet, M. (2017). Interplay between Natural Killer Cells and Anti-HER2 Antibodies: Perspectives for Breast Cancer Immunotherapy. *Front Immunol* *8*, 1544-1544.
- Nakashima, H., Terabe, M., Berzofsky, J. A., Husain, S. R., and Puri, R. K. (2011). A novel combination immunotherapy for cancer by IL-13Ralpha2-targeted DNA vaccine and immunotoxin in murine tumor models. *J Immunol* *187*, 4935-4946.
- Nawaz, S., Heindl, A., Koelble, K., and Yuan, Y. (2015). Beyond immune density: critical role of spatial heterogeneity in estrogen receptor-negative breast cancer. *Mod Pathol* *28*, 766-777.
- Neeraja, D., Engel, B. J., and Carson, D. D. (2013). Activated EGFR stimulates MUC1 expression in human uterine and pancreatic cancer cell lines. *J Cell Biochem* *114*, 2314-2322.
- Netea, M. G., Quintin, J., and van der Meer, J. W. (2011). Trained immunity: a memory for innate host defense. *Cell Host Microbe* *9*, 355-361.

- Neve, R. M., Chin, K., Fridlyand, J., Yeh, J., Baehner, F. L., Fevr, T., Clark, L., Bayani, N., Coppe, J.-P., Tong, F., *et al.* (2006). A collection of breast cancer cell lines for the study of functionally distinct cancer subtypes. *Cancer Cell* *10*, 515-527.
- Neville, M. C., Medina, D., Monks, J., and Hovey, R. C. (1998). The Mammary Fat Pad. *J Mammary Gland Biol Neoplasia* *3*, 109-116.
- Newman, A. M., Liu, C. L., Green, M. R., Gentles, A. J., Feng, W., Xu, Y., Hoang, C. D., Diehn, M., and Alizadeh, A. A. (2015). Robust enumeration of cell subsets from tissue expression profiles. *Nature methods* *12*, 453-457.
- Nguyen, H., Ramana, C. V., Bayes, J., and Stark, G. R. (2001). Roles of phosphatidylinositol 3-kinase in interferon-gamma-dependent phosphorylation of STAT1 on serine 727 and activation of gene expression. *J Biol Chem* *276*, 33361-33368.
- Ni, S., Zhao, C., Feng, G. S., Paulson, R. F., and Correll, P. H. (2007). A novel Stat3 binding motif in Gab2 mediates transformation of primary hematopoietic cells by the Stk/Ron receptor tyrosine kinase in response to Friend virus infection. *Mol Cell Biol* *27*, 3708-3715.
- Nicholson, P. R., Empeur, S., Glover, H. R., and Dilworth, S. M. (2001). ShcA tyrosine phosphorylation sites can replace ShcA binding in signalling by middle T-antigen. *EMBO J* *20*, 6337-6346.
- Nirschl, C. J., Suarez-Farinas, M., Izar, B., Prakadan, S., Dannenfels, R., Tirosh, I., Liu, Y., Zhu, Q., Devi, K. S. P., Carroll, S. L., *et al.* (2017). IFN $\gamma$ -Dependent Tissue-Immune Homeostasis Is Co-opted in the Tumor Microenvironment. *Cell* *170*, 127-141 e115.
- Nishioka, Y., Aono, Y., and Sone, S. (2011). Role of tyrosine kinase inhibitors in tumor immunology. *Immunotherapy* *3*, 107+.
- Niu, G., Briggs, J., Deng, J., Ma, Y., Lee, H., Kortylewski, M., Kujawski, M., Kay, H., Cress, W. D., Jove, R., and Yu, H. (2008). Signal transducer and activator of transcription 3 is required for hypoxia-inducible factor-1 $\alpha$  RNA expression in both tumor cells and tumor-associated myeloid cells. *Mol Cancer Res* *6*, 1099-1105.
- Niu, G., Wright, K. L., Huang, M., Song, L., Haura, E., Turkson, J., Zhang, S., Wang, T., Sinibaldi, D., Coppola, D., *et al.* (2002). Constitutive Stat3 activity up-regulates VEGF expression and tumor angiogenesis. *Oncogene* *21*, 2000-2008.
- Northey, J. J., Chmielecki, J., Ngan, E., Russo, C., Annis, M. G., Muller, W. J., and Siegel, P. M. (2008). Signaling through ShcA is required for transforming growth factor beta- and Neu/ErbB-2-induced breast cancer cell motility and invasion. *Molecular and Cellular Biology* *28*, 3162-3176.
- Northey, J. J., Dong, Z., Ngan, E., Kaplan, A., Hardy, W. R., Pawson, T., and Siegel, P. M. (2012). Distinct phospho-tyrosine dependent functions of ShcA are required for TGF $\beta$ -induced breast cancer cell migration, invasion and metastasis. *J Biol Chem*.
- O'Rourke, L., and Shepherd, P. R. (2002). Biphasic regulation of extracellular-signal-regulated protein kinase by leptin in macrophages: role in regulating STAT3 Ser727 phosphorylation and DNA binding. *Biochem J* *364*, 875-879.

- Obeid, M., Tesniere, A., Ghiringhelli, F., Fimia, G. M., Apetoh, L., Perfettini, J. L., Castedo, M., Mignot, G., Panaretakis, T., Casares, N., *et al.* (2007). Calreticulin exposure dictates the immunogenicity of cancer cell death. *Nat Med* 13, 54-61.
- Odom, D. T., Dowell, R. D., Jacobsen, E. S., Gordon, W., Danford, T. W., Maclsaac, K. D., Rolfe, P. A., Conboy, C. M., Gifford, D. K., and Fraenkel, E. (2007). Tissue-specific transcriptional regulation has diverged significantly between human and mouse. *Nature genetics* 39, 730-732.
- Oh, Y. M., Kim, J. K., Choi, Y., Choi, S., and Yoo, J. Y. (2009). Prediction and experimental validation of novel STAT3 target genes in human cancer cells. *PLoS One* 4, e6911.
- Olayioye, M. A., Beuvink, I., Horsch, K., Daly, J. M., and Hynes, N. E. (1999). ErbB Receptor-induced Activation of Stat Transcription Factors Is Mediated by Src Tyrosine Kinases. *Journal of Biological Chemistry* 274, 17209-17218.
- Ott, P. A., and Adams, S. (2011). Small-molecule protein kinase inhibitors and their effects on the immune system: implications for cancer treatment. *Immunotherapy* 3, 213-227.
- Ouedraogo, Z. G., Muller-Barthelemy, M., Kemeny, J. L., Dedieu, V., Biau, J., Khalil, T., Raoelfils, L. I., Granzotto, A., Pereira, B., Beaudoin, C., *et al.* (2016). STAT3 Serine 727 Phosphorylation: A Relevant Target to Radiosensitize Human Glioblastoma. *Brain pathology (Zurich, Switzerland)* 26, 18-30.
- Overacre-Delgoffe, A. E., Chikina, M., Dadey, R. E., Yano, H., Brunazzi, E. A., Shayan, G., Horne, W., Moskovitz, J. M., Kolls, J. K., Sander, C., *et al.* (2017). Interferon-gamma Drives Treg Fragility to Promote Anti-tumor Immunity. *Cell* 169, 1130-1141.e1111.
- Paine, I. S., and Lewis, M. T. (2017). The Terminal End Bud: the Little Engine that Could. *J Mammary Gland Biol Neoplasia* 22, 93-108.
- Paolino, M., Choidas, A., Wallner, S., Pranjic, B., Uribesalgo, I., Loeser, S., Jamieson, A. M., Langdon, W. Y., Ikeda, F., Fededa, J. P., *et al.* (2014). The E3 ligase Cbl-b and TAM receptors regulate cancer metastasis via natural killer cells. *Nature* 507, 508-512.
- Park, O. K., Schaefer, T. S., and Nathans, D. (1996). In vitro activation of Stat3 by epidermal growth factor receptor kinase. *Proc Natl Acad Sci U S A* 93, 13704-13708.
- Park, S. Y., Baik, Y. H., Cho, J. H., Kim, S., Lee, K. S., and Han, J. S. (2008). Inhibition of lipopolysaccharide-induced nitric oxide synthesis by nicotine through S6K1-p42/44 MAPK pathway and STAT3 (Ser 727) phosphorylation in Raw 264.7 cells. *Cytokine* 44, 126-134.
- Patel, S., Ngounou Wetie, A. G., Darie, C. C., and Clarkson, B. D. (2014). Cancer secretomes and their place in supplementing other hallmarks of cancer. *Advances in experimental medicine and biology* 806, 409-442.
- Patrussi, L., Savino, M. T., Pellegrini, M., Paccani, S. R., Migliaccio, E., Plyte, S., Lanfrancone, L., Pelicci, P. G., and Baldari, C. T. (2005). Cooperation and selectivity of the two Grb2 binding sites of p52Shc in T-cell antigen receptor signaling to Ras family GTPases and Myc-dependent survival. *Oncogene* 24, 2218-2228.

- Patterson, S. D., Thomas, D., and Bradshaw, R. A. (1996). Application of combined mass spectrometry and partial amino acid sequence to the identification of gel-separated proteins. *Electrophoresis* 17, 877-891.
- Patterson, S. G., Wei, S., Chen, X., Sallman, D. A., Gilvary, D. L., Zhong, B., Pow-Sang, J., Yeatman, T., and Djeu, J. Y. (2006). Novel role of Stat1 in the development of docetaxel resistance in prostate tumor cells. *Oncogene* 25, 6113-6122.
- Pawson, T. (1997). Signaling Through Scaffold, Anchoring, and Adaptor Proteins. *Science* 278, 2075-2080.
- Paz, K., Socci, N. D., van Nimwegen, E., Viale, A., and Darnell, J. E. (2004). Transformation fingerprint: induced STAT3-C, v-Src and Ha-Ras cause small initial changes but similar established profiles in mRNA. *Oncogene* 23, 8455-8463.
- Pelicci, G., Lanfrancone, L., Grignani, F., McGlade, J., Cavallo, F., Forni, G., Nicoletti, I., Grignani, F., Pawson, T., and Giuseppe Pelicci, P. (1992). A novel transforming protein (SHC) with an SH2 domain is implicated in mitogenic signal transduction. *Cell* 70, 93-104.
- Pelicci, G., Lanfrancone, L., Salcini, A. E., Romano, A., Mele, S., Grazia Borrello, M., Segatto, O., Di Fiore, P. P., and Pelicci, P. G. (1995). Constitutive phosphorylation of Shc proteins in human tumors. *Oncogene* 11, 899-907.
- Peng, W., Chen, J. Q., Liu, C., Malu, S., Creasy, C., Tetzlaff, M. T., Xu, C., McKenzie, J. A., Zhang, C., Liang, X., *et al.* (2016). Loss of PTEN Promotes Resistance to T Cell-Mediated Immunotherapy. *Cancer discovery* 6, 202-216.
- Peyser, N. D., Du, Y., Li, H., Lui, V., Xiao, X., Chan, T. A., and Grandis, J. R. (2015). Loss-of-Function PTPRD Mutations Lead to Increased STAT3 Activation and Sensitivity to STAT3 Inhibition in Head and Neck Cancer. *PLoS One* 10, e0135750.
- Platanias, L. C. (2005). Mechanisms of type-I- and type-II-interferon-mediated signalling. *Nat Rev Immunol* 5, 375-386.
- Polk, A., Svane, I. M., Andersson, M., and Nielsen, D. (2018). Checkpoint inhibitors in breast cancer - Current status. *Cancer Treat Rev* 63, 122-134.
- Polyak, K., and Hu, M. (2005). Do Myoepithelial Cells Hold the Key for Breast Tumor Progression? *J Mammary Gland Biol Neoplasia* 10, 231-247.
- Polyak, K., and Metzger Filho, O. (2012). SnapShot: breast cancer. *Cancer Cell* 22, 562-562 e561.
- Pozzi, C., Cuomo, A., Spadoni, I., Magni, E., Silvola, A., Conte, A., Sigismund, S., Ravenda, P. S., Bonaldi, T., Zampino, M. G., *et al.* (2016). The EGFR-specific antibody cetuximab combined with chemotherapy triggers immunogenic cell death. *Nat Med* 22, 624-631.
- Pratt, J. C., van den Brink, M. R. M., Igras, V. E., Walk, S. F., Ravichandran, K. S., and Burakoff, S. J. (1999). Requirement for Shc in TCR-Mediated Activation of a T Cell Hybridoma. *The Journal of Immunology* 163, 2586-2591.

Propper, D. J., Chao, D., Braybrooke, J. P., Bahl, P., Thavasu, P., Balkwill, F., Turley, H., Dobbs, N., Gatter, K., Talbot, D. C., *et al.* (2003). Low-dose IFN-gamma induces tumor MHC expression in metastatic malignant melanoma. *Clin Cancer Res* 9, 84-92.

Przanowski, P., Dabrowski, M., Ellert-Miklaszewska, A., Kloss, M., Mieczkowski, J., Kaza, B., Ronowicz, A., Hu, F., Piotrowski, A., Kettenmann, H., *et al.* (2014). The signal transducers Stat1 and Stat3 and their novel target Jmjd3 drive the expression of inflammatory genes in microglia. *Journal of molecular medicine* 92, 239-254.

QIAGEN (2015).

Qin, H. R., Kim, H. J., Kim, J. Y., Hurt, E. M., Klarmann, G. J., Kawasaki, B. T., Duhagon Serrat, M. A., and Farrar, W. L. (2008). Activation of signal transducer and activator of transcription 3 through a phosphomimetic serine 727 promotes prostate tumorigenesis independent of tyrosine 705 phosphorylation. *Cancer Res* 68, 7736-7741.

Qin, W., Golovkina, T. V., Peng, T., Nepomnaschy, I., Buggiano, V., Piazzon, I., and Ross, S. R. (1999). Mammary Gland Expression of Mouse Mammary Tumor Virus Is Regulated by a Novel Element in the Long Terminal Repeat. *Journal of Virology* 73, 368-376.

Qing, Y., and Stark, G. R. (2004). Alternative activation of STAT1 and STAT3 in response to interferon-gamma. *J Biol Chem* 279, 41679-41685.

Quinlan, A. R., and Hall, I. M. (2010). BEDTools: a flexible suite of utilities for comparing genomic features. *Bioinformatics* 26, 841-842.

Rajendrakumar, S. K., Mohapatra, A., Singh, B., Revuri, V., Lee, Y. K., Kim, C. S., Cho, C. S., and Park, I. K. (2018). Self-Assembled, Adjuvant/Antigen-Based Nanovaccine Mediates Anti-Tumor Immune Response against Melanoma Tumor. *Polymers (Basel)* 10.

Ravichandran, K. S. (2001). Signaling via Shc family adapter proteins. *Oncogene* 20, 6322-6330.

Ravichandran, K. S., Lorenz, U., Shoelson, S. E., and Burakoff, S. J. (1995). Interaction of Shc with Grb2 regulates association of Grb2 with mSOS. *Mol Cell Biol* 15, 593-600.

Real, P. J., Sierra, A., De Juan, A., Segovia, J. C., Lopez-Vega, J. M., and Fernandez-Luna, J. L. (2002). Resistance to chemotherapy via Stat3-dependent overexpression of Bcl-2 in metastatic breast cancer cells. *Oncogene* 21, 7611-7618.

Reich, M., Liefeld, T., Gould, J., Lerner, J., Tamayo, P., and Mesirov, J. P. (2006). GenePattern 2.0. *Nature genetics* 38, 500-501.

Riley, R. S., June, C. H., Langer, R., and Mitchell, M. J. (2019). Delivery technologies for cancer immunotherapy. *Nat Rev Drug Discov* 18, 175-196.

Rojas, A., Zhang, P., Wang, Y., Foo, W. C., Munoz, N. M., Xiao, L., Wang, J., Gores, G. J., Hung, M. C., and Blechacz, B. (2016). A Positive TGF-beta/c-KIT Feedback Loop Drives Tumor Progression in Advanced Primary Liver Cancer. *Neoplasia* 18, 371-386.

Ross, S. R. (2008). MMTV infectious cycle and the contribution of virus-encoded proteins to transformation of mammary tissue. *J Mammary Gland Biol Neoplasia* 13, 299-307.

Roux, K. J., Kim, D. I., Burke, B., and May, D. G. (2018). BioID: A Screen for Protein-Protein Interactions. *Current protocols in protein science* *91*, 19 23 11-19 23 15.

Roux, P. P., and Blenis, J. (2004). ERK and p38 MAPK-Activated Protein Kinases: a Family of Protein Kinases with Diverse Biological Functions. *Microbiology and Molecular Biology Reviews* *68*, 320-344.

Sade-Feldman, M., Yizhak, K., Bjorgaard, S. L., Ray, J. P., de Boer, C. G., Jenkins, R. W., Lieb, D. J., Chen, J. H., Frederick, D. T., Barzily-Rokni, M., *et al.* (2018). Defining T Cell States Associated with Response to Checkpoint Immunotherapy in Melanoma. *Cell* *175*, 998-1013.e1020.

Sakaguchi, M., Oka, M., Iwasaki, T., Fukami, Y., and Nishigori, C. (2012). Role and Regulation of STAT3 Phosphorylation at Ser727 in Melanocytes and Melanoma Cells. *Journal of Investigative Dermatology* *132*, 1877-1885.

Salcini, A. E., McGlade, J., Pelicci, G., Nicoletti, I., Pawson, T., and Pelicci, P. G. (1994). Formation of Shc-Grb2 complexes is necessary to induce neoplastic transformation by overexpression of Shc proteins. *Oncogene* *9*, 2827-2836.

Saltz, J., Gupta, R., Hou, L., Kurc, T., Singh, P., Nguyen, V., Samaras, D., Shroyer, K. R., Zhao, T., Batiste, R., *et al.* (2018). Spatial Organization and Molecular Correlation of Tumor-Infiltrating Lymphocytes Using Deep Learning on Pathology Images. *Cell Rep* *23*, 181-193.e187.

Sasaoka, T., and Kobayashi, M. (2000). The functional significance of Shc in insulin signaling as a substrate of the insulin receptor. *Endocrine journal* *47*, 373-381.

Sato, K.-i., Gotoh, N., Otsuki, T., Kakumoto, M., Aoto, M., Tokmakov, A. A., Shibuya, M., and Fukami, Y. (1997a). Tyrosine Residues 239 and 240 of Shc Are Phosphatidylinositol 4,5-Bisphosphate-Dependent Phosphorylation Sites by c-Src. *Biochemical and Biophysical Research Communications* *240*, 399-404.

Sato, K., Nagao, T., Kakumoto, M., Kimoto, M., Otsuki, T., Iwasaki, T., Tokmakov, A. A., Owada, K., and Fukami, Y. (2002). Adaptor protein Shc is an isoform-specific direct activator of the tyrosine kinase c-Src. *J Biol Chem* *277*, 29568-29576.

Sato, K., Otsuki, T., Kimoto, M., Kakumoto, M., Tokmakov, A. A., Watanabe, Y., and Fukami, Y. (1998). c-Src and phosphatidylinositol 3-kinase are involved in NGF-dependent tyrosine phosphorylation of Shc in PC12 cells. *Biochem Biophys Res Commun* *250*, 223-228.

Sato, T., Selleri, C., Young, N. S., and Maciejewski, J. P. (1997b). Inhibition of interferon regulatory factor-1 expression results in predominance of cell growth stimulatory effects of interferon-gamma due to phosphorylation of Stat1 and Stat3. *Blood* *90*, 4749-4758.

Satoh, J., and Tabunoki, H. (2013). A Comprehensive Profile of ChIP-Seq-Based STAT1 Target Genes Suggests the Complexity of STAT1-Mediated Gene Regulatory Mechanisms. *Gene regulation and systems biology* *7*, 41-56.

Savas, P., Salgado, R., Denkert, C., Sotiriou, C., Darcy, P. K., Smyth, M. J., and Loi, S. (2016). Clinical relevance of host immunity in breast cancer: from TILs to the clinic. *Nat Rev Clin Oncol* *13*, 228-241.

- Saxton, R. A., and Sabatini, D. M. (2017). mTOR Signaling in Growth, Metabolism, and Disease. *Cell* 168, 960-976.
- Schiavoni, G., Mattei, F., and Gabriele, L. (2013). Type I Interferons as Stimulators of DC-Mediated Cross-Priming: Impact on Anti-Tumor Response. *Front Immunol* 4, 483.
- Schindler, C., and Darnell, J. E., Jr. (1995). Transcriptional responses to polypeptide ligands: the JAK-STAT pathway. *Annu Rev Biochem* 64, 621-651.
- Schindler, C., Levy, D. E., and Decker, T. (2007). JAK-STAT signaling: from interferons to cytokines. *J Biol Chem* 282, 20059-20063.
- Schmid, P., Adams, S., Rugo, H. S., Schneeweiss, A., Barrios, C. H., Iwata, H., Dieras, V., Hegg, R., Im, S. A., Shaw Wright, G., *et al.* (2018). Atezolizumab and Nab-Paclitaxel in Advanced Triple-Negative Breast Cancer. *The New England journal of medicine* 379, 2108-2121.
- Schroder, K., Hertzog, P. J., Ravasi, T., and Hume, D. A. (2004a). Interferon-gamma: an overview of signals, mechanisms and functions. *J Leukoc Biol* 75, 163-189.
- Schroder, M., Kroeger, K. M., Volk, H. D., Eidne, K. A., and Grutz, G. (2004b). Preassociation of nonactivated STAT3 molecules demonstrated in living cells using bioluminescence resonance energy transfer: a new model of STAT activation? *J Leukoc Biol* 75, 792-797.
- Schuller, A. C., Ahmed, Z., Levitt, J. A., Suen, K. M., Suhling, K., and Ladbury, J. E. (2008). Indirect recruitment of the signalling adaptor Shc to the fibroblast growth factor receptor 2 (FGFR2). *Biochem J* 416, 189-199.
- Schumacher, T. N., and Schreiber, R. D. (2015). Neoantigens in cancer immunotherapy. *Science* 348, 69-74.
- Schuster, H., Shao, W., Weiss, T., Pedrioli, P. G. A., Roth, P., Weller, M., Campbell, D. S., Deutsch, E. W., Moritz, R. L., Planz, O., *et al.* (2018). A tissue-based draft map of the murine MHC class I immunopeptidome. *Sci Data* 5, 180157.
- Sedger, L. M., and McDermott, M. F. (2014). TNF and TNF-receptors: From mediators of cell death and inflammation to therapeutic giants - past, present and future. *Cytokine Growth Factor Rev* 25, 453-472.
- Sercan, Ö., Hämmerling, G. J., Arnold, B., and Schüler, T. (2006). Cutting Edge: Innate Immune Cells Contribute to the IFN- $\gamma$ -Dependent Regulation of Antigen-Specific CD8<sup>+</sup> T Cell Homeostasis. *The Journal of Immunology* 176, 735-739.
- Serrels, A., Lund, T., Serrels, B., Byron, A., McPherson, R. C., von Kriegsheim, A., Gomez-Cuadrado, L., Canel, M., Muir, M., Ring, J. E., *et al.* (2015). Nuclear FAK controls chemokine transcription, Tregs, and evasion of anti-tumor immunity. *Cell* 163, 160-173.
- Shankaran, V., Ikeda, H., Bruce, A. T., White, J. M., Swanson, P. E., Old, L. J., and Schreiber, R. D. (2001). IFN[ $\gamma$ ] and lymphocytes prevent primary tumour development and shape tumour immunogenicity. *Nature* 410, 1107-1111.

Shao, H., Cheng, H. Y., Cook, R. G., and Tweardy, D. J. (2003). Identification and characterization of signal transducer and activator of transcription 3 recruitment sites within the epidermal growth factor receptor. *Cancer Res* 63, 3923-3930.

Shay, T., Jojic, V., Zuk, O., Rothamel, K., Puyraimond-Zemmour, D., Feng, T., Wakamatsu, E., Benoist, C., Koller, D., and Regev, A. (2013). Conservation and divergence in the transcriptional programs of the human and mouse immune systems. *Proceedings of the National Academy of Sciences* 110, 2946-2951.

Shi, C.-S., Leonardi, A., Kyriakis, J., Siebenlist, U., and Kehrl, J. H. (1999). TNF-Mediated Activation of the Stress-Activated Protein Kinase Pathway: TNF Receptor-Associated Factor 2 Recruits and Activates Germinal Center Kinase Related. *The Journal of Immunology* 163, 3279-3285.

Shi, C. S., and Kehrl, J. H. (1997). Activation of stress-activated protein kinase/c-Jun N-terminal kinase, but not NF-kappaB, by the tumor necrosis factor (TNF) receptor 1 through a TNF receptor-associated factor 2- and germinal center kinase related-dependent pathway. *J Biol Chem* 272, 32102-32107.

Shi, C. S., Tuscano, J., and Kehrl, J. H. (2000). Adaptor proteins CRK and CRKL associate with the serine/threonine protein kinase GCKR promoting GCKR and SAPK activation. *Blood* 95, 776-782.

Shin, J., Rhim, J., Kwon, Y., Choi, S. Y., Shin, S., Ha, C.-W., and Lee, C. (2019). Comparative analysis of differentially secreted proteins in serum-free and serum-containing media by using BONCAT and pulsed SILAC. *Scientific reports* 9, 3096.

Shuai, K., Schindler, C., Prezioso, V. R., and Darnell, J. E., Jr. (1992). Activation of transcription by IFN-gamma: tyrosine phosphorylation of a 91-kD DNA binding protein. *Science* 258, 1808-1812.

Siegel, P. M., Ryan, E. D., Cardiff, R. D., and Muller, W. J. (1999). Elevated expression of activated forms of Neu/ErbB-2 and ErbB-3 are involved in the induction of mammary tumors in transgenic mice: implications for human breast cancer. *EMBO J* 18, 2149-2164.

Silvennoinen, O., Ihle, J. N., Schlessinger, J., and Levy, D. E. (1993). Interferon-induced nuclear signalling by Jak protein tyrosine kinases. *Nature* 366, 583-585.

Sironi, J. J., and Ouchi, T. (2004). STAT1-induced apoptosis is mediated by caspases 2, 3, and 7. *J Biol Chem* 279, 4066-4074.

Smith, M. J., Hardy, W. R., Murphy, J. M., Jones, N., and Pawson, T. (2006). Screening for PTB domain binding partners and ligand specificity using proteome-derived NPXY peptide arrays. *Molecular and Cellular Biology* 26, 8461-8474.

Snyder, M., Huang, X. Y., and Zhang, J. J. (2008). Identification of novel direct Stat3 target genes for control of growth and differentiation. *J Biol Chem* 283, 3791-3798.

Song, G., Satterfield, M. C., Kim, J., Bazer, F. W., and Spencer, T. E. (2009). Progesterone and interferon tau regulate leukemia inhibitory factor receptor and IL6ST in the ovine uterus during early pregnancy. *Reproduction (Cambridge, England)* 137, 553-565.

- Song, T. L., Nairismagi, M. L., Laurensia, Y., Lim, J. Q., Tan, J., Li, Z. M., Pang, W. L., Kizhakeyil, A., Wijaya, G. C., Huang, D. C., *et al.* (2018). Oncogenic activation of the STAT3 pathway drives PD-L1 expression in natural killer/T-cell lymphoma. *Blood* *132*, 1146-1158.
- Sonnenblick, A., Levy, C., and Razin, E. (2004). Interplay between MITF, PIAS3, and STAT3 in mast cells and melanocytes. *Mol Cell Biol* *24*, 10584-10592.
- Souma, Y., Nishida, T., Serada, S., Iwahori, K., Takahashi, T., Fujimoto, M., Ripley, B., Nakajima, K., Miyazaki, Y., Mori, M., *et al.* (2012). Antiproliferative effect of SOCS-1 through the suppression of STAT3 and p38 MAPK activation in gastric cancer cells. *Int J Cancer* *131*, 1287-1296.
- Sparmann, A., and Bar-Sagi, D. (2004). Ras-induced interleukin-8 expression plays a critical role in tumor growth and angiogenesis. *Cancer Cell* *6*, 447-458.
- Spranger, S., and Gajewski, T. F. (2018). Impact of oncogenic pathways on evasion of antitumor immune responses. *Nat Rev Cancer* *18*, 139-147.
- Spranger, S., Spaapen, R. M., Zha, Y., Williams, J., Meng, Y., Ha, T. T., and Gajewski, T. F. (2013). Up-regulation of PD-L1, IDO, and T(regs) in the melanoma tumor microenvironment is driven by CD8(+) T cells. *Science translational medicine* *5*, 200ra116.
- Staaf, J., Ringner, M., Vallon-Christersson, J., Jonsson, G., Bendahl, P. O., Holm, K., Arason, A., Gunnarsson, H., Hegardt, C., Agnarsson, B. A., *et al.* (2010). Identification of subtypes in human epidermal growth factor receptor 2--positive breast cancer reveals a gene signature prognostic of outcome. *J Clin Oncol* *28*, 1813-1820.
- Stanton, S. E., Adams, S., and Disis, M. L. (2016). Variation in the Incidence and Magnitude of Tumor-Infiltrating Lymphocytes in Breast Cancer Subtypes: A Systematic Review. *JAMA Oncol* *2*, 1354-1360.
- Stark, C., Breitkreutz, B. J., Reguly, T., Boucher, L., Breitkreutz, A., and Tyers, M. (2006). BioGRID: a general repository for interaction datasets. *Nucleic Acids Res* *34*, D535-539.
- Stark, G. R., Kerr, I. M., Williams, B. R. G., Silverman, R. H., and Schreiber, R. D. (1998). HOW CELLS RESPOND TO INTERFERONS. *Annu Rev Biochem* *67*, 227-264.
- Stevenson, L. E., and Frackelton, A. R., Jr. (1998). Constitutively tyrosine phosphorylated p52 Shc in breast cancer cells: correlation with ErbB2 and p66 Shc expression. *Breast Cancer Res Treat* *49*, 119-128.
- Street, S. E., Trapani, J. A., MacGregor, D., and Smyth, M. J. (2002). Suppression of lymphoma and epithelial malignancies effected by interferon gamma. *J Exp Med* *196*, 129-134.
- Strehl, B., Seifert, U., Kruger, E., Heink, S., Kuckelkorn, U., and Kloetzel, P. M. (2005). Interferon-gamma, the functional plasticity of the ubiquitin-proteasome system, and MHC class I antigen processing. *Immunol Rev* *207*, 19-30.
- Suenaga, A., Kiyatkin, A. B., Hatakeyama, M., Futatsugi, N., Okimoto, N., Hirano, Y., Narumi, T., Kawai, A., Susukita, R., Koishi, T., *et al.* (2004). Tyr-317 phosphorylation increases Shc structural rigidity and reduces coupling of domain motions remote from the phosphorylation site as revealed by molecular dynamics simulations. *J Biol Chem* *279*, 4657-4662.

Sumimoto, H., Imabayashi, F., Iwata, T., and Kawakami, Y. (2006). The BRAF-MAPK signaling pathway is essential for cancer-immune evasion in human melanoma cells. *J Exp Med* 203, 1651-1656.

Sun, J. C., Ugolini, S., and Vivier, E. (2014). Immunological memory within the innate immune system. *EMBO J* 33, 1295-1303.

Sun, M., Song, C.-X., Huang, H., Frankenberger, C. A., Sankarasharma, D., Gomes, S., Chen, P., Chen, J., Chada, K. K., He, C., and Rosner, M. R. (2013). HMGA2/TET1/HOXA9 signaling pathway regulates breast cancer growth and metastasis. *Proceedings of the National Academy of Sciences* 110, 9920-9925.

Suzuki, R., and Shimodaira, H. (2006). Pvcust: an R package for assessing the uncertainty in hierarchical clustering. *Bioinformatics* 22, 1540-1542.

Szklarczyk, D., Franceschini, A., Wyder, S., Forslund, K., Heller, D., Huerta-Cepas, J., Simonovic, M., Roth, A., Santos, A., Tsafou, K. P., *et al.* (2015). STRING v10: protein-protein interaction networks, integrated over the tree of life. *Nucleic Acids Res* 43, D447-452.

Takeda, K., Clausen, B. E., Kaisho, T., Tsujimura, T., Terada, N., Forster, I., and Akira, S. (1999). Enhanced Th1 activity and development of chronic enterocolitis in mice devoid of Stat3 in macrophages and neutrophils. *Immunity* 10, 39-49.

Taneja, P., Frazier, D. P., Kendig, R. D., Maglic, D., Sugiyama, T., Kai, F., Taneja, N. K., and Inoue, K. (2009). MMTV mouse models and the diagnostic values of MMTV-like sequences in human breast cancer. *Expert Rev Mol Diagn* 9, 423-440.

Tang, L.-Y., Heller, M., Meng, Z., Yu, L.-R., Tang, Y., Zhou, M., and Zhang, Y. E. (2017). Transforming Growth Factor- $\beta$  (TGF- $\beta$ ) Directly Activates the JAK1-STAT3 Axis to Induce Hepatic Fibrosis in Coordination with the SMAD Pathway. *Journal of Biological Chemistry* 292, 4302-4312.

ten Hoeve, J., de Jesus Ibarra-Sanchez, M., Fu, Y., Zhu, W., Tremblay, M., David, M., and Shuai, K. (2002). Identification of a nuclear Stat1 protein tyrosine phosphatase. *Mol Cell Biol* 22, 5662-5668.

Teo, G., Liu, G., Zhang, J., Nesvizhskii, A. I., Gingras, A. C., and Choi, H. (2014). SAINTexpress: improvements and additional features in Significance Analysis of INteractome software. *J Proteomics* 100, 37-43.

TFsearcher (2015).

Thomas, A., Routh, E. D., Pullikuth, A., Jin, G., Su, J., Chou, J. W., Hoadley, K. A., Print, C., Knowlton, N., Black, M. A., *et al.* (2018). Tumor mutational burden is a determinant of immune-mediated survival in breast cancer. *Oncoimmunology* 7, e1490854-e1490854.

Thomas, D., Patterson, S. D., and Bradshaw, R. A. (1995). Src Homologous and Collagen (Shc) Protein Binds to F-actin and Translocates to the Cytoskeleton upon Nerve Growth Factor Stimulation in PC12 Cells. *Journal of Biological Chemistry* 270, 28924-28931.

- Thuault, S., Valcourt, U., Petersen, M., Manfioletti, G., Heldin, C. H., and Moustakas, A. (2006). Transforming growth factor-beta employs HMGA2 to elicit epithelial-mesenchymal transition. *J Cell Biol* 174, 175-183.
- Thyrell, L., Arulampalam, V., Hjortsberg, L., Farnebo, M., Grander, D., and Pokrovskaja Tamm, K. (2007). Interferon alpha induces cell death through interference with interleukin 6 signaling and inhibition of STAT3 activity. *Experimental cell research* 313, 4015-4024.
- Tian, Z. J., and An, W. (2004). ERK1/2 contributes negative regulation to STAT3 activity in HSS-transfected HepG2 cells. *Cell Res* 14, 141-147.
- Tiganis, T., Bennett, A. M., Ravichandran, K. S., and Tonks, N. K. (1998). Epidermal Growth Factor Receptor and the Adaptor Protein p52Shc Are Specific Substrates of T-Cell Protein Tyrosine Phosphatase. *Molecular and Cellular Biology* 18, 1622-1634.
- Timofeeva, O. A., Tarasova, N. I., Zhang, X., Chasovskikh, S., Cheema, A. K., Wang, H., Brown, M. L., and Dritschilo, A. (2013). STAT3 suppresses transcription of proapoptotic genes in cancer cells with the involvement of its N-terminal domain. *Proc Natl Acad Sci U S A* 110, 1267-1272.
- Tkach, M., Roseblit, C., Rivas, M. A., Proietti, C. J., Díaz Flaqué, M. C., Mercogliano, M. F., Beguelin, W., Maronna, E., Guzmán, P., Gercovich, F. G., *et al.* (2013). p42/p44 MAPK-mediated Stat3 Ser727 phosphorylation is required for progestin-induced full activation of Stat3 and breast cancer growth. *Endocrine-Related Cancer*.
- Togi, S., Kamitani, S., Kawakami, S., Ikeda, O., Muromoto, R., Nanbo, A., and Matsuda, T. (2009). HDAC3 influences phosphorylation of STAT3 at serine 727 by interacting with PP2A. *Biochem Biophys Res Commun* 379, 616-620.
- Topalian, S., Drake, C., and Pardoll, D. (2012). Targeting the PD-1/B7-H1(PD-L1) pathway to activate anti-tumor immunity. *Curr Opin Immunol* 24, 207 - 212.
- Topalian, S. L., Drake, C. G., and Pardoll, D. M. (2015). Immune checkpoint blockade: a common denominator approach to cancer therapy. *Cancer Cell* 27, 450-461.
- Tsou, P., Katayama, H., Ostrin, E. J., and Hanash, S. M. (2016). The Emerging Role of B Cells in Tumor Immunity. *Cancer Res* 76, 5597-5601.
- Tumeh, P. C., Harview, C. L., Yearley, J. H., Shintaku, I. P., Taylor, E. J., Robert, L., Chmielowski, B., Spasic, M., Henry, G., Ciobanu, V., *et al.* (2014). PD-1 blockade induces responses by inhibiting adaptive immune resistance. *Nature* 515, 568-571.
- Tups, A., Stohr, S., Helwig, M., Barrett, P., Krol, E., Schachtner, J., Mercer, J. G., and Klingenspor, M. (2012). Seasonal leptin resistance is associated with impaired signalling via JAK2-STAT3 but not ERK, possibly mediated by reduced hypothalamic GRB2 protein. *Journal of comparative physiology B, Biochemical, systemic, and environmental physiology* 182, 553-567.
- Tymoszuk, P., Charoentong, P., Hackl, H., Spilka, R., Muller-Holzner, E., Trajanoski, Z., Obrist, P., Revillion, F., Peyrat, J. P., Fiegl, H., and Doppler, W. (2014). High STAT1 mRNA levels but not its tyrosine phosphorylation are associated with macrophage infiltration and bad prognosis in breast cancer. *BMC Cancer* 14, 257.

- Ursini-Siegel, J., Cory, S., Zuo, D., Hardy, W. R., Rexhepaj, E., Lam, S., Schade, B., Jirstrom, K., Bjur, E., Piccirillo, C. A., *et al.* (2010). Receptor tyrosine kinase signaling favors a protumorigenic state in breast cancer cells by inhibiting the adaptive immune response. *Cancer Res* *70*, 7776-7787.
- Ursini-Siegel, J., Hardy, W. R., Zheng, Y., Ling, C., Zuo, D., Zhang, C., Podmore, L., Pawson, T., and Muller, W. J. (2012). The ShcA SH2 domain engages a 14-3-3/PI3K signaling complex and promotes breast cancer cell survival. *Oncogene*.
- Ursini-Siegel, J., Hardy, W. R., Zuo, D., Lam, S. H. L., Sanguin-Gendreau, V., Cardiff, R. D., Pawson, T., and Muller, W. J. (2008). ShcA signalling is essential for tumour progression in mouse models of human breast cancer. *EMBO J* *27*, 910-920.
- Ursini-Siegel, J., and Muller, W. J. (2008). The ShcA adaptor protein is a critical regulator of breast cancer progression. *Cell Cycle* *7*, 1936-1943.
- van der Geer, P., Wiley, S., Gish, G. D., and Pawson, T. (1996). The Shc adaptor protein is highly phosphorylated at conserved, twin tyrosine residues (Y239/240) that mediate protein-protein interactions. *Current biology* : CB *6*, 1435-1444.
- Varnaite, R., and MacNeill, S. A. (2016). Meet the neighbors: Mapping local protein interactomes by proximity-dependent labeling with BioID. *Proteomics* *16*, 2503-2518.
- Velazquez, L., Gish, G. D., van Der Geer, P., Taylor, L., Shulman, J., and Pawson, T. (2000). The shc adaptor protein forms interdependent phosphotyrosine-mediated protein complexes in mast cells stimulated with interleukin 3. *Blood* *96*, 132-138.
- Vinkemeier, U. (2004). Getting the message across, STAT! Design principles of a molecular signaling circuit. *J Cell Biol* *167*, 197-201.
- Visvader, J. E. (2009). Keeping abreast of the mammary epithelial hierarchy and breast tumorigenesis. *Genes Dev* *23*, 2563-2577.
- Voron, T., Marcheteau, E., Pernot, S., Colussi, O., Tartour, E., Taieb, J., and Terme, M. (2014). Control of the immune response by pro-angiogenic factors. *Frontiers in oncology* *4*, 70.
- Voskoboinik, I., Whisstock, J. C., and Trapani, J. A. (2015). Perforin and granzymes: function, dysfunction and human pathology. *Nat Rev Immunol* *15*, 388-400.
- Wagner, B. J., Hayes, T. E., Hoban, C. J., and Cochran, B. H. (1990). The SIF binding element confers sis/PDGF inducibility onto the c-fos promoter. *Embo j* *9*, 4477-4484.
- Wakahara, R., Kunimoto, H., Tanino, K., Kojima, H., Inoue, A., Shintaku, H., and Nakajima, K. (2012). Phospho-Ser727 of STAT3 regulates STAT3 activity by enhancing dephosphorylation of phospho-Tyr705 largely through TC45. *Genes Cells* *17*, 132-145.
- Waks, A. G., and Winer, E. P. (2019). Breast Cancer Treatment: A Review Breast Cancer Treatment in 2019. *JAMA : the journal of the American Medical Association* *321*, 288-300.

- Walrath, J. C., Hawes, J. J., Van Dyke, T., and Reilly, K. M. (2010). Genetically engineered mouse models in cancer research. *Advances in cancer research* 106, 113-164.
- Wang, G., Wang, Y., Teng, M., Zhang, D., Li, L., and Liu, Y. (2010). Signal transducers and activators of transcription-1 (STAT1) regulates microRNA transcription in interferon gamma-stimulated HeLa cells. *PLoS One* 5, e11794.
- Wang, O. H., Azizian, N., Guo, M., Capello, M., Deng, D., Zang, F., Fry, J., Katz, M. H., Fleming, J. B., Lee, J. E., *et al.* (2016). Prognostic and Functional Significance of MAP4K5 in Pancreatic Cancer. *PLoS One* 11, e0152300.
- Wang, S., Patsis, C., and Koromilas, A. E. (2015a). Stat1 stimulates cap-independent mRNA translation to inhibit cell proliferation and promote survival in response to antitumor drugs. *Proc Natl Acad Sci U S A*.
- Wang, S., Zhou, M., Lin, F., Liu, D., Hong, W., Lu, L., Zhu, Y., and Xu, A. (2014). Interferon-gamma induces senescence in normal human melanocytes. *PLoS One* 9, e93232.
- Wang, W., Erbe, A. K., Hank, J. A., Morris, Z. S., and Sondel, P. M. (2015b). NK Cell-Mediated Antibody-Dependent Cellular Cytotoxicity in Cancer Immunotherapy. *Front Immunol* 6, 368-368.
- Wang, W. B., Levy, D. E., and Lee, C. K. (2011). STAT3 negatively regulates type I IFN-mediated antiviral response. *J Immunol* 187, 2578-2585.
- Wary, K. K., Mariotti, A., Zurzolo, C., and Giancotti, F. G. (1998). A requirement for caveolin-1 and associated kinase Fyn in integrin signaling and anchorage-dependent cell growth. *Cell* 94, 625-634.
- Webster, M. A., Hutchinson, J. N., Rauh, M. J., Muthuswamy, S. K., Anton, M., Tortorice, C. G., Cardiff, R. D., Graham, F. L., Hassell, J. A., and Muller, W. J. (1998). Requirement for Both Shc and Phosphatidylinositol 3' Kinase Signaling Pathways in Polyomavirus Middle T-Mediated Mammary Tumorigenesis. *Molecular and Cellular Biology* 18, 2344-2359.
- Wegrzyn, J., Potla, R., Chwae, Y. J., Sepuri, N. B., Zhang, Q., Koeck, T., Derecka, M., Szczepanek, K., Szlag, M., Gornicka, A., *et al.* (2009). Function of mitochondrial Stat3 in cellular respiration. *Science* 323, 793-797.
- Wellenstein, M. D., and de Visser, K. E. (2018). Cancer-Cell-Intrinsic Mechanisms Shaping the Tumor Immune Landscape. *Immunity* 48, 399-416.
- Wellings, S. R. (1980). A Hypothesis of the Origin of Human Breast Cancer from the Terminal Ductal Lobular Unit. *Pathology - Research and Practice* 166, 515-535.
- Wen, Z., and Darnell, J. E., Jr. (1997). Mapping of Stat3 serine phosphorylation to a single residue (727) and evidence that serine phosphorylation has no influence on DNA binding of Stat1 and Stat3. *Nucleic Acids Res* 25, 2062-2067.
- Wen, Z., Zhong, Z., and Darnell, J. E., Jr. (1995). Maximal activation of transcription by Stat1 and Stat3 requires both tyrosine and serine phosphorylation. *Cell* 82, 241-250.

White, D. E., Kurpios, N. A., Zuo, D., Hassell, J. A., Blaess, S., Mueller, U., and Muller, W. J. (2004). Targeted disruption of beta1-integrin in a transgenic mouse model of human breast cancer reveals an essential role in mammary tumor induction. *Cancer Cell* 6, 159-170.

White, F. M., and Wolf-Yadlin, A. (2016). Methods for the Analysis of Protein Phosphorylation–Mediated Cellular Signaling Networks. *Annual Review of Analytical Chemistry* 9, 295-315.

Whittemore, A. S., Gong, G., and Itnyre, J. (1997). Prevalence and contribution of BRCA1 mutations in breast cancer and ovarian cancer: results from three U.S. population-based case-control studies of ovarian cancer. *Am J Hum Genet* 60, 496-504.

Wiejak, J., Dunlop, J., Gao, S., Borland, G., and Yarwood, S. J. (2012). Extracellular signal-regulated kinase mitogen-activated protein kinase-dependent SOCS-3 gene induction requires c-Jun, signal transducer and activator of transcription 3, and specificity protein 3 transcription factors. *Molecular pharmacology* 81, 657-668.

Wills, M. K., and Jones, N. (2012). Teaching an old dogma new tricks: twenty years of Shc adaptor signalling. *Biochem J* 447, 1-16.

Woetmann, A., Nielsen, M., Christensen, S. T., Brockdorff, J., Kaltoft, K., Engel, A. M., Skov, S., Brender, C., Geisler, C., Svejgaard, A., *et al.* (1999). Inhibition of protein phosphatase 2A induces serine/threonine phosphorylation, subcellular redistribution, and functional inhibition of STAT3. *Proc Natl Acad Sci U S A* 96, 10620-10625.

Wohrle, F. U., Daly, R. J., and Brummer, T. (2009). Function, regulation and pathological roles of the Gab/DOS docking proteins. *Cell communication and signaling : CCS* 7, 22.

Wouters, M. C., and Nelson, B. H. (2018). Prognostic significance of tumor-infiltrating B cells and plasma cells in human cancer. *Clinical Cancer Research*, clincanres.1481.2018.

Wright, K. D., Miller, B. S., El-Meanawy, S., Tsaih, S. W., Banerjee, A., Geurts, A. M., Sheinin, Y., Sun, Y., Kalyanaraman, B., Rui, H., *et al.* (2019). The p52 isoform of SHC1 is a key driver of breast cancer initiation. *Breast Cancer Res* 21, 74.

Xia, L., Wang, L., Chung, A. S., Ivanov, S. S., Ling, M. Y., Dragoi, A. M., Platt, A., Gilmer, T. M., Fu, X. Y., and Chin, Y. E. (2002). Identification of both positive and negative domains within the epidermal growth factor receptor COOH-terminal region for signal transducer and activator of transcription (STAT) activation. *J Biol Chem* 277, 30716-30723.

Xia, Y., Medeiros, L. J., and Young, K. H. (2015). Immune checkpoint blockade: Releasing the brake towards hematological malignancies. *Blood Rev.*

Xin, H., Zhang, C., Herrmann, A., Du, Y., Figlin, R., and Yu, H. (2009). Sunitinib inhibition of Stat3 induces renal cell carcinoma tumor cell apoptosis and reduces immunosuppressive cells. *Cancer Res* 69, 2506-2513.

Yaffe, M. B., and VanHook, A. M. (2017). *Science Signaling* Podcast for 14 March 2017: The Cancer Moonshot. *Sci Signal* 10, eaan1418.

Yamamoto, T., Sekine, Y., Kashima, K., Kubota, A., Sato, N., Aoki, N., and Matsuda, T. (2002). The nuclear isoform of protein-tyrosine phosphatase TC-PTP regulates interleukin-6-mediated

signaling pathway through STAT3 dephosphorylation. *Biochem Biophys Res Commun* 297, 811-817.

Yang, J., Chatterjee-Kishore, M., Staugaitis, S. M., Nguyen, H., Schlessinger, K., Levy, D. E., and Stark, G. R. (2005). Novel roles of unphosphorylated STAT3 in oncogenesis and transcriptional regulation. *Cancer Res* 65, 939-947.

Yang, J., Huang, J., Dasgupta, M., Sears, N., Miyagi, M., Wang, B., Chance, M. R., Chen, X., Du, Y., Wang, Y., *et al.* (2010). Reversible methylation of promoter-bound STAT3 by histone-modifying enzymes. *Proceedings of the National Academy of Sciences* 107, 21499-21504.

Yang, J., Liao, X., Agarwal, M. K., Barnes, L., Auron, P. E., and Stark, G. R. (2007). Unphosphorylated STAT3 accumulates in response to IL-6 and activates transcription by binding to NFkappaB. *Genes Dev* 21, 1396-1408.

Yang, X. R., Figueroa, J. D., Falk, R. T., Zhang, H., Pfeiffer, R. M., Hewitt, S. M., Lissowska, J., Peplonska, B., Brinton, L., Garcia-Closas, M., and Sherman, M. E. (2012). Analysis of terminal duct lobular unit involution in luminal A and basal breast cancers. *Breast Cancer Res* 14, R64.

Yang, Z., and Tam, K. Y. (2018). Combination Strategies Using EGFR-TKi in NSCLC Therapy: Learning from the Gap between Pre-Clinical Results and Clinical Outcomes. *Int J Biol Sci* 14, 204-216.

Yarchoan, M., Johnson, B. A., 3rd, Lutz, E. R., Laheru, D. A., and Jaffee, E. M. (2017). Targeting neoantigens to augment antitumour immunity. *Nat Rev Cancer* 17, 209-222.

Yeh, Y. T., Ou-Yang, F., Chen, I. F., Yang, S. F., Wang, Y. Y., Chuang, H. Y., Su, J. H., Hou, M. F., and Yuan, S. S. (2006). STAT3 ser727 phosphorylation and its association with negative estrogen receptor status in breast infiltrating ductal carcinoma. *Int J Cancer* 118, 2943-2947.

Yi, M., Jiao, D., Xu, H., Liu, Q., Zhao, W., Han, X., and Wu, K. (2018). Biomarkers for predicting efficacy of PD-1/PD-L1 inhibitors. *Mol Cancer* 17, 129.

Yoon, S., Woo, S. U., Kang, J. H., Kim, K., Kwon, M. H., Park, S., Shin, H. J., Gwak, H. S., and Chwae, Y. J. (2010). STAT3 transcriptional factor activated by reactive oxygen species induces IL6 in starvation-induced autophagy of cancer cells. *Autophagy* 6, 1125-1138.

Young, Y. K., Bolt, A. M., Ahn, R., and Mann, K. K. (2016). Analyzing the Tumor Microenvironment by Flow Cytometry. *Methods in molecular biology* 1458, 95-110.

Yu, H., and Jove, R. (2004). The STATs of cancer--new molecular targets come of age. *Nat Rev Cancer* 4, 97-105.

Yu, H., Kortylewski, M., and Pardoll, D. (2007). Crosstalk between cancer and immune cells: role of STAT3 in the tumour microenvironment. *Nat Rev Immunol* 7, 41-51.

Yu, H., Lee, H., Herrmann, A., Buettner, R., and Jove, R. (2014). Revisiting STAT3 signalling in cancer: new and unexpected biological functions. *Nat Rev Cancer* 14, 736-746.

Yu, H., Pardoll, D., and Jove, R. (2009). STATs in cancer inflammation and immunity: a leading role for STAT3. *Nat Rev Cancer* 9, 798-809.

- Yue, H., Li, W., Desnoyer, R., and Karnik, S. S. (2010). Role of nuclear unphosphorylated STAT3 in angiotensin II type 1 receptor-induced cardiac hypertrophy. *Cardiovasc Res* 85, 90-99.
- Yue, P., and Turkson, J. (2009). Targeting STAT3 in cancer: how successful are we? *Expert Opin Investig Drugs* 18, 45-56.
- Zaidi, M. R., and Merlino, G. (2011). The two faces of interferon-gamma in cancer. *Clin Cancer Res* 17, 6118-6124.
- Zgheib, C., Zouein, F. A., Chidiac, R., Kurdi, M., and Booz, G. W. (2012). Calyculin A reveals serine/threonine phosphatase protein phosphatase 1 as a regulatory nodal point in canonical signal transducer and activator of transcription 3 signaling of human microvascular endothelial cells. *Journal of interferon & cytokine research : the official journal of the International Society for Interferon and Cytokine Research* 32, 87-94.
- Zhang, A. W., McPherson, A., Milne, K., Kroeger, D. R., Hamilton, P. T., Miranda, A., Funnell, T., Little, N., de Souza, C. P. E., Laan, S., *et al.* (2018). Interfaces of Malignant and Immunologic Clonal Dynamics in Ovarian Cancer. *Cell* 173, 1755-1769 e1722.
- Zhang, S., Kohli, K., Black, R. G., Yao, L., Spadinger, S. M., He, Q., Pillarisetty, V. G., Cranmer, L. D., Van Tine, B. A., Yee, C., *et al.* (2019). Systemic Interferon-gamma Increases MHC Class I Expression and T-cell Infiltration in Cold Tumors: Results of a Phase 0 Clinical Trial. *Cancer Immunol Res* 7, 1237-1243.
- Zhang, T., Ma, J., and Cao, X. (2003a). Grb2 regulates Stat3 activation negatively in epidermal growth factor signalling. *Biochem J* 376, 457-464.
- Zhang, X., Blenis, J., Li, H. C., Schindler, C., and Chen-Kiang, S. (1995). Requirement of serine phosphorylation for formation of STAT-promoter complexes. *Science* 267, 1990-1994.
- Zhang, X., Guo, A., Yu, J., Possemato, A., Chen, Y., Zheng, W., Polakiewicz, R. D., Kinzler, K. W., Vogelstein, B., Velculescu, V. E., and Wang, Z. J. (2007). Identification of STAT3 as a substrate of receptor protein tyrosine phosphatase T. *Proc Natl Acad Sci U S A* 104, 4060-4064.
- Zhang, Y., Cho, Y. Y., Petersen, B. L., Bode, A. M., Zhu, F., and Dong, Z. (2003b). Ataxia telangiectasia mutated proteins, MAPKs, and RSK2 are involved in the phosphorylation of STAT3. *J Biol Chem* 278, 12650-12659.
- Zhang, Y., Liu, G., and Dong, Z. (2001). MSK1 and JNKs Mediate Phosphorylation of STAT3 in UVA-irradiated Mouse Epidermal JB6 Cells. *Journal of Biological Chemistry* 276, 42534-42542.
- Zheng, Y., Zhang, C., Croucher, D. R., Soliman, M. A., St-Denis, N., Pasculescu, A., Taylor, L., Tate, S. A., Hardy, W. R., Colwill, K., *et al.* (2013). Temporal regulation of EGF signalling networks by the scaffold protein Shc1. *Nature* 499, 166-171.
- Zhong, Z., Wen, Z., and Darnell, J. E., Jr. (1994). Stat3: a STAT family member activated by tyrosine phosphorylation in response to epidermal growth factor and interleukin-6. *Science* 264, 95-98.
- Zhou, F. (2009). Molecular mechanisms of IFN-gamma to up-regulate MHC class I antigen processing and presentation. *Int Rev Immunol* 28, 239-260.

Zitvogel, L., Tesniere, A., and Kroemer, G. (2006). Cancer despite immunosurveillance: immunoselection and immunosubversion. *Nat Rev Immunol* 6, 715-727.